GENERAL ELECTRIC

RESEARCH AND DEVELOPMENT CENTER

SCHENECTADY, NEW YORK

FINAL REPORT

STUDY OF DYNAMIC AND STATIC SEALS FOR LIQUID ROCKET ENGINES

for Period April 1, 1967 to April 1, 1968

NASA Contract No. NAS7-434

Phase II

Prepared For

Chief, Liquid Propulsion Technology, RPL
National Aeronautics and Space Administration
Washington, D.C. 20546

S-68-1144

STUDY OF DYNAMIC AND STATIC SEALS FOR LIQUID ROCKET ENGINES

FINAL REPORT

SELECTED STUDIES FROM THE TECHNOLOGY OF MECHANICAL FACE SEALS

MAY 1, 1968

For Period April 1, 1967 to April 1, 1968

TO: Chief, Liquid Propulsion Technology, RPL
Office of Advanced Research and Technology
NASA Headquarters
Washington, D.C. 20546

NASA CONTRACT NO.: NAS 7-434 Phase II

PREPARED BY: Research and Development Center
General Electric Company
Schenectady, New York 12305

CONTRACTING COMPONENT: Missile and Space Division
General Electric Company
Philadelphia, Pennsylvania

FOREWORD

This volume comprises the Final Report prepared in complete fulfillment of the requirements of Contract NAS 7-434, Phase II. The Final Report covers the period April 1, 1967 to April 1, 1968. Contributors for the technical work reported are as follows:

J. A. Findlay
A. J. Orsino
H. J. Sneck

Significant contributions were made by J. A. Reilly, in computer programming, data reduction, literature review and editorial and publication assistance, and by H. T. Robison, in carrying out a successful experimental program and assisting with the literature review.

TABLE OF CONTENTS

I. SUMMARY

The final report consists of a single volume and presents the results and recommendations of the technical work performed under the National Aeronautics and Space Administration Contract NAS7-434, Phase II, from April 1, 1967 to April 1, 1968.

The technical work is of a fundamental nature intended to establish a basic understanding of seals and sealing mechanisms. Analytical as well as experimental efforts are described in the area of Newtonian and non-Newtonian sealing concepts. Viscoelastic experiments using a seal-like configuration were continued. A hydrostatic gas bearing was used in measuring torque in these tests. The data obtained from these tests was used in the attempt to determine a simple correlative model for non-Newtonian phenomenon. Correlation included the shear-stress shear-rate correlation and the normal stress shear-rate correlation.

Several series of Newtonian tests were run to study the effects of seal geometry on leakage and to consider the relationship of the different geometries to the phenomenon of "seal pumping". Corresponding analytical work was also carried out and through the use of digital computers, correlations were made and the derived theories were substantiated. The literature analysis and review was updated.

All technical work was accomplished by personnel of the Research and Development Center, General Electric Company, Schenectady, New York. Names of individual contributions appear on the appendix containing the full report of their particular activity. Project Engineer is J. A. Findlay. Project Manager is G. R. Fox. The work was accomplished under the direction of National Aeronautics and Space Administration Technical Manager, Mr. R. S. Weiner, Liquid Propulsion Section, Jet Propulsion Section, Jet Propulsion Laboratory, California Institute of Technology, 4800 Oak Grove Drive, Passadena, California. National Aeronautics and Space Administration Project Manager is Mr. F. E. Compitello, Liquid Propulsion Technology, RPL, Office of Advanced Research and Technology, NASA Headquarters, Washington, D.C. 20546.

II. DESCRIPTION OF PROGRAM

A. Introduction

The Research and Development Center, General Electric Company, has been engaged in a fundamental study of dynamic and static seals for the National Aeronautics and Space Administration under Contract NAS7-434, Phase II. The principal work of the study is concerned with the technology of seals and sealing mechanisms on an analytical as well as an experimental basis. The scope of the program is extremely broad and requires detailed knowledge of several technical disciplines. In view of these particular characteristics of the program, it has been necessary to select specific areas for detailed study in order to assure the development of meaningful information and data. It is expected that the results of these technical efforts would serve to form a basis for formulation of seal design criteria. A considerable amount of preliminary work, intended to provide a measure of order in the available technology of seals and sealing mechanisms was accomplished on contract NAS7-102. The work of this contract draws heavily from the findings and results of contract NAS7-102 and of Phase I of the current contract. The technical results of this work are contained in one volume..

B. Program Objective

The objective of this program is to advance the technology of dynamic and static seals for liquid rocket engines. A study of the fundamentals of sealing processes is to be carried out, in order to provide the understanding necessary to formulate design criteria for seals in future liquid rocket engines.

C. Description of Program Plan

The detailed program plan covering the technical effort under this contract is outlined below. The task designations are evolved from the contract work statement and include suitable sub-headings to facilitate description of the effort involved.

Program Plan

Task 1 - Non-Newtonian Face Seal Experiments
- Effect of Land Width
- Torque Measurements
- Leakage Speed Test

Task 2 - Non-Newtonian Correlative Model
- Review Existing Models
- Formulation of a Tentative Model
- Suggest Experiments
- Evaluate Data and Model

Task 3 - Face Seal Geometry Effects Study
- Cavitation Experiments
- Eccentric Seal Experiments
- Inertia Experiments
- Two-fluid Study

Task 4 - Seal Design
- Correlate Seal Data
- Evaluate Seal Theories
- Extend and Improve theories
- Design Data

Task 5 - Literature Review
- Updating

The planned analytical studies and experimental investigations cover areas which heretofore have not been explored in significant depth. These areas were considered to possess a high potential for improved understanding of seals and sealing mechanisms. During execution of the program, some variations in original plans were necessary. This was somewhat anticipated since it is not always possible to predict the course of fundamental technical investigations. As the work progressed, the knowledge acquired was used to reevaluate, and if necessary, to redirect the subsequent effort for each task. In all cases, the overall program objective was followed as closely as possible to assure useful results.

A discussion of the results and accomplishments for each task will be presented in a subsequent section of this report.

III. DISCUSSION OF ACCOMPLISHMENTS

1. General

The technical accomplishments of this study are reported in a single volume. The technical work reported was initiated April 1, 1967 and continued to April 1, 1968.

The results of the technical work were highly encouraging, especially the Newtonian face seal tasks. The phenomenon of "inward pumping" was found to be predictable by a theory based on radial eccentricity and misalignment. This theory is discussed in Appendix D and includes the effects of gas cavities and two different fluids on either side of the seal. These theories are confirmed by the experiments reported in Appendix C as is the inertia theory of H. J. Sneck's reported in Phase I of this contract. The Newtonian face seal theories are extended in Appendix E and F.

The very difficult task of developing a non-Newtonian face seal correlation is discussed in Appendix A and B.

The seals literature review is brought up to date in Appendix G.

2. Discussion of Tasks

A. Task 1 - Non-Newtonian Face Seal Experiments

The non-Newtonian face seal experiments conducted during this contract phase were actually an extension of experimental work previously performed. The extension was due primarily to the marginal correlation obtained with the original jet capillary experiments. During the initial face seal experiments it was found that sealing effectiveness was several orders of magnitude below the value predicted from the capillary experiments.

In the non-Newtonian face seal experiments covered by this report an effort was made to provide data for the development of a suitable correlative model. Such a correlation might provide a better understanding of the behavior of non-Newtonian fluids in face seals. Knowledge of torque level at the seal interface was considered a vital part of any effort to establish a suitable correlation. Under this task effort a hydrostatic torque device was constructed to facilitate evaluation of seal interface torque under dynamic conditions.

The experimental results provided data at several fixed clearances over a broad speed range to 12000 rpm. Tests were performed with JP5 + 3.2% poly-isobutylene, JP5 with no polymer additive and SF96 silicone oil of two different viscosities. Leakage data as well as torque, clearance and speed were obtained for all tests. No evaluation of the data was performed under this task effort. The correlation of test results was accomplished as part of a separate task of this contract phase. The test data is presented in Appendix A.

B. Task 2 - Non-Newtonian Correlative Model

The objective of this investigation was to determine if a simple correlative model could be developed with the aid of the data obtained under Task 1. While there is considerable viscometric data available for seal-like configurations, none of this data was obtained in the presence of an applied pressure gradient and non-zero leakage rates. Most viscoelastic fluid flow theories have been developed for the much simpler case of zero-net leakage in configurations which do not allow for applying pressure gradients.

It was found from an examination of the torque data obtained in Task 1 that over the entire range of shear rates tested the tangential shear stress was described quite accurately by a form of the invariant power-law. Although it has been often suggested that the invariant form of the power-law might be applicable to three dimensional flows, this is one of the few instances where such a correlation has actually been made.

As anticipated, the sealing effects of the normal stresses were found to be relatively unimportant at low shear-rates. This is because, as the results of no net leakage tests show, the normal stresses are related to the tangential shear-rate.

At high tangential shear-rates where this shear-rate predominates over the radial shear-rate due to leakage, the normal stresses can again be correlated as a function of the tangential shear-rate. Unfortunately, this correlation is not the same as the no leakage-rate correlation at low shear-rates.

In the intermediate range of tangential shear-rates where the radial and tangential shear-rates are of the same order of magnitude, it was not possible to generate a general correlation which accounted for the normal stress effects on leakage sealing.

Attempts to superimpose simultaneously the effects of degrading viscosity and improving normal stress effects failed probably due to the inherent non-linearity of viscoelastic phenomena itself. Failure to obtain a correlative theory on a global basis, i.e., by not considering the details of the phenomena is disappointing but not unexpected. The results obtained here will be very useful in the future efforts to develop such detailed theories.

C. Task 3 - Seal Geometry Effects

The experiments in this task have been keyed towards the accurate measurement of face seal geometry. The basic problem in obtaining data to substantiate the theories of Newtonian face seal operation has been the uncontrolled variations in the surface geometry. Through the use of relatively large film thicknesses

and optically flat glass as the seal face, the effects of uncontrolled surface variations was minimized. Previous literature concerning seal geometry effects have not dealt with such controlled test conditions and, thus, the data obtained under this task appears to be the most useful for correlating theories.

The experiments carried out in this task include those with concentric and misaligned seals, eccentric seals and those tests studying the effects of inertia and of fluid viscosity on seal leakage. The results of the cavitation experiments showed that the gas cavities had no effect on the leakage. The full film results verified the fact that the effect of seal eccentricity can be added directly to the hydrostatic leakage. Both of these results compared very well with the existing theories and these specific correlations are presented in Appendix C.

Tests were also conducted under this task which are concerned with the two-fluid problem in face seal operation. This phenomenon considers the changes in seal hydrodynamics which occur when the fluids on either side of the seal face are of different viscosities. These tests were run using viscosity ratios, μ_o/μ_i, ranging from 3.5 to 0.002. The data taken was correlated using this ratio. Further tests were carried out in this task which consider the inertial effect on leakage. In this series of tests, as was with all tests, GE Time Sharing Computer programs were used to reduce the data. The results of both the two fluid and the inertia tests can be seen in Appendix C.

D. Task 4

1. Seal Design I

The main effort of this task has been the extension of basic face seal theories. The "short bearing" theory developed in Phase I of this contract has been used to predict gas cavity shapes and inception points. The analysis has been extended from the wavy film thickness to the tilted seal case used in the laboratory experiments.

A full film solution has been derived for the eccentric seal case using the "short bearing" approximation. This was done to show that a combination of seal surface waviness or tilt coupled with an eccentricity between the two seal surfaces can result in a pumping of fluid against a hydrostatic pressure differential.

The GE 635 face seal computer program was used to compute seal leakage and pumping due to eccentricity in the misaligned seal. This program has been improved to give faster convergence and to compute the short bearing approximation as well as the two dimensional solution.

A further analysis of the two-fluid case was conducted. Many of the basic relationships were derived. A summary of the equations and approach to their solution is given in Appendix D.

2. Seal Design II and III

The analyses of face seal behavior are invariably based on the assumption of isothermal flow through the seal clearance. This assumption allows both the density and particularly the viscosity to be taken as constants. The analysis of thermal effects in face seals presented here formalizes the procedures whereby the designer may estimate when such simplifying assumptions are valid.

Reversed flow effects in seals are particularly interesting when the externally applied pressure in a face seal exceeds the internal pressure. Under this condition it is possible to establish counter flows within the clearance space so that there is a net exchange of internal and external fluids. The rate at which these fluids are exchanged between the inner and outer boundaries is an important design consideration. Methods for predicting these exchange rates are developed in the reversed flow analyses.

E. Task 5 - Literature Review

The literature review was patterned after the similar study under Phase I of this contract. The review of all available reference sources was updated as far as possible with most sources reviewed up to January 1968.

Abstracts were prepared for all the material considered of interest in the area of seals and sealing mechanisms for both dynamic and static seals. More than one hundred abstracts from the more than eleven major source references were prepared. In some cases the abstract was taken from the authors own prepared abstract. In other cases the abstract was prepared from a complete reading of the text.

APPENDIX A

NON-NEWTONIAN FACE SEAL EXPERIMENT

BY

A. J. Orsino

I. INTRODUCTION

The experimental study by Bernd, Reference 1, predicted increased sealing effectiveness in a face type dynamic seal for fluids containing small amounts of certain polymer additive. As a result of the work reported in Reference 1, an experimental program using a seal like configuration was undertaken in an effort to obtain a more detailed understanding of non-Newtonian fluid behavior in dynamic face seals. The results of this effort are reported in Reference 2 and show only a minimal degree of correlation with the results of the jet capillary experiments by Bernd. The fundamental reasons for the poor correlation is probably due to the significant differences in geometry between the capillary and the dynamic face seal. Transit time for the fluid in the capillary test is extremely short and perhaps of a lower value than the fluid relaxation time. This is not the case for the seal configuration. The comparatively tortuous path for the fluid in the seal, with its correspondingly longer transit time, may give rise to increased possibility for rupture of intramolecular bands. Rupture of fluid molecular bands has a strong influence on fluid properties.

In order to better understand the behavior of non-Newtonian fluids in thin films, and thereby establish a basic understanding of face seals operating with such fluids, a new series of experiments was conducted. The objective of this new testing was the acquisition of experimental data for use in evolving a suitable correlative model. The model would provide a basis for making meaningful predictions regarding face seal performance. Testing during this contract phase was an extension of previous work using the identical test equipment plus some modification to allow for torque measurements. It was expected that torque data would provide an independent means for development of a suitable correlative model. Knowledge of the torque present at the fluid interface allows detailed evaluation of viscosity and its variation with shear rate.

This Appendix describes the design of the torque device, the test procedure used and the results of the experimental data obtained for the several fluids tested. A description of the data evaluation and a discussion of the correlative model evolved are contained elsewhere in this report under the results of the Task 2 effort.

II. HYDROSTATIC TORQUE MEASURING DEVICE

The single most important feature of the test device used for the non-Newtonian seal experiments is the hydrostatic bearing arrangement designed to provide a high stiffness characteristic and a low parasitic torque. Previous designs considered a set of preloaded angular contact ball bearings with an oil mist lubrication system. However, calculations for a twenty millimeter duplex angular contact ball bearing with sufficient preload to assure a $1 \cdot 10^6$ lb/in stiffness, revealed a bearing internal torque at least one order of magnitude greater than the anticipated interface fluid torque. An added limitation on such a bearing would be the torque "ripple" due to variations in bearing surface finish as well as surface waviness. To circumvent the limitations of the rolling element bearing arrangement a hydrostatic fluid film bearing was designed. Pressurized gas was used as the bearing working fluid in order to preclude the possibility of contamination of the seal test fluid. The risk of pneumatic instability as well as lack up can be very troublesome in such bearings and, therefore, some caution is required to assure satisfactory operation. The arrangement selected for detail design featured a double acting thrust bearing combined with a journal bearing having a double row of admission holes. The design of the hydrostatic torque device is very conventional and is based on the criteria contained in Reference 3 and 4.

Figure 1 presents the overall seal assembly test device and shows the bearing arrangement in cross-section. The upper thrust bearing is supplied by 36 holes of 0.016" diameter equally spaced and supplied from a common manifold. The lower bearing is likewise supplied by 36 holes of 0.016 diameter equally spaced. Alternate gas supply ports for the lower thrust bearing are connected to the journal bearing which is fed by two rows of 18 holes each. The journal bearing holes are also 0.016" diameter. By this arrangement it is possible to supply the journal bearing and the lower thrust bearing from one common manifold. The two manifolds were supplied from separate pressure sources.

Torque measurements were made by conventional strain gauge technique employing a bridge circuit connected to an Ellis amplifier. Linearity of the strain gauge and torque arm arrangement is checked by dead weights. During operation a fixed amplifier gain is maintained to further assure system linearity. Speed was monitored on a Hewlett Packard counter connected to a magnetic pickup which received its signal from three pins mounted on the spindle shaft.

Seal interface clearance was adjusted by two sets of opposed screws which allow accurate dependable setting in the low microinch range. Determination of actual clearance is made by three "Electro-Jet" Sheffield magnetic reluctance probes mounted in close proximity to the interface. The "Electro-Jet" is a direct contact instrument capable of providing accurate measurement in the low microinch range. Provision was made for use of "Wayne Kerr" capacitance probes, however it was not possible to use them at high speed due to the difficulty of maintaining a full fluid film under the probe tip. A partial film gives rise to variations in capacitance and consequently erratic and uncertain data. The Sheffield probes are equipped with a retracting mechanism to prevent damage to the runner surface.

As for previous tests of this type a graduated tube was used as the pressurized fluid reservoir connected to the center of the stationary head by a flexible hose. An overall view of the non-Newtonian Test Assembly is shown in Figure 2. The Sheffield meter located next to the graduated reservoir is shown connected to the distance probes. Other related instrumentation can be clearly identified. Figure 3 is a close-up view of the hydrostatic torque measuring device. Flexible connections to the manifolds can be seen as well as the connecting plastic hose from the reservoir to the seal center position. The torque lever and strain gauge arrangement is clearly visible. Component parts for the hydrostatic test device including the stationary seal mating face are shown in Figure 4.

III. TORQUE DEVICE PERFORMANCE TEST

To assure adequate performance of the torque measuring device, a series of calibration tests were performed to determine the stiffness characteristics of the thrust bearings. This was accomplished by applying dead weight loads directly to the bearing and subsequently measuring the deflection in the direction of loading. Figure 5 is a plot of the load versus displacement for the upper thrust bearing at several selected pressure levels. Manifold

pressures were set rather arbitrarily but were based on equal clearance for each thrust bearing. From Figure 5 it can be seen that the required stiffness of $1 \cdot 10^6$ lb/in can be easily obtained with a pressure level of approximately 100 PSIG. For modest increases in pressure a stiffness as high as $2 \cdot 10^6$ lb/in can be obtained to match the stiffness of the support structure. Data in Figure 5 was taken on the inverted unit for convenience of loading with dead weights.

Total axial clearance in the thrust bearing is 0.00074 inches and is sufficient to provide the necessary face clearance during all conditions of test loading. For example, at a seal interface pressure of 40 PSIG a total axial load of approximately 95 pounds can be developed. With a supply manifold pressure of 100 PSIG the displacement will be limited to approximately 100 microinches. At the higher supply pressure of 140 PSIG the displacement is limited to less than 50 microinches. The actual axial movement is not critical providing sufficient clearance is maintained under load in the assembly. Clearance settings were made with pressure at the seal interface so that total axial movement of the hydrostatic torque device was properly taken into account. As part of the torque device performance testing the system breakaway torque was determined with an ARPO hand type torque meter. A breakaway torque of 0.22 oz inches was found and it was judged that steady state drag torque did not exceed approximately 0.04 oz inches.

IV. DESCRIPTION OF TEST PROCEDURE

As an initial step, a preliminary interface clearance was set without fluid in the reservoir. The final setting was accomplished with the reservoir at the proper pressure for test and with zero speed. It was necessary to establish the correct fluid level after the final clearance setting. The Electro-Jet gauges were retracted for all speed tests.

With the test fluid under pressure the desired speed was established and data was recorded. Torque, speed, temperature and flow data were taken. The flow was determined by timing the fluid level change for a fixed fluid volume change. Immediately after each test the speed was reduced to zero and with the reservoir under pressure the clearance was determined with the Electro-Jet gauges. The running clearance then became the average of the readings before and after test. This correction accounted for any heating which developed during test within the drive spindle and was of only second order of significance. Minimum thermal expansion was present in the seal mating parts since they were made

from invar. No change in interface clearance was present due to speed alone. This had been determined independently with the capacitance probes operating without interface fluid.

V. LOW SHEAR RATE VISCOSITY TEST

Viscosity data, employing a conventional Cannon and Fenske glass capillary viscometer, was obtained for samples of JP5 containing 3.2% Vistanex polymer additive. The results indicate a viscosity of 4471 centistokes (20,650 Saybolt Secon Seconds) at 77°F. This value of viscosity is approximately 2200 times greater than the viscosity of the base JP5 fluid. In effect this data provides the zero shear rate viscosity value and agrees quite well with data for the same fluid taken on the Weissenberg Rheogoniometer.

Additional viscosity data was obtained from the rheogoniometer located at the General Electric Research and Development Center. The data for JP5 with 3.2% Vistanex of molecular weight 2×10^5 and 10^5 are shown in Figure 6. The data covers only the low shear rate range. Also shown is the normal stress for the Vistanex 200 mixture. This data was obtained in an effort to provide additional information useful in establishing the correlative model of Task 2.

VI. DISCUSSION OF TEST DATA

Tests were conducted at nominal clearances of 0.001, 0.002, 0.003 and 0.004 inches with JP5 plus 3.2% polyisobutylene. The major portion of the testing was conducted with a 1/2 inch wide interface land as used in prior testing. Tests with a 1/4 inch wide land were also completed. Data for the JP5 plus 3.2% polyisobutylene is contained in Tables 1, 2, 3 and 4 for each of the nominal clearances and at several pressures. The data is plotted in Figures 7, 8, 9 and 10 and shows the same trend as previously seen with other viscoelastic fluids. This is characterized by a change in rate of torque increase as speed is increased. In each case the change occurs between 1000 and 1500 RPM. This slope variation is due to the influence of shear rate on viscosity. The specific relationship will be analyzed in greater depth as part of Task 2. The data covers testing to 12000 RPM. In the lower speed range, below 100 RPM, the torque readings contain some scatter due to the low level of interface torque. This difficulty was recognized at an early date and provision was made to obtain low shear rate data from a separate source. The low shear data was obtained on a rheogoniometer available at the General

Electric Research and Development Center. The data at the lower shear is shown in Figure 6. This low shear rate data will be used as an additional input to the correlation study of Task 2. It should be noted that the rheogoniometer is limited to shear rates of 10^3 reciprocal seconds.

As a further comparison Table 5 presents data for plain JP5 at a reservoir pressure of 5 PSIG. Due to the extremely low viscosity it was possible to test at a clearance of 0.001 inches only. In Figure 11 the torque verses speed from Table 5 is plotted. The straight line relationship characteristic of such a fluid is evident.

The data from the tests with the narrow land is shown in Table 6 and Table 7 for the 0.002 inch clearance and the 0.003 inch clearance respectively. The distinct change in slope is seen for each clearance in Figures 12 and 13 for the same clearances.

As an additional source of information for correlations of the viscosity data, several tests were performed with silicone fluids. Silicone SF96 of two different viscosity values (50 and 100) were tested up to 1000 RPM. Fairly good correlation was achieved between measured torque values and torque values computed from flow rates. Test data for the silicone fluids evaluated is shown in Table 8.

VII. LIST OF FIGURES

XIII. LIST OF TABLES

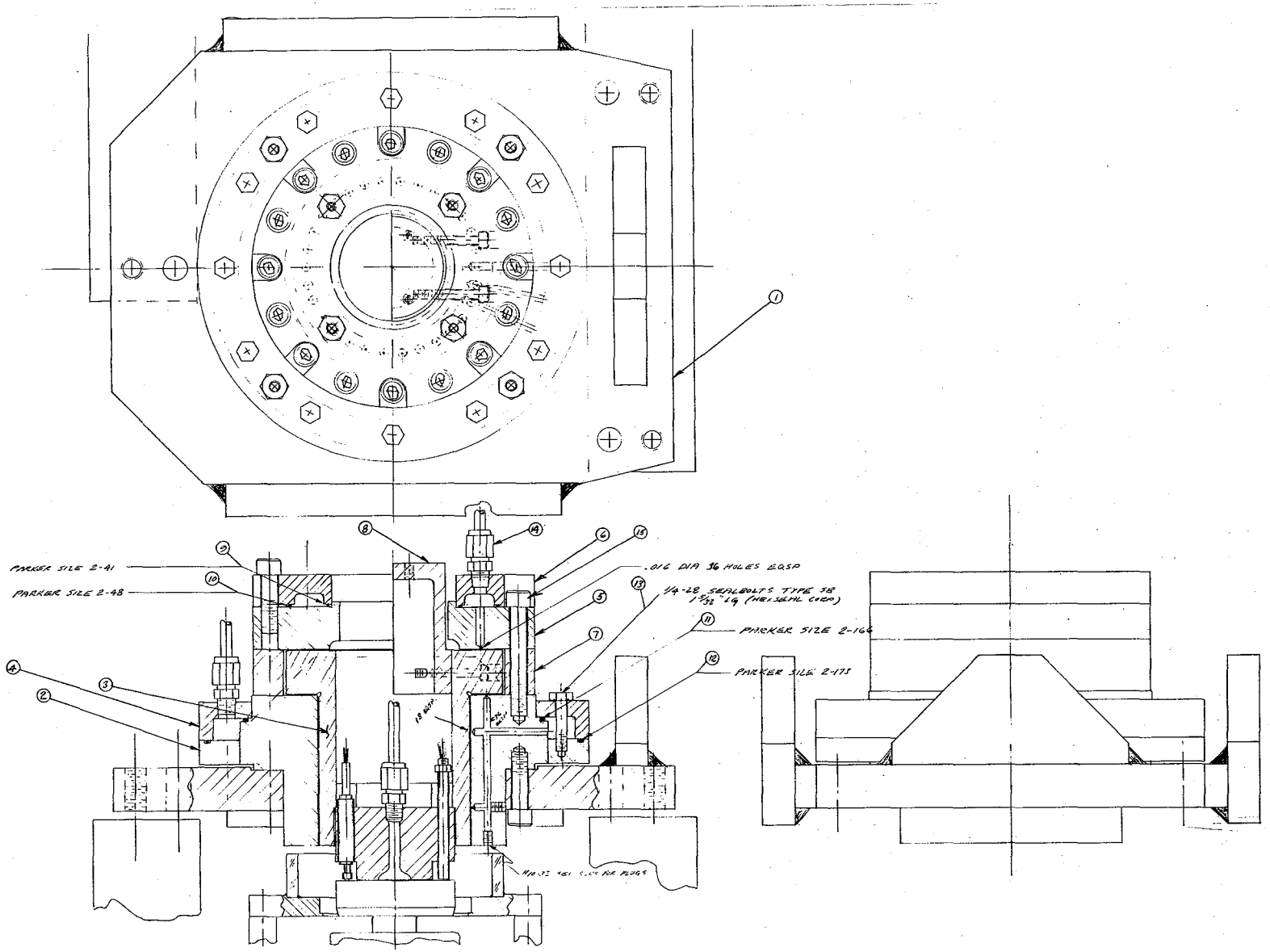

Figure 1. Non-Newtonian Seal Test Device (see parts list, Table 9)

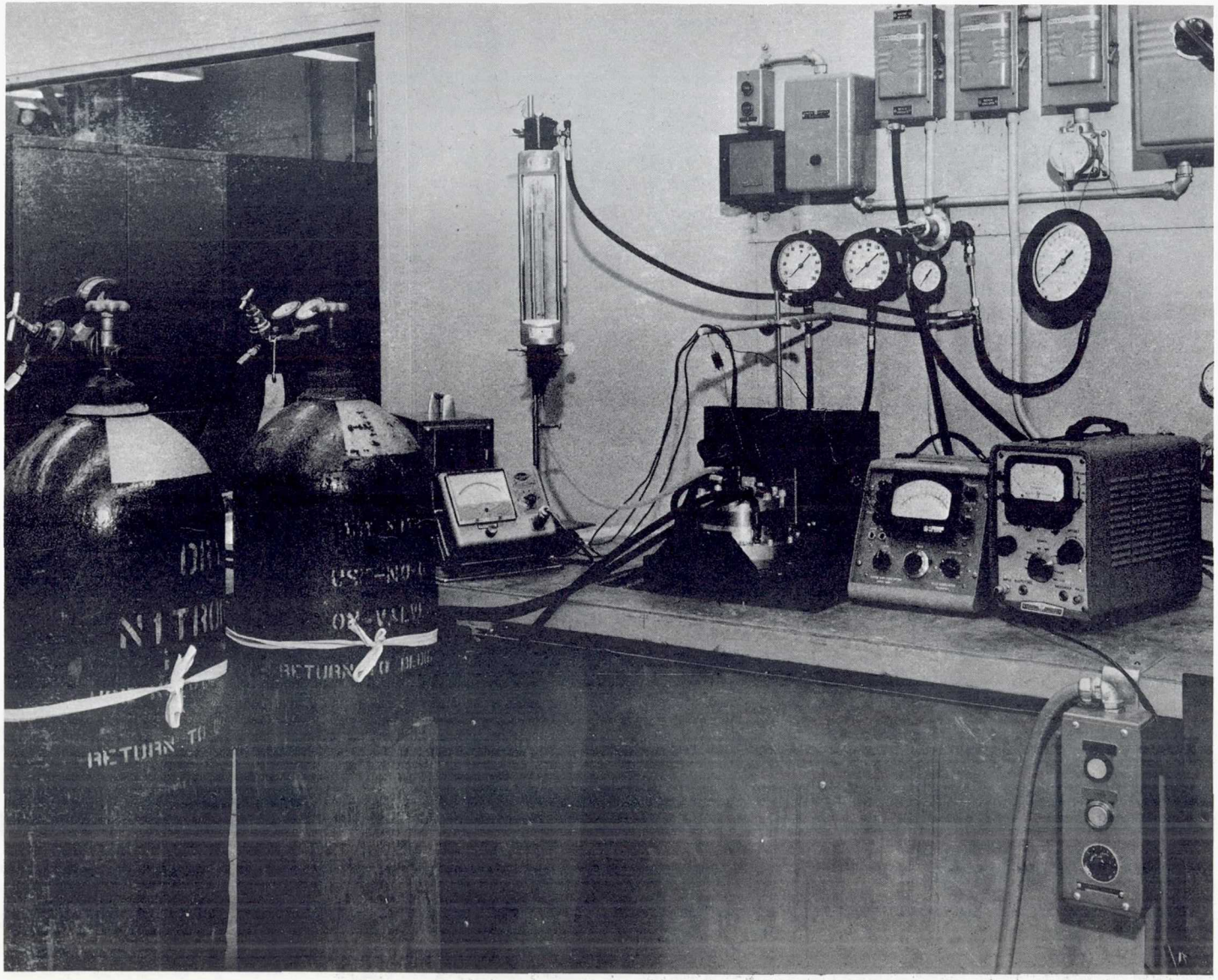

Figure 2. Non-Newtonian Test Assembly

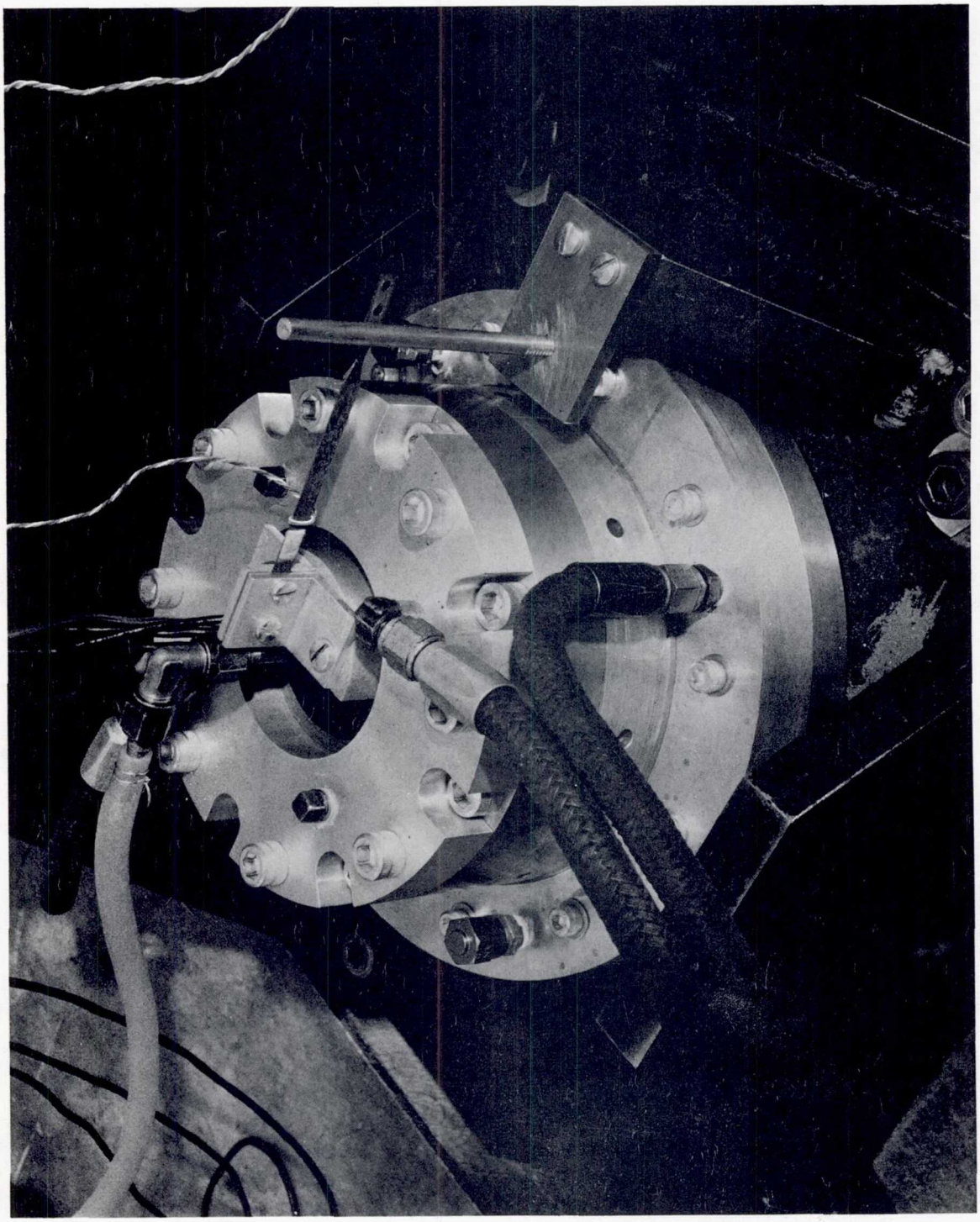

Figure 3. Hydrostatic Torque Device

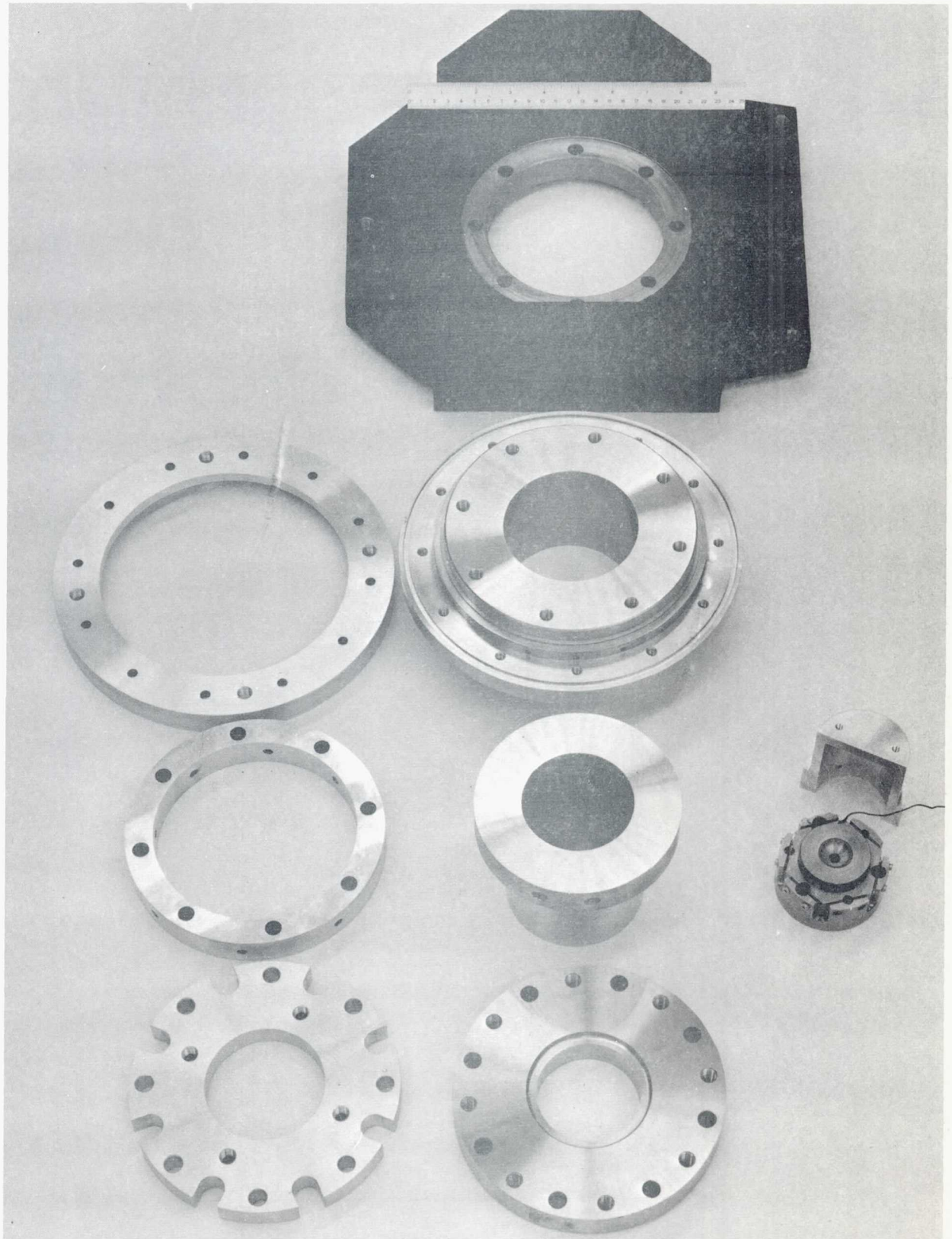

Figure 4. Hydrostatic Torque Device (component parts)

THRUST BEARING STIFFNESS

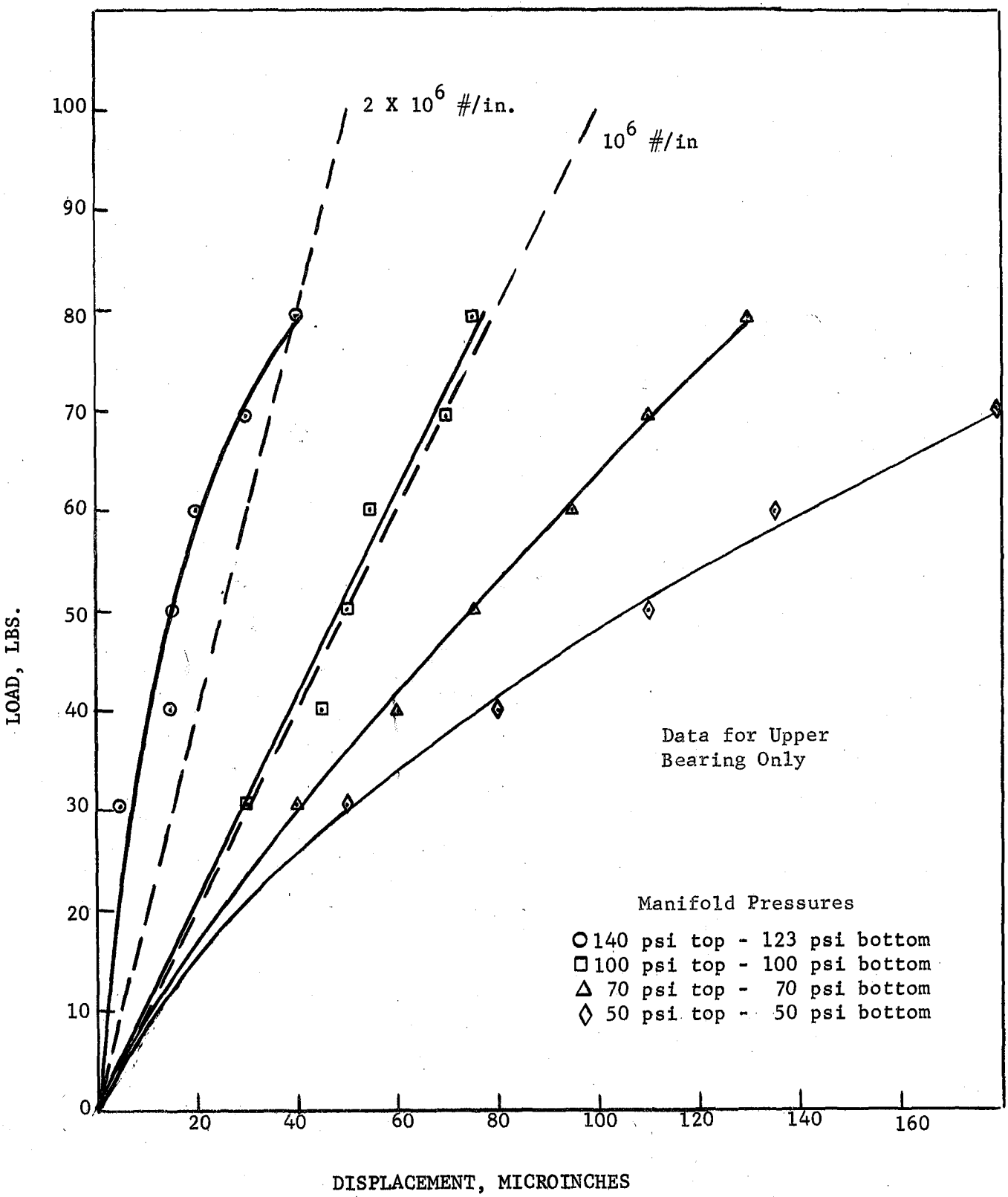

FIGURE 5

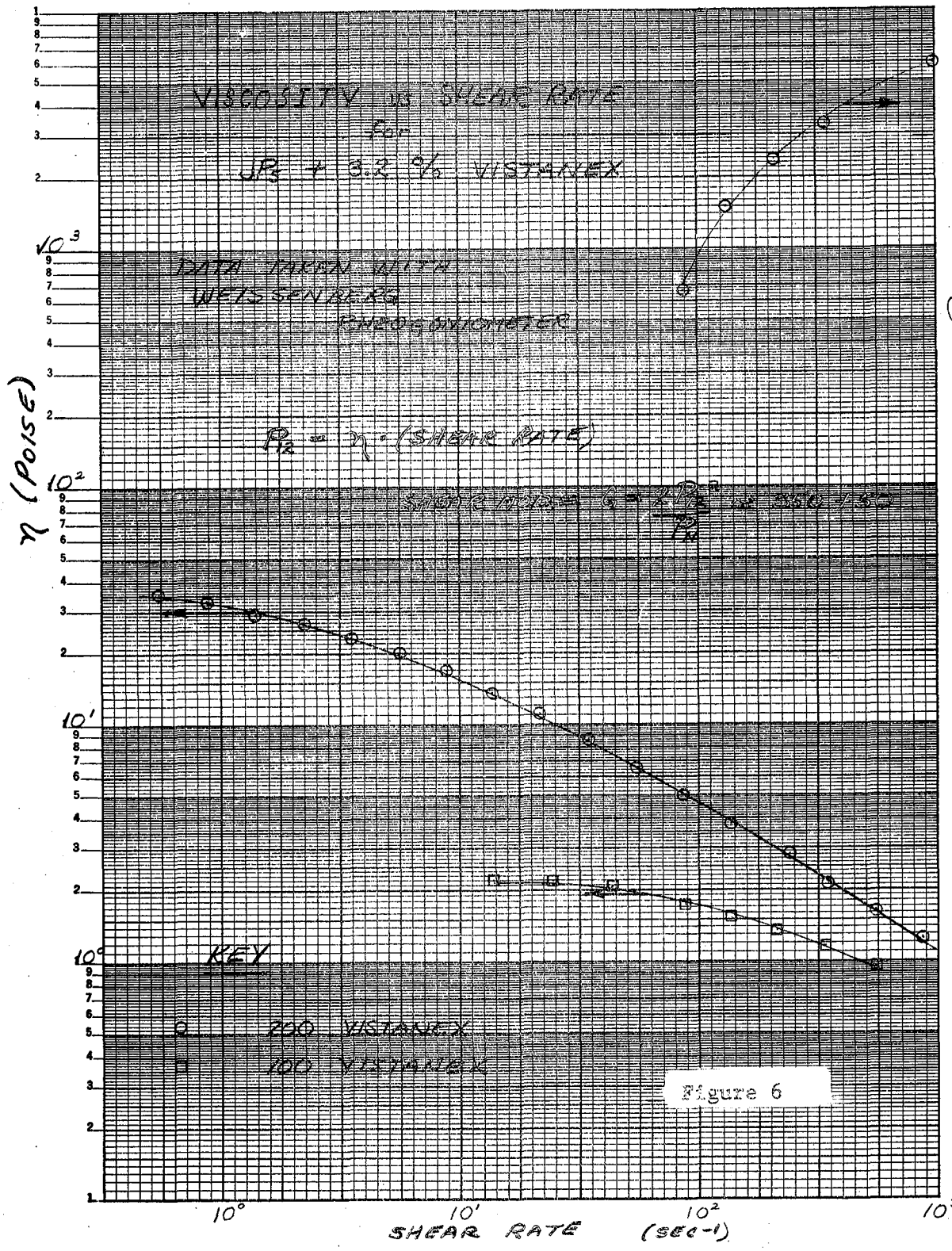
VISCOSITY vs SHEAR RATE
FOR
JP5 + 3.2 % VISTANEX
DATA TAKEN WITH
WEISSENBERG
RHEOGONIOMETER
$P_{12} = \eta \cdot$ (SHEAR RATE)
SHEAR STRESS = $G = \frac{F}{A} = P_{12}$ = 350 DYNES/CM²
KEY
200 VISTANEX
100 VISTANEX
η (POISE)
SHEAR RATE (SEC⁻¹)
P_{12} DYNES/CM²

Figure 6

INTERFACE TORQUE VS. SHAFT SPEED

JP5 + 3.2% POLYISOBUTYLENE

NOMINAL CLEARANCE .001 in

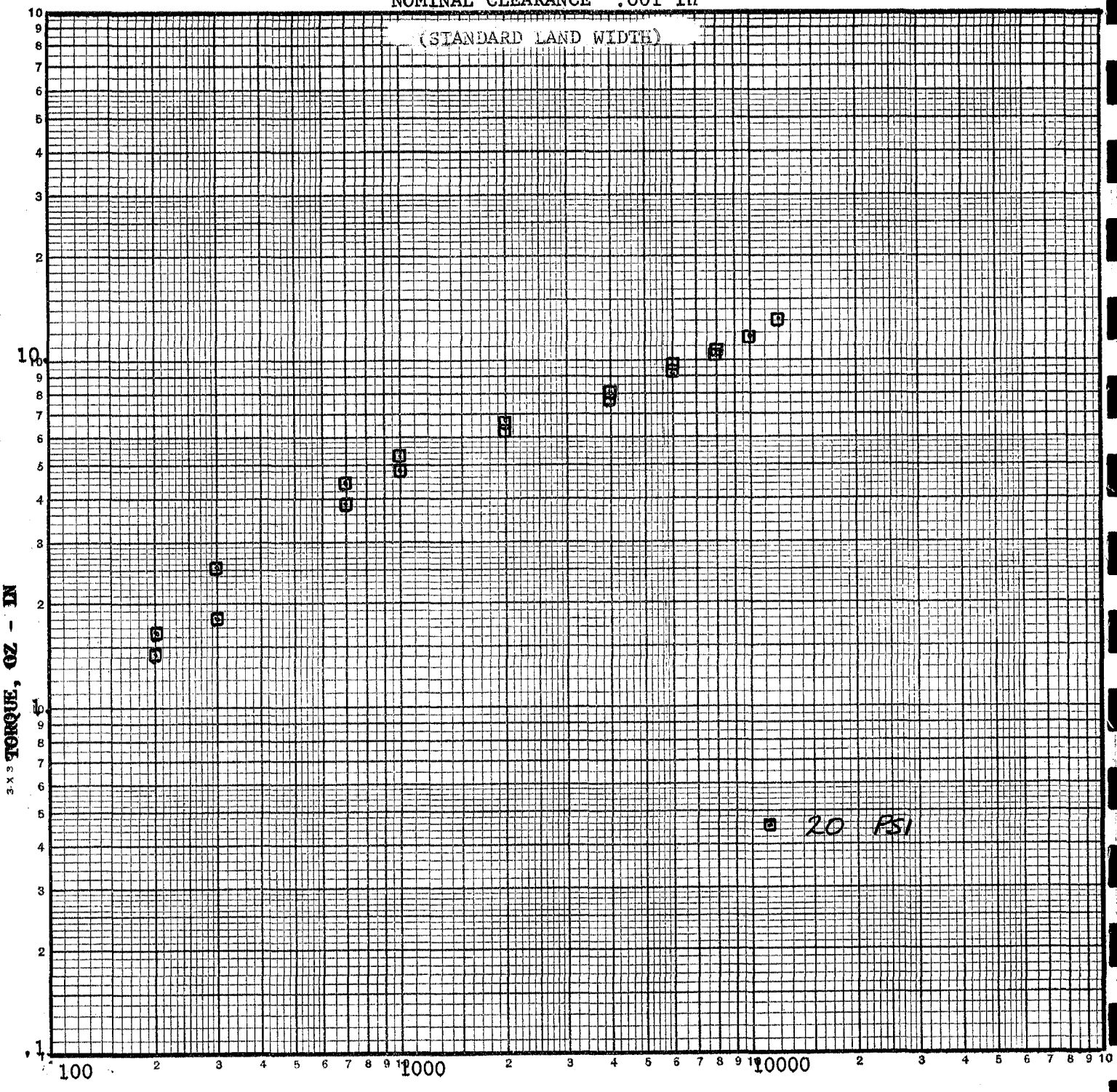

FIGURE 7

GL360 (Feb. 1962)

INTERFACE TORQUE VS SHAFT SPEED

JP5 + 3.2% POLYISOBUTYLENE

NOMINAL CLEARANCE .002 IN
(STANDARD LAND WIDTH)

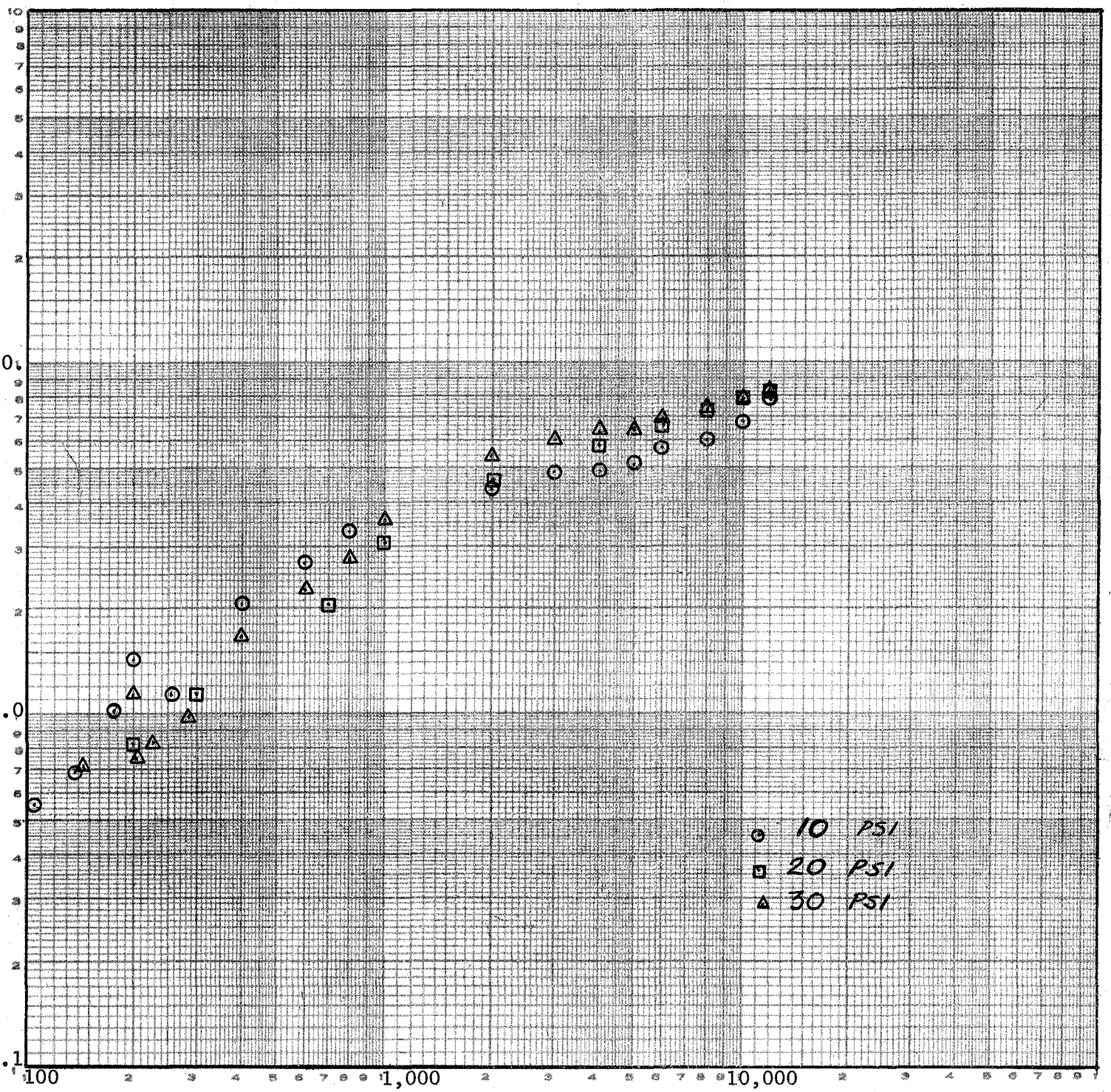

FIGURE 8

INTERFACE TORQUE VS SHAFT SPEED

JP5 + 3.2% POLYISOBUTYLENE

NOMINAL CLEARANCE .003 IN

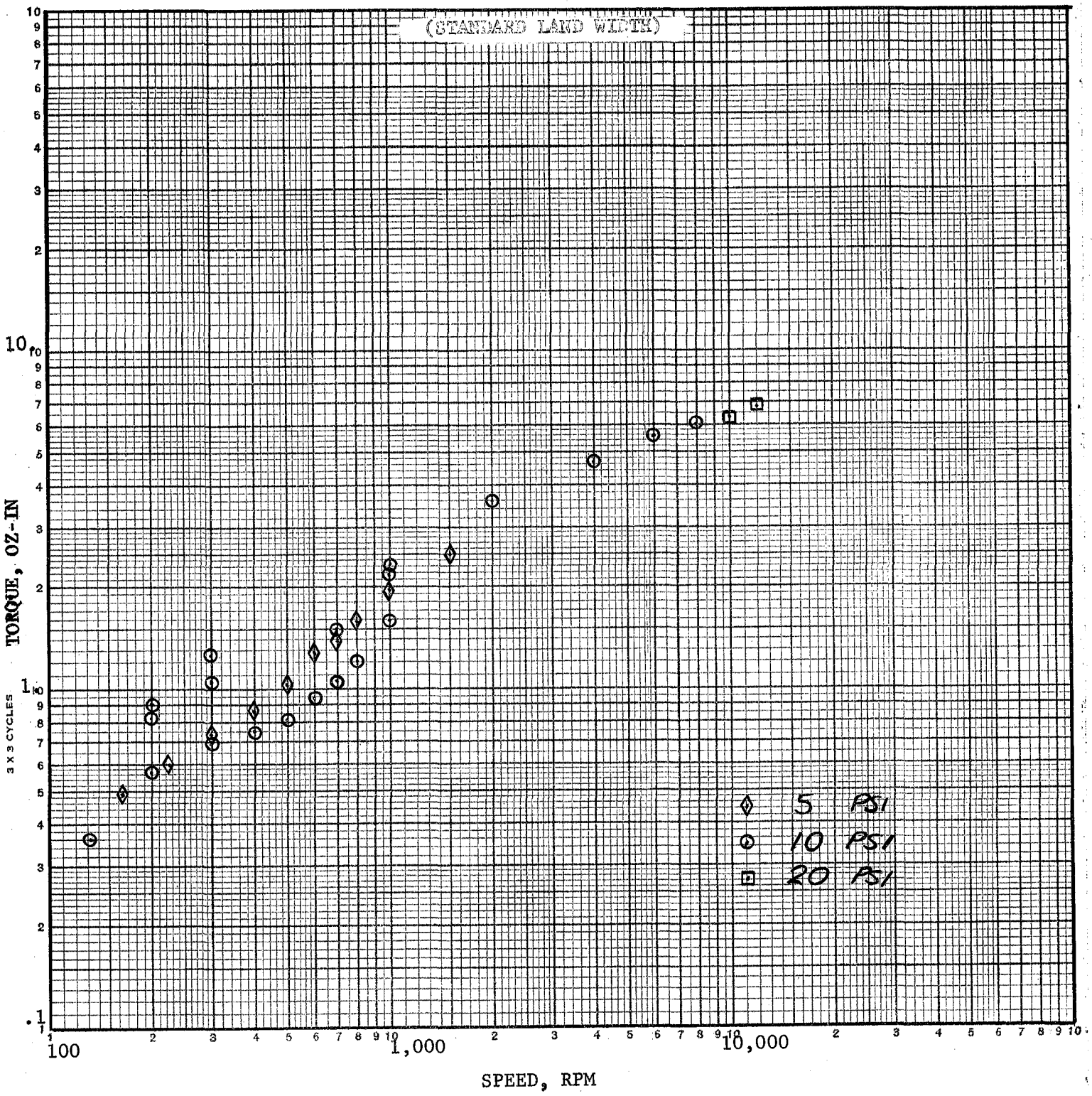

FIGURE 9

GL360 (Feb. 1962)

INTERFACE TORQUE VS SHAFT SPEED

JP5 + 3.2% POLYISOBUTYLENE

NOMINAL CLEARANCE .004 IN

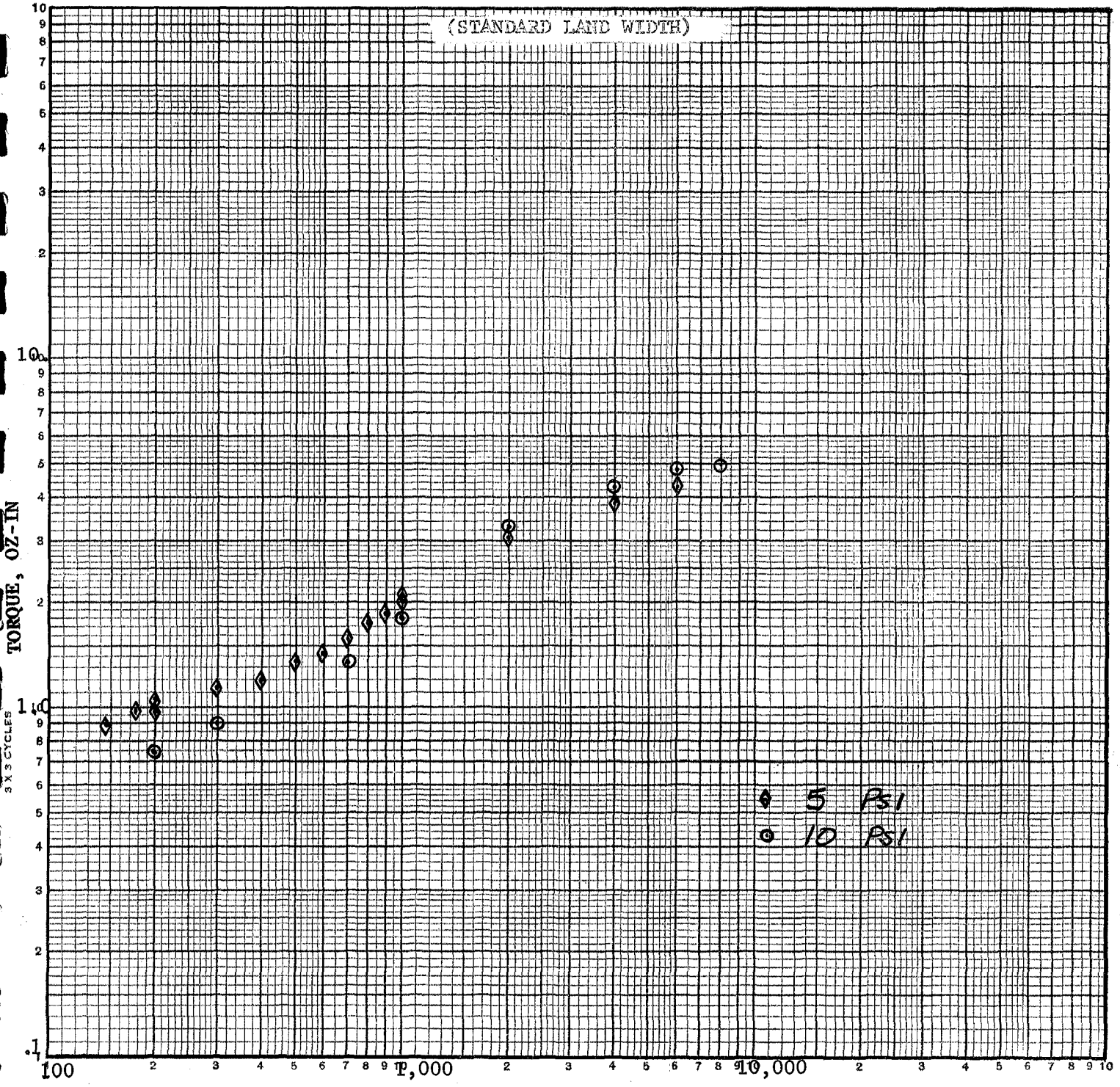

FIGURE 10

GL360 (Feb. 1962)

INTERFACE TORQUE VS SHAFT SPEED

JP-5

NOMINAL CLEARANCE .001 IN

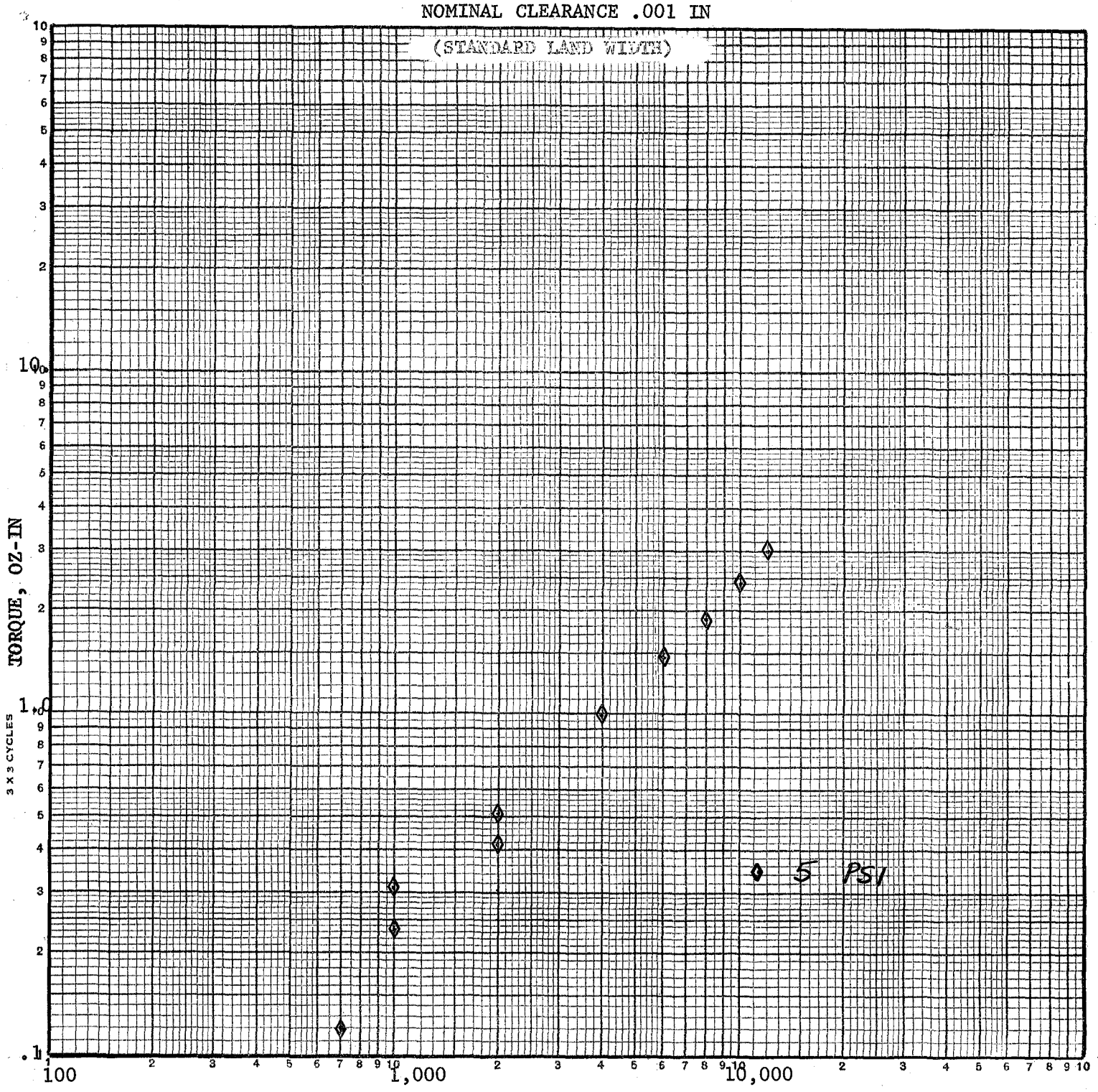

FIGURE 11

GL360 (Feb. 1962)

INTERFACE TORQUE VS SHAFT SPEED

JP5 + 3.2% POLYISOBUTYLENE

NOMINAL CLEARANCE .002 IN

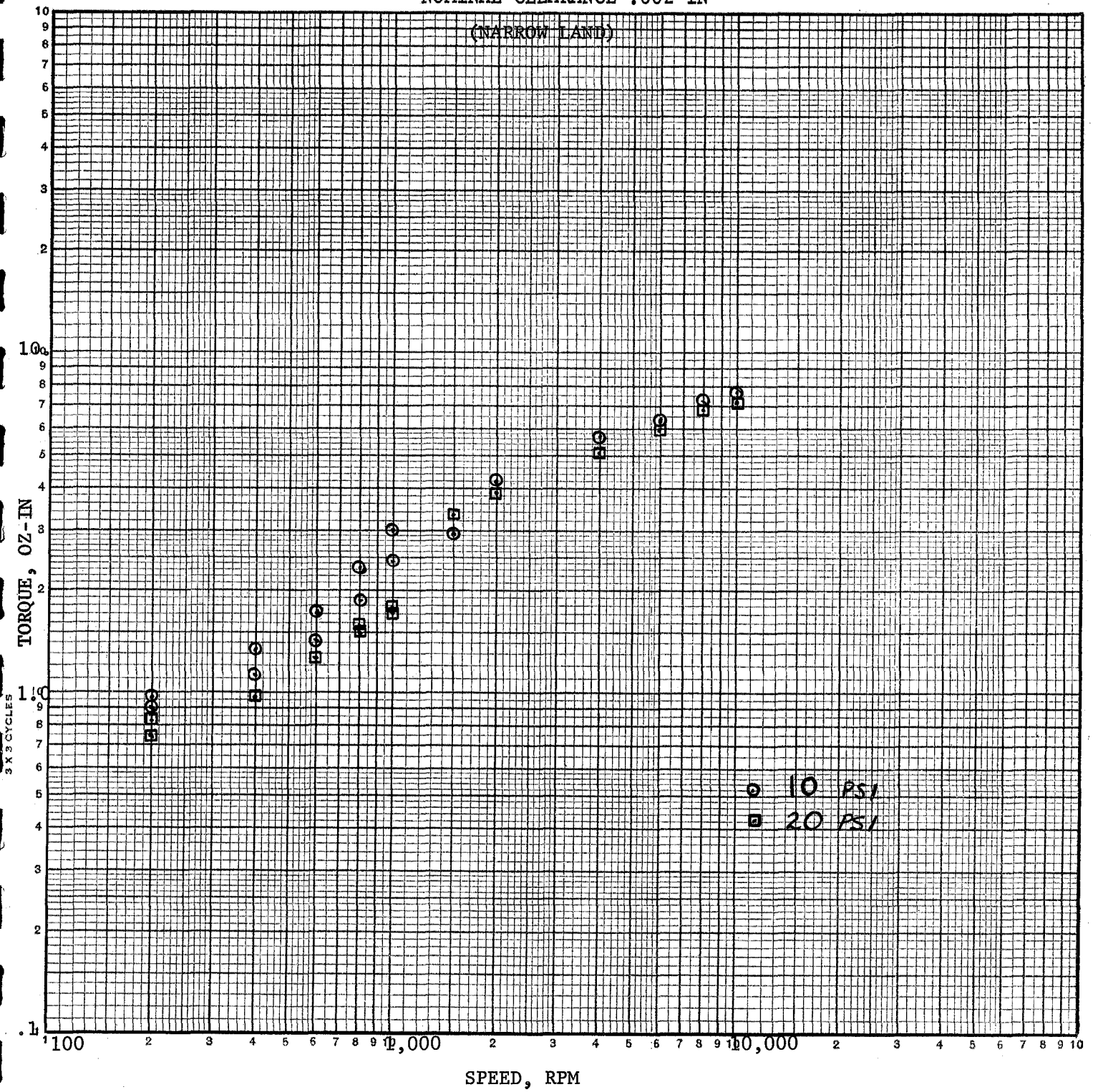

FIGURE 12

INTERFACE TORQUE VS SHAFT SPEED

JP5 + 3.2% POLYISOBUTYLENE

NOMINAL CLEARANCE .003 IN

(NARROW LAND)

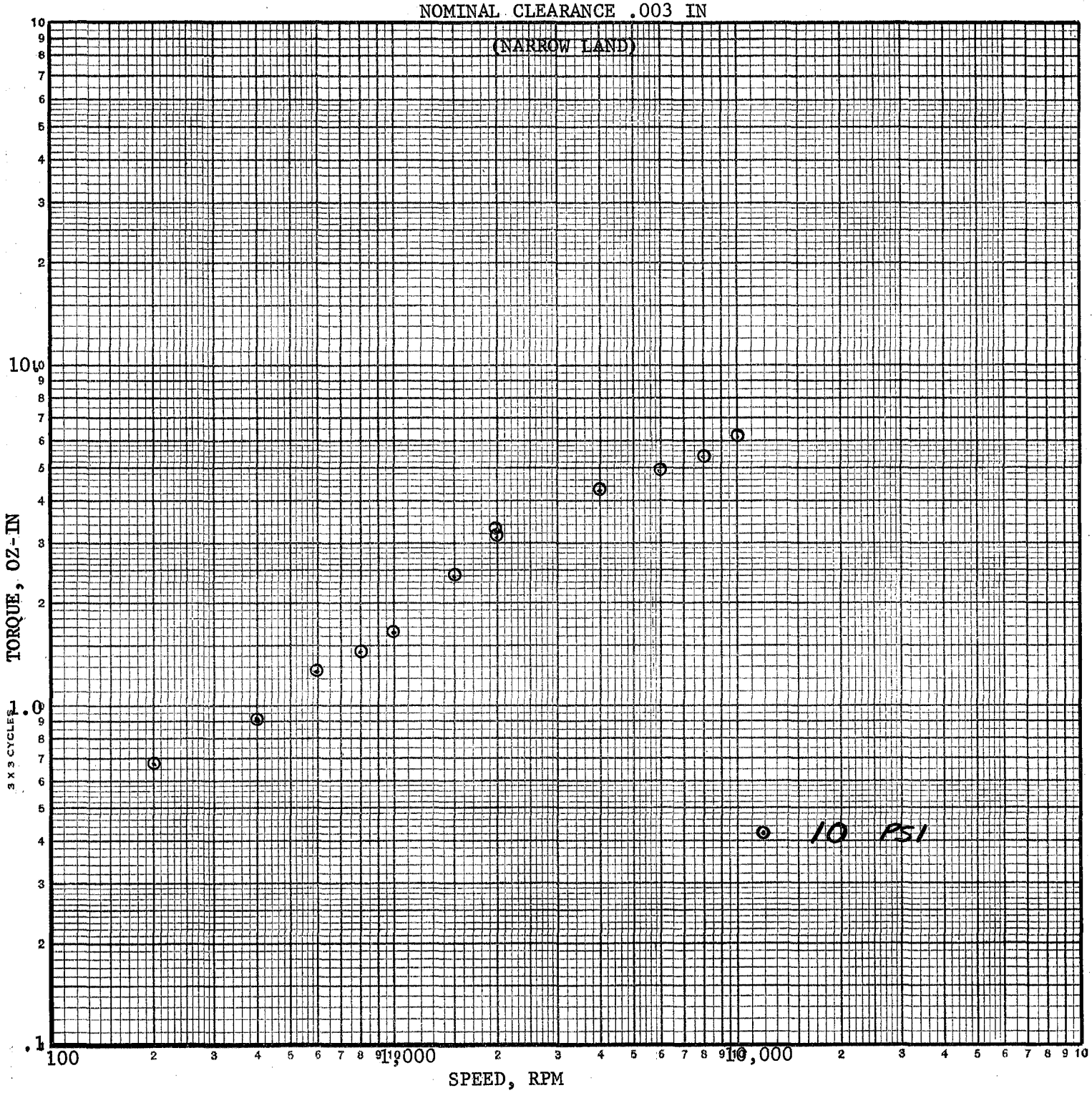

FIGURE 13

GL360 (Feb. 1962)

TABLE 1

JP5 + 3.2% VISTANEX 200

NOMINAL CLEARANCE 0.001 IN.
(STANDARD LAND WIDTH)

RESERVOIR PRESSURE 20 PSI
AMB. TEMPERATURE 77°F

RPM	Q in^3/sec	h in.	Torque oz-in
INITIAL TEST			
0	.00218	.00114	--
200	.0048	.00114	1.65
300	.00451	.00114	2.55
700	.00188	.00113	4.5
1000	.00204	.00113	4.8
2000	.0019	.00108	6.45
4000	.0025	.00103	8.1
6000	.00277	.00097	9.6
8000	.00371	.00086	10.8
10000	.00389	.00077	11.85
12000	.00399	.00070	13.05
REPEAT TEST			
0	.0015	.00111	--
200	.00383	.00113	1.42
300	.0040	.00112	1.8
700	.00191	.00111	3.83
1000	.00164	.00110	5.34
2000	.00156	.00109	6.83
4000	.00183	.00105	7.8
6000	.00222	.00100	9.16
8000	.00297	.00095	10.65
10000	.00356	.00087	11.86
12000	.00361	.00078	13.07

TABLE 2

JP5 + 3.2% VISTANEX 200

NOMINAL CLEARANCE 0.002 IN
(STANDARD LAND WIDTH)

Reservoir Pressure - 10 PSI
Amb. Temperature 78°F

RPM	Q in^3/sec	h in.	Torque Oz-in
0	.00407	.00216	-
8	.00428	.00206	.225
25	.00500	.00206	.27
36	.00473	.00206	.27
60	.00623	.00206	.375
105	.00718	.00206	.555
137	.0078	.00206	.69
179	.00877	.00206	1.01
200	.00948	.00208	1.42
262	.00865	.00206	1.12
400	.0104	.00208	2.03
600	.0838	.00211	2.7
800	.00509	.00214	3.3
1000	.00314	.00226	3.15
2000	.00169	.00212	4.35
3000	.00305	.00198	4.80
4000	.00337	.00197	4.80
5000	.00198	.00200	5.10
6000	.00300	.00194	5.65
8000	.00359	.00183	6.00
10000	.00363	.00175	6.75
12000	.00451	.00161	7.65

Reservoir Pressure - 20 PSI
Amb. Temperature 77°F

RPM	Q in^3/sec	h in.	Torque Oz-in
0	.0225	.00216	-
200	.0269	.00216	.825
300	.0293	.00215	1.12
700	.0271	.00214	2.03
1000	.132	.00213	3.15
2000	.00501	.00211	4.65
4000	.00446	.00207	5.85
6000	.00594	.00203	6.6
8000	.00687	.00197	7.2
10000	.00800	.00188	7.8
12000	.00983	.00179	8.25

Reservoir Pressure - 30 PSI
Amb. Temperature

RPM	Q in^3/sec	h in.	Torque Oz-in
0	.0539	.00222	--
18	.0444	.00218	.30
35	.0504	.00218	.375
85	.0473	.00218	.69
143	.0533	.00218	.705
202	.0515	.00218	.75
226	.0377	.00218	.84
286	.0584	.00218	.975
200	.0558	.00223	1.12
400	.0633	.00222	1.65
600	.0702	.00222	2.25
800	.0592	.00220	2.78
1000	.0526	.00220	3.53
1000	.0406	.00218	3.45
2000	.0103	.00216	5.4
3000	.0084	.00213	6.0
4000	.00808	.00209	6.45
5000	.00838	.00206	6.6
6000	.00850	.00204	6.9
8000	.0100	.00199	7.2
10000	.0107	.00195	7.8
12000	.0128	.00189	8.25

TABLE 3

JP5 WITH 3.2% VISTANEX 200

NOMINAL CLEARANCE 0.003 IN.**

Reservoir Pressure - 5 PSI
Amb. Temperature 78°F

RPM	Q in^3/sec	h in.	Torque Oz-In
0	.00411	.00303	--
52	.00688	.00303	.405
83	.00801	.00301	.435
166	.0140	.00300	.495
228	.00936	.00298	.60
300	.00920	.00297	.735
400	.00920	.00295	.855
500	.00935	.00294	1.02
600	.00773	.00294	1.29
700	.00676	.00294	1.38
800	.00495	.00293	1.59
1000	.00197	.00293	1.98
1500	.00125	.00293	2.50

Reservoir Pressure - 10 PSI
Amb. Temperature 78°F

RPM	Q in^3/sec	h in.	Torque Oz-In
0	.0163	.00308	--
200	.0272	.00308	.825
300	.0301	.00307	1.05
700	.0332	.00307	1.5
1000	.0217	.00307	2.17
2000	.00371	.00305	3.6
4000	.00252	.00303	4.65
6000	.00421	.00301	5.55
8000	.00395	.00294	6.0
*10000	.0151	.00276	6.3
*12000	.0177	.00271	6.75
0	.0164	.00312	--
200	.0275	.00312	.9
300	.0316	.00312	1.26
1000	.025	.00312	2.32

Reservoir Pressure - 10 PSI
Amb. Temperature 78°F

RPM	Q in^3/sec	h in.	Torque Oz-In
0	.0160	.00307	--
35	.016	.00306	.15
73	.0213	.00306	.27
131	.0232	.00306	.36
200	.0259	.00305	.57
300	.0269	.00303	.69
400	.0303	.00303	.75
500	.0320	.00303	.81
600	.0324	.00303	.93
700	.0287	.00303	1.05
800	.0271	.00302	1.2
1000	.0186	.00302	1.59

* Fluid Pressure - 20 PSI
** Standard Land Width

TABLE 4

JP5 WITH 3.2% VISTANEX 200

NOMINAL CLEARANCE 0.004 IN.*

Reservoir Pressure - 5 PSI
Amb. Temperature 79°F

RPM	Q in^3/sec	h in.	Torque Oz-In
0	.00944		--
37	.0118	.00400	.6
63	.0140		.75
91	.0148		.825
144	.0190		.9
179	.0190		.975
200	.0192		1.05
300	.0200		1.12
400	.0219		1.2
500	.0235		1.35
600	.0225		1.42
700	.0242		1.57
800	.0201		1.72
900	.0172		1.87
1000	.0154		2.02
0	.0102	.00398	--
200	.0203	.00400	.976
300	.0214	.00399	1.12
700	.0210	.00399	1.57
1000	.0148	.00397	2.1
2000	.00225	.00397	3.08
4000	.00218	.00395@	3.82
6000	.00383	.00390	4.27
8000	.00562	.00385	3.45

Reservoir Pressure - 10 PSI
Amb. Temperature 80°F

RPM	Q in^3/sec	h in.	Torque Oz-In
0	.0409	.00399	--
200	.0536	.00399	.75
300	.0583	.00399	.90
700	.0648	.00398	1.35
1000	.0565	.00397	1.8
2000	.0078	.00397	3.3
4000	.00451	.00396	4.28
6000	.0060	.00395	4.8
8000	.00823	.00398	4.95

*Standard Land Width

TABLE 5

JP5

NOMINAL CLEARANCE 0.001 IN
(STANDARD LAND WIDTH)

RESERVOIR PRESSURE - 5 PSI
AMB. TEMPERATURE 80°F

RPM	Q_3 in^3/sec	h in.	Torque Oz-In
0	.0289	.00113	--
200	.0294	.00107	.045
300	.0278	.00107	.0525
700	.0279	.00105	.12
1000	.0266	.00104	.233
2000	.0277	.00104	.51
0	.0259	.00109	--
1000	.0271	.00106	.308
2000	.0232	.00105	.413
4000	.0258	.00102	.99
6000	.0294	.00095	1.47
8000	.0367	.00089	1.89
10000	.0402	.00081	2.4
12000	.0281	.00070	3.00

TABLE 6

JP5 WITH 3.2% VISTANEX 200

NOMINAL CLEARANCE 0.002 IN*

Reservoir Pressure - 20 PSI
Amb. Temperature 75°F

RPM	Q in^3/sec	h in.	Torque Oz-In
0	.0877	.00216	--
200	.0998	.00216	.75
400	.0998	.00216	.975
600	.118	.00216	1.27
800	.0948	.00216	1.5
1000	.0998	.00216	1.72
2000	.0149	.00215	3.98
4000	.0155	.00214	5.18
6000	.0180	.00210	6.00
8000	.0225	.00207	6.9
10000	.0300	.00201	7.2
200	.0748	.00216	..826
400	.0860	.00216	..976
600	.0972	.00216	1.28
800	.0842	.00216	1.57
1000	.0842	.00216	1.80
1500	.0220	.00216	3.38

Reservoir Pressure - 10 PSI
Amb. Temperature 70°F

RPM	Q in^3/sec	h in.	Torque Oz- In
0	.0152	.00199	--
200	.0177	.00199	.975
400	.0214	.00199	1.35
600	.0204	.00199	1.72
800	.0103	.00199	2.32
1000	.00518	.00199	3.00
2000	.00366	.00197	4.2
4000	.00421	.00195	5.77
6000	.00633	.00190	6.3
8000	.00712	.00183	7.05
10000	.0109	.00175	7.65
0	.0136	.00206	--
200	.0211	.00206	..90
400	.0252	.00206	1.12
600	.0223	.00206	1.42
800	.00945	.00206	1.88
1000	.00043	.00206	2.48
1500	.00484	.00206	2.93

*Standard Land Width

TABLE 7

JP5 WITH 3.2% VISTANEX 200

NOMINAL CLEARANCE 0.003 IN
(STANDARD LAND WIDTH)

RESERVOIR PRESSURE - 10 PSI
AMB. TEMPERATURE 75°F

RPM	Q in^3/sec	h in.	Torque Oz-In
0	.0563	.00306	--
200	.0728	.00306	.675
400	.0789	.00306	.90
600	.0823	.00306	1.27
800	.0823	.00306	1.43
1000	.0823	.00306	1.65
2000	.0104	.00303	3.3
4000	.00992	.00303	4.28
6000	.0118	.00298	4.87
8000	--	.00292	5.4
10000	.0203	.00290	6.15
1000	.0842	.00296	1.65
1500	.0315	.00294	2.4
2000	.0115	.00292	3.15

TABLE 8

NOMINAL CLEARANCE 0.002 IN.
(STANDARD LAND WIDTH)

Silicone SF 96 (50)

Reservoir Pressure = 10 psi

rpm	Q in^3/sec	h in	torque oz-in
0	0.0114	0.00209	--
109	0.0119	0.00205	0.36
300	0.0104	0.00205	0.99
700	0.00924	0.00198	1.83
1000	0.0146	0.00195	2.76

Silicone SF 96 (100)

Reservoir Pressure = 40 psi

rpm	Q in^3/sec	h in	torque oz-in
0	0.0297	0.00222	--
200	0.0271	0.00219	1.12
300	0.0260	0.00218	1.87
700	0.0277	0.00218	4.72
1000	0.0257	0.00207	6.82

TABLE 9

PARTS LIST
(Drwg. No. 422D466)
NON NEWTONIAN SEAL TEST DEVICE

Part No.	Description
1	Mounting Plate
2	Journal Bearing
3	Journal
4	Manifold Ring
5	Thrust Bearing
6	Thrust Bearing Manifold
7	Spaur Ring
8	Torque Arm Support
9	Seal
10	Seal
11	Seal
12	Seal
13	Sealbolt
14	Connector
15	Screw

REFERENCES

1. Study of Dynamic and Static Seals for Liquid Rocket Engines - dated November 5, 1965, Contract NAS7-102

2. Study of Dynamic and Static Seals for Liquid Rocket Engines - dates January 17, 1965, Contract NAS7-434, Phase II.

3. Grassam, N. S. and Powell, J. W., Gas Lubricated Bearings, Butterworths, London

4. Lund, J. W., Gas Bearings Design Charts, Volume 2, AD-615920, Unclassified available through clearinghouse for Federal Scientific and Technical Information, Department of Commerce, Washington, D. C.

APPENDIX B

NON-NEWTONIAN CORRELATIVE MODEL

BY

H. J. SNECK

I. INTRODUCTION

Viscometric tests of Newtonian fluids containing viscoelastic additives has shown that it is possible to generate a radial pressure gradient between two rotating disks such that the pressure at the center of the disks is larger than at the perimeter. If such a pressure gradient can also be created in a face seal, this pressure gradient could have a beneficial effect on the outward leakage rate.

Early experiments (Ref. 1) indicated that such a beneficial effect can be obtained. Further tests have been performed, this time including torque measurements, with the view to obtaining if possible a simple correlative model which describes the seal performance characteristics in terms of measurable fluid properties. The results of this attempt are reported on the following pages.

II. CALIBRATION TESTS USING A NEWTONIAN FLUID

An initial check-out of the test-rig performance was made using several known Newtonian fluids. The fluids used were JP-5 and two silicone fluids, SF96(50) and SF96(100).

Because JP-5 has such a low viscosity it was not feasible to make tests with an applied pressure differential above 5 psi. The viscosity calculated from torque measurements was found to be constant at $1.5(10^{-7})$ reyns over the shear-rate range 10^4 to 10^6 sec^{-1}. This viscosity was then used to compute the leakage rate from the equation

$$Q = \frac{\pi C^3}{6\mu \ln \frac{R_2}{n_1}} \left\{ P_1 - P_2 + \frac{3}{20} \rho (R_2 \omega)^2 \left[1 - \left(\frac{R_1}{R_2} \right)^2 \right] \right\}$$

The agreement between measured and predicted leakage-rate was within 10%, which is an acceptable correlation considering the effects which small clearance measurement errors can introduce. (The nominal clearance at 5 psi was 0.001 inches.)

The two silicone fluids were also tested at pressures of 10, 30, and 40 psi using a nominal gap of 0.002 inches. Torque measurements yielded viscosities of 29 centipoise for SF96(50) and 69 centipoise for SF96(100). As with the JP-5 the calculated leakage was somewhat larger than the measured values, the maximum error in this case being of the order of 15% for shear rates ranging from 5×10^3 to 5×10^4 sec^{-1}.

The measured viscosities are 60 to 70% of the manufacturers indicated viscosity and about 80 to 90% of the values required to compute the measured leakage-rates. The Newtonian fluid check-out of the apparatus indicates that reasonably accurate viscosities can be obtained from the torque measurements, and what is more important, these viscosities are constant throughout the shear-rate range and consistant with regard to leakage-rates.

III. ANALYTICAL FORMULATION OF THE PROBLEM

The equations of motion for the fluid are

$$-\rho \frac{v^2}{r} = \frac{\partial}{\partial r} (p - P_{rr}) + \frac{P_{rr} - P_{\theta\theta}}{r} + \frac{\partial \tau_{zr}}{\partial z} \qquad (1)$$

$$0 = -\frac{\partial}{\partial z}(p-P_{zz}) \tag{2}$$

$$0 = \frac{\partial \tau_{z\theta}}{\partial z} \tag{3}$$

Where the P_{rr}, $P_{\theta\theta}$, and P_{zz} are the deviatoric components of the stress. The last equation indicates that the shear stress is constant across the clearance. For laminar flow this suggests the approximation

$$v = r\omega\left(\frac{z}{c}\right) \tag{4}$$

Integrating the first equation across the clearance yields

$$\tau_{zr} = \frac{\partial \bar{P}}{\partial r} z + \int \left(\frac{P_{\theta\theta}-P_{rr}}{r}\right) dz \tag{5}$$

$$-\frac{\rho}{r}\left(\frac{r\omega}{c}\right)^2 \int_0^z z^2 dz + f(r,\theta) \tag{6}$$

where $\bar{P} = p-P_{rr}$. Assuming that the viscosity isotropic allows the shear-stresses to be related by

$$\tau_{zr} = \tau_{z\theta}\left(\frac{du}{\partial z}\Big/\frac{\partial v}{\partial z}\right) \tag{7}$$

where $\tau_{z\theta}$ is independent of z.

Integrating the radial momentum equation once again with respect to z gives

$$\tau_{z\theta} u = \frac{r\omega}{c}\left\{ zf(r,\theta) + \frac{z^2}{2}\frac{\partial \bar{p}}{\partial r} + \int_0^z\int_0^\xi \left(\frac{P_{\theta\theta}-P_{rr}}{r}\right) d\xi dz - \frac{\rho}{r}\left(\frac{r\omega}{c}\right)^2 \frac{z^4}{12}\right\} + g(r,\theta) \tag{8}$$

If it is assumed that $P_{\theta\theta}-P_{rr}$ is independent of z, then

$$\int_0^z\int_0^\xi \left(\frac{P_{\theta\theta}-P_{rr}}{r}\right) d\xi dz = \frac{z^2}{2}\left(\frac{P_{\theta\theta}-P_{rr}}{r}\right) \tag{9}$$

Applying the boundary conditions that u = o at z = o, c allows the arbitrary functions $f(r,\theta)$ and $g(r,\theta)$ to be evaluated. As a result

$$\frac{\tau_{z\theta} u}{\left(\frac{r\omega}{c}\right)} = \left[\frac{\partial \bar{P}}{\partial r} + \frac{P_{\theta\theta}-P_{rr}}{r}\right]\left(\frac{z^2-cz}{z}\right) - \frac{\rho}{r}\left(\frac{r\omega}{c}\right)^2 \left(\frac{z^4-cz^3}{12}\right) \tag{10}$$

The volumetric leakage rate is calculated from

$$Q = \int_0^c 2\pi u r dr \tag{11}$$

When this flow-rate is evaluated it becomes

$$\frac{Q\tau_{z\theta}}{2\pi r\left(\frac{r\omega}{c}\right)} = -\left[\frac{\partial \bar{P}}{\partial r} + \frac{P_{\theta\theta}-P_{rr}}{r}\right]\frac{c^3}{12} + \frac{1}{12}\left(\frac{3}{10}\right)\frac{\rho}{r}\left(\frac{r\omega}{c}\right)^2 c^5 \tag{12}$$

Integrating this equation with respect to r using the boundary conditions

$$\bar{P} = \bar{P}_1 \text{ @ } r = R_1$$
$$\bar{P} = \bar{P}_2 \text{ @ } r = R_2 \tag{13}$$

yields

$$\frac{6Q}{c^3\pi}\int_{R_1}^{R_2}\frac{\tau_{z\theta}}{r\left(\frac{r\omega}{c}\right)}dr = \bar{P}_1 - \bar{P}_2 + \frac{3}{20}\rho\omega^2\left(R_2^2 - R_1^2\right) + \int_{R_1}^{R_2}\left(\frac{P_{rr} - P_{\theta\theta}}{r}\right)dr \tag{14}$$

The left hand side of this equation may also be written in the form

$$\frac{6Q}{\pi c^3}\int_{R_1}^{R_2}\frac{\tau_{zr}}{r\left(\frac{\partial v}{\partial z}\right)}dr \tag{15}$$

IV. NO-ROTATION LEAKAGE CORRELATIONS

For the purpose of determining the basic behavior of the fluid the seal may be considered as a slightly divergent rectangular slit. When there is no rotation the slit may be considered analogous to a circular pipe in that the flow is caused only by a pressure differential. Rabinowitsch and Mooney (1, 2) have devised a general expression relating pressure drop, leakage-rate and geometry which is independent of fluid properties. A log-log plot of the parameters in this expression is shown in Figure 1 for the no-rotation test results for 3.2% Vistanex 200 in JP-5. These results are for pressure differences between 5 and 30 psi and clearances of 1, 2, 3 and 4 mils. It may be concluded that the fluid follows a power-law relation from the fact that the results generally lie along a straight line in this plot.

The quantity

$$c\left(\frac{\bar{P}_1 - \bar{P}_2}{R_2 - R_1}\right)$$

is related to the radial shear stress τ_{zr} for parallel disks by the expression

$$\frac{c\left|\bar{P}_1-\bar{P}_2\right|}{R_2-R_1} = \frac{6Q}{\pi c^2\left|R_2-R_1\right|}\int_{R_1}^{R_2}\frac{\tau_{zr}}{r\left|\frac{\partial u}{\partial r}\right|}\,dr \tag{16}$$

The data shown in Figure 1 is correlated using the expression

$$\frac{c\left|\bar{P}_1-\bar{P}_2\right|}{R_2-R_1} = 2.86\ (10^{-3})\ \left|\frac{Q}{c^2}\right|^{0.4} \tag{17}$$

If it is assumed that

$$\tau_{zr}\Big/ r\frac{\partial u}{\partial z} = \frac{K}{r^{0.4}} \tag{18}$$

the last two equations yield the power law expression

$$\tau_{zr} = 1.222\ (10^{-3})\ \left|\frac{Q}{c^2 r}\right|^{-0.6}\ \frac{\partial u}{\partial z} \tag{19}$$

where the viscosity can be taken to be

$$\mu = 1.222\ (10^{-3})\ \left|\frac{Q}{c^2 r}\right|^{-0.6} \qquad \text{(reyns)} \tag{20}$$

V. RESULTS OF TORQUE TESTS

The torque test data can be reduced assuming that

$$\tau_{z\theta} = \mu\,\dot{\gamma}_{z\theta} = \mu\,\frac{rw}{c} \tag{21}$$

in the absence of actual velocity profile data. If μ is constant, then the torque is given by

$$T = \frac{1}{2}\left|\frac{\mu\omega\pi}{c}\right|\left|R_2^4-R_1^4\right| \tag{22}$$

The viscosity calculated from the data using this equation is shown in Figure 2 as a function of

$$\frac{R_2\omega}{c} .$$

There is considerable scatter in the results up to about

$$\frac{R_2\omega}{c} \sim 5(10^5)$$

after which there is a good correlation for all applied pressure differences and clearances. In this range it is obvious that the viscosity follows a power-law relationship of the form

$$\mu = \mu_o \left(\frac{r\omega}{c}\right)^n \tag{23}$$

If the torque is now calculated on the basis of the power-law viscosity relation, the equation for the torque becomes

$$T = 2\left(\frac{\mu_o \omega \pi}{c}\right)\left(\frac{\omega}{c}\right)^n \left[\frac{R_2^{n+4} - R_1^{n+4}}{n+4}\right] \tag{24}$$

A first estimate of n can be obtained from Figure 2 and then the test data processed through the revised form of the torque equation to determine the constant μ_o. Carrying out this calculation yields the correlation

$$\mu = 2.7(10^{-3})\left(\frac{r\omega}{c}\right)^{-0.60} \quad \text{(reyns)} \tag{25}$$

for

$$\frac{r\omega}{c} > 5(10^4)$$

VI. INVARIANT POWER LAW CORRELATION

The scatter in the low shear rate viscosity is undoubtedly due to the fact that the radial and tangential shear rates are of the same order of magnitude in this range. At higher rotational speeds, the tangential shear rate

predominates so that the simple correlation given above is quite accurate. The invariant form of the power-law is

$$\tau_{ij} = \mu_o \left| \left(\frac{\partial u}{\partial z}\right)^2 + \left(\frac{\partial v}{\partial z}\right)^2 \right|^{\frac{n-1}{2}} \dot{\gamma}_{ij} \tag{26}$$

where the viscosity is given by

$$\mu = \mu_o \left| \left(\frac{\partial u}{\partial z}\right)^2 + \left(\frac{\partial v}{\partial z}\right)^2 \right|^{\frac{n-1}{2}} \tag{27}$$

From the two previous correlations it is clear that n-1 = -0.6. Since

$$\frac{dv}{dz} \cong \left|\frac{r\omega}{c}\right|$$

the quantity μ_o is equal to 2.7 (10^{-3}). The quantity Q/c^2r used in equation (20) is not equal to $\partial u/\partial z$ but only a measure of it. Bearing this in mind, the discrepancy in coefficients can be accommodated by writing the viscosity as

$$\mu = 2.7\ (10^{-3}) \left| \left(\frac{r\omega}{c}\right)^2 + \left(\frac{kQ}{c^2 r}\right)^2 \right|^{-0.30} \tag{28}$$

If k is chosen equal to 3.75, then this expression also agrees with the no-rotation correlation for ω = o.

The final expression for the viscosity is then

$$\mu = 2.7\ (10^{-3}) \left| \left(\frac{r\omega}{c}\right)^2 + \left(\frac{3.75\ Q}{c^2 r}\right)^2 \right|^{-0.30} \quad \text{(reyns)} \tag{29}$$

The total torque can now be calculated from the expression

$$T \doteq 2.7\ (10^{-3})\ 2\pi \int_{R_1}^{R_2} \frac{\left|\frac{r\omega}{c}\right| r^2 dr}{\left| \left(\frac{r\omega}{c}\right)^2 + \left(\frac{3.75Q}{rc^2}\right)^2 \right|^{0.3}} \tag{30}$$

The predictions of this equation are in fairly good agreement with the experimental results over the entire operating range of the seal.

VII. NO-LEAKAGE PRESSURE RISE

Tests were also performed with no initially applied internal pressure. It was found that the internal pressure increased with time due to inward pumping of the fluid. This pressure eventually reached an equilibrium value when the net leakage-rate vanished. This effect is obviously a manifestation of the so-called "Weissenberg effect."

Figure 3 shows the result of these tests where $\Delta\bar{P}_{tot}$ is the measured pressure corrected for centrifugal effects. The pressure difference is plotted in the figure against the parameter

$$\frac{R_2\omega}{c}\sqrt{c}$$

because the data indicates a size effect.

It should be recalled that this pressure difference is related to the normal stresses through the expression

$$\bar{P}_1-\bar{P}_2 = -\int_{R_1}^{R_2}\left(\frac{P_{rr}-P_{\theta\theta}}{r}\right)dr \tag{31}$$

When the right-hand-side of this equation is evaluated for a laminar Newtonian flow it is found to be dependent on the shear-rate, as well as the clearance. This normal stress term for Newtonian flow is extremely small and ordinarily neglected. The important fact is that even in such a simple case this term is not just a function of the shear rate.

It should also be noted that it was assumed earlier that $P_{\theta\theta}-P_{rr}$ was independent of the coordinate z, and following that assumption three integrations with respect to z where performed on $P_{\theta\theta}-P_{rr}$. The effect of performing these integrations is to introduce the clearance into the integrated result. The way in which the normal stresses depend on the local shear rate determines how the clearance enters the integrated expression given above.

If it is assumed that $P_{rr}-P_{\theta\theta}$ is proportional to shear stress square as some experimenters suggest, then

$$\int\left(\frac{P_{\theta\theta}-P_{rr}}{r}\right)dr \propto \left(\frac{r\omega}{c}\right)^{0.8} \tag{32}$$

Since

$$\frac{r\omega}{c}$$

is only an approximation for the tangential shear rate, a small error in it could account for the experimentally observed $\sqrt{c}$ factor.

Correlating the result of Figure 3 yields

$$\int_{R_1}^{R_2} \left(\frac{P_{\theta\theta} - P_{rr}}{r} \right) dr = 1.582 \ (10^{-3}) \ \frac{R_2\omega}{c} \sqrt{c} \tag{33}$$

where the constant absorbs the effects of the radius R_1.

VIII. LEAKAGE AT LOW RPM WITH AN APPLIED PRESSURE DIFFERENTIAL

Having examined the performance of the fluid under the special conditions of no-leakage and no-rotation, we are now in a position to compare these results with the actual performance of the fluid under more general operating conditions.

Since such an excellent correlation for the non-rotating performance was obtained, it seems logical to first investigate the perturbing effects of modest rotational speeds. Because the rotational speeds are small, the centrifugal pumping effect will be negligible and any changes in leakage rate can be attributed to changes in fluid properties.

Of the quantities so far investigated, probably the term containing $P_{rr}-P_{\theta\theta}$ is the one in greatest doubt and least understood from a fundamental point of view. On the other hand the term containing

$$\tau_{z\theta} \Big/ \frac{r\omega}{c}$$

which is equal to the viscosity, is by comparison a much better understood quantity and, therefore, on a much firmer foundation. This suggests that the best way to examine the experimental data for general operating conditions is to compute the quantity

$$\bar{P}_1 - \bar{P}_2 + \frac{3}{20} \rho\omega^2 \left(R_2^2 - P_1^2 \right) - \frac{6Q}{\pi c^3} \int_{R_1}^{R_2} \frac{\mu}{r} \, dr \tag{34}$$

which is equal to the apparent value of

$$\int_{R_1}^{R_2} \frac{P_{\theta\theta}-P_{rr}}{r}\, dr \qquad (35)$$

and compare the result with the values of the latter quantity obtained for the special case of Q = o. In the first expression above (33), μ is given by the invariant power law derived earlier [equation (28)].

The results of such computations clearly indicate that when $Q/rc^2 > r\omega/c$ the first expression (33) is very nearly equal to zero (i.e., within probable experimental error), so that the Weissenberg effect or contribution of

$$\int_{R_1}^{R_2} \frac{P_{\theta\theta}-P_{rr}}{r}\, dr$$

is negligible or overwhelmed by the viscous effects. Typically, this occurs at the higher pressure differentials ($\bar{P}_1-\bar{P}_2 \sim 20$ to 30 psi) which, of course, correspond to high leakage rates. Actually, for tests made, $r\omega/c$ was always less than $10^4 sec^{-1}$ when $r\omega/c < Q/rc^2$. According to the no-leakage test results, negligible Weissenberg effects would be expected under these circumstances.

The only disquieting aspect of the calculated results was the fact that the small residual was always negative indicating that μ_o may be a little too large by a factor of about 1.2.

IX. LEAKAGE AT HIGH RPM WITH AN APPLIED PRESSURE DIFFERENTIAL

When the data is run through the equation above for high $r\omega/c$ where $r\omega/c$ is about ten times Q/cr^2, the apparent value of

$$\int_{R_1}^{R_2} \left(\frac{P_{\theta\theta}-P_{rr}}{r}\right) dr$$

exhibits several interesting features.

The first is the rapidity with which the viscous term becomes insignificant. At total shear rates of the order of $10^5 sec^{-1}$, where the total shear rate is given by

$$\dot{\gamma} = \left[\left(\frac{r\omega}{c}\right)^2 + \left(\frac{3.75Q}{rc^2}\right)^2\right]^{1/2}$$

the pressure and inertial terms entirely overwhelm the viscous term so that the apparent value of

$$\int_{R_1}^{R_2} \left| \frac{P_{\theta\theta} - P_{rr}}{r} \right| dr$$

is positive and practically independent of Q. This condition is almost the same as the no-leakage case studied earlier and warrants comparison with it. Such a comparison reveals that the apparent values are always higher than those measured for the no-leakage case, sometimes almost twice as much for the same shear rate without leakage. The no-leakage form of the equation

$$\int_{R}^{R_2} \left| \frac{P_{\theta\theta} - P_{rr}}{r} \right| dr = 1.582\ (10^{-3})\ \frac{\bar{P}_2^{\omega}}{c}\ \sqrt{c}$$

is, therefore, a conservative estimate of its value for seal operation when $Q \neq o$.

X. LEAKAGE AT INTERMEDIATE RPM WITH AN APPLIED PRESSURE DIFFERENTIAL

This regime of operation is the most interesting and also the most difficult, since it cannot be compared directly with either of the limiting cases previously examined.

The first important feature of note in this regime is the relative weakness of the viscous effects. While more influential than in the limiting case of extremely high shear rate, the viscous term is still quite small compared to the pressure and inertia effects. The apparent value of the normal stress term amounts to a variation around the applied pressure differential with slight corrections for inertial effects. The result is that in the total shear rate range $2\ (10^4)$ to (10^6) the quantity $P_{\theta\theta} - P_{rr}$ is proportional to

$$\left[\left(\frac{r\omega}{c} \right)^2 + \left(\frac{3.75Q}{rc^2} \right)^2 \right]^{0.15}$$

for a given clearance and pressure difference.

In this range the leakage contribution to the total shear-rate is quite small so that to a high degree of accuracy

$$P_{\theta\theta}-P_{rr} \alpha \left(\frac{r\omega}{c}\right)^{0.3}$$

which is clearly quite different from the no-leakage results.

Because the pressure term dominates the viscous term in equation 33 the normal stress difference is also proportional to the applied pressure difference P_1-P_2 so that for a given clearance

$$P_{\theta\theta}-P_{rr} \alpha (P_1-P_2) \left[\left(\frac{r\omega}{c}\right)^2 + \left(\frac{3.75Q}{rc^2}\right)^2\right]^{0.15}$$

There seems to be no simple expression which will correlate the effects of clearance. As noted, the proportion above holds only for a given nominal clearance. When the clearance is changed the normal stress difference changes, but not in a regular or consistent manner. In fact, there seems to be an optimum clearance (about 2 mils) at which the viscoelastic effects are the strongest. This is at variance with the no-leakage results where there was a definite nonotonic trend with clearance changes.

XI. CONCLUSION

It is clear from these findings, as well as those for very high shear-rates, that the advent of radial leakage has a significant effect on the performance of the viscoelastic fluids on face seals at high shear-rates (of the order 10^4 or greater). Since these effects can only be inferred indirectly, rather than measured directly, it is natural that one would like to assign observed unexplainable peculiarities to poor experimental values of the measured quantities.

In particular, it would be nice if the peculiar behavior at moderate rpm could be laid at the doorstep of poorly measured viscosity. This is not a plausible explanation since it is in this range of shear-rates where the most consistent viscosities were obtained.

Even more surprising is the fact that the best overall correlation (and the most believable) was obtained at low shear-rates where the viscosity correlation is its poorest. At least in this region the normal stress difference is relatively unimportant and, therefore, does not introduce added complications.

Considering all the evidence, it is obvious that the normal stress difference $P_{\theta\theta}-P_{rr}$ is dependent on more than just the tangential shear-rate as might be supposed from the examination of viscometer test data where the net leakage-rate is zero. As pointed out by several investigators, zero net leakage flow fields cannot be the simple flows which are usually pictured, but must contain rather complicated secondary flows involving radial and axial velocity components.

From the results obtained here, it is obvious that radial velocity components play a significant role in the behavior of the fluid. The major clue in this regard is the normal stress difference dependence on the applied pressure difference. This pressure difference is probably unimportant in itself, its importance lies in the fact that it is symptomatic of higher leakage-rates and high radial shear-rates.

The key to understanding high shear performance is in determining how normal stress difference depends on the radial shear rate. The analysis used above avoids a detailed investigation of the velocity field and deals only with the gross features of the seal performance, i.e., leakage, applied pressure difference, etc. Obviously, this is not sufficient when the normal stress difference is of the order of the applied pressure difference. Its dependence on clearance is evidence that more detailed knowledge is required.

To carry out a detailed analysis is by no means a simple task. It requires first a model constitutive equation, and second, a computer program for solving the equations of motion and predicting the overall performance characteristics since these equations will not be simple. This is a formidable task, but unfortunately there seems to be no alternative.

FIGURE 1

$$c\,\frac{(P_1-P_2)}{R_2-R_1} \text{ vs } \frac{Q}{c^2}$$

No Leakage

3.2% Vistanex 200 in JP-5

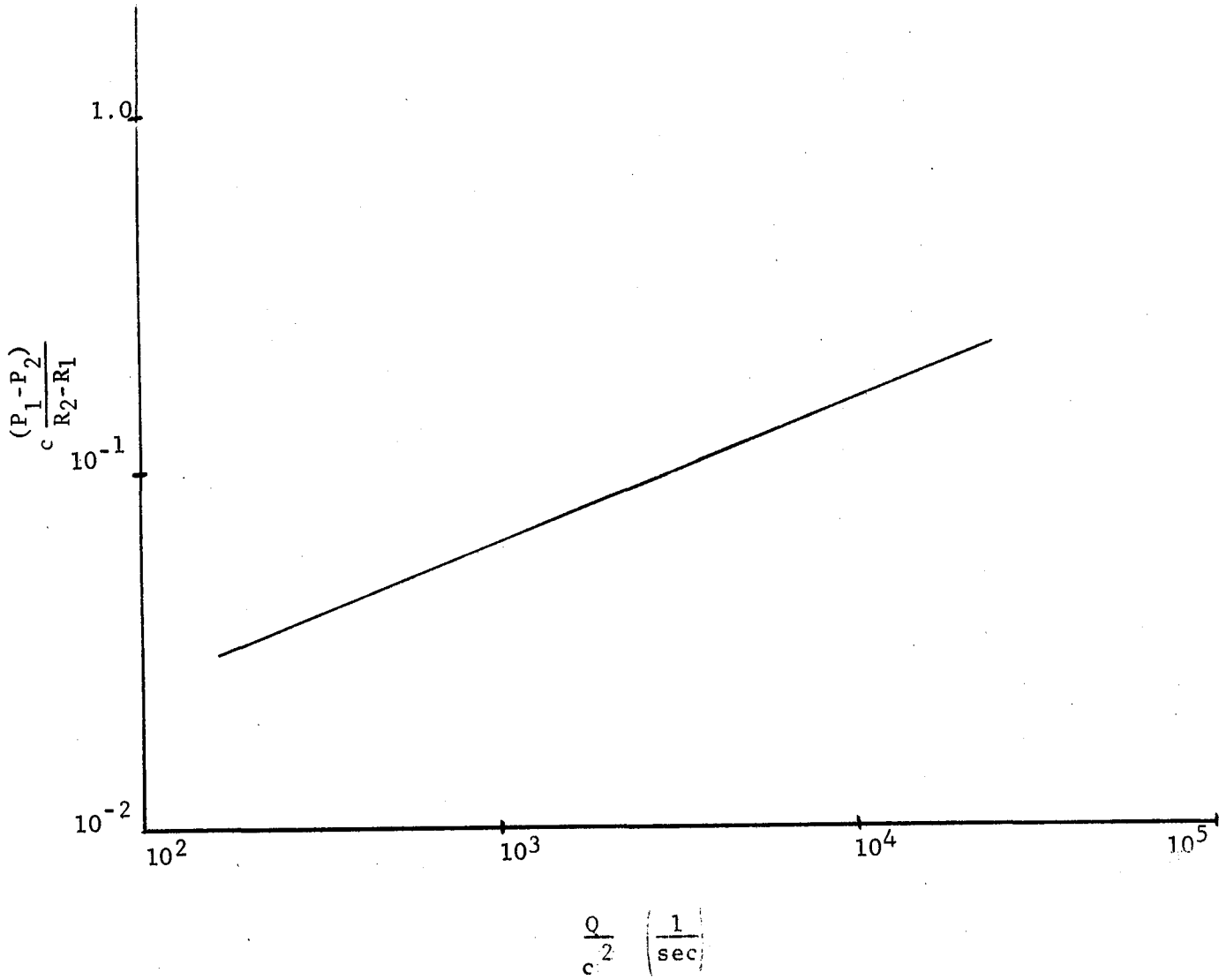

FIGURE 3

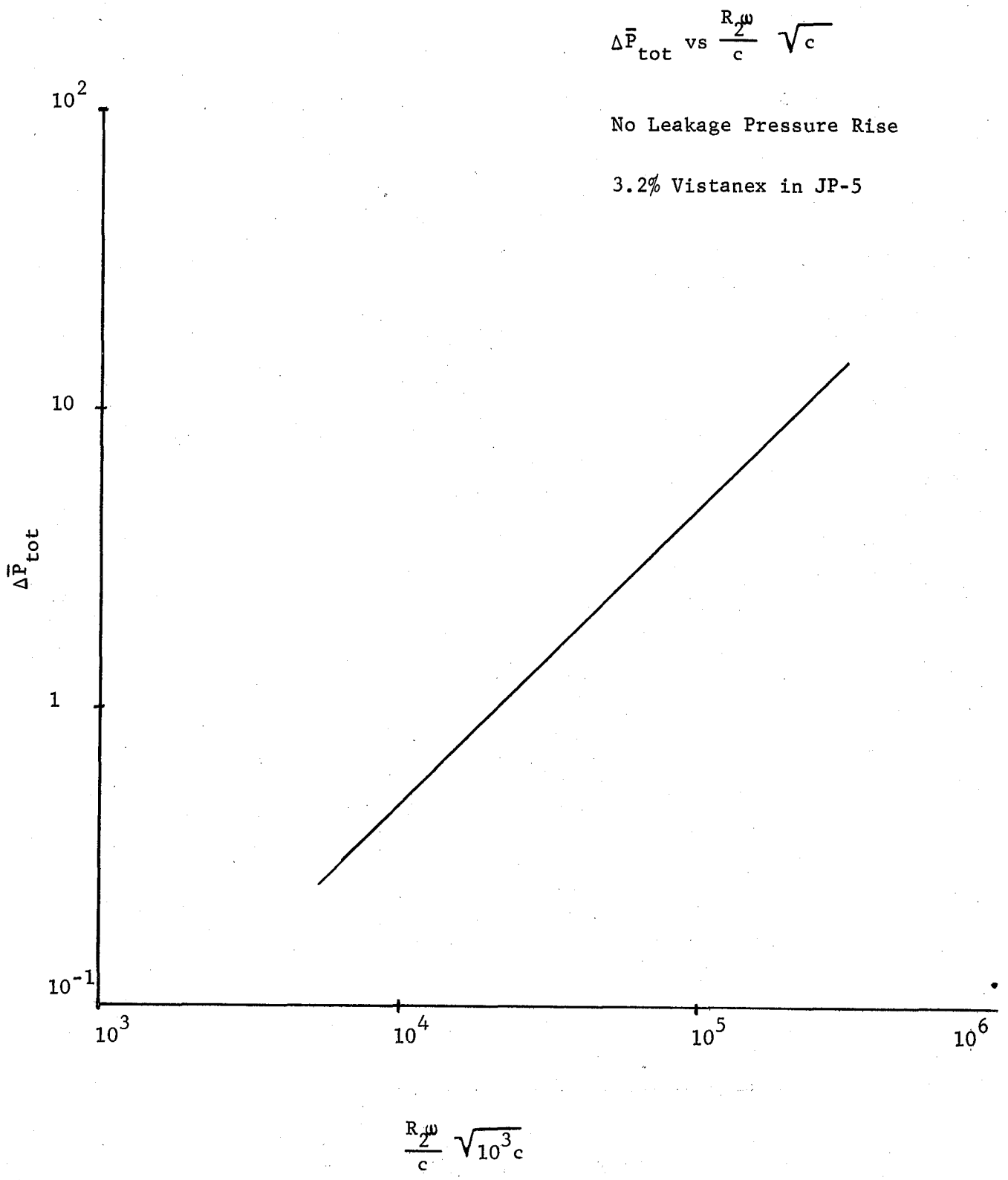
$\Delta\bar{P}_{tot}$ vs $\frac{R_2\omega}{c}\sqrt{c}$
No Leakage Pressure Rise
3.2% Vistanex in JP-5
10^2
10
1
10^{-1}
$\Delta\bar{P}_{tot}$
10^3
10^4
10^5
10^6
$\frac{R_2\omega}{c}\sqrt{10^3 c}$

FIGURE 2

SHEAR-STRESS, SHEAR-RATE CORRELATION

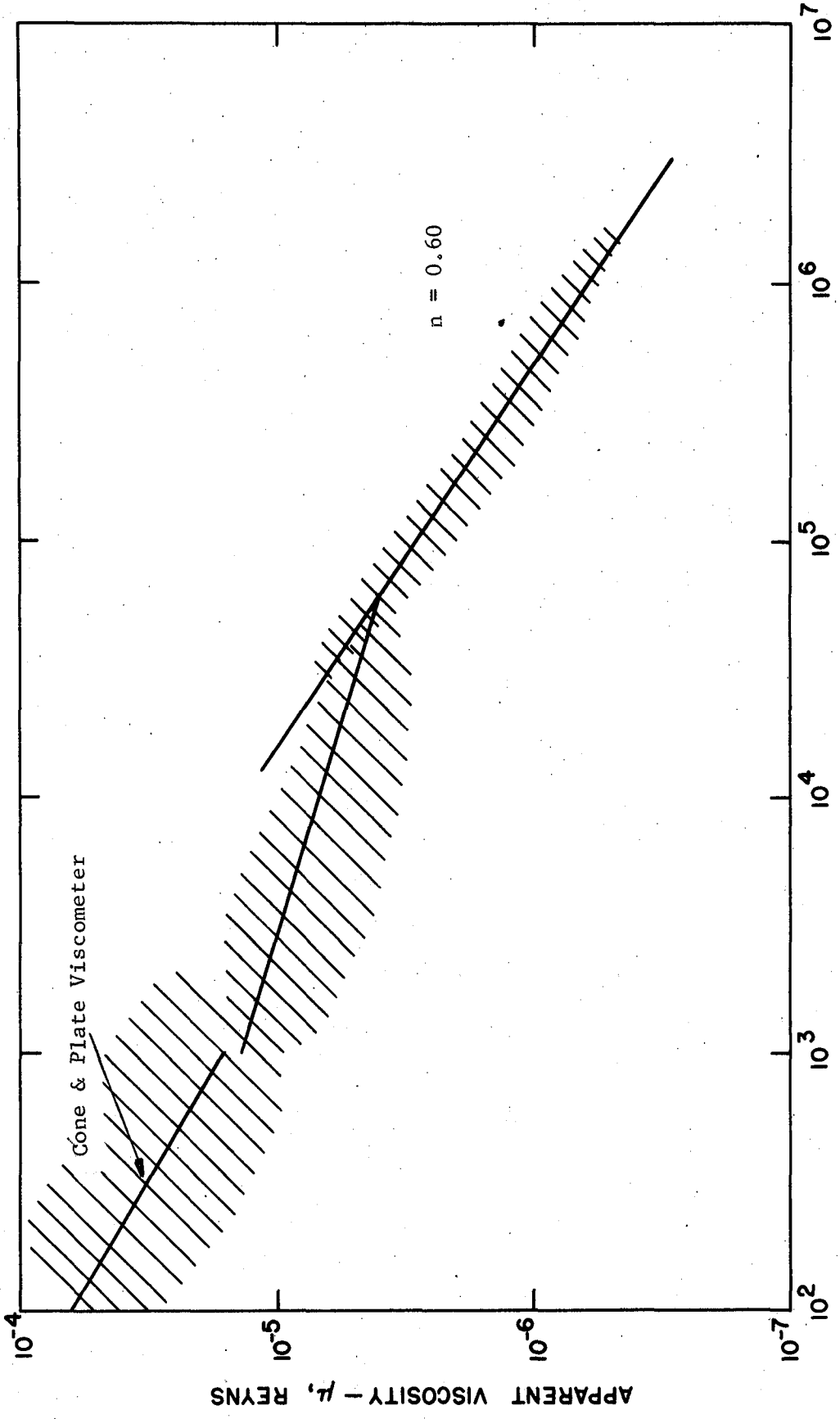

NOMENCLATURE

c = seal clearance

n = invariant power-law index

p = isotropic pressure

$\bar{P}$ = $p-P_{rr}$

P_{rr} = radial component of the deviatoric normal stress

$P_{\theta\theta}$ = tangential component of the deviatoric normal stress

$\Delta\bar{P}_{tot} = \bar{P}_1-\bar{P}_2 + \frac{3}{20}\rho\omega^2 (R_2^2-R_1^2)$

Q = volumetric leakage-rate

r = radial coordinate

R_1 = seal inner radius

R_2 = seal outer radius

T = total seal torque

u = radial component of the velocity

v = tangential component of the velocity

z = axial coordinate

$\dot{\gamma}$ = total shear-rate

$\dot{\gamma}_{z\theta}$ = tangential component of the shear-rate

μ = viscosity

μ_o = consistency index

ρ = density

$\tau_{z\theta}$ = tangential component of shear stress

τ_{zr} = radial component of shear stress

ω = angular velocity of seal rotation

REFERENCES

1. Study of Dynamic and Static Seals for Liquid Rocket Engines, Final Rpt., Vol. 1, 1 Jan., 1966-14 Feb., 1967, NAS 7-434

2. B. Rabinowitsch, Z. Phys. Chem., 1929, A145 1

3. M. Mooney, J. Rheology, 1931, 2, 210

APPENDIX C

SEAL GEOMETRY EFFECTS

BY

J. A. FINDLAY

I. INTRODUCTION

The purpose of this study is to provide an experimental verification of the Newtonian face seal theories developed under this contract. These theories include the inward pumping theory, the effects of inertia and turbulence on dynamic face seals and cavitation effects in the fluid passages which are typical of these thin film seals.

The basic problem in deriving an adequate theory for face seal behavior is the lack of accurate data. In general, this is a difficult experimental area because at the close clearances required for face seal operation, small, uncontrolled variations in surface geometry play a major role. Thus, the key to successful face seal experiments is the controlled, accurate measurement of the face seal geometry. These experiments have been designed with this factor as an outstanding guide. This allows accurate measurement of face seal performance characteristics, such as, leakage, normal force and power loss, as a function of known face seal geometry. Thus, the objective of obtaining data adequate for precise correlation and understanding of the physics of face seal behavior may be attained. Thus, the situation of having what appears to be comprehensive seal data, when actually the seal interface geometry is unknown, will thereby be avoided.

The experiments of this task substantiate the theories within the limits of the assumptions made. The actual correlation of the experiments with the theories follows in this Appendix.

II. TEST EQUIPMENT AND PROCEDURE

The rotating and stationary faces of the test seal are shown in Figures 1, 2, and 3. The metal face of Figure 1 is B6H3 steel which was heat treated before grinding was completed. After grinding, the measured runout was $\pm$ 0.000025 in. and the flatness was within $\sim$ 0.000005 in. both of which are within specifications. Figure 2 shows one of the transparent seal faces mounted on the bridge plate which is used to position it. Figure 3(a) shows another transparent seal face. This one has a narrower land than the one shown in Figure 2. Both of these transparent seal faces are 7740 pyrex glass optical polished plates from

Corning Glass. These glass faces are mounted on lucite, a transparent, heat resistent acrylic compound. The metal stationary seal face shown in Figure 3(b) has the same dimensions as the transparent seal face shown in Figure 2. The pressure taps can be seen in the metal face.

A cross-section of the face seal experiment is shown in Figure 4. In this figure, the center feed pipe and film thickness probes are shown. The Sheffield displacement sensors were used to set the initial film thicknesses. Three sensors were used and from these three readings any combination of average film thickness, $\bar{h}_i$, and tilt eccentricity, ϵ_t, could be set. It was found, however, that as the supply pressure to the seal was increased the film thickness opened up. A static calibration was made using the Sheffield's which showed that the film thickness increased uniformly with pressure. Therefore, if only one sensor could be read the change in $\bar{h}_i$ and ϵ_t could be determined by assuming the same increase in film thickness at the other two sensor locations. This was very important since the Sheffield's could only be used for static measurements and during the dynamic tests the Wayne-Kerr capacitance probe had to be used. Because Wa yne-Kerr probes were useful only when a film of oil could be maintained between them and the rotating seal face, only one of the probes could be used. If three were used they would wipe the oil off the rotating face and no readings of any value could be obtained.

The Wayne-Kerr probe was calibrated using the test fluid, 350 centistoke silicone oil, and the measurements taken with it during the dynamic tests were used to correct $\bar{h}_i$ and ϵ_t. This was accomplished using a data reduction program

Two other corrections to the raw data were made using the data reduction program. They were: (1) a pressure correction due to the hydrostatic pressure head of oil in the graduated supply reservoir (see Figures 5 and 6) and (2) a viscosity correction due to temperature changes measured by a thermocouple in the leakage oil. The leakage rate was also calculated using the data reduction program using as input the initial and final oil levels in the graduated reservoir and the time interval.

This data reduction program is referred to as No. 1 and its listing is given at the end of this Appendix. Data reduction program No. 2 is used for calculating the pumping component of leakage in the eccentric seal tests. Its listing is also given. Data reduction program No. 3 is similar to No. 1, but has the inertia component of leakage added to it.

These three data reduction programs take the raw data from the tests and reduce it down to a form suitable for comparison with the theoretical curves shown in Figures 10 and 11 of Appendix D.

Photographs were taken for all the test conditions where gas cavities appeared. Figures 9, 10, 11 and 12 are samples of some of these figures. Figures 9 and 10 are for the concentric seal showing cavities of different sizes. Figures 11 and 12 are for the eccentric seal. Both of these latter figures show air being pumped into the center of the seal against a moderate pressure differential (about 1 psi). In Figure 11 a small spiral of bubbles may be seen. In Figure 12 much more air is being pumped in and it appears as the blurred black regions in the center of the seal.

Figure 5 shows a photograph of the transparent test seal set up. The glass face seal is clearly shown as are the Sheffield displacement probes and the Wayne-Kerr capacitance probe. The tube connected to the center of the seal is, of course, the oil supply line. A more complete view of the oil supply line, graduated reservoir and supply pressure system may be seen in Figure 6. This figure also shows the movie camera used to take motion pictures of the gas cavities and the inward pumping of air.

III. CAVITY EXPERIMENTS (CONCENTRIC, MISALIGNED SEAL)

A. INTRODUCTION

The first seal theory to be studied experimentally was that of gas cavities in the fluid film between the seal faces. The short bearing theory developed during Phase I of this contract indicated that these gas cavities, under certain conditions would influence the hydrodynamic forces but not the leakage. This was true at least for the concentric seal. That is, the leakage would be the same as for the hydrostatic seal. However, the numerical solutions obtained on the GE 635 Computer Program gave leakage rates that increased with Λ and, therefore, cavity size. It was suspected at the time that this was the result of inadequately describing the boundary shape of the cavity in the GE 635 Program (Reference 1).

B. TEST PROCEDURES

The experimental program schedule was set up to settle the difference between the two methods of analyses described above. Tests were performed on the transparent test seal described in Part II.

In these experiments the oil was fed to the inside of the seal under pressures from 1 to 40 psig and the outside diameter of the seal was exposed to air. The stationary seal member was held at a fixed tilt to the rotating member so that a "converging-diverging" film shape was obtained between the seal

faces with a film thickness variation of about two-to-one. For these conditions, air was "sucked" into the seal interface in the diverging film region forming a gas cavity at ambient pressure. A range of pressures and speeds were used so that relative magnitude of the hydrodynamic effects could be varied. Therefore, leakage measurements were obtained for conditions ranging from the hydrostatic up to $\Lambda = 1000$. A summary of the concentric seal experiments is given in Table I. It will be noted that only a few tests were made with the wide land seal. This seal was cracked during one of the tests and the remainder of the experiments were carried out using the narrow land seal. The wide land seal is shown in Figure 2 and the narrow land seal in Figure 3(a).

C. RESULTS

1. Flow Rates

a. Wide Land Seal

The data taken with the side land seal are given in Table II and shown correlated in Figures 14 and 15. The correlation is not as good as hoped for but this is attributed to the fact that no correction was made for the hydrostatic pressure head in the supply line and the difficulty experienced in obtaining close control on the film thickness measurements.

The maximum error in this correlation of the flow coefficient was about 100%. This could be due to an error of only 30% in the film thickness. Most of the data correlated within about 25%. This would represent a film thickness error of only 8%.

The important thing to note is that the rotational speed had no measurable effect on the leakage. Since the gas cavities, which were photographed, increased in size with speed it can be concluded that the presence and size of the gas cavities had no effect on the seal leakage.

Observing a set of points, in Figure 14 and 15, for a constant speed it can be noted that the pressure level did effect the accuracy of the correlation. Since the pressure level influences the film thickness, this further indicates that the accuracy of the film thicknesses may be the weak link in this correlation.

b. Narrow Land Seal

The correlation of data with theory is much better in these experiments. Again the scatter of the data is attributed mainly to the accuracy of the film thickness measurements. Also the conclusion that the cavity does not affect the leakage, is again substantiated.

The data for these experiments are summarized in Table III and Figures 16, 17, 18, 19 and 20.

2. Cavity Shapes and Inception

One of the objectives of these experiments was to see if the observed cavity shapes could be predicted, and if the conditions under which the cavity first appeared could be predicted. These correlations are not yet complete, but some general observations can be made at this time.

First of all, for a given geometry the theory says that the cavity will first appear for a given, fixed value of Λ. That is, as the pressure across the seal is increased so must the rotational speed be increased. This observation has been confirmed. What is more difficult to confirm is the exact value of Λ for which the cavity first appears. This is due to the fact that the cavity appears gradually and an observation cannot be made until a finite cavity appears.

Secondly, the cavity shapes are generally the same as predicted in the Phase I study for the wavy seal. However, cavity shapes have not yet been calculated for the misaligned seal although the two cases are similar in geometry. The theory assumes that there are many small ribbons of oil flowing through the cavity. However, with the relatively large film thicknesses used in these experiments there are only a few large ribbons of oil. This will affect the correlation of the theory and experiments but not drastically.

A summary of cavity shapes and corresponding seal conditions is given in Figure 8 and Table XI. Most of data taken for the concentric seal leakage tests had photographs.

Many of these, while showing the gas cavities, are not clear enough for publication. However, some measurements were taken from these photographs. As noted before, the value of Λ necessary for a cavity to first form (inception) was very difficult to measure. A correlation between θ_a (cavity nose) and Λ has not been pursued to any extent. However, a few measurements were made of R_{crit} vs Λ. A correlation of these measurements against theory is shown in Figure 34. So far this correlation, also, is rather crude. The observations made do indicate that the cavity shapes are given to a fair approximation by the theory. This correlation could be extended in the future.

The theoretical curve shown in Figure 34 was obtained from the Phase I cavity theory for the wavy seal and is, therefore, an approximation to this case. The data points were taken from experiments on a misaligned or tilted seal.

IV. SEAL PUMPING EXPERIMENTS (ECCENTRIC, MISALIGNED SEAL)

A. INTRODUCTION

In Appendix D, an analysis is developed for the wavy, radially eccentric face seal showing the existence of a "pumping" leakage. This pumping leakage occurs because of the combined effects of a once per rev film thickness variation, due either to waviness or misalignment, and a radial displacement of the seal center from the center of rotation.

The assumption made in this analysis was that a complete fluid film exists between the seal surfaces. Since in the misaligned seal experiments gas cavities usually occurred, the pumping experiments were broken down into three groups: (1) inward pumping, with cavities, (2) inward pumping, no cavities, and (3) outward pumping, no cavities. A fourth category, "full film with different fluids on either side of the seal," is discussed in Part V.

B. TEST PROCEDURES

In the group (1) experiments the seal radial eccentricity was in such a direction, in relation to the seal misalignment, so that the hydrodynamic pumping action was inward, or opposed to the hydrostatic leakage. Also in these experiments the outer circumference of the seal was exposed to air. This resulted in the air being drawn into the seal film where the surfaces diverged, thus forming gas cavities. The gas cavities reduce the generation of hydrodynamic pressures in the seal film and thus reduce the pumping action that occurs because of the seal eccentricity. For the high Λ tests some air was pumped through the seal to the inside against the pressure.

The inward pumping experiments with no cavities (group 2) were accomplished by building up an oil dam on the rotating seal face outside of the stationary seal face; and supplying oil between the dam and the seal. Thus, the outside circumference of the seal was flooded with oil, and no gas cavities were formed in the seal film during these experiments. The pumping action in the seal was exactly as predicted and in a direction to oppose the hydrostatic leakage. Under high Λ conditions a net inward leakage was obtained against the hydrostatic pressure head of the oil in the graduated reservoir. The experimental set-up for this experiment is shown in Figure 13. This figure shows the rubber tubing and bulb used to supply the oil to the outside of the seal. This oil was dyed blue and as it was pumped into the center of the seal it filled the normal supply line and flowed up into the oil reservoir. This dark colored oil can be seen in Figure 13 also.

The group (3) experiments were performed with the radial eccentricity set in a position 180° from that in the group (1) and (2) experiments. This changed the cos α term in the pumping equation from -1 to +1. In this case, the pumping action was outward, in the same direction as the hydrostatic leakage. No gas cavities formed during these experiments and the data correlated very well with the theoretical predictions. The leakage in these experiments was greater than the hydrostatic leakage and increased linearly with Λ.

C. RESULTS

From the preceeding discussion it should be clear that the inward and outward experiments with no cavities should correlate with the theory developed in Appendix D. This correlation is shown in Figures 21, 22 and 23. Figure 21 shows the q pump/ε_t data from the outward pumping experiments and its comparison with the identical curve for $\varepsilon_r = 0.091$. As can be seen, the correlation is very good.

Figure 22 shows the leakage coefficient data from the inward pumping, without cavities, experiment. Again the comparison with the theoretical curve is very good.

Both of the preceeding sets of data are plotted in Figure 23 using the invariant parameter q pump/$\Lambda\varepsilon_r\varepsilon_t \cos\alpha$. For the seal tested, $R_i = 0.83$, the theoretical value of this parameter is 2.63 as obtained from Appendix D. The correlation on this basis does not look as good but all the errors are magnified in this type of plot. In addition, it is difficult to obtain accurate pumping flows since they must be determined by subtracting the measured leakage from the theoretical concentric seal leakage. Since the concentric seal correlations showed some scatter, it is obvious that the accuracy of the pumping flow measurements must be affected even more since a difference in flows is involved.

Figures 24 through 29 show the inward pumping data for seals containing gas cavities. The first conclusion that can be drawn from these curves is that the presence of cavities decreases the inward pumping effect.

In Figures 24 and 25 the same data is plotted in two different ways. From these curves, it can be seen that at the low values of Λ, where no cavities exist in the fluid film, the data compares quite closely to the noncavity seal pumping theory. However, at the higher values of Λ, where gas cavities do form, the effect of seal pumping decreases.

Figures 26 through 29 also show the decrease in seal pumping with increased Λ. There is more scatter in this data, however. It is felt that the reason for

this is that the data in these figures is for smaller film thicknesses, and the accuracy of the measurements and, therefore, the leakage correlation is not as good as for the larger film thickness tests. Even the static leakage correlation for $\bar{h}_i = 0.001"$ was not sufficiently accurate to allow meaningful values of the pumping coefficient to be determined. However, in Figure 27, where some of this data is plotted, still shows the general trend of decreasing leakage with increasing Λ due to the seal eccentricity, i.e., inward pumping.

Figure 29 illustrates the data for $\epsilon_t = 0.20$. At this low value of tilt eccentricity the pumping effect is small and, therefore, the accuracy in measuring it is relatively poor. Thus the data points in Figure 29 show quite a bit of scatter.

The low pressure, inward pumping tests were repeated with a slightly different feed system. This was done because some of the low pressure inertia tests showed a great deal of scatter. In looking into the problem it was found that air was trapped in the supply tube and thus giving a lower hydrostatic pressure at the inside of the seal than assumed.

The feed system was modified so that the reservoir stand pipe was placed directly over the feed hole in the center of the stationary face seal. This reservoir was then connected to the feed hole by a piece of transparent plastic tubing. All air was thereby eliminated from the feed system and the scaling pressure could be accurately determined by the height of the oil in the reservoir.

This set up was used to: (1)repeat the low pressure, inward pumping experiments with no cavities, (2) repeat the low pressure inward pumping experiments with cavities, (3) perform the no cavity inward pumping tests with two different fluids on either side of the face seal, and (4) perform the inertia experiments.

Figure 30 shows the results of the low pressure, inward pumping experiments, with and without cavities. The experiments without cavities correlates very well with the theory developed in Appendix D. Both of these experiments were carried out with silicone oils of two different viscosities, i.e., 350 and 100 centistokes. The correlations between the two fluids is excellent.

It will again be noted that the presence of gas cavities in the film reduces the inward pumping action of the eccentric seal. At low values of Λ the two curves are identical. However, as Λ increases and a cavity starts to form, in the oil-air experiments, the two curves diverge and the inward pumping component of leakage reaches a limiting value. This is demonstrated by the fact that the net leakage reaches a steady value as Λ increases. This can also be seen in Figure 32 for values of Λ up to 4100.

The analytical relationships for the "inward pumping with cavity" case has been set up in Appendix D, but no solutions have as yet been obtained. Part of this has been set up on the computer, but the final programming was not accomplished in the time allowed. It is recommended that this work be continued.

V. TWO FLUID, PUMPING EXPERIMENTS

A. INTRODUCTION

Up to this point, the very important phenomenon of seal pumping has been investigated for the single fluid cases. Another very important application is where the face seal separates two different fluids.

If a hydrodynamic film exists between the two seal surfaces, then the two fluids will meet in the seal interface and the seal hydrodynamics will be modified.

This problem has been set up in Appendix D, but again, time did not permit the completion of this solution. However, experiments have been run and the data correlated with the viscosity ratio. As suspected, if the viscosity of the fluid on the outside of the seal is lower than the viscosity of the fluid on the inside of the seal, then the pumping action is reduced.

B. TEST PROCEDURE

The experimental apparatus was set up with stand pipe reservoir directly over the feed hole in the center of the stationary face seal, as explained in IV. Silicone oil of one viscosity was supplied to the center of the seal under hydrostatic pressure by means of this stand pipe. A fluid dam was mounted on the rotating seal face, the same as for the inward pumping - no cavity experiments. This outside reservoir, at ambient pressure, was flooded with a silicone oil of a different viscosity.

Two things modified the procedure somewhat. The first was that at high speeds (high Λ) cavities started to form because not enough oil could be supplied to the outer reservoir. Therefore, the maximum value of Λ for these experiments was limited. The second was that the net leakage of the fluids through the seal would "contaminate" the other fluid. That is, at low Λ the inside fluid leaked to the outside reservoir and mixed with the other oil there. Thus, the viscosity of the oil on the outside of the seal tended to be variable. At high Λ the outer fluid was pumped into the center of the seal, thus mixing with the fluid there and modifying its viscosity.

Therefore, periodically the experiments were stopped and the inner and outer reservoirs flushed before continuing the measurements.

C. RESULTS

The measurements taken in these experiments are correlated in Figures 31 and 32. Viscosity ratios, μ_o/μ_i, ranging from 3.5 to 0.002 were used. Although for the single fluid case, $\mu_o/\mu_i = 1$, the data showed very little scatter, and lay on a straight line; the two fluid data scattered and it is not certain that the correlations should be straight lines or not. Theoretical solutions have not yet been obtained for this case. Because of the fluid mixing, as discussed above, the two fluid data scattered and repeating the same conditions would yield slightly different results depending on whether or not the reservoirs had just been flushed or whether the net leakage had been inward or outward. Since it takes a finite length of time to obtain a single data point, and fluid mixing starts immediately, it was not possible to eliminate the scatter even when the reservoirs were flushed frequently.

VI. INERTIA EXPERIMENTS

A. INTRODUCTION AND TEST PROCEDURE

In the Newtonian study performed under Phase I by H. J. Sneck, laminar flow with inertia effects was considered. The results of this analysis showed that the leakage solution was unchanged except for the addition of a centrifugal inertia term. Thus, the concentric, misaligned seal leakage coefficient is

$$q = \frac{-h_i^3}{\left[(p_i - p_o) + \frac{3}{20}\rho\omega^2\left(r_o^2 - r_i^2\right)\right]} \frac{12\mu Q}{} = -\frac{2\pi\left(1 + a\epsilon_t^2\right)}{\ln R_i}$$

The experiments performed up to this point have been at low speed and with high viscosity oils. Thus, large hydrodynamic pressures could be generated while the inertia terms were minimized. In order to obtain significant inertia effects, it was necessary to run the seal experiments at high speeds. To do this, a low viscosity oil (5-10 centistokes) had to be used in order to reduce the friction and, therefore, the torque required and heat generated. A compromise between oil viscosity and average film thickness had to be arrived at so that the leakage rates would not be too great nor the film thickness error too large. Values of 10 centistokes and 0.003 inches were used. Both aligned tests and a tilt eccentricity, ϵ_t, of 0.56 were used.

B. RESULTS

The experimental measurements are correlated with the theoretical values in Figure 33. The leakage equation was rearranged as follows

$$-q \ln R_i / 2\pi (1 + a \epsilon_t^2) = 1$$

The inertia term

$$\frac{3}{20} \rho \omega^2 (r_o^2 - r_i^2)$$

assumes that all the inertia effects take place within the seal interface. However, it was quite obvious that because of the rotating plate, rather than a rotating ring, the inertia effects were felt throughout the seal.

The final correlations showed that if an inertia term of

$$\frac{3}{20} \rho \omega^2 r_o^2$$

was used, the correlation was quite good. This can be seen in Figure 33.

VI. CONCLUSIONS

Although some scatter was found in certain of the data, there was sufficient consistency in most of the data to confirm the misaligned seal leakage theory, with and without inertia effects, and the eccentric seal pumping theory.

Since the eccentric, misaligned seal theories for pumping with cavities and with two fluids have not been completed, no verification of these theories have been made. However, sufficient data has been obtained to evaluate the effect and give a basis for evaluating the theory.

These theories should be completed and incorporated in the digital computer SEAL PROGRAM.

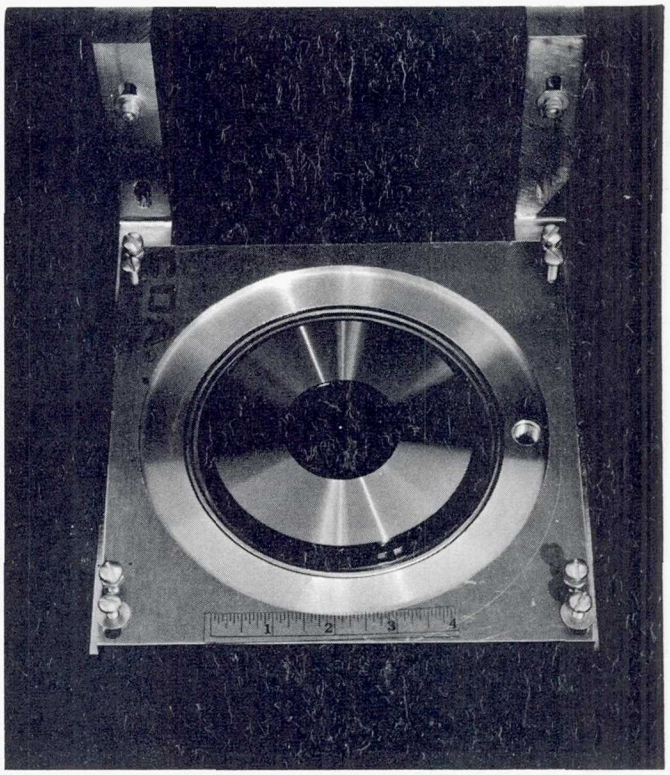

Figure 1. Rotating Seal Face

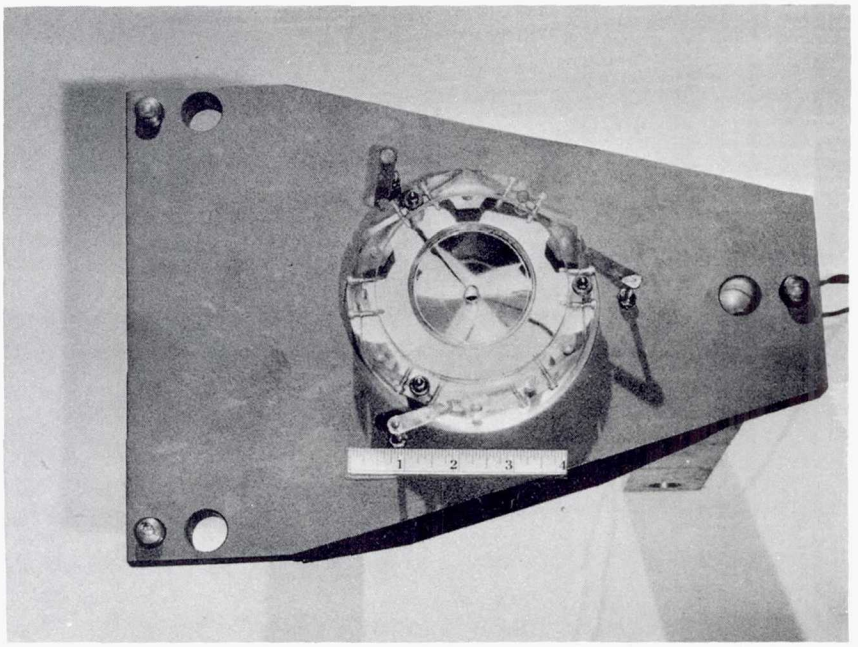

Figure 2. Transparent Stationary Seal Face Mounted on the Bridge Plate. (Sheffield displacement sensors are shown.) I.D. = 2.25 in. – O.D. = 3.50 in.

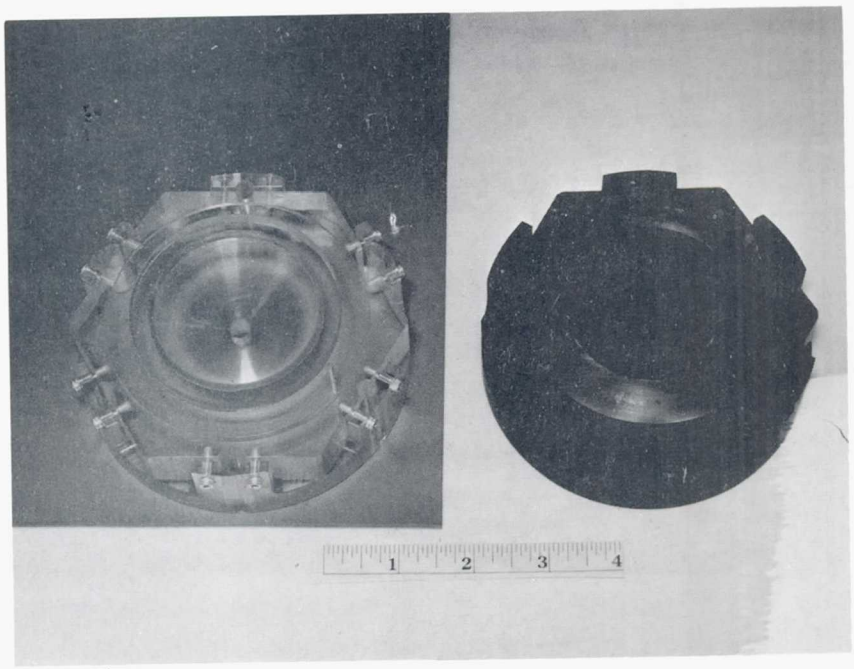

(a)
Transparent Stationary
Seal Face
I. D. = 2.25 in.
O. D. = 2.75 in.

(b)
Steel Stationary
Seal Face
I. D. = 2.25 in.
O. D. = 3.50 in.

Figure 3

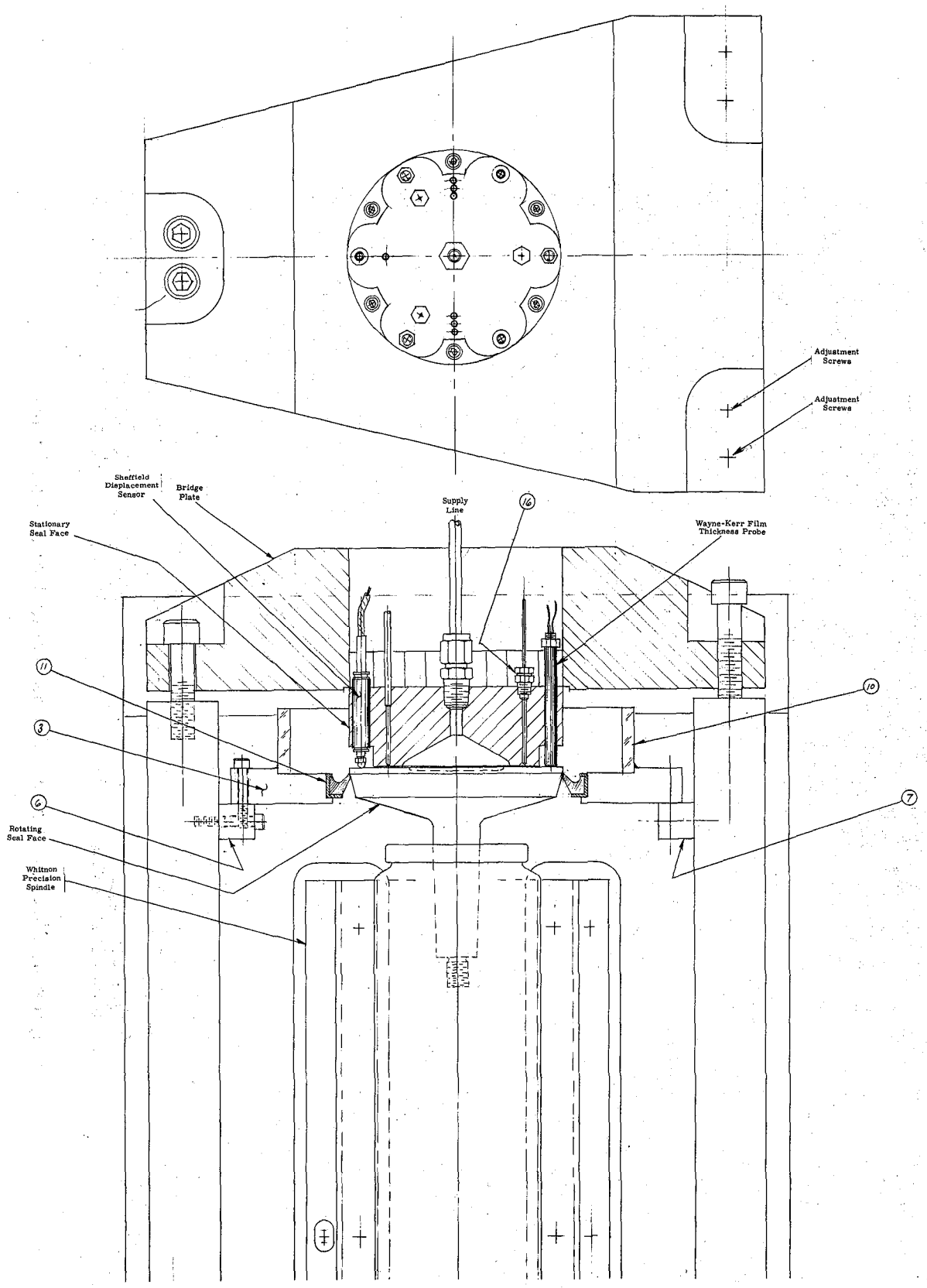

Figure 4. Newtonian Face Seal Experiment

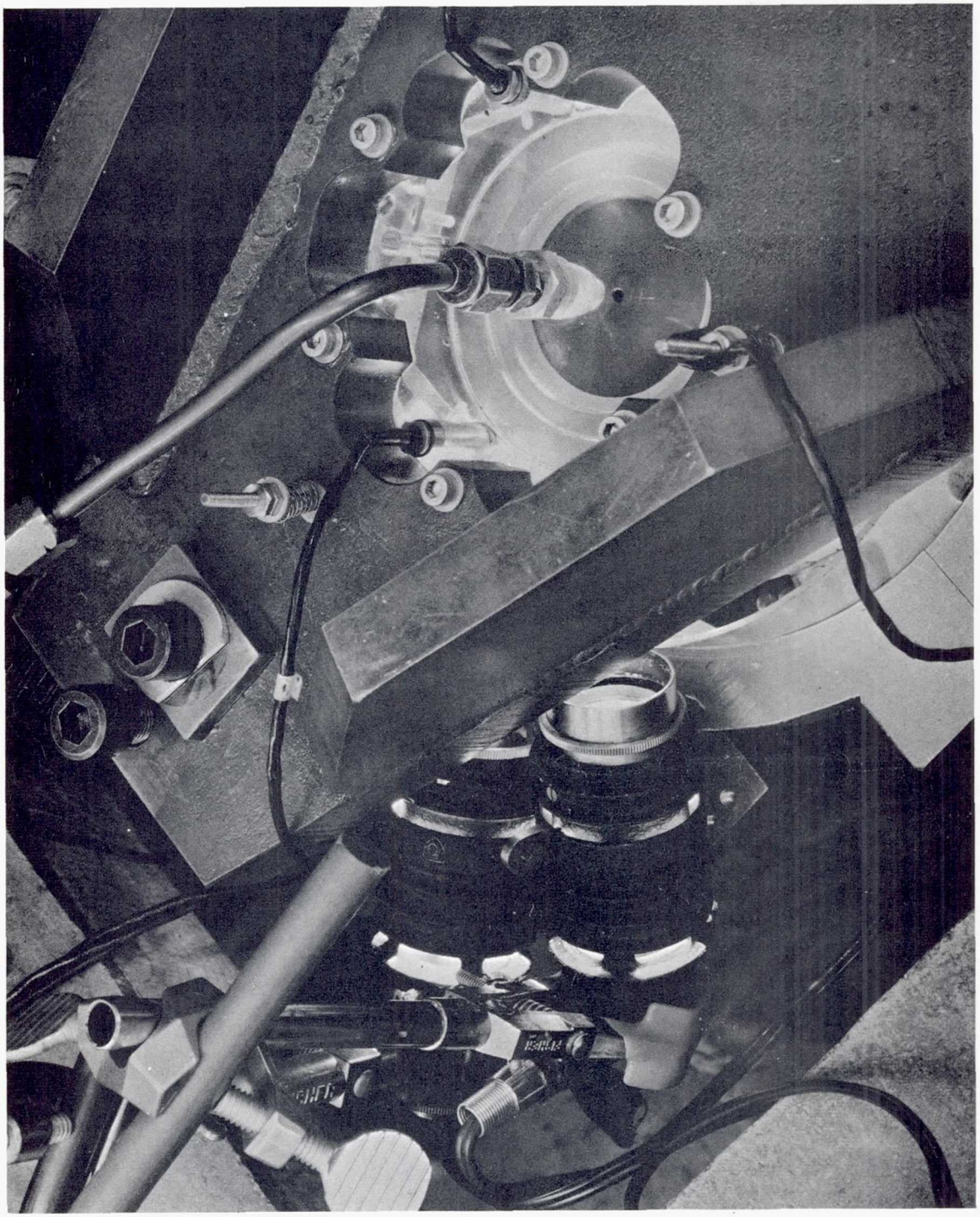

Figure 5. Narrow Land, Transparent Face Seal Setup

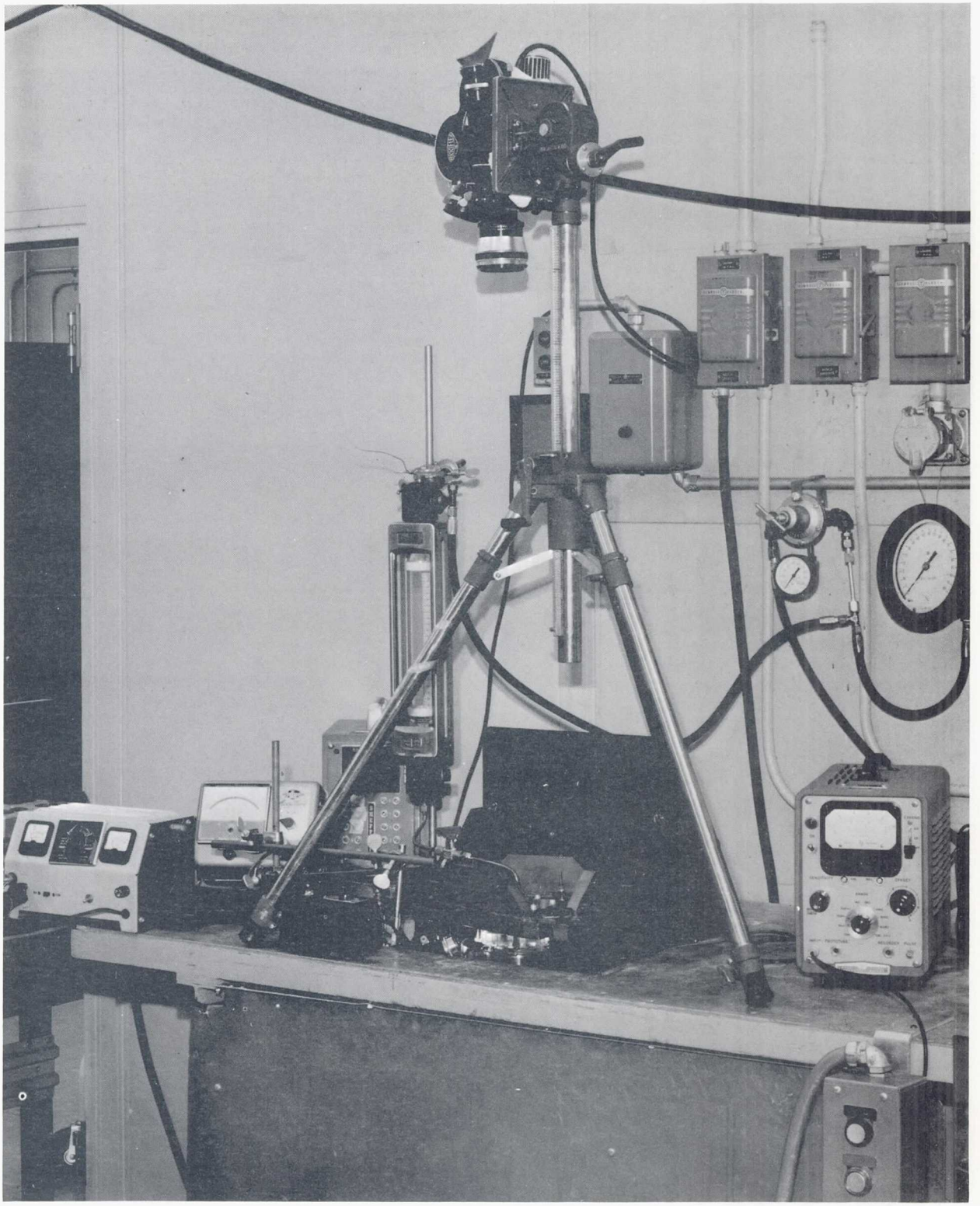

Figure 6. Face Seal Experiment Showing Movie Camera

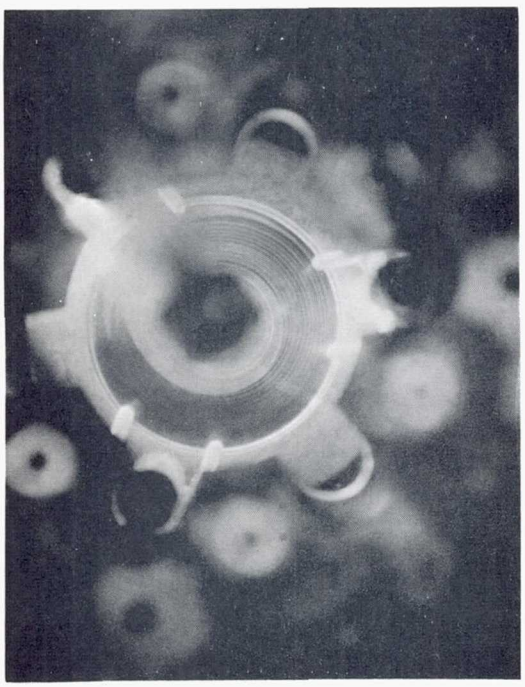

(a)

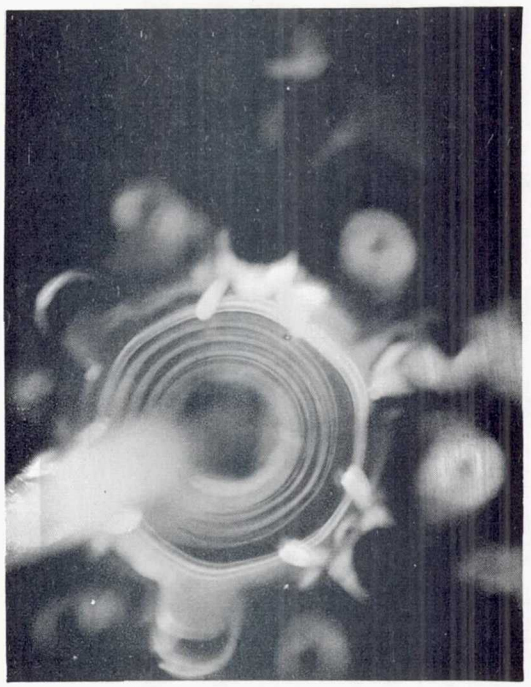

(b)

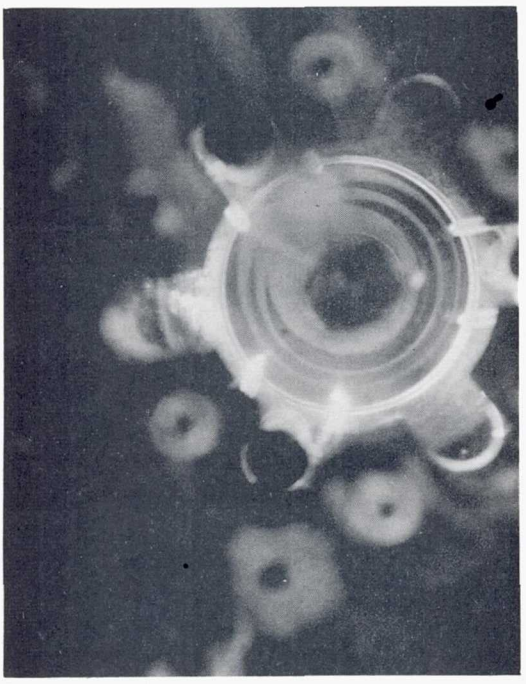

(c)

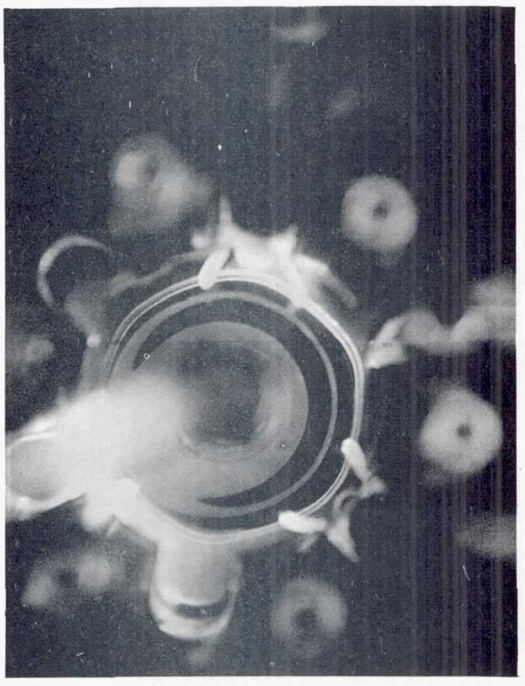

(d)

Figure 7. Gas Cavities in a Transparent Face Seal. (The dark areas are the gas cavities and the light areas oil. Rotation is in the clockwise direction with the minimum film thickness, of the misaligned seal faces, coinciding with the full film region)

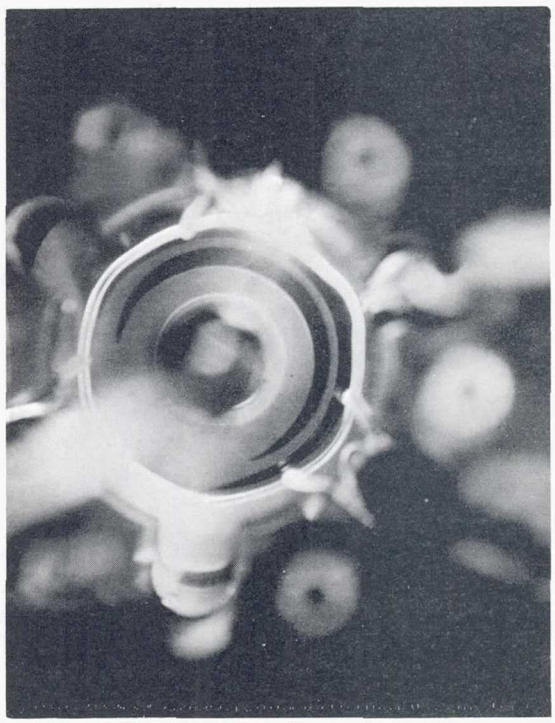

(e)

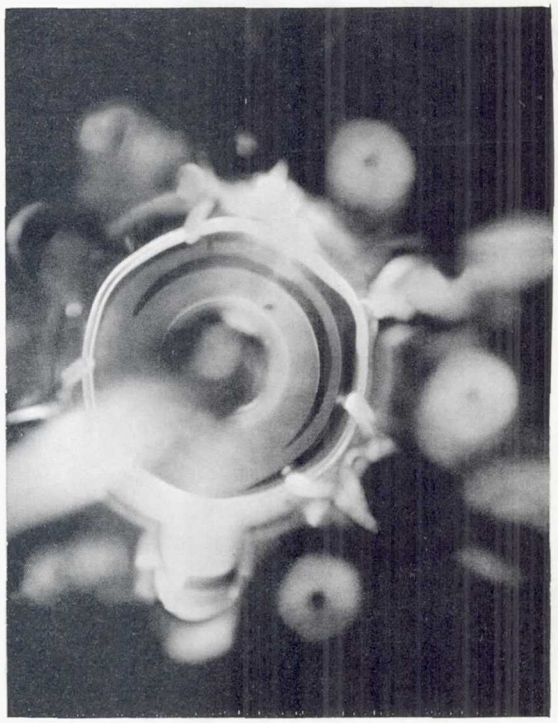

(f)

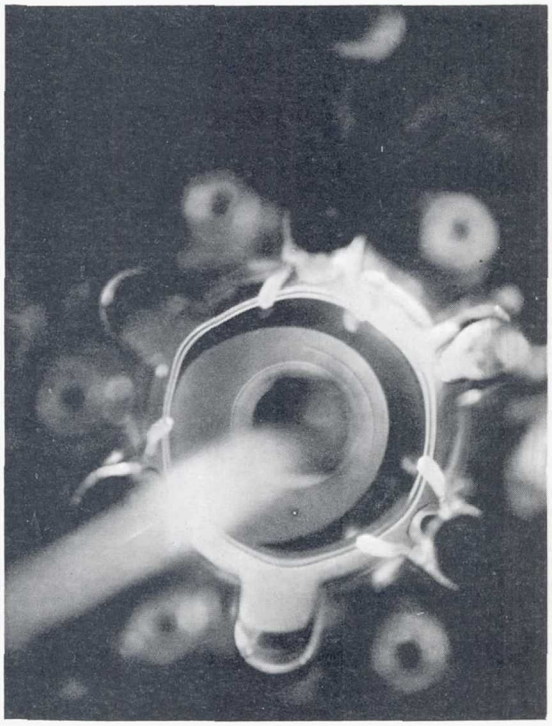

(g)

Figure 7 (continued)

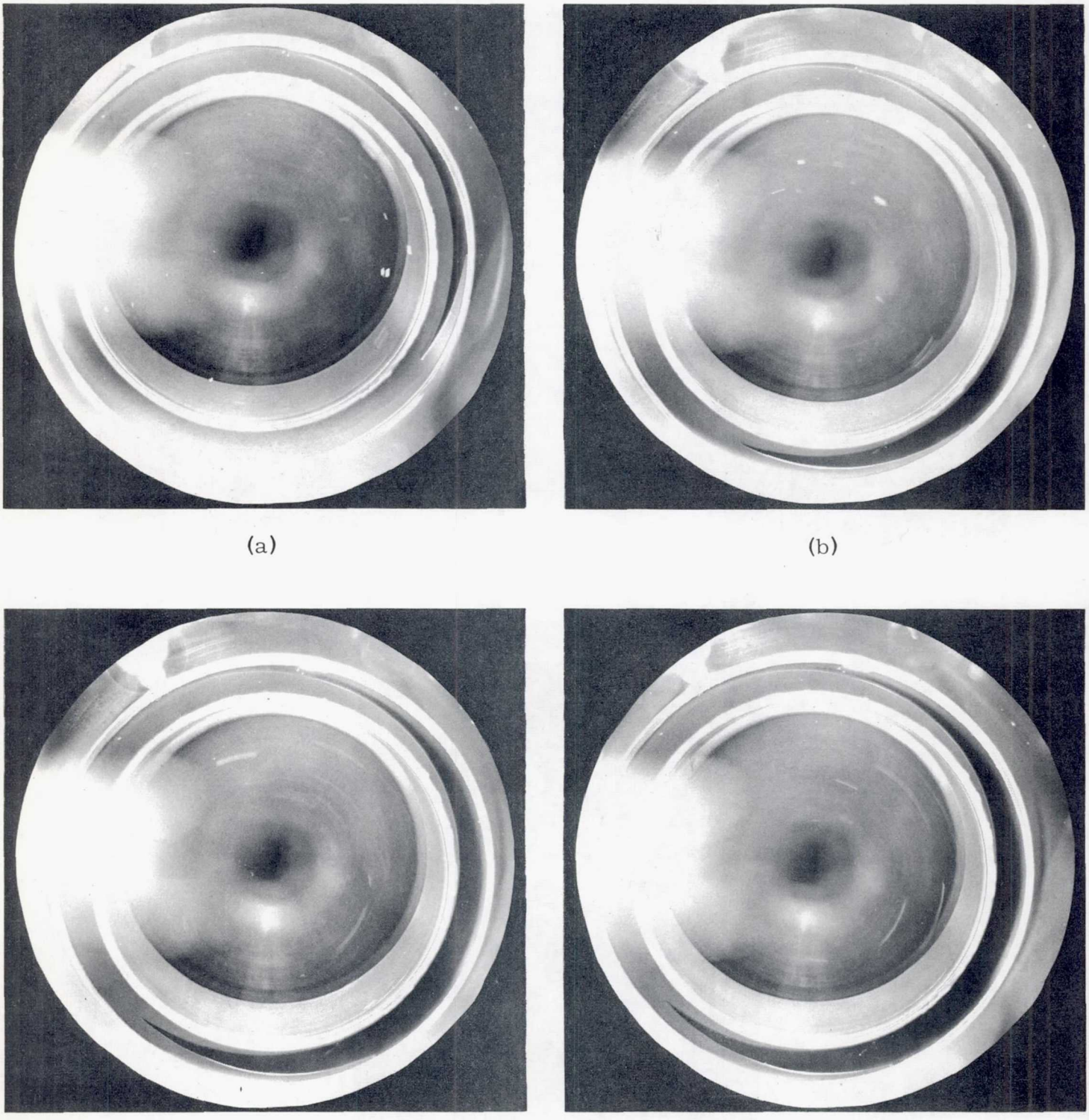

(a) (b)

(c) (d)

Figure 8. Gas Cavities in the Narrow Land Transparent Face Seal, $R_i = 0.83$. (The dark areas are the gas cavities and the light areas oil. Rotation is in the clockwise direction with the minimum film thickness, of the misaligned seal faces, at the left of the photos.) See Table XI.

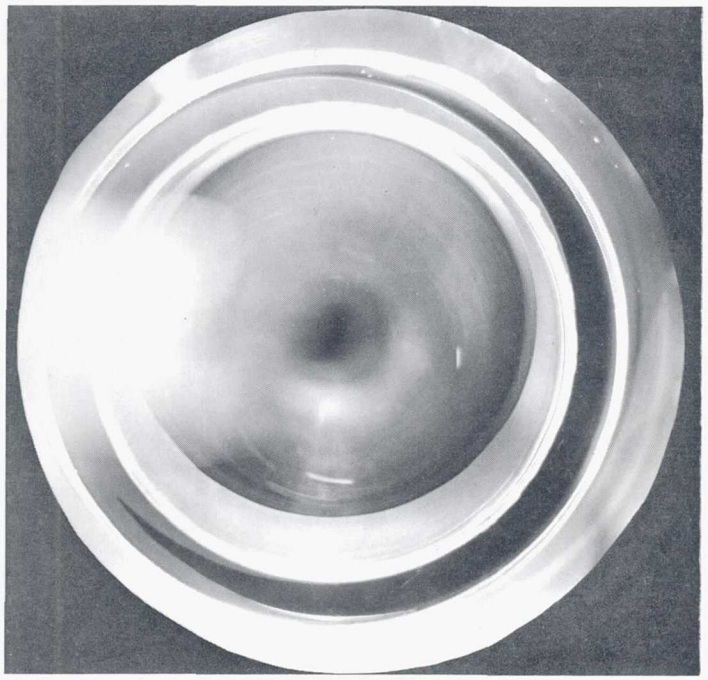

(e)

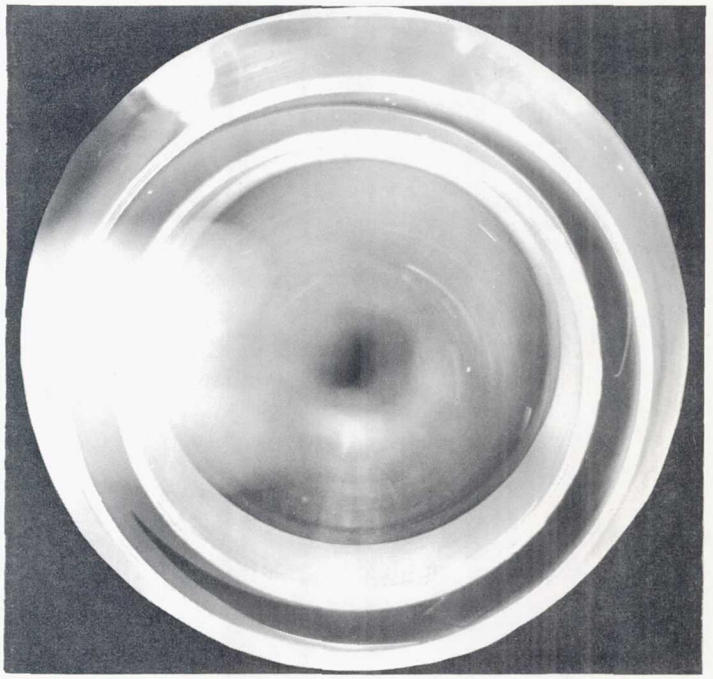

(f)

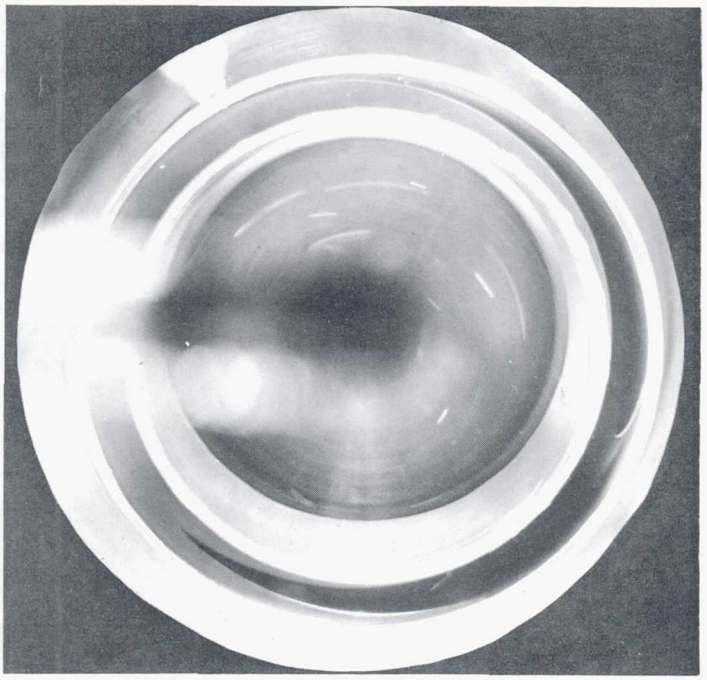

(g)

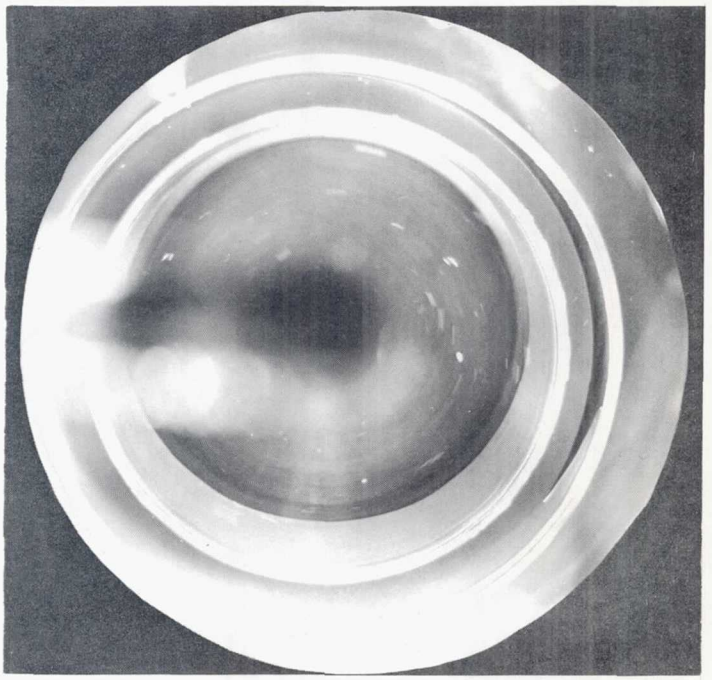

(h)

Figure 8 (Continued)

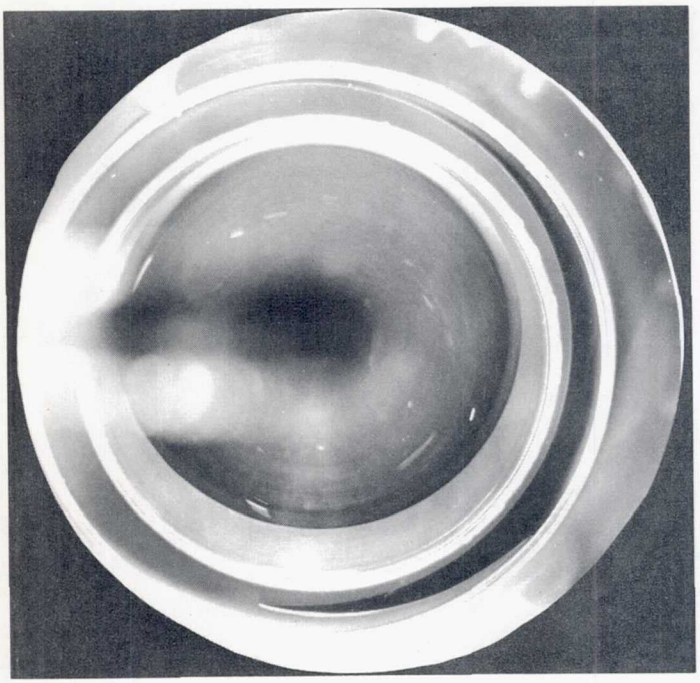

(i)

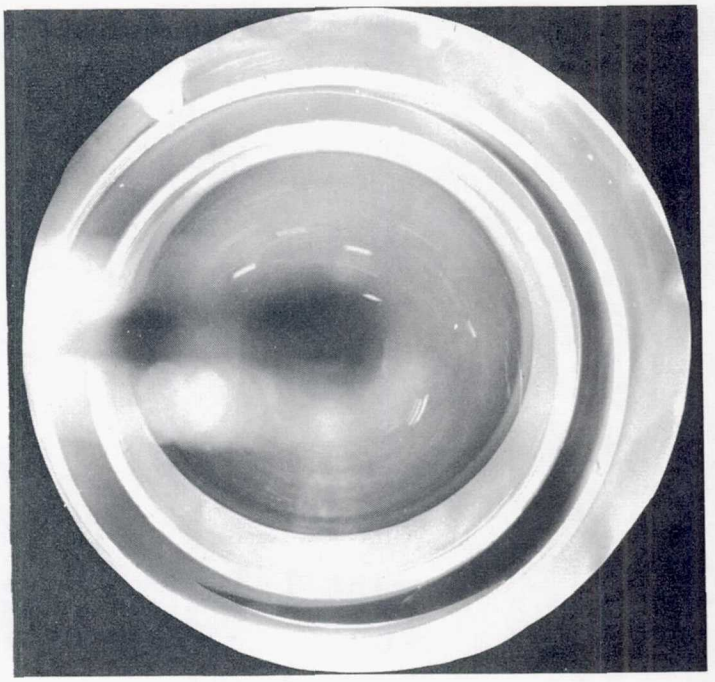

(j)

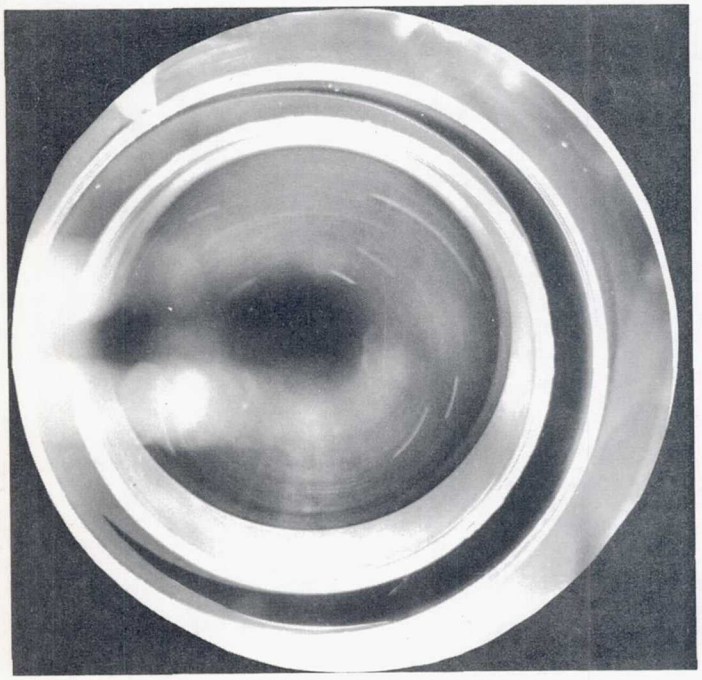

(k)

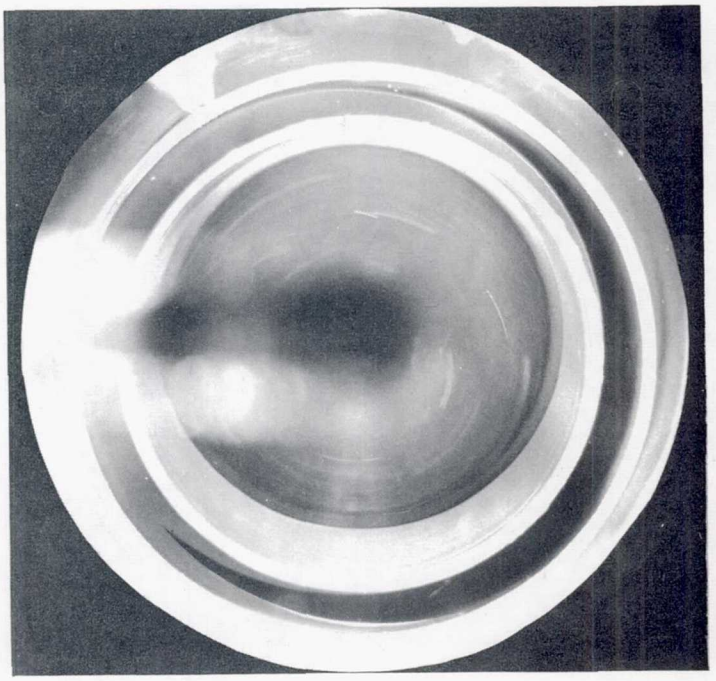

(l)

Figure 8 (Continued)

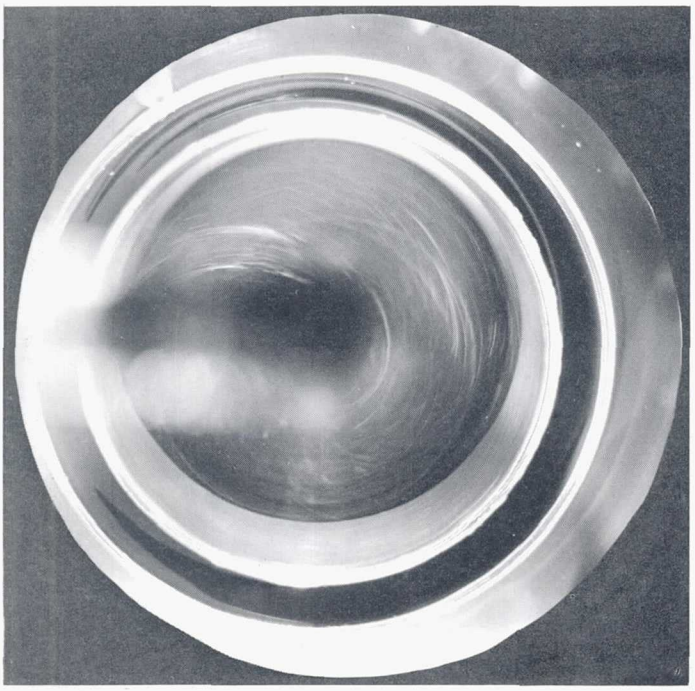

(m)

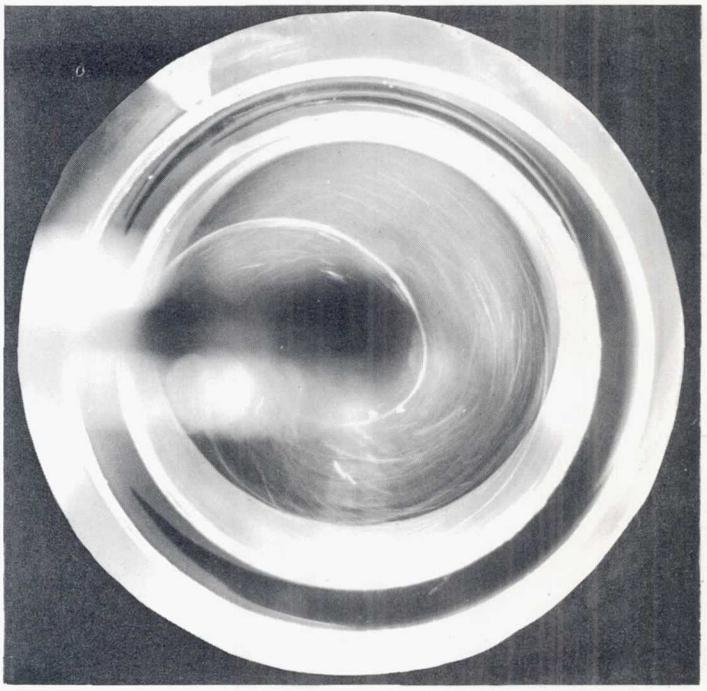

(n)

(o)

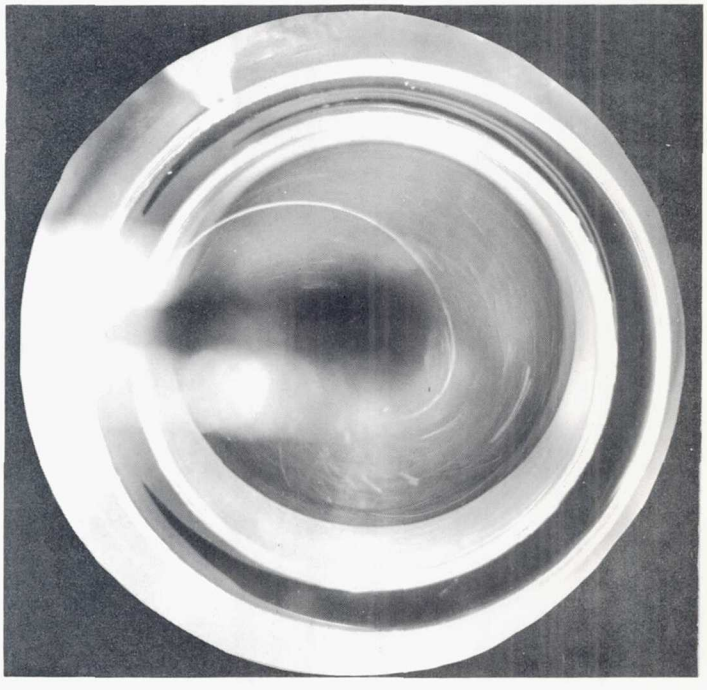

(p)

Figure 8 (Continued)

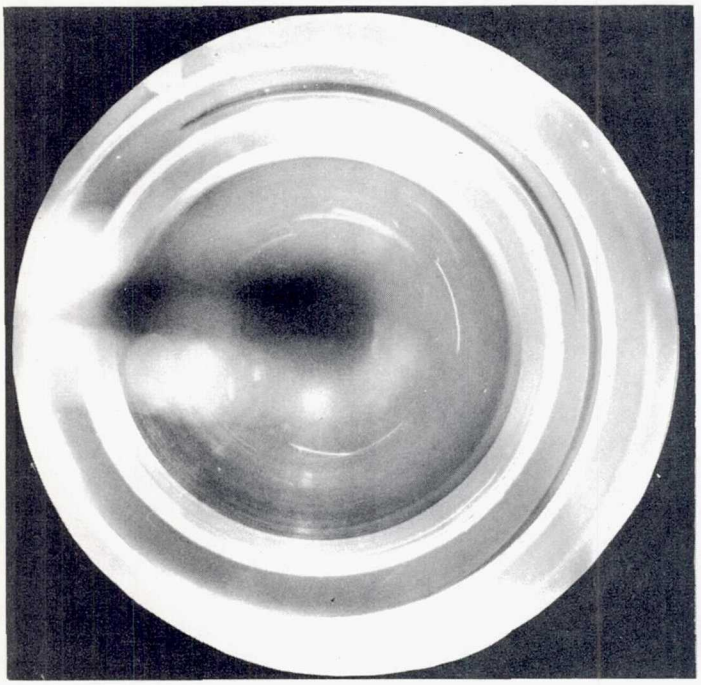

(q)

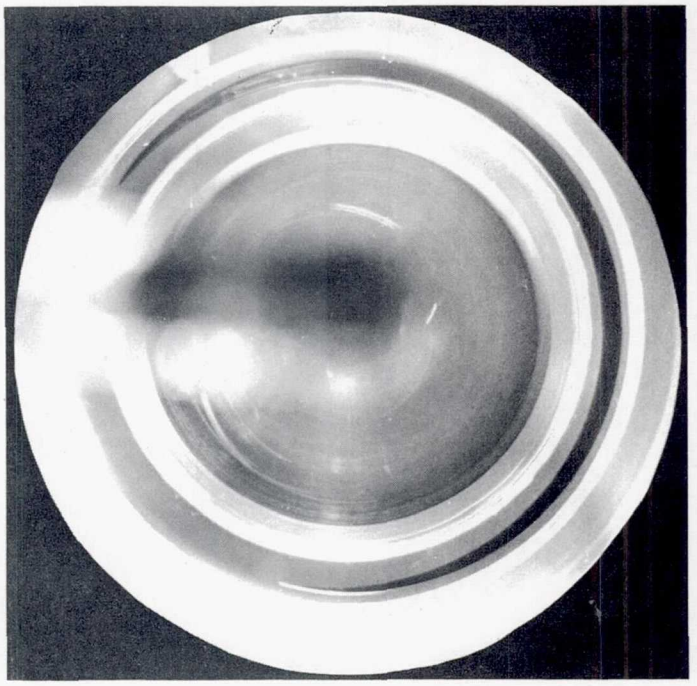

(r)

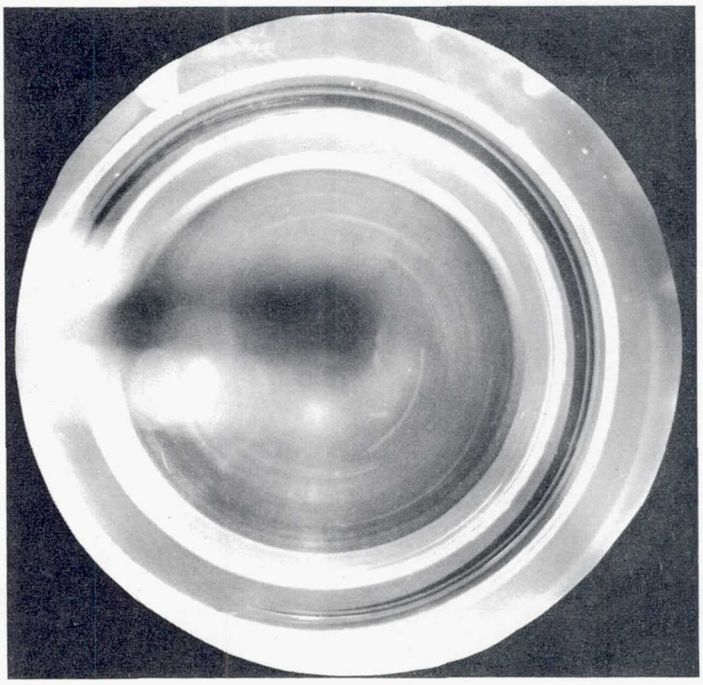

(s)

Figure 8 (Continued)

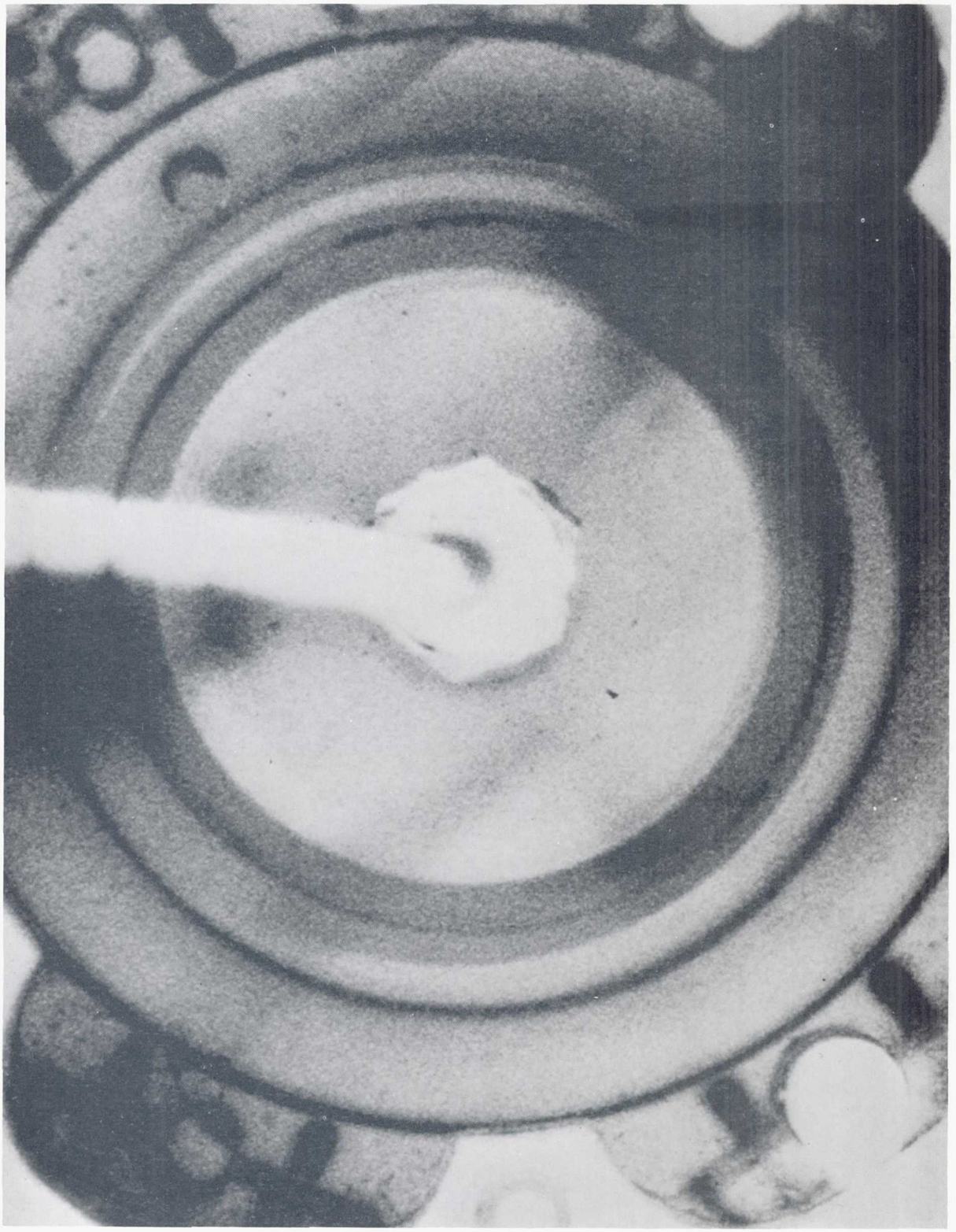

Figure 9. Concentric, Transparent Face Seal Showing Gas Cavity

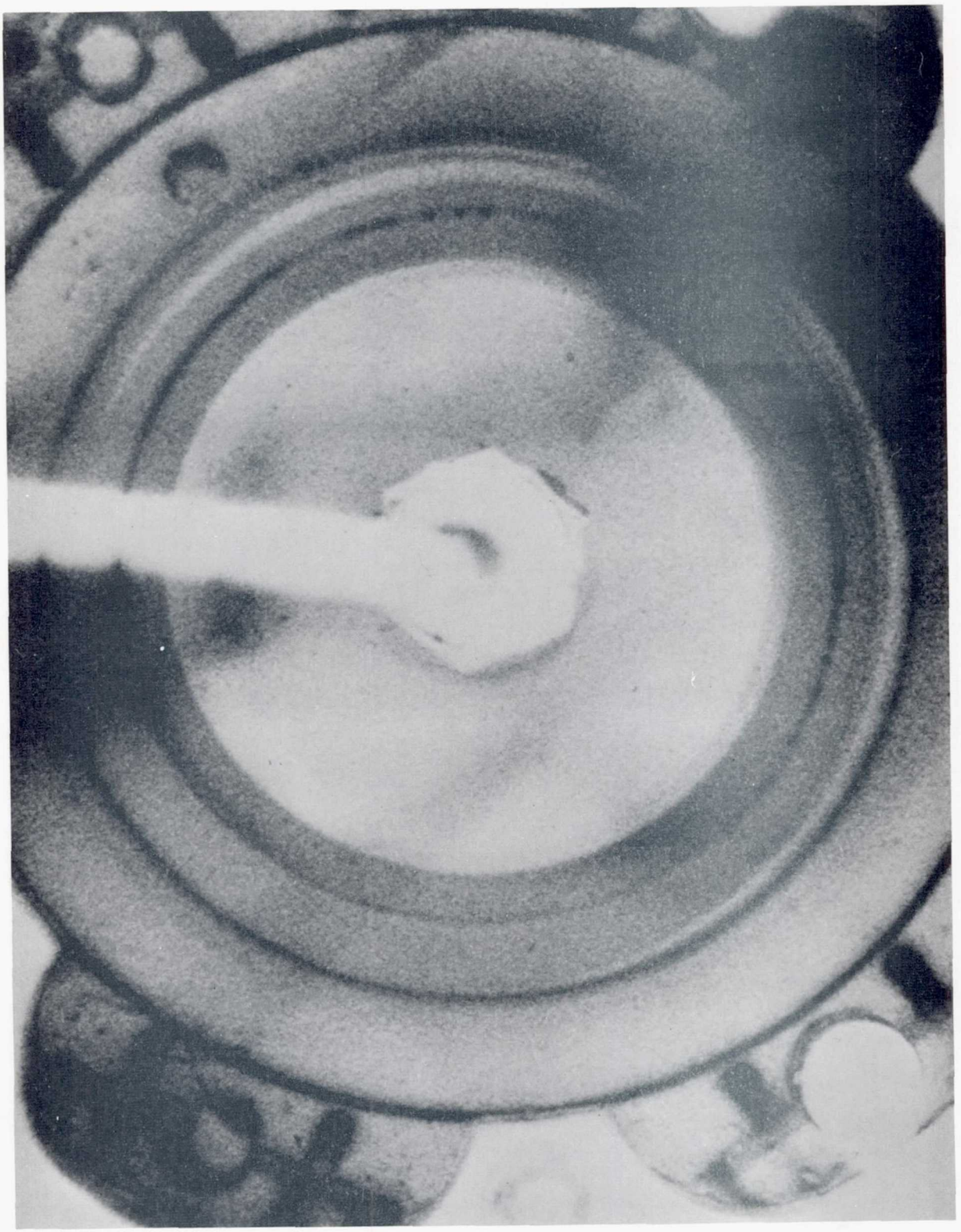

Figure 10. Concentric, Transparent Face Seal Showing Gas Cavity. (Smaller cavity, lower speed)

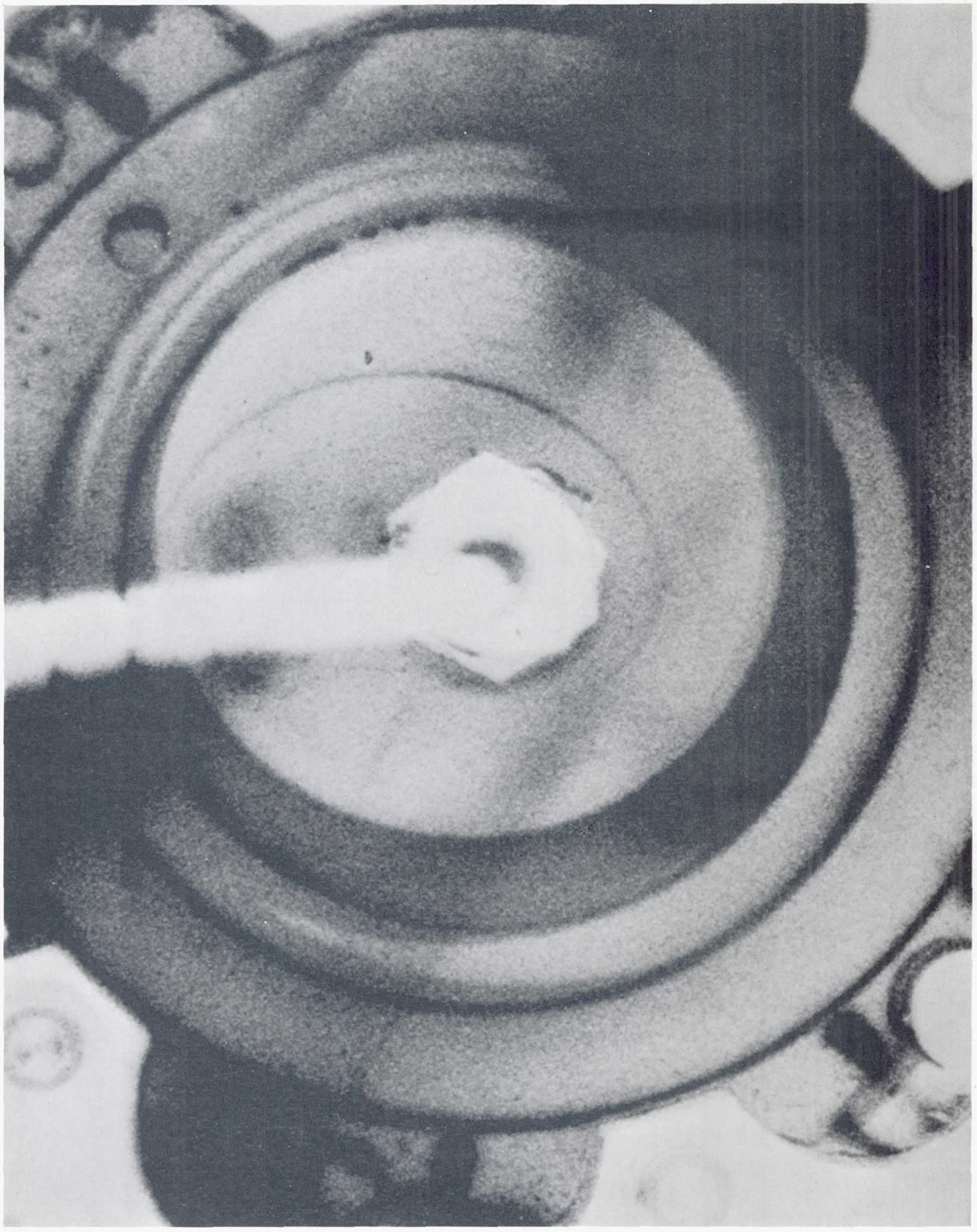

Figure 11. Eccentric, Transparent Face Seal Showing Gas Cavity and Inward Pumping of Air. (Note spiral of bubbles in center)

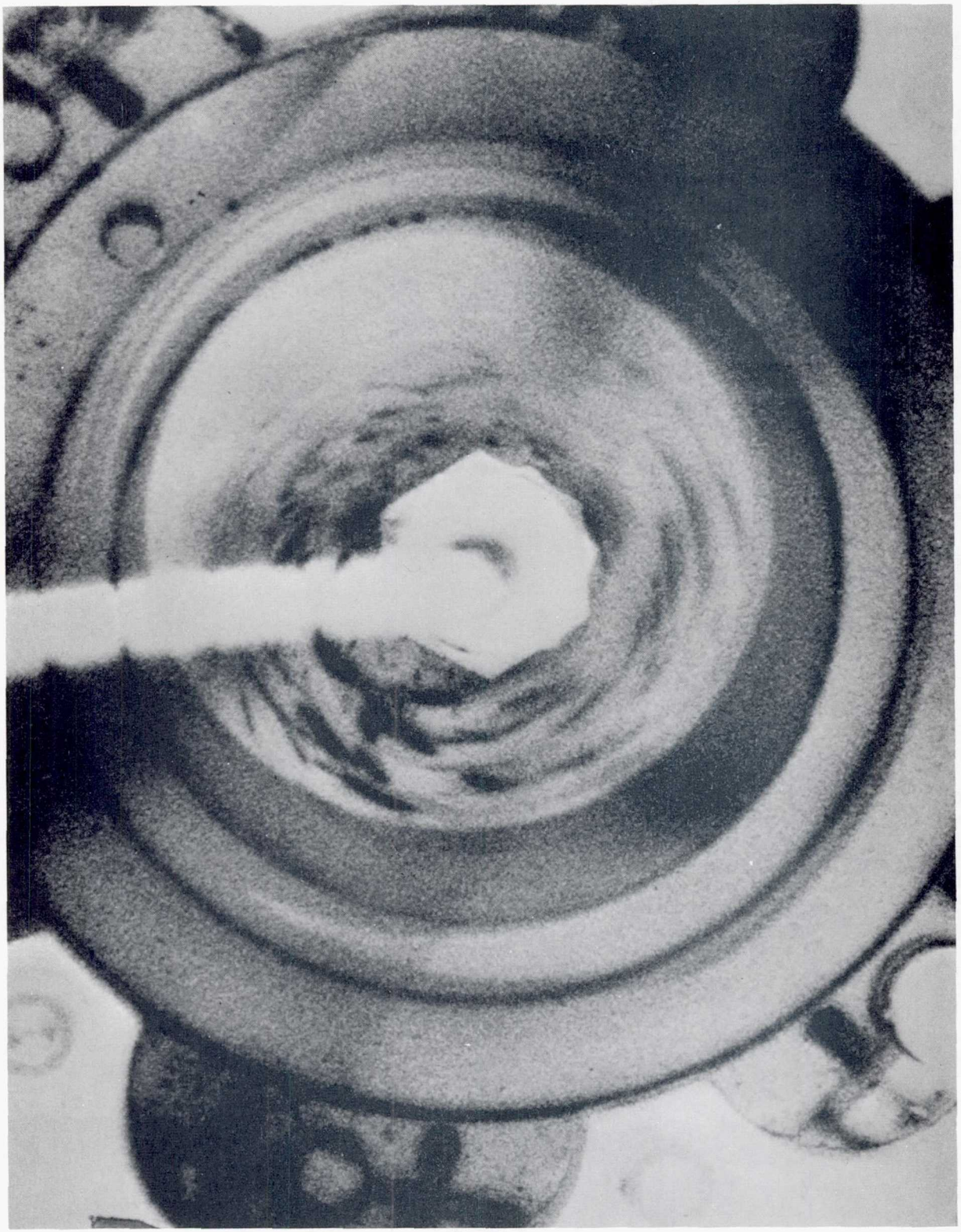

Figure 12. Eccentric, Transparent Face Seal Showing Gas Cavity. (Note many bubbles in center due to higher speed)

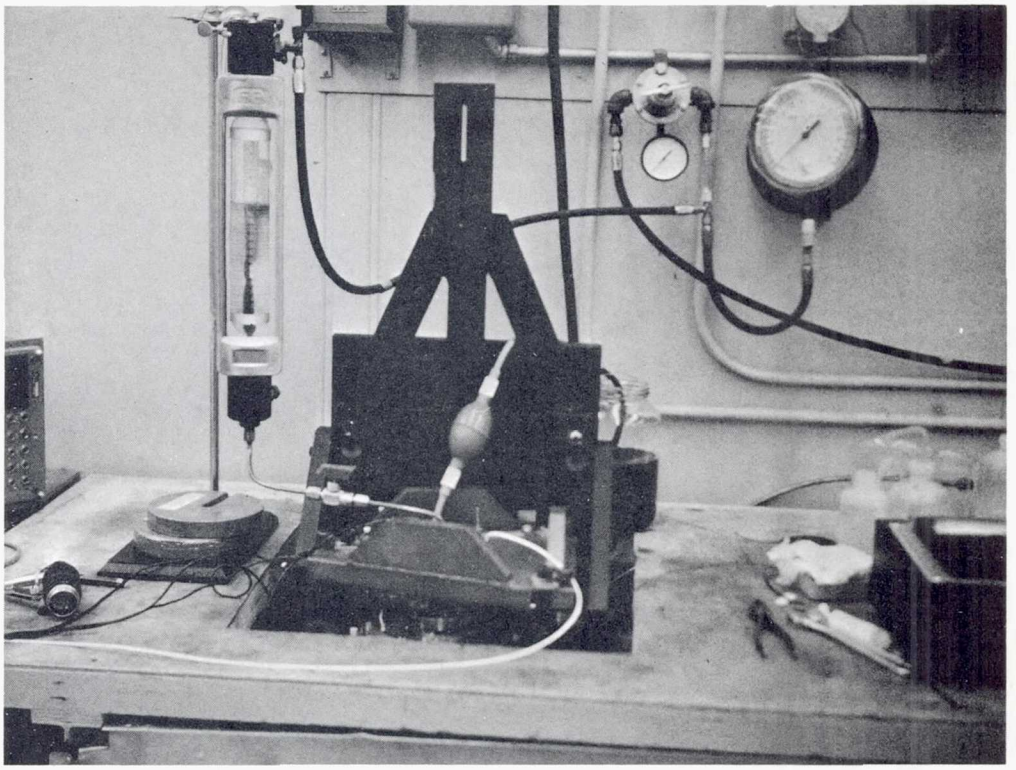

Figure 13. Face Seal Experiment Setup for Flooded Seal

FIGURE 14

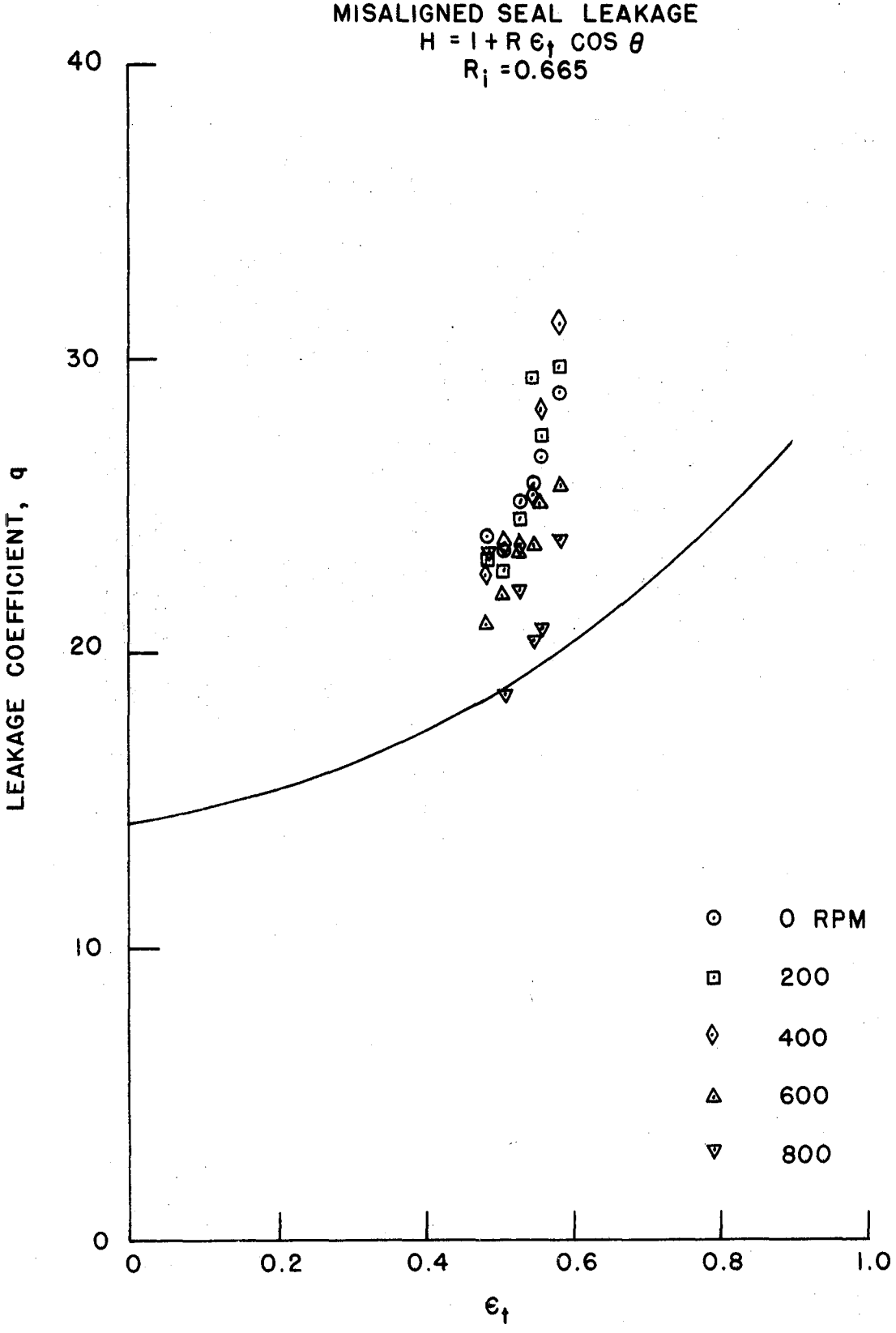
MISALIGNED SEAL LEAKAGE
H = 1 + R ε_t COS θ
R_i = 0.665
LEAKAGE COEFFICIENT, q
40
30
20
10
0
0
0.2
0.4
0.6
0.8
1.0
ε_t
0 RPM
200
400
600
800

FIGURE 15
MISALIGNED SEAL LEAKAGE
$H = 1 + R\epsilon_t \cos\theta$
$R_i = 0.665$

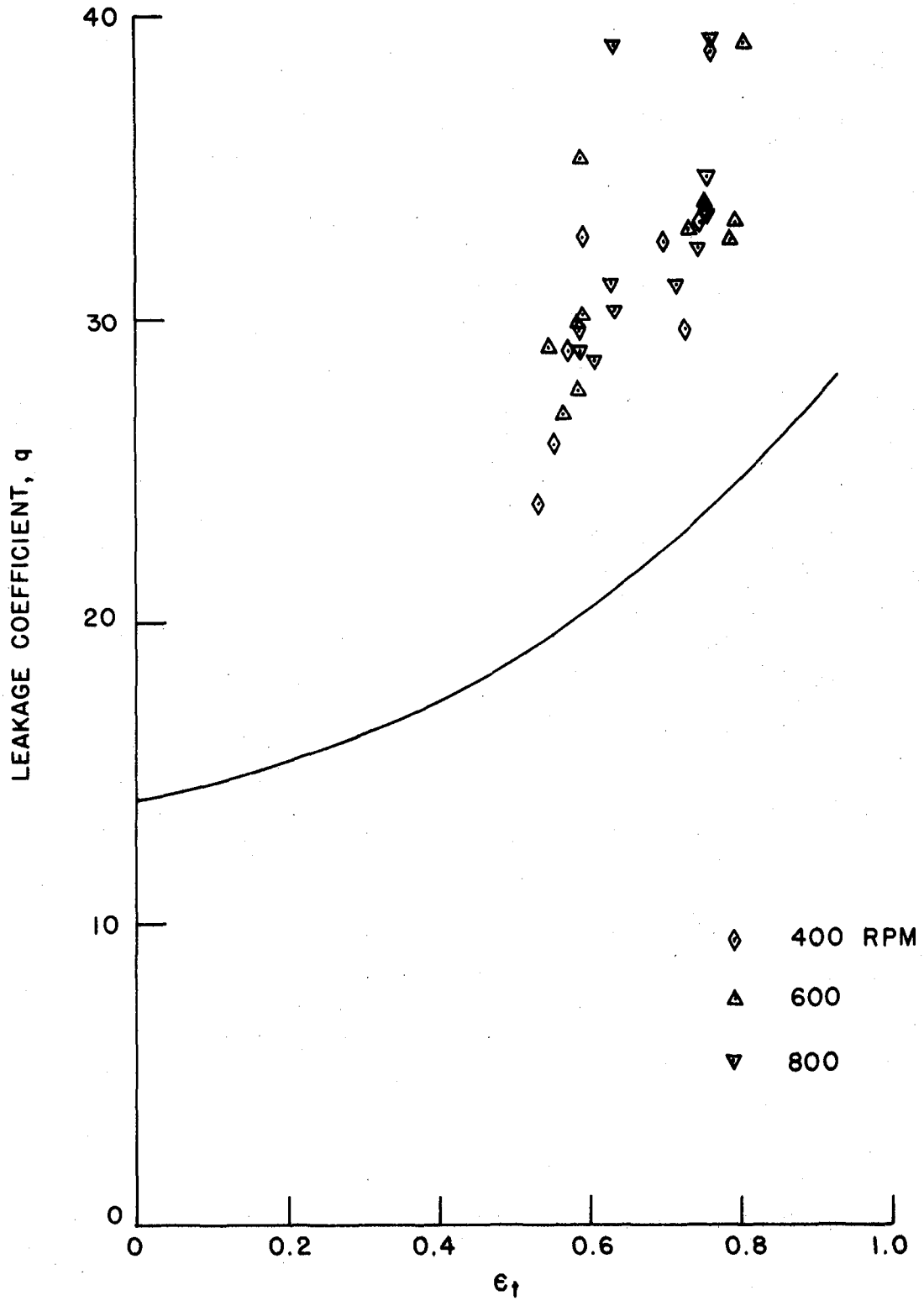

FIGURE 16
MISALIGNED SEAL LEAKAGE
$H = 1 + R\epsilon_t \cos\theta$
$R_i = 0.83$

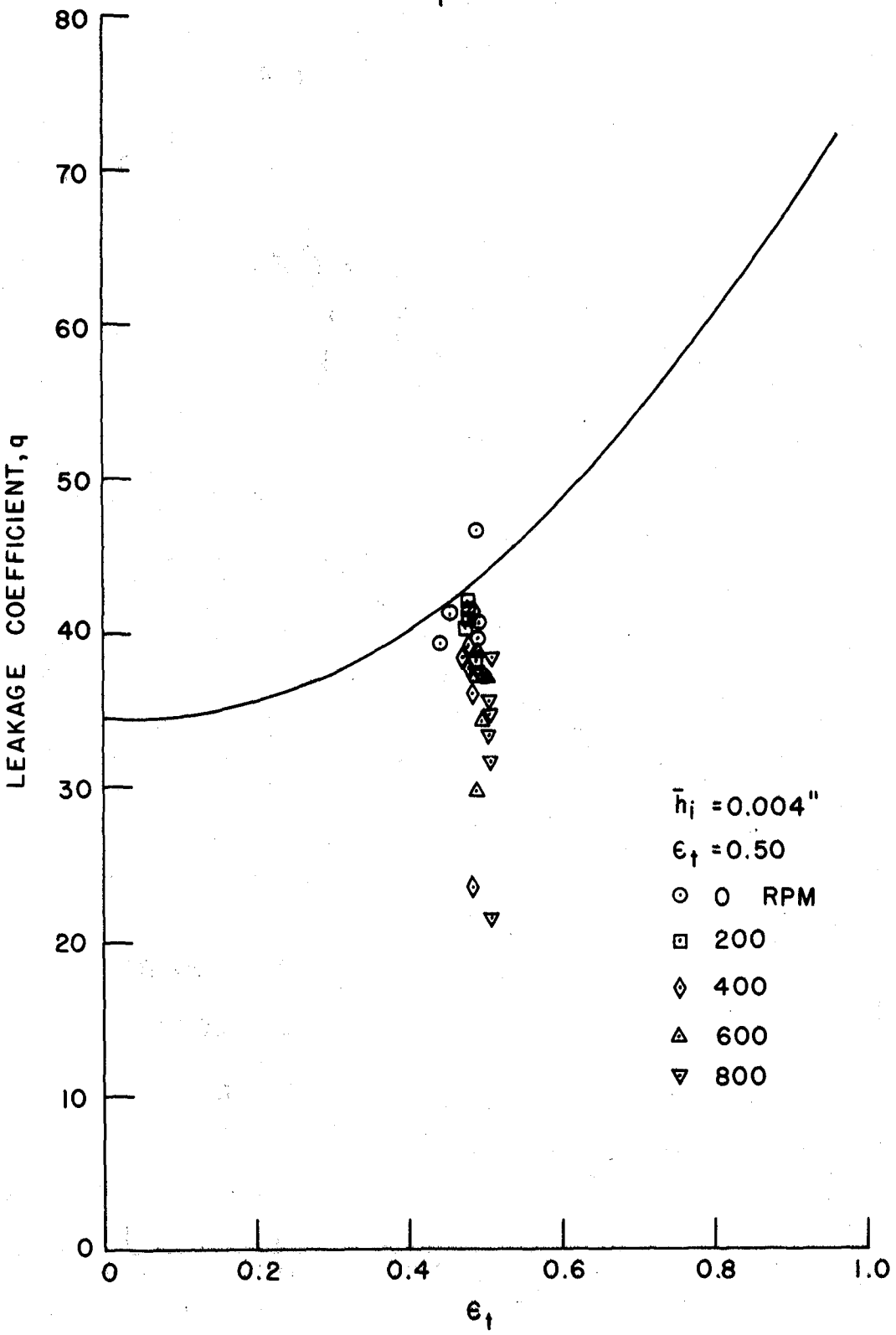

FIGURE 17
MISALIGNED SEAL LEAKAGE
$H = 1 + R\epsilon_t \cos\theta$
$R_i = 0.83$

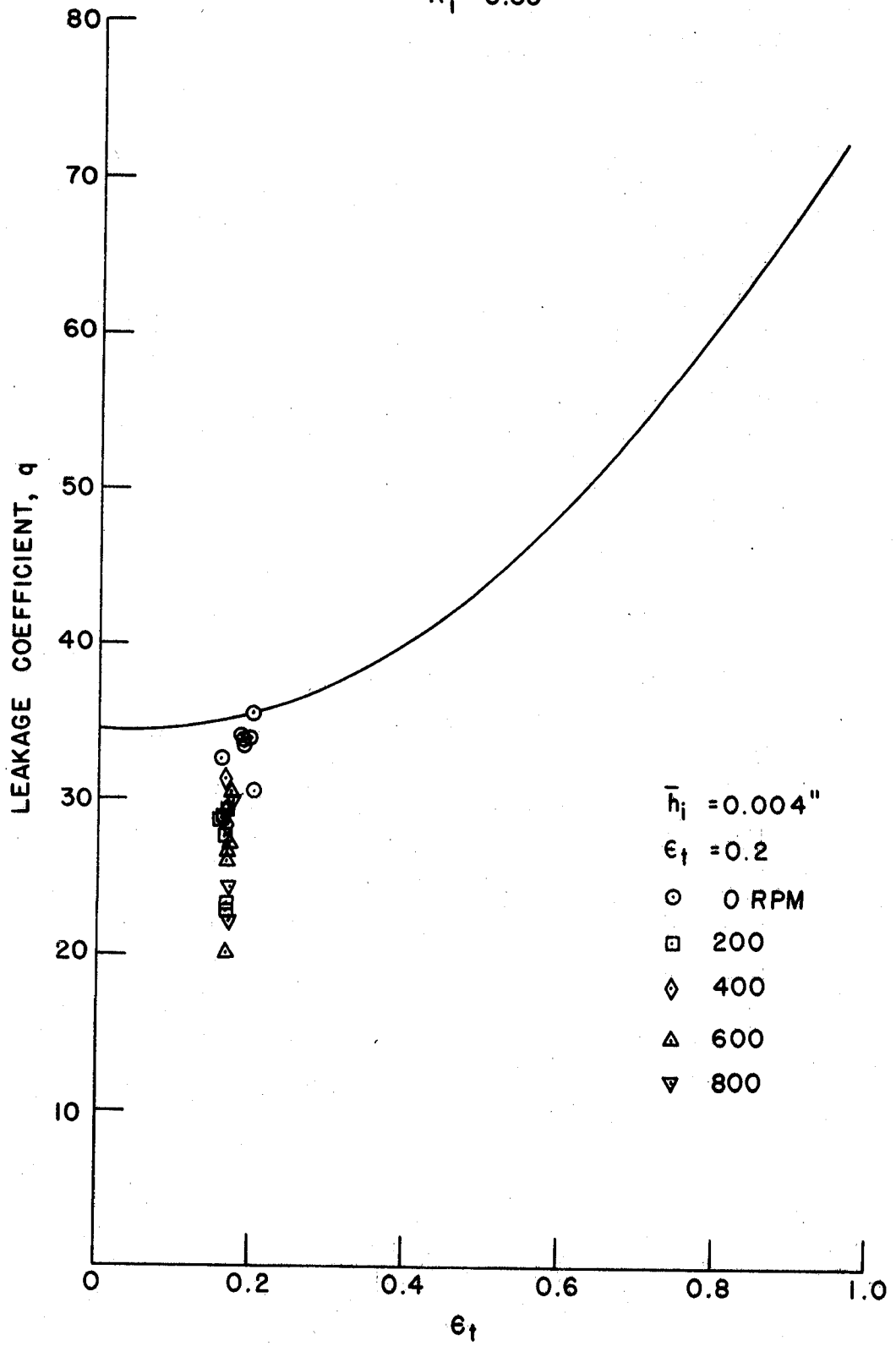

FIGURE 18
MISALIGNED SEAL LEAKAGE
$H = 1 + R\,\epsilon_t \cos\theta$
$R_1 = 0.83$

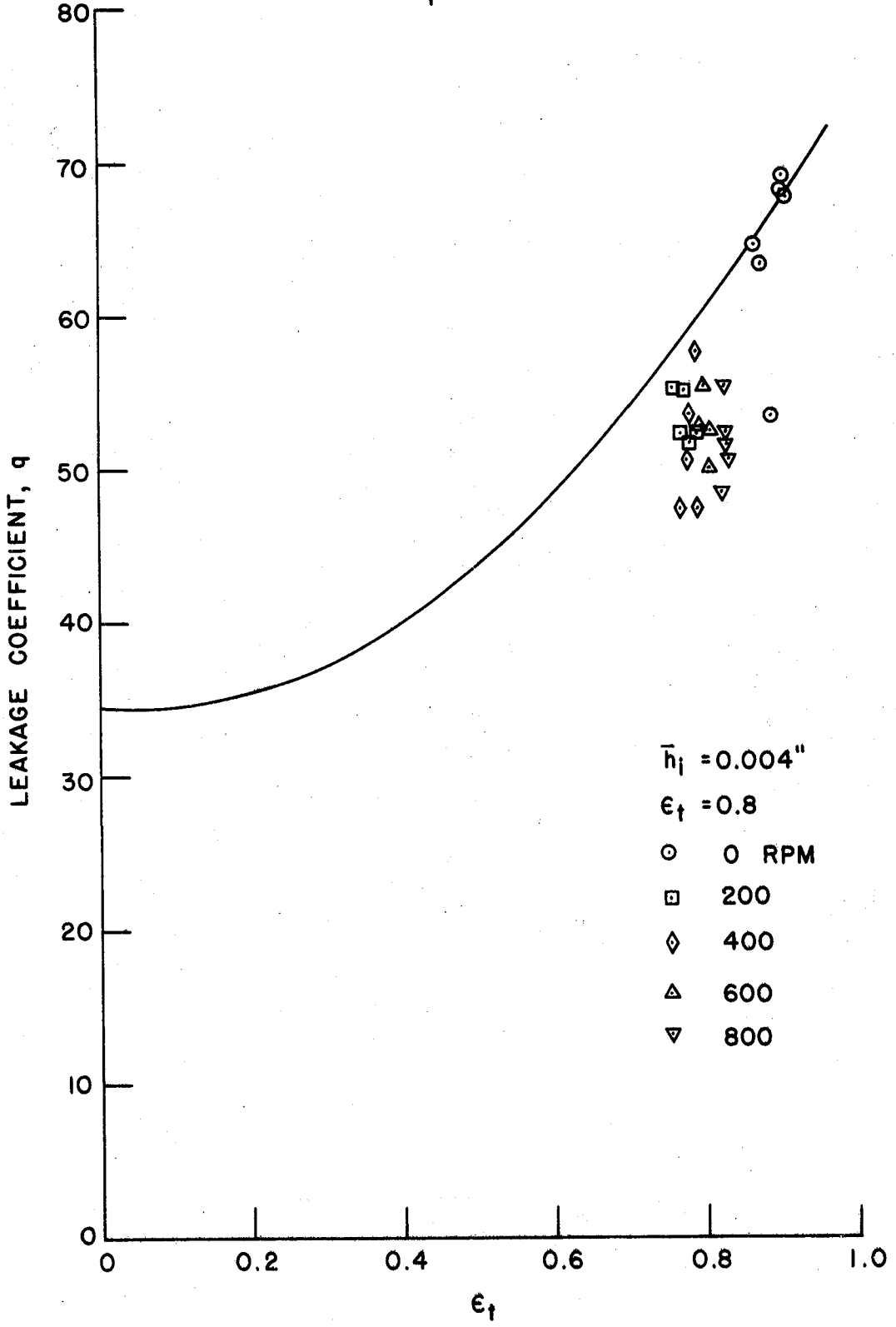

FIGURE 19
MISALIGNED SEAL LEAKAGE
$H = 1 + R\,\epsilon_t \cos\theta$
$R_i = 0.83$

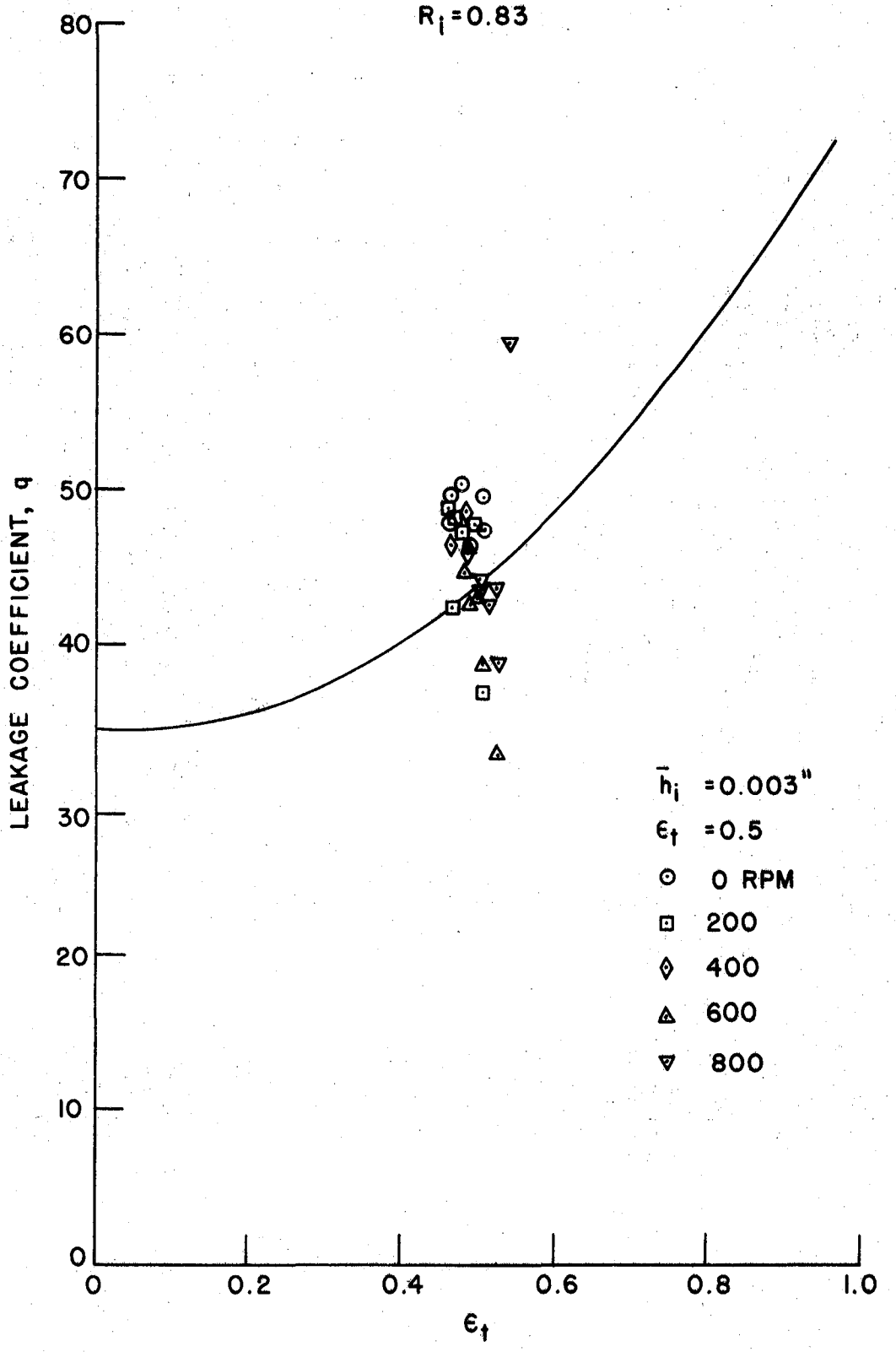

FIGURE 20

MISALIGNED SEAL LEAKAGE

$H = 1 + R\epsilon_t \cos\theta$

$R_j = 0.83$

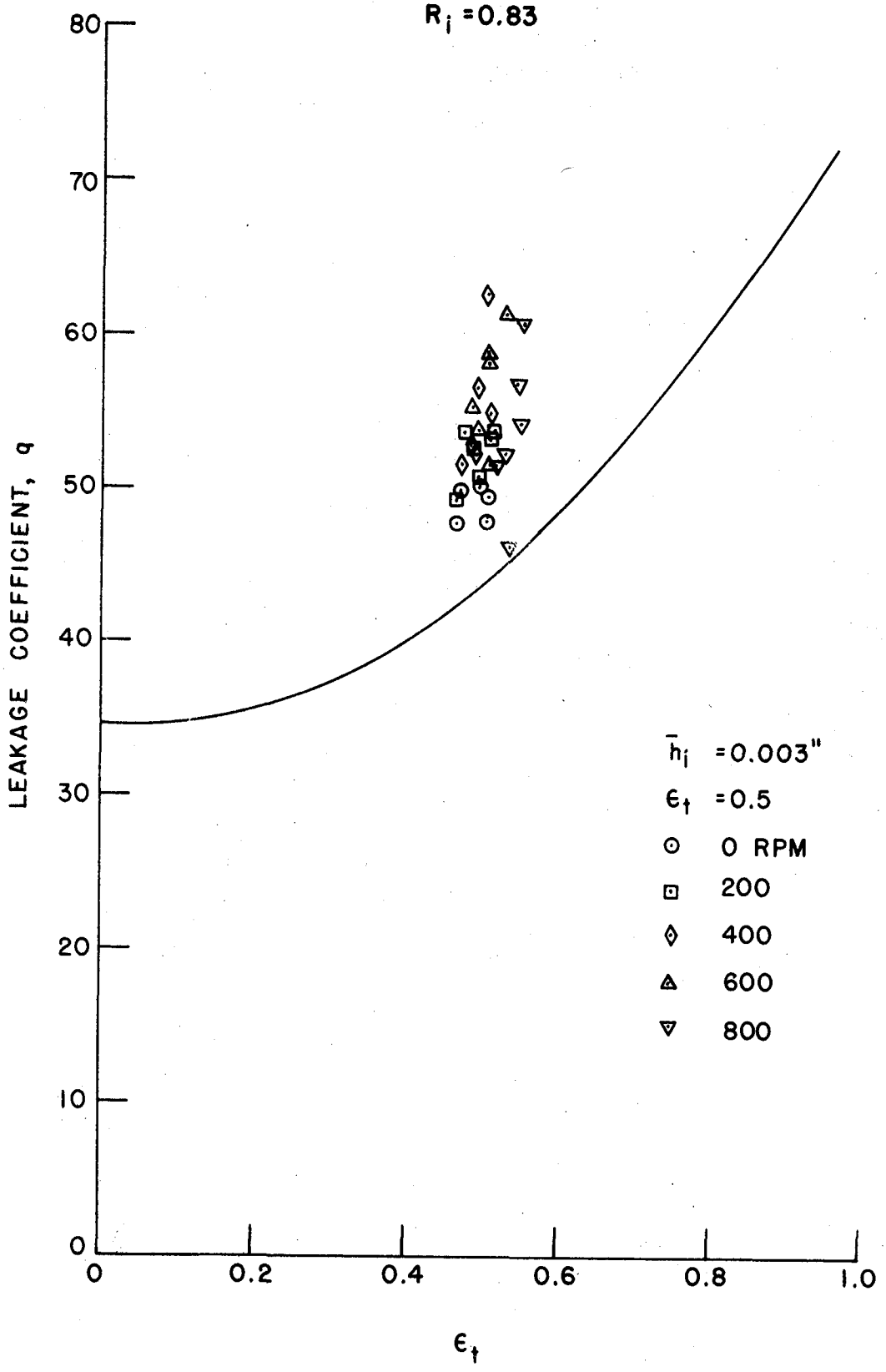

FIGURE 21
OUTWARD PUMPING
DUE TO
RADIAL ECCENTRICITY
(NO CAVITY)

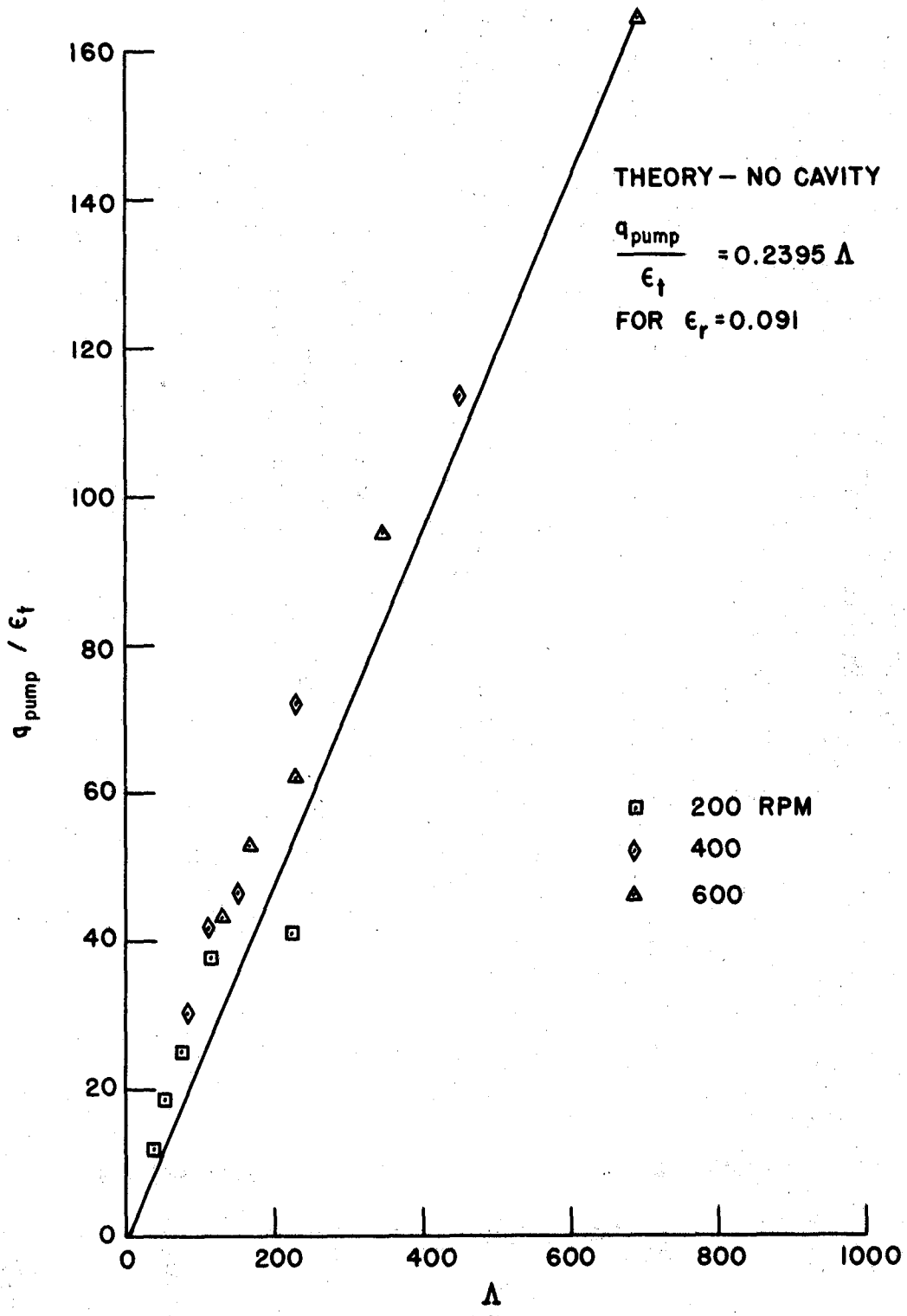

FIGURE 22
LEAKAGE COEFFICIENT
SHOWING THE EFFECTS
OF INWARD PUMPING

$\epsilon_r = 0.091 \quad \epsilon_t = 0.518$
(NO CAVITY)

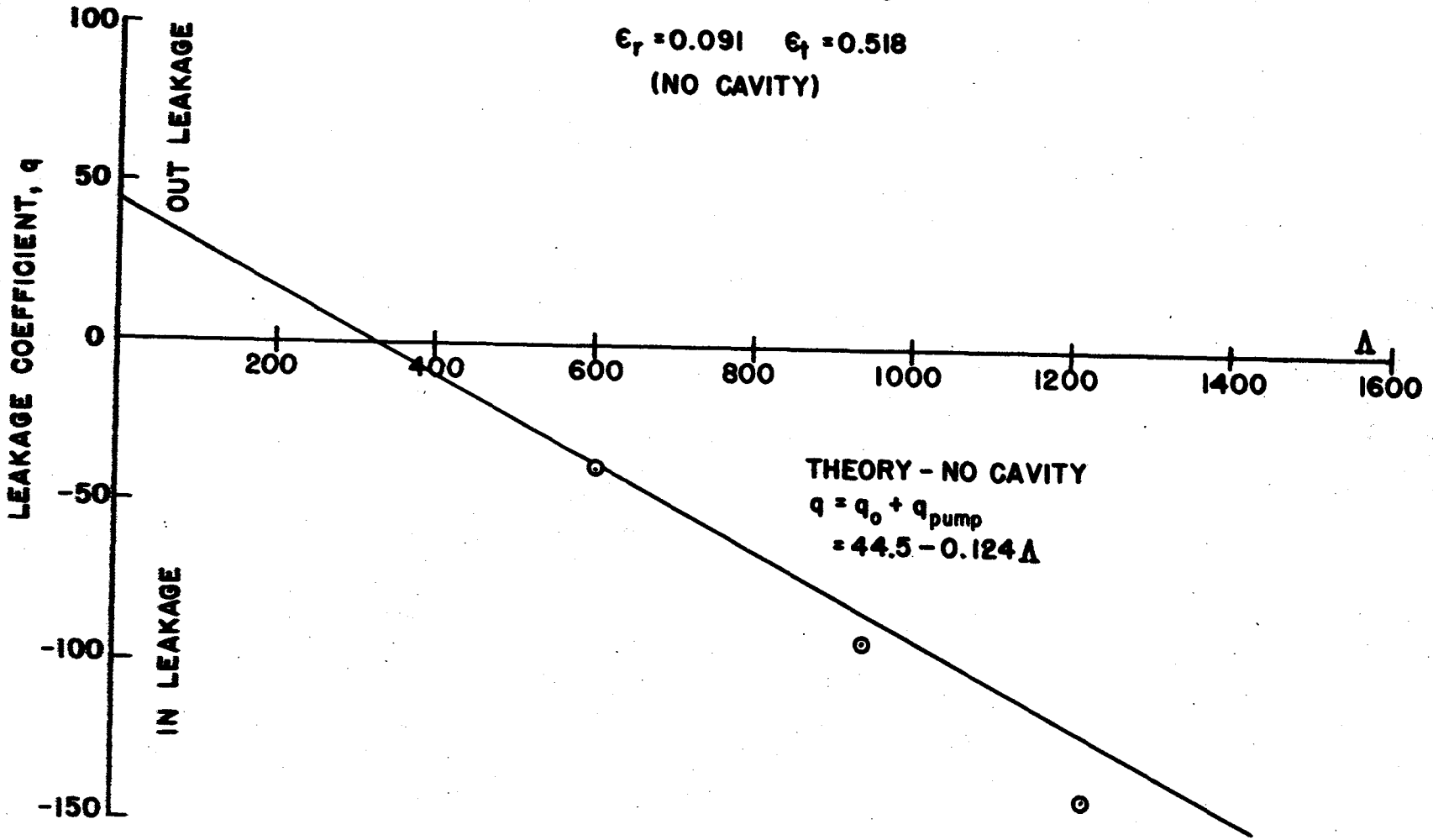

FIGURE 23

CORRELATION OF INWARD AND OUTWARD PUMPING EFFECTS DUE TO SEAL ECCENTRICITY (NO CAVITY)

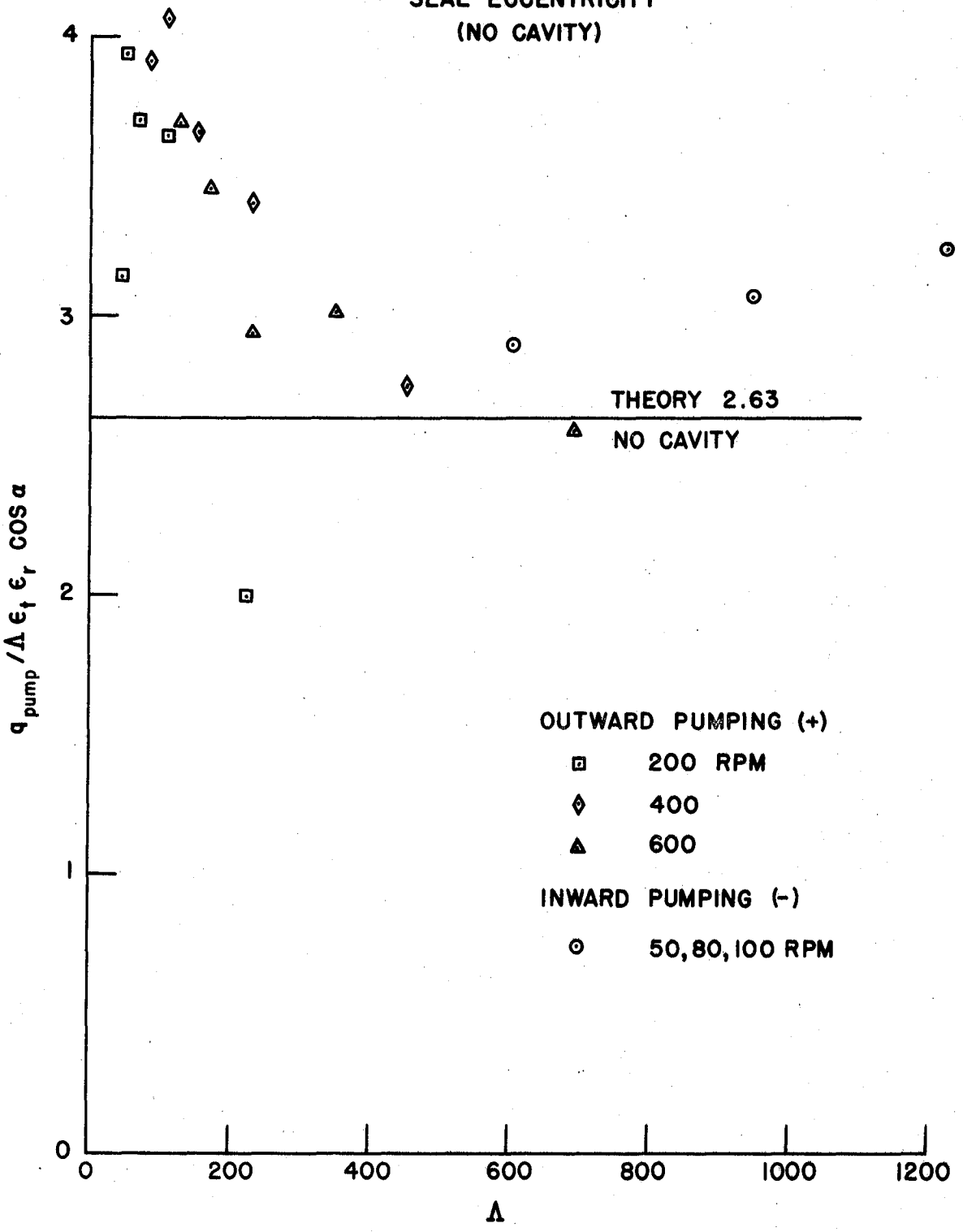

FIGURE 24

PUMPING COEFFICIENT

FOR

ECCENTRIC FACE SEAL

WITH CAVITIES

$R_i = 0.83$, $\epsilon_r = 0.091$

$\bar{h}_i = 0.004"$, $\epsilon_t = 0.50$

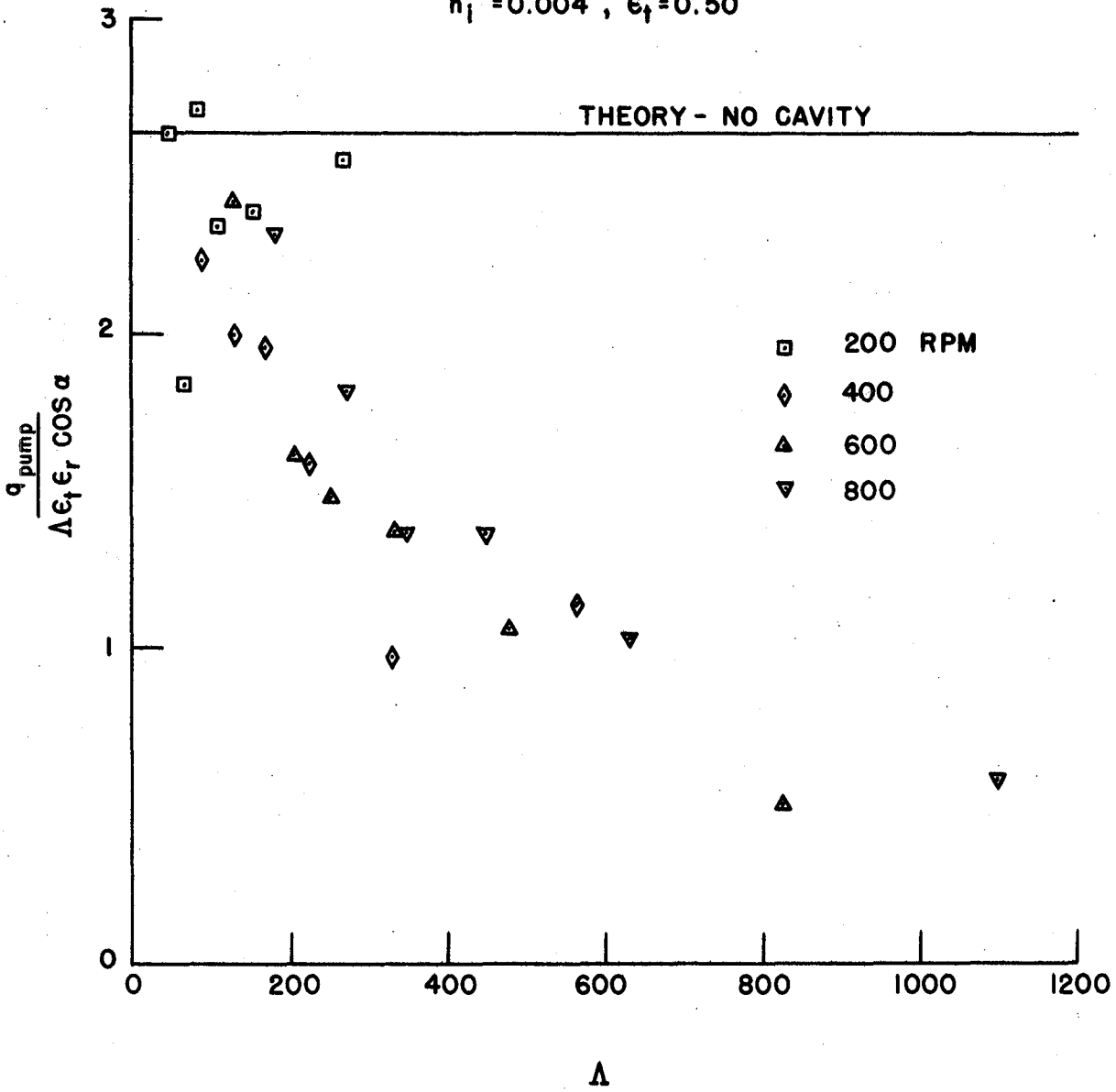

FIGURE 25
PUMPING COEFFICIENT
FOR
ECCENTRIC FACE SEAL
WITH CAVITIES
$R_i = 0.83$, $\epsilon_r = 0.091$
$\bar{h}_i = 0.004"$, $\epsilon_t = 0.50$

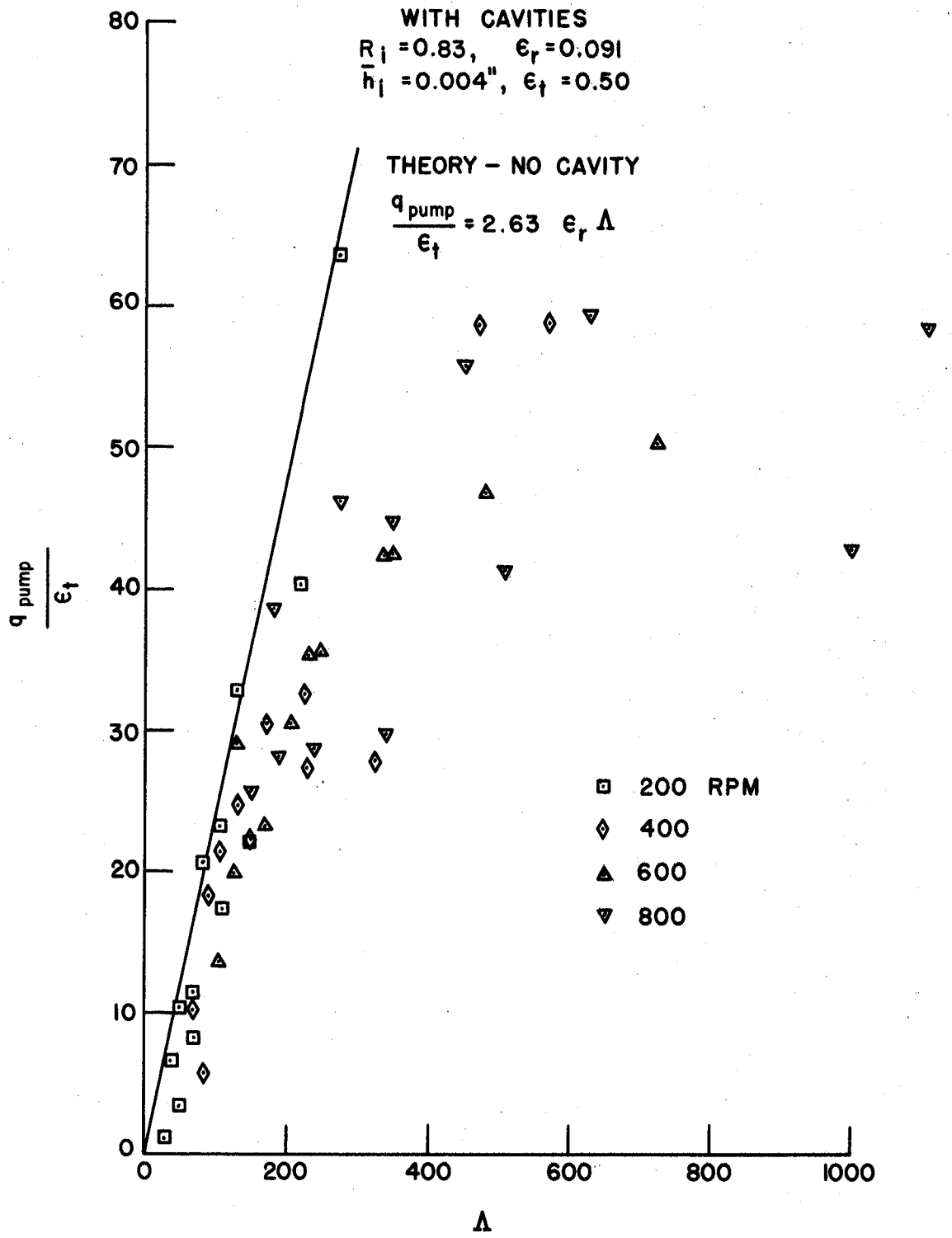

FIGURE 26
PUMPING COEFFICIENT
FOR
ECCENTRIC FACE SEAL
WITH CAVITIES
$R_i = 0.83$, $\epsilon_r = 0.091$
$\bar{h}_i = 0.003''$, $\epsilon_t = 0.50$

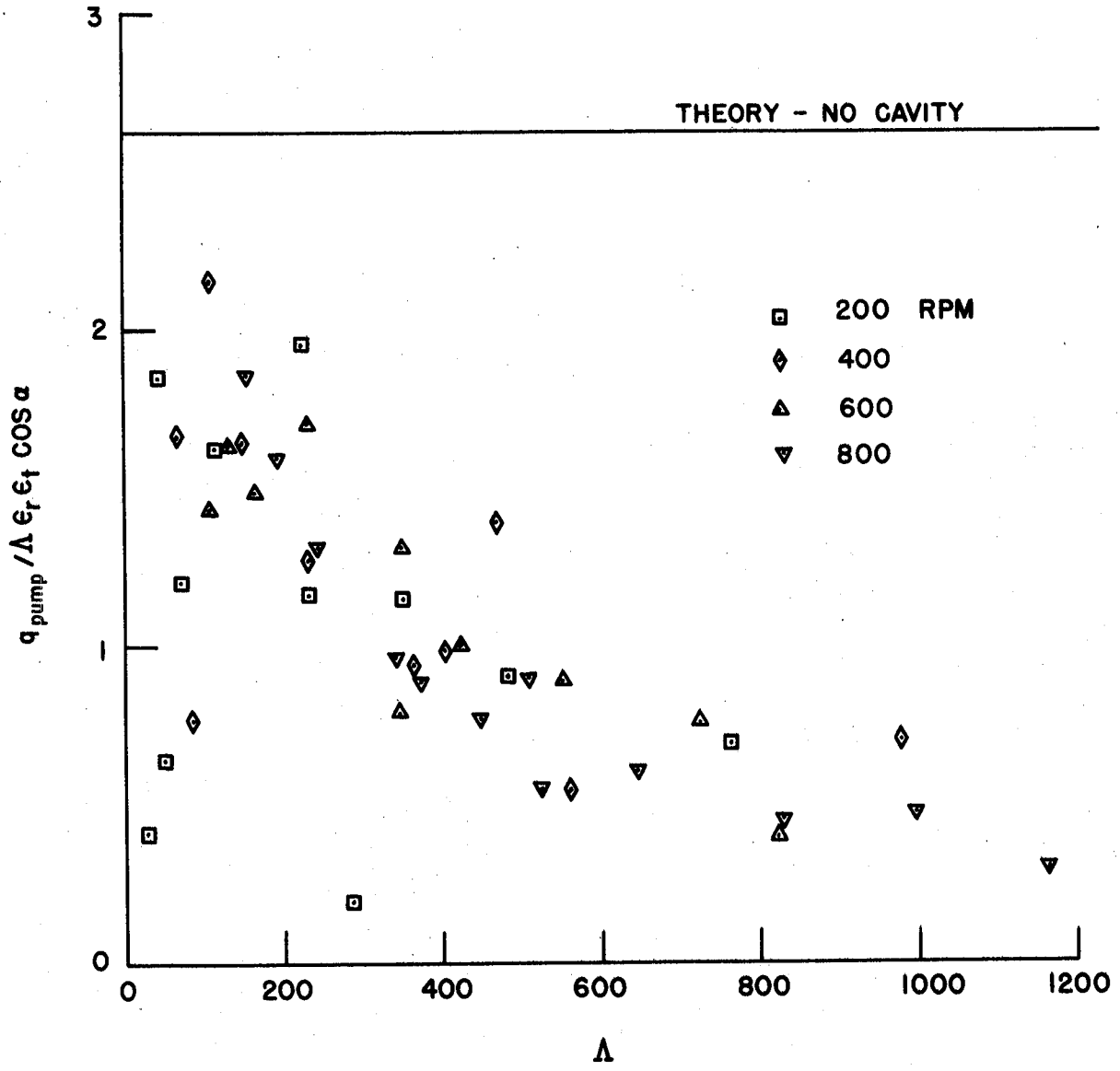

FIGURE 27
LEAKAGE COEFFICIENT
FOR
ECCENTRIC FACE SEAL
WITH CAVITIES
$R_1 = 0.83$, $\epsilon_r = 0.091$
$\bar{h}_1 = 0.001"$, $\epsilon_t = 0.50$

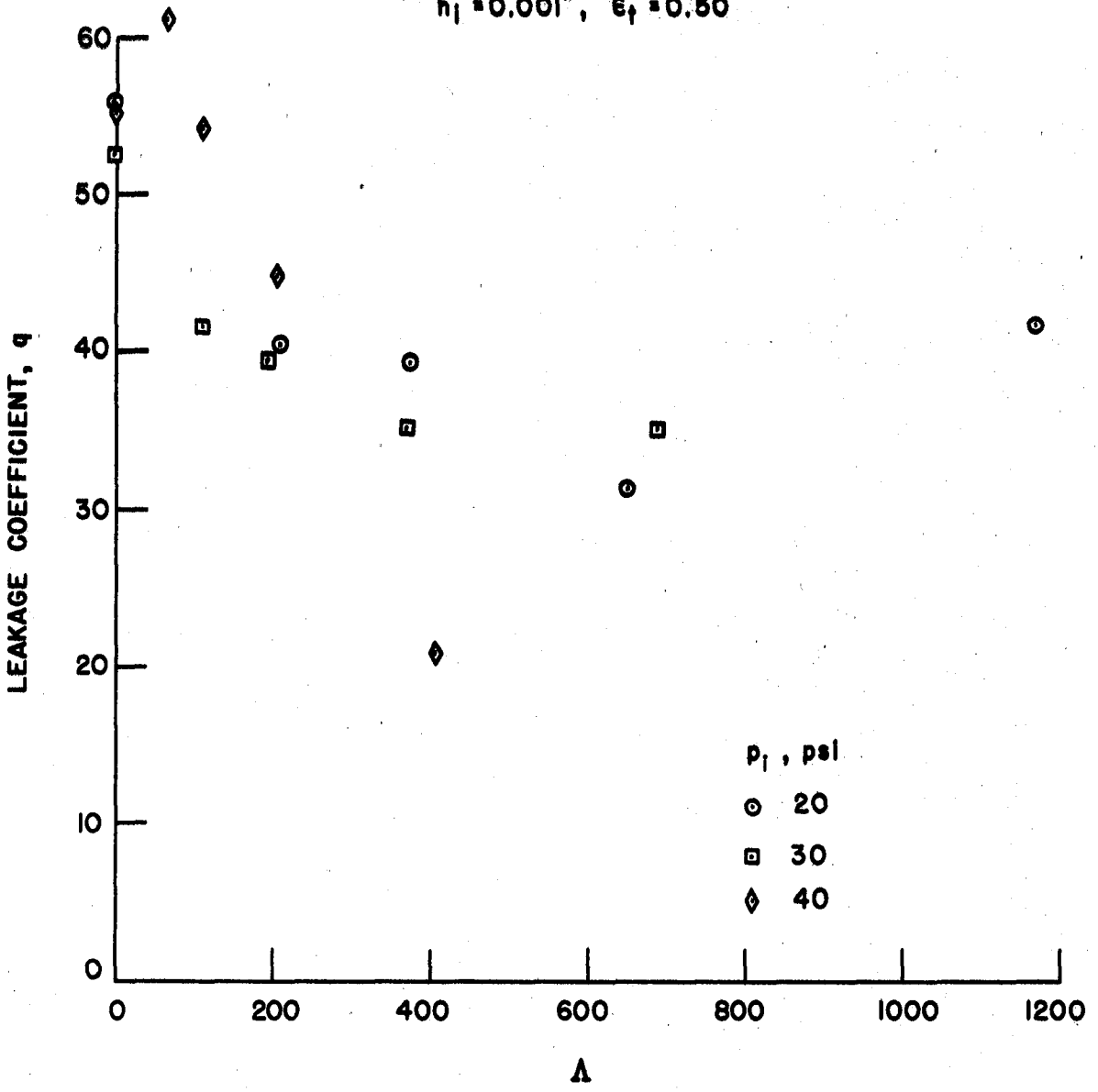

FIGURE 28
PUMPING COEFFICIENT
FOR
ECCENTRIC FACE SEAL
WITH CAVITIES
$R_i = 0.83$, $\epsilon_r = 0.091$
$\bar{h}_i = 0.003"$, $\epsilon_t = 0.80$

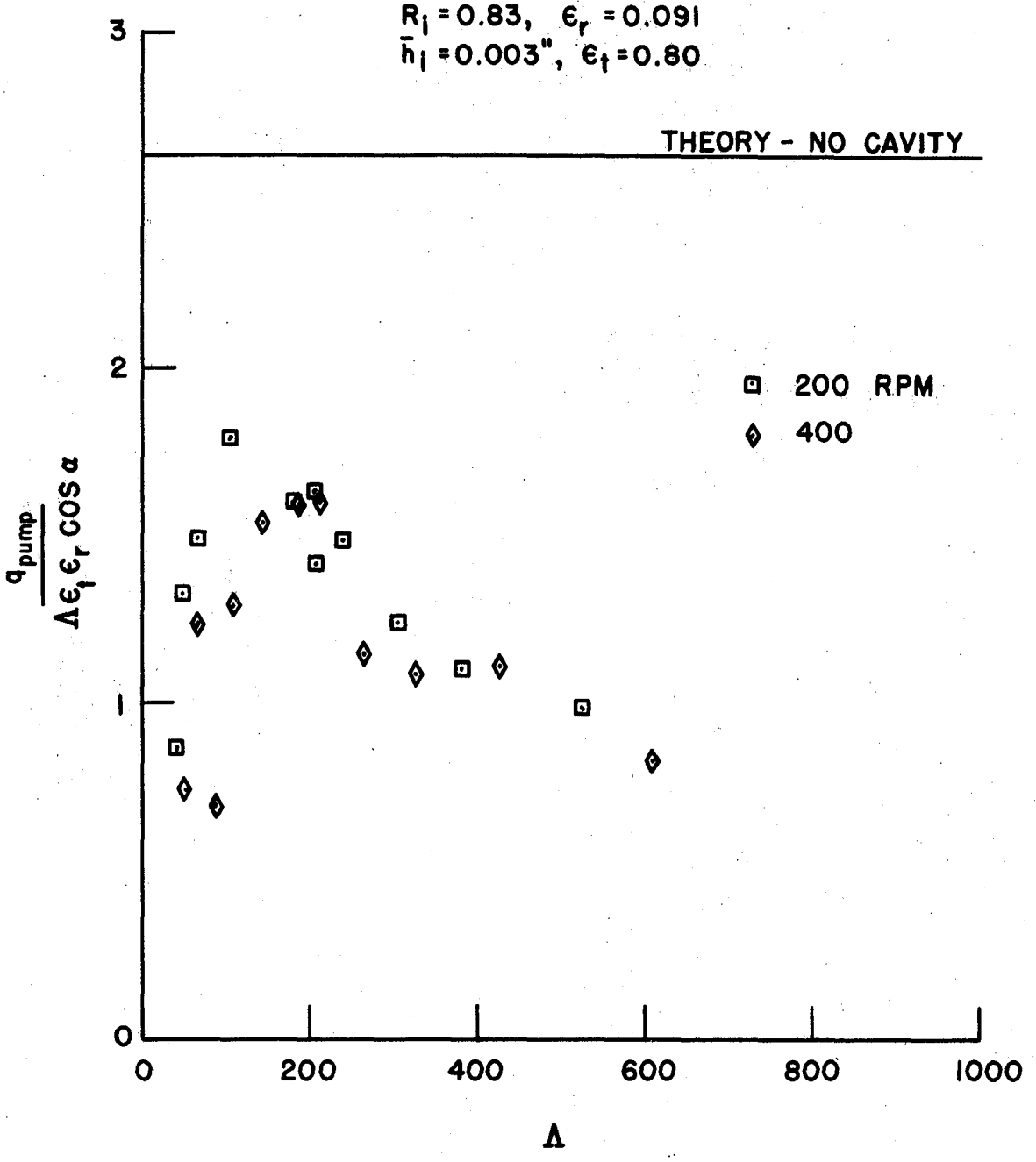

FIGURE 29
PUMPING COEFFICIENT
FOR
ECCENTRIC FACE SEAL
WITH CAVITIES
$R_i = 0.83$, $\epsilon_r = 0.091$
$\bar{h}_i = 0.003"$, $\epsilon_t = 0.20$

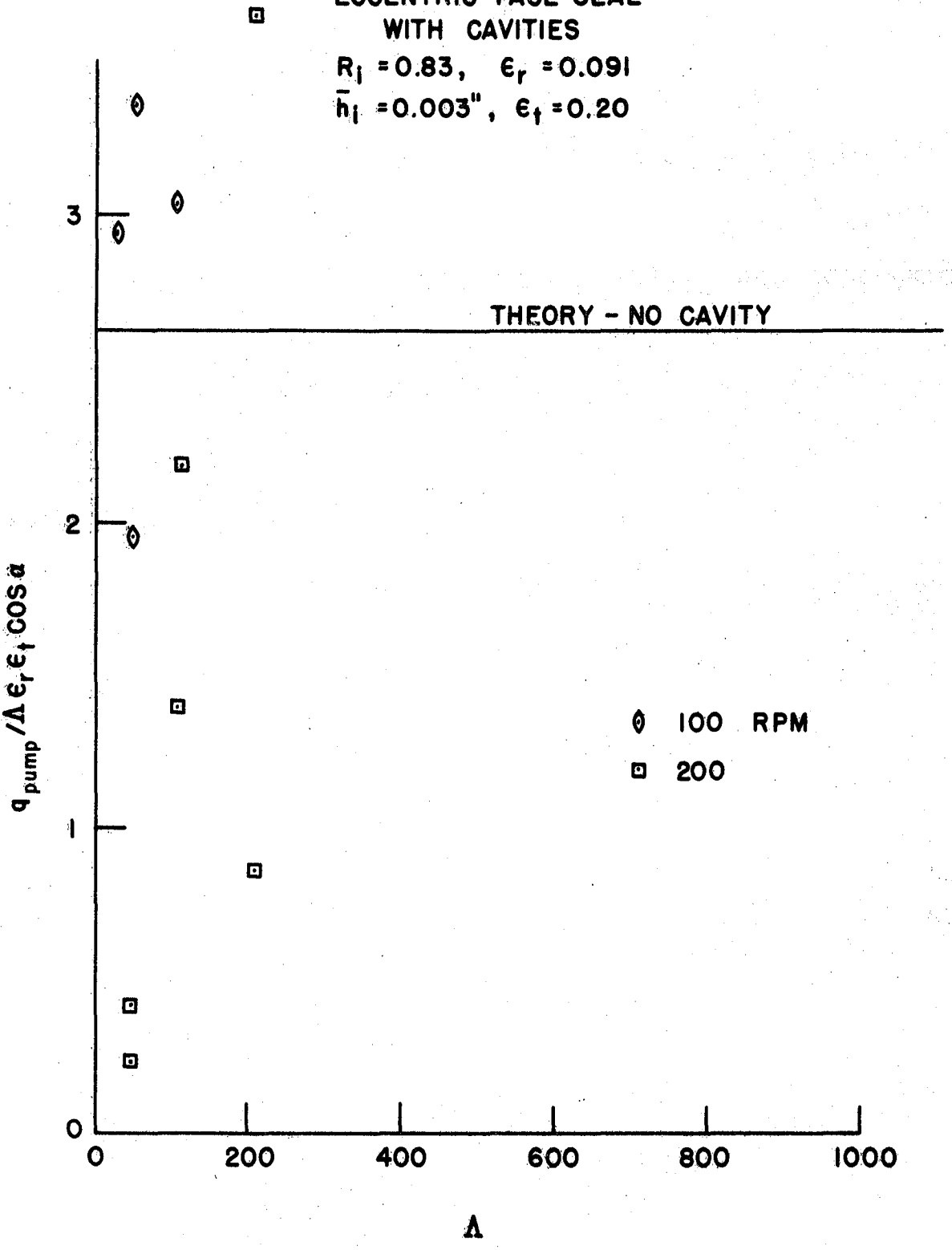

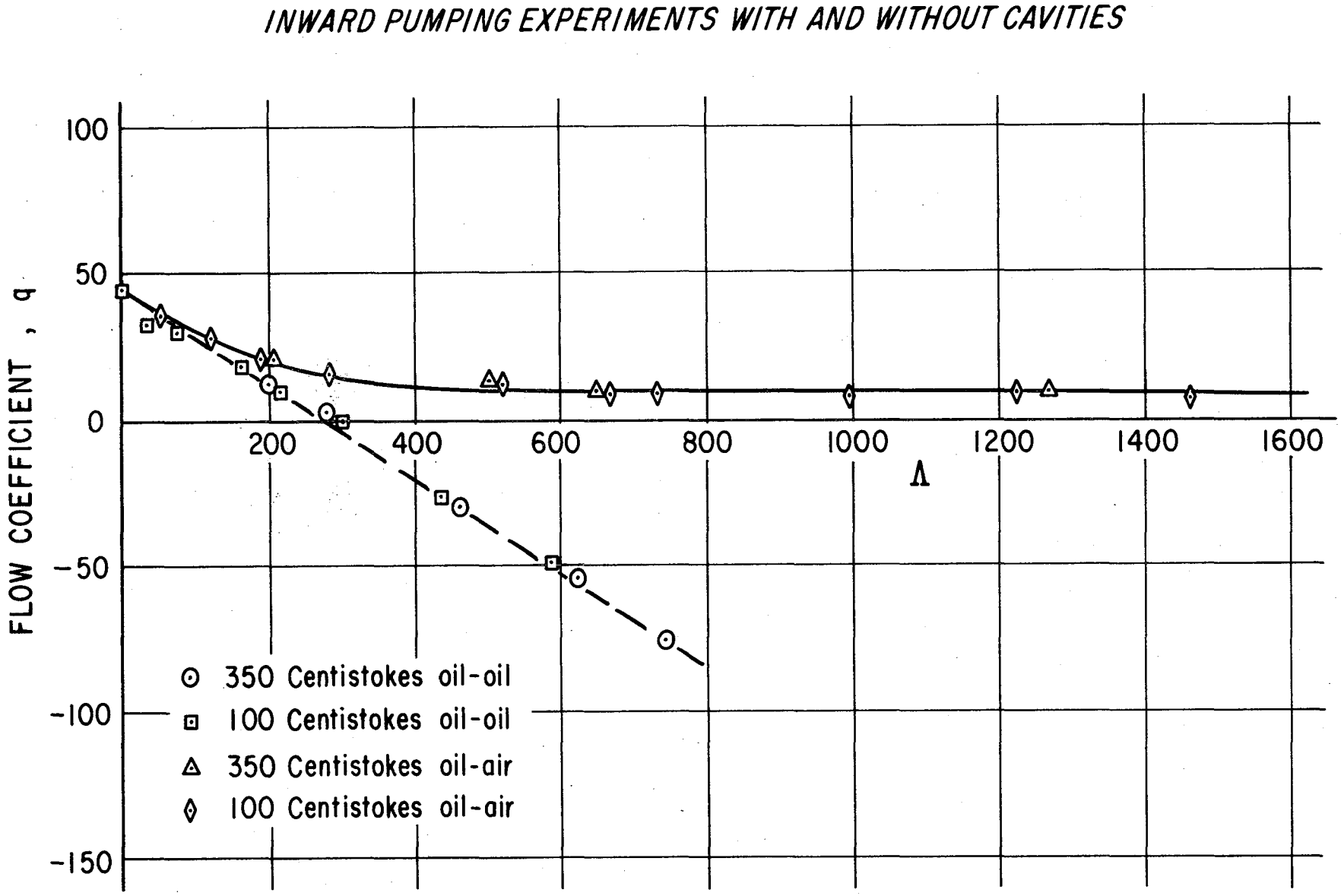
INWARD PUMPING EXPERIMENTS WITH AND WITHOUT CAVITIES
FLOW COEFFICIENT , q
100
50
0
-50
-100
-150
200
400
600
800
1000
1200
1400
1600
Λ
350 Centistokes oil-oil
100 Centistokes oil-oil
350 Centistokes oil-air
100 Centistokes oil-air

Figure 30

FIGURE 31
INWARD PUMPING EXPERIMENTS
TWO FLUIDS

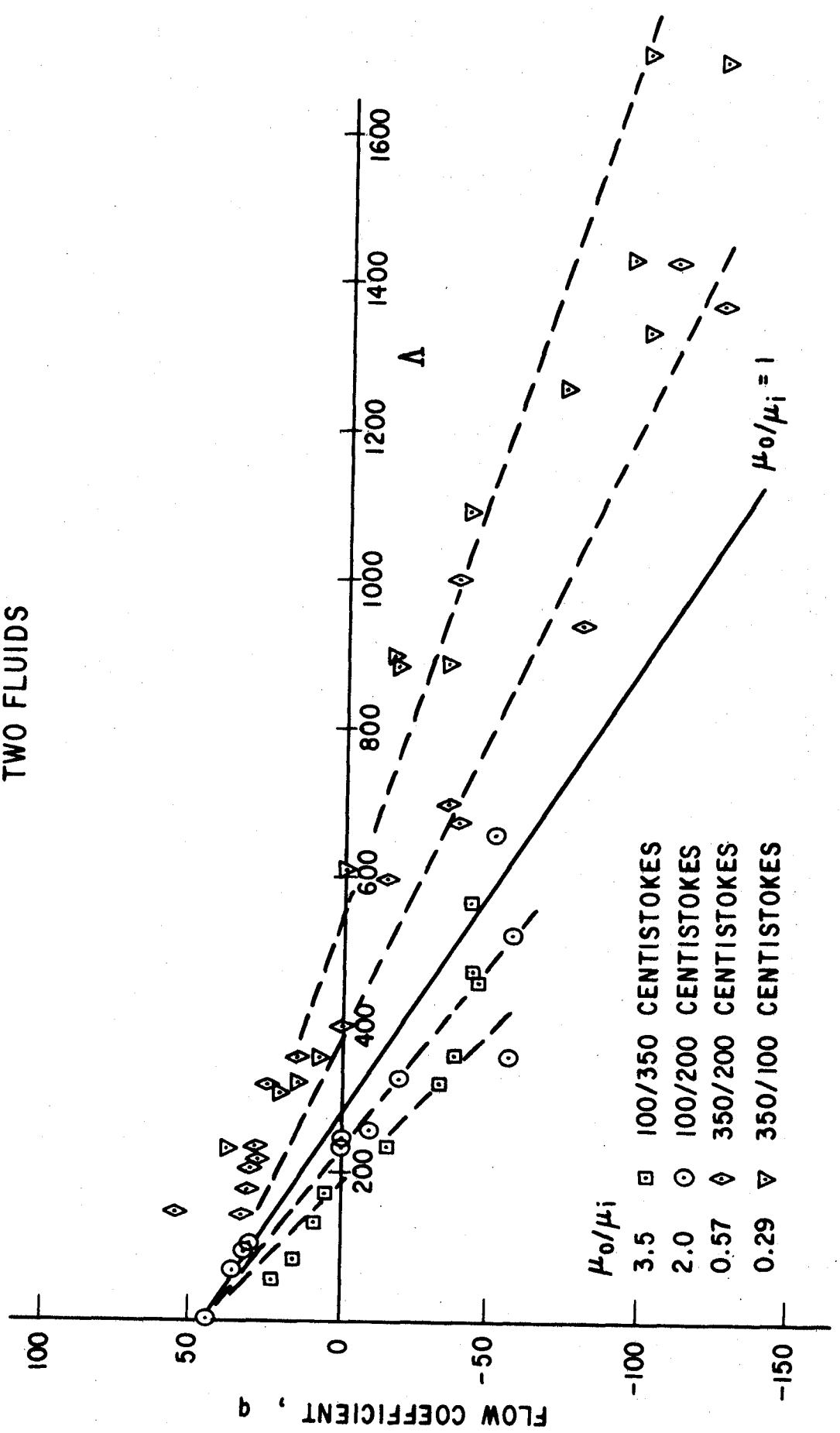

FIGURE 32
INWARD PUMPING EXPERIMENTS
TWO FLUIDS

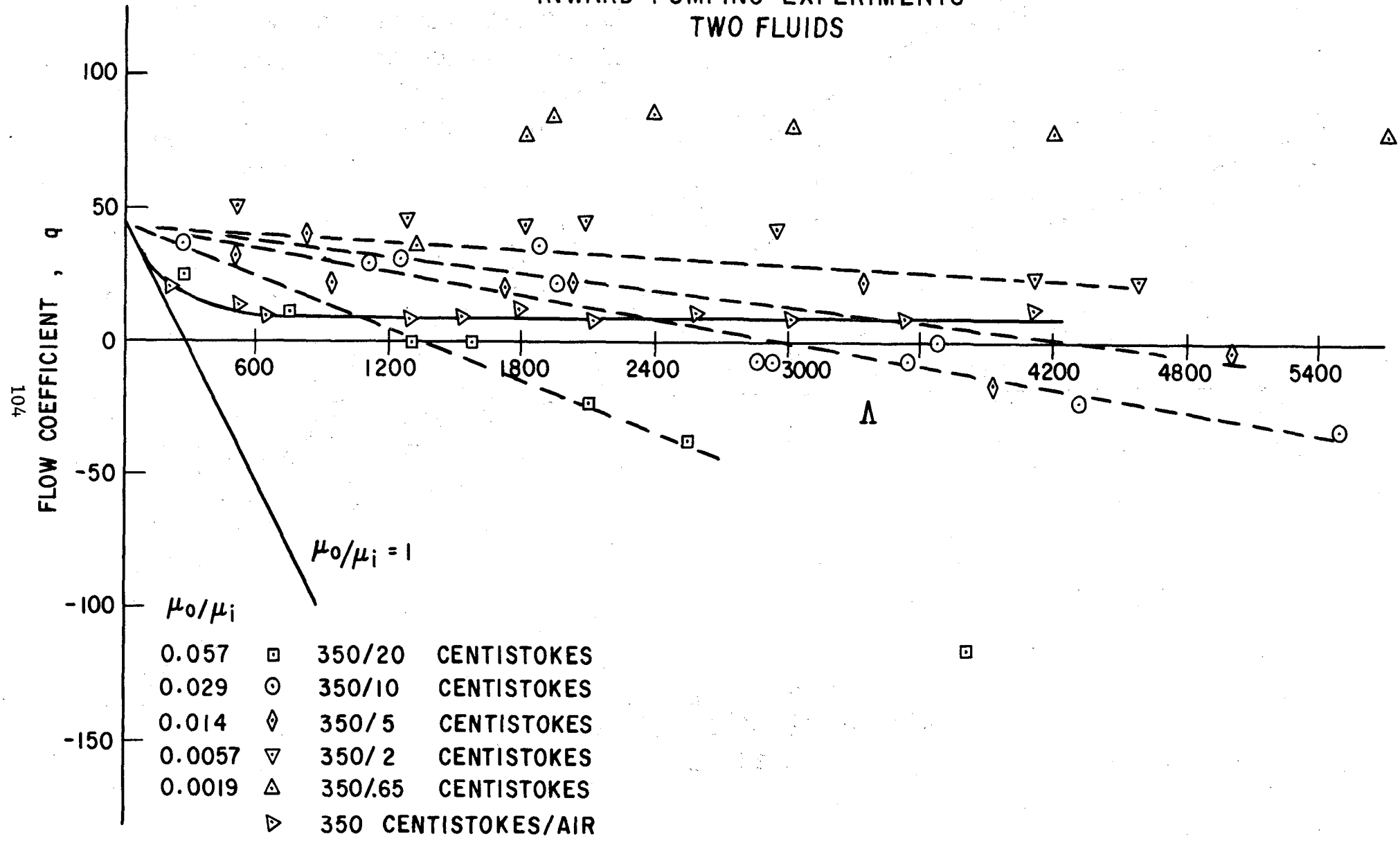

FIGURE 33

INERTIA EXPERIMENTS

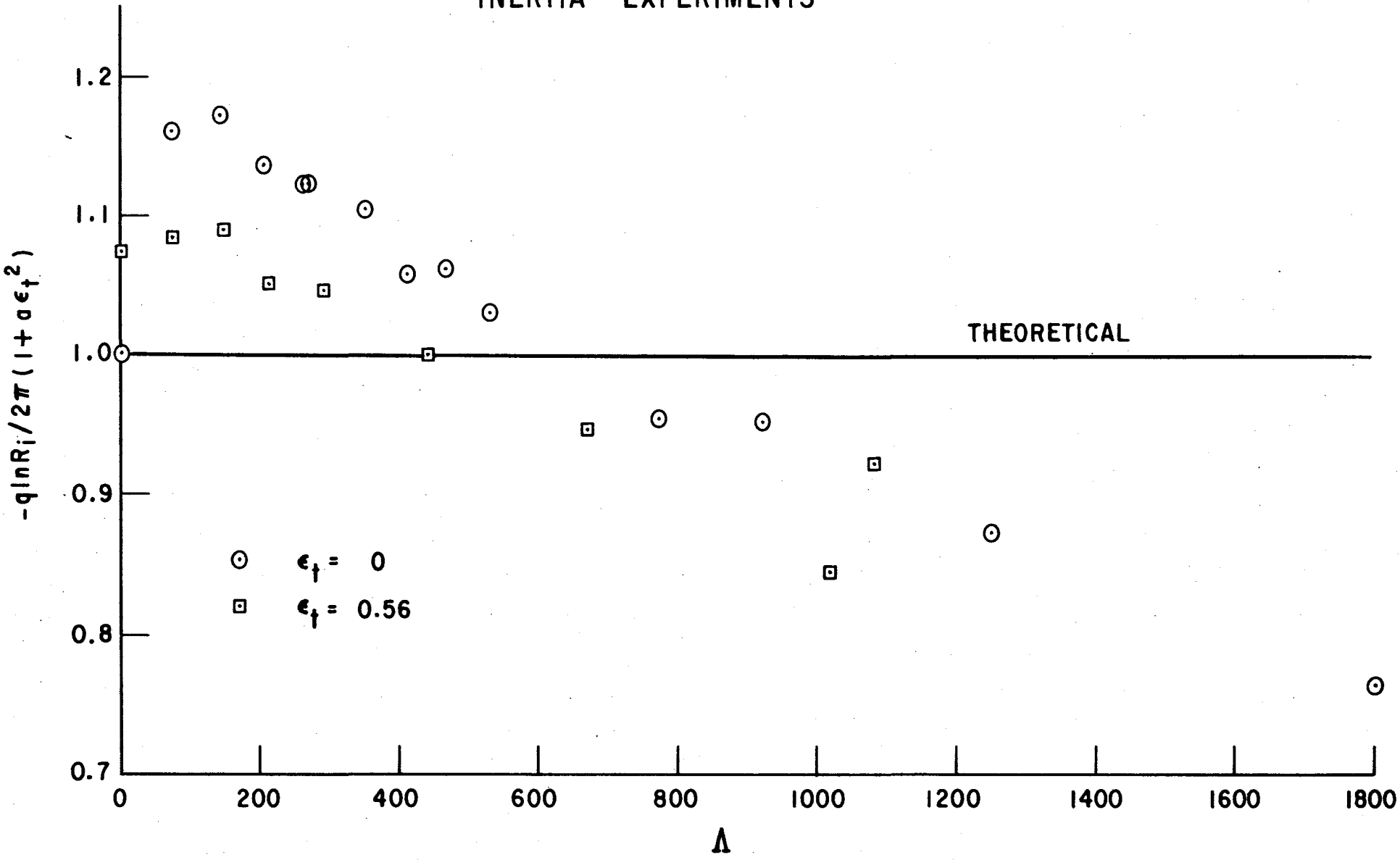

FIGURE 34

CORRELATION OF CAVITY SHAPES

(R_{CRIT})

$\epsilon = 0.5$, $\bar{h}_i = 0.005"$

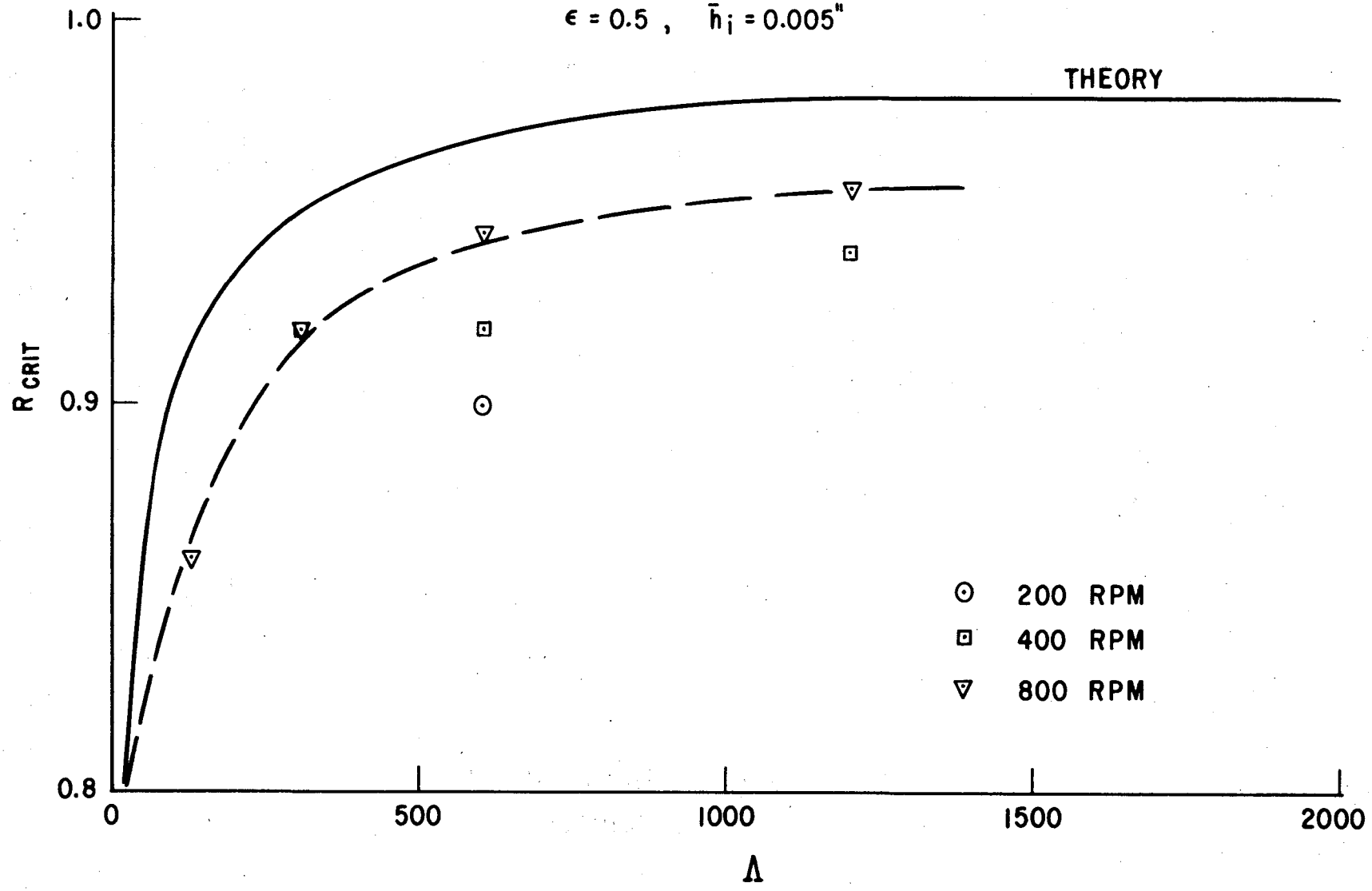

TABLE I

SUMMARY OF CONCENTRIC SEAL TESTS

Table No.	h_i, in	ϵ_t	Remarks	Figures
II - 1	.004	.50	Wide land seal	14
II - 2	"	.60	" " "	15
II - 3	"	.70, .80	" " "	15
III - 1	"	.50	Narrow land seal	16
III - 2	"	.20	" " "	17
III - 3	"	.80	" " "	18
III - 4	.003	.50	" " "	19
III - 5	.003	.50	" " "	20

TABLE II

Wide Land Seal Data - Concentric

d_o = 3.469 inch; d_i = 2.312 inch; R_i = 0.665 inch

1. This set of data had no dynamic film thickness measurements or viscosity temperature correction (Figure 14).

p_i psi	N rpm	$\bar{h}_i$ in.	ε_t	Q in³/sec	q
5	0	0.00417	0.581	0.0176	28.9
10	0	.00430	.560	.0351	26.6
15	0	.00436	.555	.0540	25.7
20	0	.00448	.535	.0766	25.2
30	0	.00468	.510	.1225	23.5
40	0	.00492	.485	.1905	23.8
5	200			0.0181	29.7
10	200			.0361	27.4
15	200	(Assumed to be the		.0619	29.4
20	200	same as above)		.0746	24.6
30	200			.1190	22.8
40	200			.1856	23.2
5	400			0.0189	31.2
10	400			.0373	28.4
15	400	(Assumed to be the		.0534	25.4
20	400	same as above)		.0723	23.8
30	400			.1238	23.6
40	400			.1810	22.6
5	600			0.0156	25.6
10	600			.0331	25.2
15	600	(Assumed to be the		.0495	23.6
20	600	same as above)		.0702	23.2
30	600			.1145	22.0
40	600			.1679	21.0
5	800			0.0146	24.0
10	800			.0273	20.8
15	800	(Assumed to be the		.0427	20.4
20	800	same as above)		.0672	22.2
30	800			.0970	18.6
40	800			.1881	23.5

Table II (continued)

2. This set of data includes a temperature correction on viscosity and dynamic film thickness connections (Figure 15).

p_i psi	N rpm	$\bar{h}_i$ in.	ϵ_t	Q in^3/sec	q
5	400	0.004107	0.595	0.0193	32.8
10	400	.00415	.590	.0378	29.6
15	400	.00425	.575	.0576	29.0
20	400	.004375	.558	.0794	25.9
30	400	.00455	.538	.129	23.8
5	600	0.00416	0.587	0.0230	35.4
10	600	.004147	.590	.0418	30.1
15	600	.00416	.587	.0605	29.7
20	600	.004188	.585	.0794	27.7
30	600	.004336	.565	.130	26.9
40	600	.004472	.545	.206	29.2
5	800	0.003812	0.640	0.0227	42.0
10	800	.003853	.635	.0408	39.2
15	800	.003853	.635	.0518	30.4
20	800	.003893	.627	.0734	31.1
30	800	.004027	.605	.1130	28.6
40	800	.004188	.585	.1630	28.3
3. $\bar{h}_i$ = 0.004; ϵ_t = 0.70; 0.80 (Figure 15).					
5	400	0.004153	0.760	0.0247	43.2
10	400	.004153	.760	.0471	38.9
15	400	.004181	.756	.0640	33.6
20	400	.004234	.746	.0878	33.3
30	400	.004368	.723	.1280	29.6
40	400	.004516	.700	.2050	32.5
5	600	0.003929	0.804	0.0224	43.5
10	600	.003929	.804	.0414	39.1
15	600	.003993	.791	.0624	33.3
20	600	.004033	.785	.0827	32.6
30	600	.004181	.756	.1320	33.8
40	600	.004315	.732	.1890	33.0
5	800	0.004261	0.741	0.0238	32.4
10	800	.004153	.760	.0517	39.2
15	800	.004153	.760	.0750	34.6
20	800	.004181	.756	.0974	33.4
30	800	.004261	.741	.1490	32.4
40	800	.004422	.715	.2150	31.2

TABLE III*

Narrow Land Seal Data - Concentric

d_o = 2.750 inch; d_i = 2/281 inch; R_i = 0.83 inch

1. h_i = 0.004 inch, ϵ_t = 0.50 (Figure 16).

p_i psi	N rpm	$\bar{h}_i$ in.	ϵ_t	Q in^3/sec	q
2	0	0.00400	0.492	0.0138	46.8
4	0	.00403	.490	.0206	39.5
6	0	.00406	.484	.0301	39.9
8	0	.00401	.480	.0424	42.2
10	0	.00413	.478	.0513	40.6
15	0	.00421	.469	.0798	40.9
20	0	.00428	.459	.1117	41.2
30	0	.00443	.445	.1750	39.4
2	200	0.00397	0.497	0.0107	37.4
4	200	.00402	.490	.0197	38.5
6	200	.00407	.484	.0311	40.8
8	200	.00409	.482	.0410	41.2
10	200	.00410	.480	.0521	41.9
15	200	.00418	.471	.0787	40.7
2	400	0.00402	0.490	0.0073	23.4
4	400	.00403	.489	.0195	36.1
6	400	.00403	.489	.0301	39.3
8	400	.00405	.487	.0380	37.9
10	400	.00407	.484	.0515	41.1
15	400	.00415	.474	.0756	38.5
2	600	0.00395	0.499	0.0090	29.6
4	600	.00394	.500	.0193	37.4
6	600	.00394	.500	.0254	34.4
8	600	.00397	.497	.0365	37.5
10	600	.00398	.495	.0461	38.2
15	600	.00405	.487	.0713	37.6
2	800	0.00378	0.522	0.0059	21.7
4	800	.00378	.522	.0151	31.6
6	800	.00378	.522	.0230	33.1
8	800	.00378	.522	.0344	38.2
10	800	.00378	.522	.0396	35.4
15	800	.00381	.518	.0586	34.4

*NOTE: These data were reduced using data reduction program No. 1.

Table III (continued)

2. $\bar{h}_i$ = 0.004 inch, ϵ_t = 0.20 (Figure 17)

p_i psi	N rpm	$\bar{h}_i$ in.	ϵ_t	Q in^3/sec	q
2	0	0.00405	0.206	0.0108	35.2
4	0	.00409	.204	.0163	30.2
6	0	.00413	.204	.0266	33.9
8	0	.00414	.199	.0344	33.5
10	0	.00417	.200	.0430	33.4
15	0	.00426	.194	.0677	33.7
20	0	.00432	.191	.0938	34.0
30	0	.00455	.161	.1549	32.5
2	200	0.00433	0.169	0.0084	23.0
4	200	.00437	.168	.0150	23.1
6	200	.00440	.167	.0276	29.5
8	200	.00443	.166	.0345	28.0
10	200	.00444	.165	.0451	29.6
15	200	.00453	.162	.0690	29.0
2	400	0.00433	0.169	0.0102	29.0
4	400	.00435	.169	.0176	28.3
6	400	.00437	.168	.0281	31.0
8	400	.00440	.167	.0356	29.2
10	400	.00443	.166	.0445	28.8
15	400	.00445	.165	.0661	28.6
2	600	0.00427	0.172	0.0069	20.0
4	600	.00428	.171	.0159	26.1
6	600	.00427	.172	.0261	30.3
8	600	.00429	.171	.0305	26.9
10	600	.00433	.169	.0389	27.2
15	600	.00439	.167	.0625	28.7
2	800	0.00421	0.174	0.0075	23.1
4	800	.00416	.176	.0126	22.4
6	800	.00416	.176	.0217	26.8
8	800	.00416	.176	.0260	24.1
10	800	.00415	.177	.0395	29.5
15	800	.00421	.174	.0562	27.3

Table III (continued)

3. $\bar{h}_i$ = 0.004 inch, ϵ_t = 0.80 (Figure 18)

p_i psi	N rpm	$\bar{h}_i$ in.	ϵ_t	Q in^3/sec	q
2	0	0.00380	0.915	0.0163	67.8
4	0	.00385	.902	.0298	69.3
6	0	.00386	.901	.0419	68.0
8	0	.00389	.892	.0394	48.2
10	0	.00392	.887	.0645	63.1
15	0	.00399	.870	.1029	64.9
2	200	0.00401	0.796	0.0126	43.9
4	200	.00403	.791	.0263	52.4
6	200	.00406	.786	.0401	55.2
8	200	.00409	.780	.0497	52.0
10	200	.00410	.778	.0621	52.4
15	200	.00417	.765	.1009	55.3
2	400	0.00401	0.796	0.0082	28.6
4	400	.00403	.791	.0239	47.5
6	400	.00403	.791	.0405	56.8
8	400	.00406	.786	.0510	53.6
10	400	.00409	.780	.0601	50.6
15	400	.00414	.770	.0879	47.6
2	600	0.00393	0.812	0.0107	41.6
4	600	.00395	.807	.0249	52.5
6	600	.00395	.807	.0339	50.0
8	600	.00398	.802	--	--
10	600	.00398	.802	.0629	55.1
15	600	.00401	.796	.0902	52.7
2	800	0.00382	0.835	--	--
4	800	.00387	.824	.0221	48.2
6	800	.00385	.829	.0323	50.7
8	800	.00385	.829	.0447	52.5
10	800	.00385	.829	.0541	51.3
15	800	.00387	.824	.0885	55.6

Table III (continued)

4. $\bar{h}_i$ = 0.003 inch, ϵ_t = 0.50 (Figure 19)

p_i psi	N rpm	$\bar{h}_i$ in.	ϵ_t	Q in^3/sec	q
5	0	0.00311	0.515	0.0134	47.4
10	0	.00319	.502	.0282	49.6
15	0	.00327	.490	.0415	46.3
20	0	.00334	.482	.0629	50.2
25	0	.00343	.467	.0830	49.4
30	0	.00351	.461	.1031	47.7
5	200	0.00310	0.515	0.0106	37.0
10	200	.00318	.502	.0276	47.8
15	200	.00326	.490	.0431	47.4
20	200	.00335	.478	.0544	42.2
25	200	.00340	.471	.0804	48.0
30	200	.00345	.463	.1025	48.9
5	400	0.00310	0.515	0.0121	43.3
10	400	.00318	.502	.0217	38.2
15	400	.00324	.494	.0419	46.2
20	400	.00329	.486	.0605	48.2
25	400	.00335	.478	.0793	47.9
30	400	.00343	.467	.0972	46.3
5	600	0.00302	0.529	0.0089	32.7
10	600	.00310	.515	.0212	38.4
15	600	.00318	.502	.0379	42.6
20	600	.00324	.494	.0528	42.4
25	600	.00326	.490	.0732	46.3
30	600	.00332	.482	.0902	44.6
5	800	0.00294	0.544	0.0155	59.8
10	800	.00300	.534	.0202	38.8
15	800	.00302	.529	.0342	43.5
20	800	.00308	.520	.0478	42.3
25	800	.00310	.515	.0622	43.2
30	800	.00317	.504	.0826	43.7

Table III (continued)

5. $\bar{h}_i$ = 0.003 inch, ϵ_t = 0.50 (Figure 20)

p_i psi	N rpm	$\bar{h}_i$ in.	ϵ_t	Q in³/sec	q
5	200	0.00309	0.518	0.0151	53.5
10	200	.00317	.504	.0303	53.1
15	200	.00324	.494	.0450	50.8
20	200	.00332	.482	.0662	52.7
25	200	.00337	.474	.0879	53.8
30	200	.00345	.463	.1035	49.4
5	400	0.00308	0.520	0.0151	54.2
10	400	.00316	.507	.0352	62.5
15	400	.00321	.498	.0489	56.5
20	400	.00326	.490	.0642	52.5
25	400	.00332	.482	.0860	52.9
30	400	.00337	.474	.1050	51.6
5	600	0.00300	0.534	0.0159	61.6
10	600	.00310	.515	.0313	58.5
15	600	.00313	.511	.0469	58.4
20	600	.00318	.502	.0586	51.6
25	600	.00324	.494	.0816	54.0
30	600	.00326	.490	.1020	55.2
5	800	0.00289	0.554	0.0128	54.6
10	800	.00294	.544	.0286	61.0
15	800	.00297	.539	.0330	46.1
20	800	.00300	.534	.0557	56.9
25	800	.00302	.529	.0651	52.1
30	800	.00309	.518	.0848	51.5

TABLE IV

DATA REDUCTION PROGRAM NO. 1

A. Listing

```
3 LET K=0
4 FOR R= 200 TO 400 STEP 200
5 READ S
8 FOR I= 1 TO S
10 READ P1,Y1,Y2,T,F,W
11 LET H1=-.5
12 LET H2= 4.7
20 LET X1=-2
25 LET X2= 1
27 LET D= 2.75
30 LET H1= H1*1E-3
35 LET H2= H2*1E-3
37 LET B= (H2-H1)/(X2-X1)
40 LET A= H1-B*X1
50 LET K= K+1
60 LET WO= W*1E-6*268
70 LET H= A+WO
80 LET P2= (((Y1+Y2)/2)-52)/66.7
90 LET Q1= (Y2-Y1)*.938/T
100 LET P= P1-P2
110 LET M= EXP(6.68-.0104*F)
115 LET E= B*D/(2*H)
120 LET Q= (1.7E-6*M*Q1)/(P*H↑3)
125 LET L= 1.675E-7*R*M/(P*H↑2)
130 PRINT "RUN";K,"Q1=";Q1,"HBAR=";H
140 PRINT
150 PRINT "E SUB T=";E,"FLOW=";Q,"LAMBDA=";L
160 PRINT
210 NEXT I
211 PRINT
212 PRINT
220 NEXT R
900 DATA 6
901 DATA 5,1.8,2.4,52,81,.4
902 DATA 10,2.9,3.4,19.2,81,.5
903 DATA 15,4.1,5,19.4,81,.8
904 DATA 20,6.5,7.5,15.1,81,1
905 DATA 25,8.5,9.5,11,81,1.3
906 DATA 30,10.5,12,12.8,81,1.5
```

The input data at statement 901 is

P = 5 psig

Y_1 = 1.8

Y_2 = 2.4

T = 52 sec

F = 81°F

W = .4

Table IV (continued)

B. Program Description

1. Input: P1 = supply pressure read from gage, psig

Y1 = initial reading from graduated supply reservoir

Y2 = final reading from graduated supply reservoir

T = time between Y1 and Y2, sec.

F = oil outlet temperature, ^{o}F

W = Wayne-Kerr proximity probe reading

H1 = initial (static) setting of Sheffield probe No. 1

H2 = initial (static) setting of Sheffield probe No. 2

D = Outside diameter of the seal, in

2. Output:

Q1, Q = leakage rate, in^3/sec

HBAR, $\bar{h}_i$ = average film thickness, in.

E Sub T, ϵ_t = tilt eccentricity

FLOW, q = flow coefficient

3. Calculations

a. Leakage Rate: Q1 = (Y2 - Y1).938/T, in^3/sec

The constant .938 is obtained from the calibration of the graduated reservoir.

b. Average Film Thickness, $\bar{h}_i$: H = A + WO

A = H1 - B X1 = initial $\bar{h}_i$ setting

WO = W(268×10^{-6}) = Wayne Kerr film thickness correction, in

B = (H2 - H1)/(X2 - X1) = misalignment slope

X1 = location of H1 probe from the center of the seal, in

X2 = location of H2 probe from the center of the seal, in

C. Tilt Eccentricity, ϵ_t : E SUB T = $\frac{B\ D}{2A}$

This equation is derived as follows:

First, the film thickness for the misaligned seal is given by

$h = \bar{h}_i\ (1 + R\ \epsilon_t \cos\theta)$.

Therefore $(h_o)_{max} = \bar{h}_i\ (1 + \epsilon_t)$ and $(h_o)_{min} = \bar{h}_i(1 - \epsilon_t)$. Thus solving for the tilt eccentricity we have

Table IV (continued)

$$\varepsilon_t = \left[(h_o)_{max} - (h_o)_{min} \right] / 2\bar{h}_i.$$

= misalignment slope x outside diameter / $2\bar{h}_i$

= B D/2A.

D. Average Supply Pressure: P = P1 - P2

P1 = supply pressure read from gage, psig

P2 = (Y1 + Y2)/2 - 52 /66.7

= hydrostatic pressure head correction

E. Viscosity: M = EXP (6.68 - .0104F)

The constants 6.68 and .0104 were obtained from a graph of viscosity vs temperature for 350 centistoke silicone oil.

F. Leakage Coefficient, q: FLOW = $1.7 \times 10^{-6} M(Q1) / P(H)^3$

TABLE V

SUMMARY OF ECCENTRIC SEAL TESTS

Radial Eccentricity 0.125"

$\epsilon_r = .091$

Narrow Land Seal

$R_i = .83$

TABLE	FIGURE	$\bar{h}_i$ in	ϵ_t	REMARKS
VI	21, 23	.003	.50	Outward Pumping(cos α = -1) No Cavity
VI	22, 23	.003	.50	Inward Pumping(cos α = 1) No Cavity (Oil dam used around outside of seal)
VII	24, 25	.004	.50	Inward Pumping (cos α = 1) With Gas Cavities
"	26	.003	.50	"
"	27	.001	.50	"
"	28	.003	.80	"
"	29	.003	.20	"

TABLE VI

ECCENTRIC, MISALIGNED FACE SEAL DATA

NARROW LAND SEAL $R_i = .83$

RADIAL ECCENTRICITY .125" , $\epsilon_r = .091$

1. Cos α = -1, i.e. Outward Pumping and No Cavities

P_i psi	N rpm	Λ	h_i in	ϵ_t	Q in^3/sec	q	$\frac{q_{pump}}{\epsilon_t}$	$\frac{q_{pump}}{\Lambda \epsilon_t \epsilon_r \cos\alpha}$
5	200	226	.00311	.487	.0171	63.2	41.0	2.00
10	"	114	.00320	.473	.0335	60.5	37.6	3.64
15	"	73	.00329	.459	.0474	53.5	24.7	3.71
20	"	54	.00336	.450	.0625	50.5	19.2	3.94
25	"	41	.00344	.439	.0769	46.6	11.7	3.13
5	400	454	.00308	.491	.0265	99.1	113.4	2.75
10	"	234	.00313	.483	.0411	77.9	72.0	3.40
15	"	153	.00320	.473	.0533	64.5	46.2	3.66
20	"	113	.00324	.467	.0701	62.0	41.8	4.07
25	"	85	.00332	.455	.0861	55.8	30.2	3.93
5	600	694	.00300	.504	.0323	126.5	163.9	2.59
10	"	347	.00311	.487	.0474	89.4	94.9	3.01
15	"	231	.00315	.481	.0586	72.8	61.9	2.94
20	"	170	.00320	.473	.0756	67.8	53.1	3.45
25	"	129	.00327	.463	.0938	62.4	43.3	3.70 (Theoretical Value 2.63)

2. Cos α = 1, Inward Pumping with No Cavities

0(1)	50	603.6	.00292	.518	- .0009	- 38.0	- 159(2)	- 2.89
0	80	945.3	.00292	.518	- .0022	- 91.9	- 264	- 3.07
0	100	1222	.00295	.513	- .0033	-140.3	- 360	- 3.24 (Theoretical Value -2.63)

(1) Hydrostatic pressure only, i.e., 1 psig.

(2) For $\epsilon_t = .518$, $\epsilon_r = 0$, q = +44.5.
This value was used to calculate q_{pump}

TABLE VII

ECCENTRIC SEAL DATA

Radial Eccentricity 0.125"

$\epsilon_r = .091$

Narrow Land Seal

$R_i = .83$

1. $h_i = .004$, $\epsilon_t = .50$, (Figures 24,25)

p_i psi	N rpm	Λ	$\bar{h}_i$ in	ϵ_t	Q in^3/sec	q	$\frac{q_{pump}}{\epsilon_t}$	$\frac{q_{pump}}{\Lambda \epsilon_r \epsilon_t \cos \alpha}$
2	200	273	.00402	.490	.00357	12.3	63.4	2.56
4	"	157	.00405	.487	.01386	27.3	32.8	2.39
6	"	109	.00407	.484	.02345	31.9	23.2	2.34
8	"	84	.00409	.482	.03180	33.1	20.7	2.71
10	"	67	.00413	.477	.04560	37.5	11.2	1.84
15	"	44	.00421	.468	.07090	37.6	10.5	2.64
2	400	572	.00399	.494	.00397	14.4	58.9	1.13
4	"	333	.00397	.497	.01400	29.8	27.9	.96
6	"	225	.00402	.490	.01934	27.4	32.5	1.59
8	"	171	.00405	.487	.02658	28.5	30.4	1.95
10	"	136	.00407	.484	.03689	31.2	24.7	1.99
15	"	90	.00413	.478	.06171	34.2	18.3	2.23
2	600	826	.00397	.497	.00695	24.5	38.6	.51
4	"	480	.00397	.497	.00994	20.3	46.9	1.07
6	"	338	.00397	.497	.01563	22.5	42.4	1.38
8	"	259	.00397	.497	.02365	26.1	35.3	1.50
10	"	208	.00399	.494	.03234	28.5	30.5	1.61
15	"	132	.00407	.484	.05302	29.1	29.0	2.41
2	800	1100	.00394	.500	.00408	14.5	58.6	.59
4	"	632	.00394	.500	.00690	14.0	59.4	1.03
6	"	450	.00391	.504	.01078	15.7	55.9	1.37
8	"	347	.00389	.507	.01876	21.3	44.8	1.36
10	"	278	.00386	.511	.02255	20.6	46.1	1.82
15	"	182	.00394	.500	.04188	24.5	38.5	2.32

2. $h_i = .003$, $\epsilon_t = .50$, (Figure 26)

p_i psi	N rpm	Λ	$\bar{h}_i$ in	ϵ_t	Q in^3/sec	q	$\frac{q_{pump}}{\epsilon_t}$	$\frac{q_{pump}}{\Lambda \epsilon_r \epsilon_t \cos \alpha}$
5	200	225	.00313	.483	.00651	23.8	40.1	1.96
10	"	115	.00321	.471	.01907	34.5	17.2	1.64
15	"	76	.00327	.463	.03272	38.5	8.3	1.20
20	"	55	.00335	.452	.04873	40.5	3.1	.63
25	"	41	.00348	.434	.06425	38.3	6.9	1.85
30	"	34	.00348	.434	.08156	40.7	1.3	.42
5	400	467	.00311	.487	.00381	14.5	59.0	1.39
10	"	236	.00319	.474	.01590	29.8	27.3	1.27
15	"	149	.00324	.467	.02759	32.2	22.2	1.64
20	"	108	.00332	.455	.03955	32.5	21.1	2.15
25	"	84	.00338	.448	.06212	39.2	5.9	.77
30	"	68	.00343	.441	.07346	37.0	10.3	1.67
5	600	725	.00303	.500	.00458	18.5	50.4	.76
10	"	353	.00311	.487	.01173	22.6	42.5	1.32
15	"	229	.00319	.474	.02132	26.0	35.5	1.70
20	"	171	.00321	.471	.03518	31.7	23.2	1.49
25	"	134	.00327	.463	.04786	33.1	20.0	1.64
30	"	105	.00332	.455	.06700	35.8	13.7	1.43
5	800	999	.00289	.523	.00507	22.2	42.8	.47
10	"	512	.00295	.513	.01048	23.1	41.2	.89
15	"	342	.00297	.509	.01975	28.9	30.0	.96
20	"	241	.00305	.495	.02931	29.4	28.7	1.31
25	"	193	.00300	.504	.03643	29.8	28.1	1.60
30	"	151	.00311	.487	.05003	30.8	25.6	1.86
1	200	763	.00303	.500	.00155	19.8	47.8	.69
2	"	485	.00303	.500	.00295	24.0	39.6	.90
3	"	355	.00303	.500	.00426	25.4	36.7	1.14
4	"	286	.00300	.504	.00856	41.5	4.8	.19
5	"	236	.00300	.504	.00782	31.2	25.2	1.17
2	400	980	.00300	.504	.00159	13.2	61.0	.69
4	"	562	.00300	.504	.00630	29.9	27.7	.54
6	"	402	.00297	.509	.00763	26.2	35.2	.97
7	"	363	.00292	.518	.00902	28.5	30.8	.94
4	600	821	.00305	.495	.00631	28.7	30.0	.40
6	"	555	.00311	.487	.00716	21.6	44.4	.88
8	"	423	.00312	.485	.01062	24.4	38.8	1.00
10	"	347	.00311	.487	.01657	31.3	24.5	.78

p_i psi	N rpm	Λ	$\bar{h}_i$ in	ϵ_t	Q in^3/sec	q	$\frac{q_{pump}}{\epsilon_t}$	$\frac{q_{pump}}{\Lambda \epsilon_r \epsilon_t \cos \alpha}$
4	800	1165	.00297	.509	.00581	28.9	29.9	.28
6	"	829	.00295	.513	.00763	27.2	33.2	.44
8	"	642	.00293	.516	.00938	26.1	35.4	.61
10	"	522	.00293	.516	.01366	30.8	26.2	.55
12	"	443	.00292	.518	.01477	28.4	30.9	.77
14	"	379	.00293	.516	.01753	28.8	30.2	.88
3. h_i = .001, ϵ_t = .50, (Figure 27)								
15	125	322	.00121	.413	.00197	42.4		
20	"	210	.00131	.383	.00309	40.4		
25	"	150	.00139	.361	.00545	48.0		
30	"	110	.00148	.338	.00690	41.8		
40	"	66	.00167	.300	.01914	61.1		
15	200	564	.00116	.432	.00211	52.2		
20	"	374	.00124	.404	.00256	39.2	2.3	.07
25	"	255	.00135	.371	.00364	35.0	10.6	.46
30	"	198	.00140	.357	.00552	39.6		
40	"	112	.00161	.310	.01538	54.2		
15	300	932	.00110	.453	.00105	30.1	26.3	.31
20	"	643	.00116	.432	.00167	31.4	22.8	.39
25	"	483	.00120	.417	.00243	33.2	17.9	.41
30	"	370	.00125	.399	.00350	35.1	12.3	.37
40	"	207	.00145	.344	.00924	44.7		
15	400	1563	.00100	.501	.0090	35.6	16.3	.11
20	"	1156	.00101	.495	.00144	41.7	3.7	.035
25	"	907	.00102	.488	.00167	37.6	11.7	.14
30	"	686	.00108	.464	.00218	35.2	15.4	.22
40	"	409	.00121	.413	.00372	31.9	20.7	.55
10	0	0	.00122	.417	.00153	48.5	0	0
20	"	"	.00141	.365	.00521	56.0	"	"
30	"	"	.00159	.324	.00932	47.1	"	"
40	"	"	.00177	.277	.01924	52.6	"	"
50	"	"	.00197	.254	.03442	55.4	"	"

4. $h_i = .003$, $\epsilon_t = .80$, (Figure 28)

p_i psi	N rpm	Λ	$\bar{h}_i$ in	ϵ_t	Q in^3/sec	q	$\frac{q_{pump}}{\Lambda \epsilon_r \epsilon_t \cos \alpha}$
2	0	0	.00300	.798	.01078	89.1	0
4	"	"	.00305	.791	.01363	62.4	"
6	"	"	.00305	.787	.01954	62.7	"
8	"	"	.00309	.776	.02565	61.1	"
10	"	"	.00313	.771	.03722	69.9	"
15	"	"	.00322	.751	.05154	60.5	"
20	"	"	.00330	.733	.07248	60.0	"
2	200	527	.00291	.818	.00249	22.9	.99
3	"	388	.00290	.821	.00439	29.8	1.10
4	"	304	.00291	.818	.00586	31.0	1.24
5	"	243	.00293	.814	.00821	34.7	1.49
6	"	207	.00293	.814	.01017	36.6	1.63
7	"	181	.00293	.814	.01288	40.3	1.60
2	400	609	.00290	.822	.00178	9.5	1.16
4	"	610	.00290	.822	.00445	23.7	.85
6	"	430	.00289	.826	.00695	26.2	1.11
8	"	327	.00290	.822	.01242	35.6	1.09
10	"	261	.00290	.822	.01746	39.8	1.15
12	"	216	.00293	.814	.01934	36.1	1.60
14	"	184	.00294	.811	.02490	39.6	1.60
5	200	212	.00307	.775	.01082	37.8	1.42
10	"	111	.00310	.769	.02443	44.5	1.80
15	"	72	.00318	.749	.04352	50.2	1.49
20	"	53	.00323	.737	.06212	51.8	1.33
25	"	41	.00331	.719	.08527	53.2	.87
30	"	33	.00337	.708	.10992	54.8	-
15	400	144	.00318	.749	.03703	42.6	1.53
20	"	107	.00321	.743	.05814	49.6	1.30
25	"	86	.00323	.737	.07689	51.6	.70
30	"	68	.00332	.719	.09571	50.0	1.24
35	"	57	.00337	.708	.12129	52.0	.75
40	"	48	.00342	.696	.15129	54.3	-

5. $h_i = .003$, $\epsilon_t \doteq .20$, (Figure 29)

p_i psi	N rpm	Λ	$\bar{h}_i$ in	ϵ_t	Q in^3/sec	q	$\frac{q_{pump}}{\Lambda \epsilon_r \epsilon_t \cos \alpha}$
5	0	0	.00307	.195	.01150	41.1	0
10	"	"	.00317	.188	.02233	39.0	"
15	"	"	.00325	.180	.03518	38.7	"
20	"	"	.00333	.176	.05133	39.9	"
25	"	"	.00342	.173	.06764	39.2	"
30	"	"	.00351	.170	.08716	39.3	"
35	"	"	.00357	.168	.10619	39.2	"
40	"	"	.00367	.163	.13132	39.1	"
5	100	104	.00313	.191	.00788	26.7	4.9
10	"	53	.00321	.186	.02132	35.8	-
15	"	34	.00329	.181	.03350	35.7	-
20	"	25	.00334	.178	.04841	37.3	-
25	"	19	.00344	.173	.06700	38.3	-
30	"	15	.00353	.169	.08527	37.6	-
35	"	13	.00358	.166	.10196	37.0	-
40	"	11	.00368	.162	.12849	37.9	-
5	100	104	.00313	.191	.00885	29.9	3.03
10	"	53	.00321	.186	.01927	32.3	3.36
15	"	34	.00329	.181	.03212	34.1	1.95
20	"	25	.00334	.178	.04425	34.0	2.94
25	"	19	.00344	.173	.06194	35.4	-
30	"	15	.00353	.167	.07949	35.1	-
35	"	13	.00358	.166	.09670	35.1	-
40	"	11	.00368	.162	.12342	36.4	-
5	200	212	.00310	.192	.00929	32.2	.87
10	"	110	.00315	.189	.01857	32.8	1.40
20	"	51	.00332	.180	.04467	35.2	.24
30	"	32	.00348	.171	.07688	35.5	-
40	"	22	.00361	.165	.12563	39.1	-
50	"	16	.00377	.158	.17370	38.1	-
60	"	13	.00393	.152	.23450	37.9	-
5	200	212	.00310	.192	.00634	22.0	3.66
10	"	110	.00315	.189	.01770	31.2	2.18
20	"	51	.00332	.180	.04425	34.9	.42
30	"	32	.00348	.171	.07817	36.1	-
40	"	22	.00361	.165	.12026	37.4	-
50	"	16	.00377	.158	.16456	36.1	-
60	"	13	.00393	.152	.23848	38.6	-

TABLE VIII

DATA REDUCTION PROGRAM No. 2

A. Listing

```
 10 PRINT " RUN", "Q PUMP ", "LAMBDA"
 15 PRINT
 20 FOR I = 17 TO 23
 30 READ E,Q,L
 40 LET Q 1 = 25 + 37.5*E
 50 LET P = (Q1-Q)/(E*.091*L)
 60 PRINT I,P,L
 70 NEXT I
900 DATA .191
```

B. Program Description

This program takes the output from data reduction program No. 1, $q, \Lambda, \epsilon_t, \epsilon_r, \cos\alpha$, and calculates the pumping variable, $q_{pump}/\Lambda\epsilon_r\epsilon_t\cos\alpha$. The pumping coefficient, q_{pump}, is found by subtracting the theoretical q for $\epsilon_r = 0$ from the measure (input) q. The theoretical value of q for $\epsilon_r = 0$ is calculated in the program from an approximate equation for $q(\epsilon_t)$ for the misaligned seal.

TABLE IX

ECCENTRIC MISALIGNED FACE SEAL DATA
NARROW LAND SEAL, Ri = 0.83
RADIAL ECCENTRICITY 0.125", ϵ_r = 0.091
COS α = 1, INWARD PUMPING

1. No cavities (oil/oil), 350/350 centistokes

Oil Level Y1-Y2	N rpm	Λ	$\overline{hi}$ in	ϵ_t	Q in^3/sec	q
58.5 - 53.5	0	0	0.00290	0.5690	0.00109	45.99
52 - 47	0	0	0.00290	0.5690	0.00103	44.97
38 - 38	22	298	0.00290	0.5690	0.0	0.0
39 - 39	40	537	0.00290	0.5690	-0.00096	- 45.33
42 - 45	66	863	0.00290	0.5690	-0.00196	- 89.86
41 - 40	15	200	0.00290	0.5690	0.00029	13.48
42 - 47	47	615	0.00290	0.5690	-0.00161	- 53.15
44 - 43.7	21	273	0.00290	0.5690	0.00010	4.72
44 - 45	35	453	0.00290	0.5690	-0.00064	- 28.91
46 - 49	58	737	0.00290	0.5690	-0.00167	- 74.17
52 - 55	82	1003	0.00290	0.5690	-0.00252	-107.71
57 - 61	108	1310	0.00286	0.5723	-0.00330	-141.91

2. No cavities (oil/oil), 350/200 centistokes

68 - 67	28	316	0.00292	0.5629	0.00063	24.59
58.5 - 57	12	144	0.00291	0.5648	0.00132	55.29
56.5 - 56	29	352	0.00291	0.5648	0.00037	15.84
56 - 56.5	49	595	0.00291	0.5648	-0.00031	- 12.92
57.5 - 60.5	115	1373	0.00291	0.5648	-0.00296	-123.04
62 - 63	60	701	0.00291	0.5648	-0.00081	- 32.96
64.5 - 66.5	87	999	0.00291	0.5648	-0.00090	- 36.09
68 - 70.5	127	1428	0.00291	0.5648	-0.00272	-106.58
73 - 77	185	2052	0.00289	0.5732	-0.00532	-207.30
58 - 57	18	203	0.00292	0.5627	0.00083	32.55
56.5 - 55.5	19	216	0.00292	0.5627	0.00073	29.01
55 - 54	20	229	0.00292	0.5627	0.00076	30.22
51 - 50	15	176	0.00292	0.5627	0.00079	32.19
49 - 48	12	143	0.00292	0.5627	0.00081	33.62
48 - 48	33	393	0.00292	0.5627	0.0	0.0
48.5 - 49.5	57	675	0.00292	0.5627	-0.00091	- 37.51
50.5 - 52.5	80	940	0.00291	0.5646	-0.00188	- 77.21

3. No cavities (oil/oil), 350/100 centistokes

Oil Level Y1-Y2	N rpm	Λ	$\overline{hi}$ in	ϵ_t	Q in^3/sec	q
58 - 57	18	214	0.00290	0.5667	0.00042	17.46
57.5 - 58.5	80	950	0.00290	0.5667	-0.00072	- 29.93
59 - 59	47	555	0.00290	0.5667	0.0	0.0
61 - 64	116	1340	0.00290	0.5667	-0.00253	-102.35
68.5 - 69.5	78	882	0.00288	0.5705	-0.00043	- 17.29
66.5 - 65	20	230	0.00288	0.5705	0.00095	38.64
64.5 - 64	47	546	0.00288	0.5705	0.00028	11.39
64 - 65	88	1021	0.00288	0.5705	-0.00091	- 37.28
63 - 63.5	77	894	0.00289	0.5686	-0.00032	- 13.03
66 - 69	126	1427	0.00289	0.5686	-0.00234	- 93.02
73.5 - 78.5	166	1810	0.00287	0.5704	-0.00407	-156.68
*61 - 61	52	608	0.00290	0.5619	0	0
62 - 64	109	1259	0.00290	0.5619	-0.0018	- 72.89
**65 - 65.5	71	822	0.00288	0.5680	-0.00026	- 10.68
59.5 - 61	91	1091	0.00287	0.5677	-0.00095	- 40.13
53 - 54	71	887	0.00287	0.5677	-0.00077	- 33.89
55 - 58	139	1704	0.00287	0.5677	-0.00288	-124.85
**39 - 38	12	164	0.00285	0.5741	0.00073	35.62
37 - 36	11	153	0.00285	0.5741	0.00060	29.68
35.5 - 34.5	11	156	0.00284	0.5760	0.00068	34.43
**76.5 - 76	31	341	0.00284	0.5760	0.00020	8.01
75.5 - 75	32	354	0.00284	0.5760	0.00023	9.01
75.5 - 74	33	367	0.00284	0.5760	0.00044	17.31
74 - 73	32	357	0.00284	0.5760	0.00046	18.43
**65.5 - 64.5	25	293	0.00284	0.5760	0.00057	24.04
64 - 63	26	307	0.00284	0.5760	0.00050	20.93
63 - 62	26	311	0.00283	0.5781	0.00036	15.59

4. No cavities (oil/oil), 350/20 centistokes

**42.5 - 41.5	21	279	0.00294	0.5706	0.00055	25.09
41 - 40.5	56	751	0.00294	0.5706	0.00027	12.43
40 - 40	95	1301	0.00092	0.5720	0	0
**55 - 55	125	1568	0.00290	0.5762	0	0
55 - 56	168	2101	0.00290	0.5762	-0.00053	- 23.00
56.5 - 57.5	205	2540	0.00290	0.5762	-0.00085	- 36.83
59 - 61	310	3834	0.00288	0.5825	-0.00266	-115.84

5. No cavities (oil/oil), 350/10 centistokes

Oil Level Y1-Y2	N rpm	Λ	$\overline{hi}$ in	ϵ_t	Q in^3/sec	q
70.5 - 69.5	23	255	0.00297	0.5600	0.00098	37.31
65.5 - 64.5	95	1092	0.00296	0.5643	0.00075	29.58
64 - 63	168	1949	0.00296	0.5643	0.00055	22.00
63 - 63.2	246	2860	0.00296	0.5643	-0.00015	- 5.88
61.6 - 61.8	249	2919	0.00296	0.5643	-0.00015	- 6.22
62 - 62.2	303	3544	0.00296	0.5643	-0.00015	- 6.14
62.5 - 63	355	4319	0.00289	0.5758	-0.00052	-22.08
59.5 - 58.5	101	1257	0.00289	0.5758	-0.00070	30.61
58 - 57	149	1871	0.00289	0.5758	-0.00081	35.87
57 - 57	291	3664	0.00289	0.5758	0	0
57.5 - 58.5	434	5508	0.00287	0.5774	-0.00077	-34.41

6. No cavities (oil/oil), 350/5 centistokes

**47 - 46	37	492	0.00290	0.5712	0.00068	31.71
45.5 - 45	70	938	0.00290	0.5712	0.00057	21.49
44 - 43.5	127	1719	0.00290	0.5712	0.00043	20.23
**39 - 38	60	836	0.00290	0.5712	0.00081	39.36
37.5 - 37	144	2023	0.00291	0.5692	0.00046	22.44
37 - 36.5	238	3355	0.00291	0.5692	0.00047	23.19
36.5 - 37	278	3919	0.00291	0.5692	-0.00032	-15.81
33 - 33	284	4111	0.00291	0.5692	0.0	0
33 - 33.1	337	5002	0.00287	0.5749	-0.00007	- 3.44

7. No cavities (oil/oil), 350/2 centistokes

46 - 44	40	490	0.00291	0.5645	0.00118	50.54
43 - 42	102	1268	0.00291	0.5645	0.00104	45.27
41 - 40	144	1812	0.00291	0.5645	0.00097	43.33
39 - 38	163	2077	0.00291	0.5645	0.00102	45.29
37 - 36	228	2942	0.00291	0.5645	0.00094	44.45
35.5 - 35	316	4110	0.00291	0.5645	0.00053	24.09
34.5 - 34	344	4577	0.00288	0.5707	0.00049	23.10

8. No cavities (oil/oil), 350/0.65 centistokes

Oil Level Y1-Y2	N rpm	Λ	$\overline{hi}$ in	ϵ_t	Q in^3/sec	q
56.5 - 55.5	105	1321	0.00290	0.5738	0.00086	37.78
53 - 51.5	141	1816	0.00290	0.5738	0.00174	78.21
50.5 - 48.5	182	2385	0.00290	0.5738	0.00189	86.64
47 - 45.5	225	3011	0.00290	0.5738	0.00172	80.53
**42.5 - 40.5	142	1929	0.00293	0.5700	0.00180	84.68
39 - 37	302	4202	0.00293	0.5700	0.00164	79.38
36 - 34.5	395	5602	0.00293	0.5700	0.00160	78.93
33.5 - 32	430	6082	0.00296	0.5643	0.00135	65.68

9. Cavities (oil/air), 350 centistokes/air

99.5 - 98.5	21	204	0.00292	0.5676	0.00064	21.72
98 - 97	51	501	0.00292	0.5676	0.00040	13.65
95 - 94	65	648	0.00292	0.5676	0.00029	9.95
94 - 93	126	1272	0.00291	0.5694	0.00027	9.52
91 - 90	150	1537	0.00291	0.5694	0.00026	9.42
90 - 89	173	1786	0.00291	0.5694	0.00032	11.52
87 - 86	201	2107	0.00291	0.5694	0.00023	8.49
86 - 85	240	2594	0.00287	0.5773	0.00027	10.43
81 - 80	267	3004	0.00285	0.5789	0.00022	8.81
77 - 76	307	3554	0.00284	0.5834	0.00024	9.73
74 - 73	343	4104	0.00282	0.5899	0.00031	13.24
77 - 72	0	0	0.00291	0.5692	0.00151	58.52
71 - 66	0	0	0.00292	0.5696	0.00149	59.04
65 - 60	0	0	0.00293	0.5700	0.00138	56.06
58 - 53	0	0	0.00293	0.5703	0.00138	57.88
95 - 90	0	0	0.00292	0.5698	0.00161	55.93
88 - 83	0	0	0.00292	0.5698	0.00153	54.89
82 - 77	0	0	0.00292	0.5698	0.00152	56.11
96 - 94	0	0	0.00293	0.5700	0.00161	54.74
93 - 83	0	0	0.00293	0.5700	0.00155	54.75
81 - 79	0	0	0.00293	0.5700	0.00153	56.25
75 - 65	0	0	0.00293	0.5700	0.00141	54.71
63 - 61	0	0	0.00293	0.5702	0.00134	54.43

10. No cavities (oil/oil), 100/100 centistokes

Oil Level Y1-Y2	N rpm	Λ	$\overline{h}_i$ in	ϵ_t	Q in^3/sec	q
73 - 63	0	0	0.00291	0.5694	0.00362	42.63
60 - 50	0	0	0.00291	0.5694	0.00344	43.72
48 - 38	0	0	0.00291	0.5694	0.00321	44.09
36 - 26	0	0	0.00291	0.5694	0.00301	44.99
72.5 - 67.5	10	34	0.00289	0.5733	0.00321	38.21
65 - 62	21	74	0.00289	0.5733	0.00255	31.49
53.5 - 51.5	43	162	0.00289	0.5733	0.00153	20.19
51 - 51	80	303	0.00289	0.5733	0.	0.
51.5 - 53.5	116	436	0.00289	0.5733	-0.00194	-25.58
54.5 - 58	160	587	0.00289	0.5733	-0.00368	-47.48

11. No cavities (oil/oil), 100/350 centistokes

52 - 50	15	56	0.00290	0.5691	0.00184	23.87
49 - 48	35	132	0.00290	0.5691	0.00184	8.48
48 - 47	45	170	0.00290	0.5691	0.00049	6.46
47.5 - 51	122	457	0.00290	0.5691	0.00343	-44.86
53 - 54.5	65	237	0.00290	0.5691	-0.00122	-15.55
56 - 59	131	471	0.00289	0.5757	-0.00335	-42.88
**55 - 54	22	80	0.00289	0.5757	0.00123	15.75
54.5 - 57	88	319	0.00289	0.5757	-0.00250	-31.81
58.5 - 61	100	354	0.00289	0.5757	-0.00298	-37.06
62.5 - 65	162	566	0.00288	0.5752	-0.00339	-41.83

12. No cavities (oil/oil), 100/200 centistokes

87.5 - 83.5	30	92	0.00291	0.5692	0.00306	32.91
80 - 76	32	103	0.00291	0.5692	0.00281	31.39
74 - 74	74	242	0.00291	0.5692	0.	0.
74 - 71	35	116	0.00291	0.5692	0.00244	28.08
68.5 - 65	19	65	0.00291	0.5692	0.00312	37.19
**55 - 55	64	237	0.00289	0.5733	0.	0.
55.5 - 56.5	70	258	0.00289	0.5733	-0.00065	- 8.45
57.5 - 59	90	326	0.00289	0.5733	-0.00148	- 18.85
**56.5 - 61.5	99	355	0.00288	0.5753	-0.00431	- 54.40
64 - 68	149	520	0.00288	0.5753	-0.00457	- 56.20
71 - 74	196	659	0.00288	0.5753	-0.00421	- 49.88

13. Cavities (oil/air), 100 centistokes/air

Oil Level Y1-Y2	N rpm	Λ	$\overline{hi}$ in	ϵ_t	Q in^3/sec	q
62.5 - 59.5	35	123	0.00289	0.5665	0.00223	27.33
57 - 54	14	51	0.00289	0.5665	0.00288	36.53
52 - 50	51	190	0.00289	0.5665	0.00164	21.45
49 - 47	74	281	0.00289	0.5665	0.00127	16.87
46 - 44.5	77	297	0.00289	0.5665	0.00121	16.32
43.5 - 42.5	133	522	0.00289	0.5665	0.00094	12.84
37 - 36	129	533	0.00288	0.5683	0.00081	11.86
35.5 - 34.5	164	687	0.00288	0.5705	0.00069	10.24
67 - 66	284	995	0.00285	0.5789	0.00060	7.52
51.5 - 50.5	318	1223	0.00285	0.5789	0.00066	9.03
50 - 49	372	1461	0.00283	0.5832	0.00051	7.13

TABLE X

HIGH SPEED INERTIA TESTS
CONCENTRIC MISALIGNED FACE SEAL DATA
NARROW LAND SEAL, Ri = 0.83

1. 10 centistoke oil, $\epsilon_t = 0.0$

Oil Level Y1-Y2	N rpm	Λ	$\overline{h}_i$ in	ϵ_t^2	Q in^3/sec	q	P_{corr}
95 - 75	0	0	0.00300	9.25E-6	0.0346	1.010	0.0066
65 - 55	0	0	0.00300	9.25E-6	0.0346	1.010	0.0066
45 - 25	0	0	0.00300	9.25E-6	0.0258	1.016	0.0080
80 - 60	250	74	0.00300	2.34E-6	0.0388	1.165	0.1169
90 - 70	500	142	0.00298	0.	0.0435	1.171	0.1702
100 - 80	750	203	0.00297	0.	0.0486	1.134	0.2167
100 - 80	1000	274	0.00295	0.	0.0537	1.124	0.3037
100 - 80	1250	348	0.00293	0.	0.0601	1.110	0.4104
100 - 80	1500	417	0.00292	2.47E-6	0.0664	1.057	0.4895
100 - 80	1650	464	0.00290	0.	0.0721	1.064	0.5934
Realign Spindle							
100 - 80	1000	266	0.00299	9.38E-6	0.0561	1.124	0.3034
100 - 80	2000	535	0.00297	5.94E-7	0.0935	1.031	0.7938
75 - 55	2500	778	0.00295	5.43E-6	0.1098	0.9594	1.0617
90 - 50	3000	924	0.00291	5.58E-6	0.1403	0.9511	1.5139
90 - 50	4000	1256	0.00287	5.74E-6	0.2020	0.8745	2.3388
80 - 40	5000	1816	0.00275	2.78E-6	0.2295	0.7640	2.8972

2. 10 centistoke oil, $\epsilon_t = 0.56$

100 - 80	0	0	0.00288	0.3065	0.0468	1.4627	0.0514
95 - 75	250	75	0.00287	0.3087	0.0468	1.4797	0.0715
100 - 80	500	146	0.00286	0.3112	0.0515	1.4905	0.1147
100 - 80	750	215	0.00286	0.3112	0.0561	1.4361	0.1464
100 - 70	1000	291	0.00286	0.3112	0.0631	1.4321	0.2295
100 - 70	1500	440	0.00285	0.3132	0.0815	1.3830	0.4281
80 - 40	2000	675	0.00284	0.3180	0.0990	1.3019	0.6503
40 - 10	2500	1082	0.00280	0.3275	0.1222	1.2795	0.9893
80 - 40	3000	1021	0.00280	0.3275	0.1578	1.1727	1.2002

*Reservoir first flooded with 350 centistoke oil, siphoned out and then filled with 100 centistoke oil.

**Siphon out and refill reservoir.

TABLE XI

SEAL CONDITIONS
FOR THE
CAVITY SHAPE EXPERIMENTS
(SEE FIGURES 8(a) - (s))
$R_i = 0.83$, $\bar{h} = 0.003$ in

1. $\epsilon_t = 0.56$, $\epsilon_r = 0.091$

Oil Level Y1-Y2	N rpm	Λ	$\bar{h}_i$ in	ϵ_t	Q in^3/sec	q	Figure No.
79 - 78	39	432	0.00293	0.5633	0.00052	20.02	8(a)
77.5 - 76.5	101	1128	0.00293	0.5633	0.00053	20.45	8(b)
76 - 75	160	1801	0.00293	0.5633	0.00051	19.71	8(c)
74.5 - 73.5	190	2197	0.00291	0.5692	0.00048	19.25	8(d)
69 - 68	234	2793	0.00291	0.5692	0.00046	19.10	8(e)
67.5 - 66.5	298	3647	0.00288	0.5730	0.00044	18.75	8(f)
85.5 - 84.5	173	1866	0.00292	0.5651	0.00026	9.79	8(g)
80 - 79	34	378	0.00292	0.5651	0.00047	18.09	8(h)
78.5 - 77.5	78	874	0.00292	0.5651	0.00031	11.99	8(i)
77 - 76	126	1423	0.00292	0.5651	0.00029	11.25	8(j)
75.5 - 74.5	210	2409	0.00291	0.5623	0.00025	9.93	8(k)
70.5 - 69.5	281	3325	0.00291	0.5621	0.00028	11.76	8(l)
--	600	--	--	--	--	--	8(m)
--	600	--	--	--	--	--	8(n)
58 - 57	385	5134	0.00284	0.5739	0.00026	12.18	8(o)
53 - 52	503	7057	0.00282	0.5801	0.00036	18.44	8(p)

2. $\epsilon_t = 0.56$, $\epsilon_r = 0.0$

Oil Level Y1-Y2	N rpm	Λ	$\bar{h}_i$ in	ϵ_t	Q in^3/sec	q	Figure No.
62 - 60	31	376	0.00294	0.5658	0.00143	60.09	No Cavity
59 - 57	121	1497	0.00293	0.5656	0.00138	59.24	No Cavity
53 - 51	154	1980	0.00293	0.5656	0.00134	59.75	No Cavity
49 - 47	203	2680	0.00293	0.5656	0.00136	62.34	No Cavity
46 - 44	241	3246	0.00293	0.5656	0.00144	67.25	No Cavity
43 - 41	312	4360	0.00291	0.5670	0.00134	65.45	8(q)
37 - 35	380	5541	0.00291	0.5670	0.00122	62.03	8(r)
34 - 32	505	7706	0.00288	0.5728	0.00120	60.30	8(s)

TABLE XII

DATA REDUCTION PROGRAM NO. 3

A. Listing

```
1 PRINT "    ORDER OF OUTPUT"
2 PRINT
3 LET K= 0
4 PRINT "  RUN NO","FLOW","H BAR","E SUB T↑2"
5 READ S,S0,E0
6 PRINT
7 PRINT "  Q","LAMBDA 1","QPUMP","QPUMP/L*ER*E"
8 FOR I= 1 TO S
10 READ R,Y1,Y2,T,H1,H2,F
13 LET P1=0.
15 LET W= 0.
20 LET X1=-2
25 LET X2= 1
27 LET D= 2.75
30 LET H1= H1*1E-3
35 LET H2= H2*1E-3
37 LET B= (H2-H1)/(X2-X1)
40 LET A= H1-B*X1
50 LET K= K+1
60 LET W0= W*1E-6*268
70 LET H= A+W0
80 LET P2= (((Y1+Y2)/2)+107.5)*.00351
85 LET P3= 2.68E-7*R↑2
90 LET Q1= (Y1-Y2)*.02525/T
100 LET P= P1+P2+P3
110 LET M= EXP(2.9876-.0089*F)
115 LET E= B*D/(2*H)
120 LET Q= 1.76E-6*M*Q1/(P*H↑3)*.0296
125 LET L1= 1.67E-7*R*M/((P-P3)*H↑2)
130 LET Q0= 1.+S0*E↑2
135 LET Q9= Q/Q0
140 LET R1=0.
150 PRINT
160 PRINT K,Q1,H,E↑2
165 PRINT Q,L1,Q9,R1
210 NEXT I
211 PRINT
212 PRINT
900 DATA 9,1.18,0
```

B. Program Description

This program is very similar to data reduction program No. 1 but it has the inertia component of leakage added to it. This can be seen as P3 in the program listing. This program was used to reduce the data to that shown in Table X.

NOMENCLATURE

A - seal area, in^2

A_f - flow area, in^2

h - film thickness, in

$\bar{h}_i$ - average film thickness at inside radius, in

e - displacement between seal center and shaft center, in

y - coordinate across the film, in

ρ - coordinate measured from center of shaft, in

ρ - density, lb/in^3

r - coordinate measured from center of seal, in

θ - angular coordinate, radian

β - $\alpha + \theta$, radian

α - phase angle between waviness and eccentricity, radian

γ - angle measured to ρ, radian

ψ - tilt phase angle, radian

t - time, seconds

U - fluid velocity, in/sec

ω - rotational speed, radian/sec

Q - flow rate, in^3/sec

p - pressure, psi

τ - shear stress, psi

W - seal load capacity, lb_f

SM - shaft friction moment, $in\text{-}lb_f$

C_p - specific heat, $Btu/lb\,^oF$

k - thermal conductivity, $Btu/sec\ in\ ^oF$

T - temperature, ^oF

Φ - dissipation function, sec^{-1}

μ - dynamic viscosity, psi-sec

Dimensionless Terms

R - radius ratio = r/r_o

H - film thickness ratio = $h/\bar{h}_i$

P - pressure ratio = p/p_o

Λ = seal number = $\frac{6\mu\omega}{P_o}\left(\frac{r_o}{\bar{h}_i}\right)^2$

ϵ - waviness parameter

ϵ_r - radial eccentricity

ϵ_t - tilt eccentricity

C_L - load coefficient = $\frac{W}{p_o r_o^2}$

C_f - friction coefficient = $\frac{SM}{\bar{h}_i^3 p_o r_o^2 /6}$

q - flow coefficient = $\frac{12\mu Q}{\bar{h}_i^3 p_o}$

U' - pumping velocity variable = $\frac{U}{r_o\omega}$

ξ - radius variable = $\frac{r - r_i}{r_o - r_i}$

λ - film thickness variable = $\frac{h_o - \bar{h}_i}{\bar{h}_i}$

n - number of circumferential waves

E_{ij} - numerical grouping

D_i - numerical grouping

Subscripts

o - at the outside radius of the seal

i - at the inside radius of the seal

C - within the cavitated film

REFERENCES

1. "Study of Dynamic and Static Seals for Liquid Rocket Engines", NASA Contract No. 7-434, Phase I, Appendix C.

APPENDIX D

SEAL DESIGN I

BY

J. A. FINDLAY

I. INTRODUCTION

The work on this task has been concerned primarily with the extension of the basic theories of seal cavitation to the misaligned eccentric seal and thus to include inward pumping. Expressions have been derived so that either the "wavy" seal or the tilted seal may be considered. The theories derived in this task have been used in making supporting calculations for the cavitation and pumping experiments of Task III. This was accomplished using a GE 635 computer program. The iterative method used in this program was improved so that a numerical solution to the short bearing approximation is obtained in one sweep. Subsequent iterations include the two-dimensional effects. Convergence is attained in fewer iterations than the previous method. Work has also been done towards modifying this computer program so that cavity solutions can be obtained for the eccentric seal.

Further analytical work has been done on the two-fluid problem. This considers the case when the fluids on either side of the face seal are of different viscosities. The effect of the viscosity of both the inside and outside fluids on the leakage rates has been studied.

II. INWARD PUMPING IN MECHANICAL FACE SEALS

A. INTRODUCTION

Hydrodynamic effects have been shown to exist in mechanical face seals.[1] Seal forces and leak rates are primary considerations in the design and application of face seals. Therefore, it is important to understand the basic principles of face seal operation. (See Figure 1.)

An anomolous behavior observed in face seal experiments by Denny [1], Nau [2] and others, is that of "inward pumping". This is a condition where fluid or air leaks through the seal in the opposite direction to the hydrostatic pressure drop across the seal. The term "inward pumping" was attached to this

[1] Numbers in parentheses refer to similarly numbered references in bibliography at end of Appendix.

phenomena because in the seal experiments where it was observed the inside of the seal was pressurized. Therefore, any leakage in the outward direction was attributed to the hydrostatic pressure differential while observed leakage toward the center of the seal and against the pressure was attributed to a pumping action in the seal.

So far no satisfactory explanation of this phenomenon has been set forth. Nau[3] in a recent paper based on experiments using a transparent seal apparatus confirmed his earlier postulate [4] that lubricant cavitation was the cause for "inward pumping". He also concluded that this pumping action occurred only in the inward direction.

Lyman and Saibel [5], using an approximate solution to the face seal hydrodynamic problem with gas cavities, were able to calculate an "inward pumping" rate for the case of no pressure difference across the seal.

Findlay[6], [7] and [8] showed analytically that cavity solutions using the Swift-Floberg [14], [15] boundary conditions, i.e., conservation of flow at the cavity boundaries, did not result in any "inward pumping". Subsequent experimental results reported here and in [9] confirm this conclusion and substantiate the short bearing theory put forth in [6].

A theory is developed here which shows that a combination of radial eccentricity and misalignment, or one circumferential film thickness wave will result in a "pumping" leakage which may be either inward or outward. Experimental results reported here and in [9] confirm this theory, which was developed for a full film, i.e., no gas cavities. Experiments and theory for the eccentric seal with gas cavities show that rather than causing "inward pumping" the cavities reduce the pumping effect.

B. DERIVATION OF THE SHORT BEARING PUMPING SOLUTION

1. General Equations for the Wavy Seal

Reynolds' equation for the radially eccentric face seal is

$$\frac{\partial}{\partial R}\left[RH^3\,\frac{\partial P}{\partial R}\right] + \frac{1}{R}\,\frac{\partial}{\partial \theta}\left[H^3\,\frac{\partial P}{\partial \theta}\right] = \Lambda\left\langle \frac{\partial}{\partial R}\left[RH\,U_r'\right] + \frac{\partial}{\partial \theta}\left[H\,U_\theta'\right]\right\rangle \qquad (1)$$

where, from Fig. 2, the relative seal surface velocities are given by the following expressions

$$U_r' = \epsilon_r \cos\beta \qquad (2)$$

$$U_\theta' = R + \epsilon_r \sin\beta \qquad (3)$$

Using the short bearing approximation, where the $\partial p/\partial\theta$ term is neglected, and assuming that the film thickness is a function of θ only, as in the wavy seal case, equation (1) reduces to

$$\frac{d}{dR}\left[RH^3\,\frac{dP}{dR}\right] = \Lambda\,(R + \epsilon_r \sin\beta)\,\frac{dH}{d\theta} \tag{4}$$

Integration of this expression gives the following general solution,

$$P = \frac{\Lambda}{H^3}\left(\frac{R^2}{4} + R\,\epsilon_r \sin\beta\right)\frac{dH}{d\theta} + \frac{C_1}{H^3}\,\ell nR + C_2 \tag{5}$$

where C_1 and C_2 are constants of integration which are determined from the boundary conditions on the pressure.

For the case where gas cavities may be present in the fluid film [6], there are three separate film regions and three sets of boundary conditions where equation (5) must be applied. These regions, shown in Fig. 3, are:

1. The full film region where the film extends across the face of the seal.
2. The outer film region where the film extends from the outer edge of the cavity to the outer edge of the seal.
3. The inner film region where the film extends from the inner edge of the seal to the inner edge of the cavity.

There is also the cavity region where the pressure is constant and equations (4) and (5) do not apply.

The general form of the boundary conditions is

$$P = P_m \;@\; R = R_m \text{ and } P = P_n \;@\; R = R_n \tag{6}$$

where the specific values for each region are given by the following table:

	P_m	P_n	R_m	R_n	R_c
Full film region	P_i	P_o	R_i	1	-
Inner film region	P_i	P_c	R_i	R_1	R_1
Outer film region	P_c	P_o	R_2	1	R_2

The pressure and radial pressure gradient in any region have the following general form

$$(P - P_n) = \frac{\ell n(R/R_n)}{\ell n(R_m/R_n)} (P_m - P_n) + \frac{\Lambda}{4H^3} \frac{dH}{d\theta} \left\{ (R^2 - R_n^2) + 4 (R - R_n) \epsilon_r \sin\beta + \frac{\ell n(R/R_n)}{\ell n(R_m/R_n)} \left[(R_m^2 - R_n^2) + 4 (R_m - R_n) \epsilon_r \sin\beta \right] \right\} \quad (7)$$

$$\frac{dP}{dR} = \frac{(P_m - P_n)}{R \ell n R_m/R_n} + \frac{\Lambda}{4H^3} \frac{dH}{d\theta} \left\{ \left[2R + \frac{(R_n^2 - R_m^2)}{R \ell n(R_m/R_n)} \right] + 4 \left[1 + \frac{(R_n - R_m)}{R \ell n(R_m/R_n)} \right] \epsilon_r \sin\beta \right\} . \quad (8)$$

2. Full Film - Single Fluid Case

If it is assumed that the same fluid is present on both sides of the seal and that the fluid film is complete, i.e., no gas cavities, then, equation (8) becomes

$$\frac{dP}{dR} = \frac{(P_i - P_o)}{R \ell n R_i} + \frac{\Lambda}{4H^3} \frac{dH}{d\theta} \left\{ \left[2R + \frac{(1 - R_i^2)}{R \ell n R_i} \right] + 4 \epsilon_r \sin\beta \left[1 + \frac{(1 - R_i)}{R \ell n R_i} \right] \right\} \quad (9)$$

The leakage coefficient for the radially eccentric seal is defined as

$$q = \int_o^{2\pi} \left[\Lambda H U_r' - H^3 \frac{dP}{dR} \right] R \, d\theta \quad (10)$$

Therefore, integrating at $R = R_o = 1$ we have

$$q = \int_o^{2\pi} \left\{ -\Lambda H \epsilon_r \cos\beta - H^3 \frac{(P_i - P_o)}{\ell n R_i} - \frac{\Lambda}{4} \frac{dH}{d\theta} \left[2 + \frac{1 - R_i^2}{\ell n R_i} \right] - \Lambda \frac{dH}{d\theta} \epsilon_r \sin\beta \right. \quad \text{(con't)}$$

$$- \Lambda \frac{dH}{d\theta} \epsilon_r \sin\beta \frac{(1 - B_i)}{\ell n R_i} \Bigg\} d\theta$$

$$= - \frac{(P_i - P_o)}{\ell n R_i} \int_o^{2\pi} H^3 \, d\theta - \Lambda \epsilon_r \frac{(1 - R_i)}{\ell n R_i} \int_o^{2\pi} \frac{dH}{d\theta} \sin\beta \, d\theta$$

$$- \frac{\Lambda}{4} \left[2 + \frac{1 - R_i^2}{\ell n R_i} \right] \int_o^{2\pi} \left| \frac{dH}{d\theta} \right| d\theta - \Lambda \epsilon_r \int_o^{2\pi} \frac{d}{d\theta} \left[H \sin\beta \, d\theta \right]. \quad (11)$$

If a wavy seal surface is assumed the film thickness is given by

$$H = 1 + \epsilon \cos n\theta \quad (12)$$

For this case the leakage coefficient becomes

$$q = - \frac{(P_i - P_o)}{\ell n R_i} \int_o^{2\pi} (H \epsilon \cos n\theta)^3 \, d\theta$$

$$- \Lambda \epsilon_r \frac{(1 - R_i)}{\ell n R_i} \int_o^{2\pi} (- \epsilon \, n \sin n\theta) \sin(\alpha + \theta) \, d\theta$$

$$= - \frac{(P_i - P_o)}{\ell n R_i} \, 2\pi \, (1 + 1.5 \epsilon^2) + \Lambda \epsilon_r \epsilon \pi \frac{(1 - R_i)}{\ell n R_i} \cos\alpha \quad (13)$$

for n = 1. It will be noted that for n > 1 the hydrostatic leakage is unchanged but the pumping leakage becomes zero.

The first term in equation (13) is the seal leakage due to the hydrostatic pressure differential. The second term is the leakage due to the radial eccentricity of the seal coupled with the circumferential variation in the film thickness. This second leakage term may either be inward or outward depending upon α, the phase angle between the surface waviness and the eccentricity vector (Fig. 2), or upon the direction of rotation, ω, which appears in Λ.

The shaft-seal radial eccentricity that will make the net leakage zero is

$$e = \epsilon_r r_o = \frac{(p_i - p_o) h_i^2 (1 + 1.5 \epsilon^2)}{3 \mu \omega (r_o - r_i) \epsilon \cos\alpha} \quad (14)$$

For the minimum value of e in equation (14) we find that

$$\cos \alpha = 1; \ \alpha = 0^{o} \tag{15}$$

$$(1 + 1.5\ \epsilon^{2})/\epsilon = 2.45 \quad \epsilon = 0.817 \tag{16}$$

Note that $0 \leq \epsilon \leq 1$ and at $\epsilon = 1$, $(1 + 1.5\ \epsilon^{2})/\epsilon = 2.50$.

Substituting (15) and (16) into (14) and using the test seal conditions, i.e., $r_o = 1.75$ in, $r_i = 1.125$ in, $\mu = 4.95 \times 10^{-5}$ psi/sec (350 centistokes), the result is

$$e = 2.52 \times 10^{5}\ (p_i - p_o)\ h_i^2 \ /\ N\ (\text{rpm}) \tag{17}$$

In order to estimate the order-of-magnitude of e let the following conditions be assumed,

$$(p_i - p_o) = 5 \text{ psi}$$
$$h_i = 10^{-3} \text{ in}$$
$$N = 10^{3} \text{ rpm}$$

Therefore, for this numerical example

$$e = 1.26 \times 10^{-3} \text{ in} \tag{18}$$

It would not be unusual to have a shaft-seal radial eccentricity of this magnitude. Even though the viscosity assumed in this calculation was quite high, the film thickness was much larger than normally would occur in a face seal. Further, if the equation for the seal leakage is written in dimensional terms, i.e.,

$$Q = - \frac{2\pi\ (1 + 1.5\ \epsilon^{2})\ \bar{h}_i^{3}\ (p_i - p_o)}{12\ \mu\ \ell n\ R_i} + 6\pi\omega\ r_o^{2}\ \epsilon_r\ \epsilon\ \frac{(1 - R_i)}{12\ \ell n\ R_i}\ h_i \cos\alpha$$

$$= Q_o + Q_{pump} \tag{19}$$

then it will be noted that

$$Q_o \propto \bar{h}_i^{3}$$

$$Q_{pump} \propto \bar{h}_i \tag{20}$$

Therefore, as the average seal film thickness, $\bar{h}_i$ decreases, the pumping component of the leakage becomes relatively more significant.

Thus it has been shown that for mechanical face seals the pumping leakage due to radial eccentricity can be a very important factor and for the small film thicknesses that normally occur only a small radial eccentricity is needed. In fact, it becomes a question whether or not this phenomenon can be completely eliminated from face seal experiments and applications.

C. MISALIGNED-ECCENTRIC SEAL

As will be explained later the experimental results were obtained for the misaligned-radially eccentric seal rather than the wavy-radially eccentric seal. Therefore, an analysis of this problem is of importance in verifying the seal hydrodynamic theory developed in this paper.

The wavy and misaligned cases approach one another as the seal radius ratio, R_i, approaches unity. The wavy solution is presented because it is much easier to obtain and the form of the final expression for leakage is simple and, thus, more readily understood.

It was found to be more convenient to obtain solutions to the misaligned, full-film problem using numerical computer solutions. The FORTRAN IV program used on the GE 635 computer for this purpose is explained in more detail in Part IV. The approach used shows that the "short bearing" approximation is very good.

For the misaligned seal the film thickness distribution is given by

$$H = 1 + R\,\epsilon_t \cos\theta \tag{21}$$

and, therefore, is no longer a function of θ only. Thus equation (1) becomes,

$$\frac{\partial}{\partial R}\left[RH^3\,\frac{\partial P}{\partial R}\right] + \frac{1}{R}\,\frac{\partial}{\partial \theta}\left[H^3\,\frac{\partial P}{\partial R}\right] = \Lambda\left\{R\,U_r'\,\frac{\partial H}{\partial R} + U_\theta'\,\frac{\partial H}{\partial \theta}\right\}$$

$$= \Lambda\left\{(-R\,\epsilon_r\cos\beta)\,(\epsilon_t\cos\theta) + (R + \epsilon_r\sin\beta)\,(-R\,\epsilon_t\sin\theta)\right\}$$

$$= \Lambda\left\{-R\,\epsilon_r\,\epsilon_t\cos\alpha - R^2\,\epsilon_t\sin\theta\right\} \tag{22}$$

The "short bearing" approximation could be used here to obtain a solution. However, this approach requires using some series approximations. Since a numerical computer program was already available it was decided to use it instead. Equation (22) was solved in two parts. The first was for the hydrostatic

leakage where ϵ_r, the radial eccentricity ratio, was zero and the boundary conditions were $P = P_i$ @ $R = R_i$, $P = P_o$ @ $R = 1$. These solutions are plotted in Fig. 4 and take the following form,

$$-\frac{q_o \ell n\, R_i}{2\pi(P_i - P_o)} = \frac{Q_o\, 12\, \mu\, \ell n\, R_i}{2\pi\, \bar{h}_i^3 (p_i - p_o)} = 1 + a\, \epsilon_t^2 \tag{23}$$

where the slope, a, is a function of R_i and is shown in Fig. 5.

The second part of the solution to equation (22) is for the pumping component and is obtained by using a finite value for ϵ_r and applying the boundary conditions $P_i = P_o = 0$. As can be seen from equation (22) the result will be in terms of the constant factor $\Lambda\, \epsilon_r\, \epsilon_t \cos\alpha$, the same as for the wavy case. Values for

$$\frac{q_{pump}}{\Lambda\, \epsilon_r \epsilon_t \cos\alpha} = \frac{2\, Q_{pump}}{\epsilon_r \epsilon_t \cos\alpha\, \bar{h}_i \omega r_o^2} = f\,(R_i, \epsilon_t) \tag{24}$$

are plotted in Fig. 10.

D. ECCENTRIC SEAL WITH CAVITY

Once the equation (8) for the radial pressure gradient has been formulated, two equations can be determined for the cavity boundary shape from the cavity boundary conditions. Using the short bearing approximation, the upstream cavity boundary condition is

$$(\nabla P)_c = \left(\frac{dP}{dR}\right)_c = 0 \tag{25}$$

and for the downstream cavity boundary condition

$$(H_2 - H_1)\,\Lambda \left[\frac{U'_\theta}{R} - U'_r \left.\frac{d\theta}{dR}\right|_c\right] = H_2^3 \left[\frac{1}{R^2}\frac{\partial P}{\partial \theta} - \frac{\partial P}{\partial R}\left.\frac{d\theta}{dR}\right|_c\right] \tag{26}$$

$$= H_2^3 \left[\left.\frac{dP}{dR}\right|_c \left.\frac{d\theta}{dR}\right|_c\right] \tag{27}$$

The circumferential pressure gradient, $\partial P/\partial\theta$, has been neglected as in the original assumption.

The equation for the upstream cavity boundary shape is found by substituting equation (8) into equation (25),

$$\frac{1}{H^3}\frac{dH}{d\theta} = \frac{(P_m - P_n)}{\frac{\Lambda}{4}\left\{2R_c^2 \ell n\, R_n/R_m + (R_m^2 - R_n^2) + 4\,\epsilon_r \sin\beta\left[R_c \ell n\, R_n/R_m + (R_m - R_n)\right]\right\}}$$

The equation describing the downstream cavity boundary shape is obtained by substituting equation (8) into equation (27),

$$\left(\frac{dR}{d\theta}\right)_c = \frac{H_2^3 R_c}{(H_1 - H_2)\, U'_\theta\, \Lambda}\left(\frac{dP}{dR}\right)_c + \frac{R_c U'_r}{U'_\theta}$$

$$= \frac{H_2^3 R_c}{(H_1 - H_2)\, U'_\theta\, \Lambda}\left\{\frac{P_m - P_n}{R_c \ell n\, R_m/R_n} + \frac{\Lambda}{4H_2^3}\frac{dH_2}{d\theta}\left[2R_c + \frac{(R_n^2 - R_m^2)}{R_c \ell n\, R_m/R_n} + 4\,\epsilon_r \sin\beta\left[1 + \frac{(R_n - R_m)}{R_c \ell n\, R_m/R_n}\right]\right]\right\} + \frac{R_c U'_r}{U'_\theta} \qquad (29)$$

It should be noted that when the appropriate substitutions are made for n, and m, for the various regions discussed before, R_1 will be the inner cavity boundary, i.e., the boundary closest to R_i, and R_2 will be the outer cavity boundary, i.e., closest to R_o. This nomenclature is not to be confused with H_1, which is the film thickness on the upstream boundary of the cavity and H_2 the film thickness on the downstream boundary (Fig. 3). By definition, the upstream cavity boundary is where the fluid streamers leave the complete film region and enter the cavity region, and the downstream cavity boundary is where these same streamers re-enter the full film region.

The point where the cavity boundary is tangent to the relative surface velocity vector distinguishes the difference between the upstream and the downstream cavity boundaries. This point, therefore, is located where the following expression is satisfied,

$$\left(\frac{dR}{d\theta}\right)_c = \frac{R_c U'_r}{U'_\theta} \qquad (30)$$

Note that equations (29) and (30) are consistent since at this point of intersection the upstream boundary condition, equation (25), also applies and equation (29) reduces to equation (30).

The remaining required expression is the one needed to solve for H_1. The H_1 which corresponds to a given H_2 in equation (29), i.e., to a specific point on the downstream boundary, is found by tracing the streamer path through the cavity. That is, the proper H_1 for a given H_2 is obtained by determining the departure point on the upstream boundary for the fluid streamer entering the downstream boundary at H_2 (see Fig. 3). For a given point on the downstream boundary of the cavity (R_d, θ_d), the required coordinates on the upstream boundary (R_u, θ_u) are obtained from the following equation

$$R_u^2 + 2\, e_r\, R_u \sin\beta_u = R_d^2 + e_r\, R_d \sin\beta_d \tag{31}$$

These equations are sufficient to calculate the dimensions of the gas cavity and thus yield the solution for pressure in the seal film. From this solution the load, flow and torque coefficients may be calculated,

$$C_L = \int_0^{2\pi} \int_{R_I}^{1} PRDRd\theta \tag{32}$$

$$q = \int_0^{2\pi} \left(\Lambda\, H\, U_r' - H^3 \frac{\partial P}{\partial R} \right) Rd\theta, \quad R = \text{const.} \tag{33}$$

$$C_f = \int_0^{2\pi} \int_{R_I}^{1} \left(\Lambda \frac{U_\theta'}{H} + \frac{3H}{R} \frac{\partial P}{\partial \theta} \right) R^2\, dRd\theta \tag{34}$$

Note that equation (34) represents the torque about the center of the seal.

E. EXPERIMENTAL RESULTS

The experimental apparatus used is described in Appendix C. (Figures referenced in this Part E are in Appendix C.) Figure 21 shows the comparison between theory and experiment for the full film outward pumping case. Fig. 22 shows the comparison for the inward pumping case. In the latter set of data it was difficult to supply enough oil to the reservoir surrounding the outside of the seal because of the net inward pumping taking place. Therefore, only low speed data was obtained.

When the outside of the seal is not flooded, gas cavities appear in the seal interface as shown in Figures 9, 10, 11 and 12. When this occurs the inward pumping effect is diminished as can be seen by the data plotted in Figures 19, 20, 21 and 23.

F. DISCUSSION

1. Correlation of Theory

For the full film case the correlation between experiment and theory was quite good. As yet numerical results have not been obtained from the theory developed for the radially eccentric seal containing gas cavities. The equations for the full film - two fluid problem have been derived but not set up for solution as yet. It is hoped that these two solutions can be pursued further.

2. Previous Investigations

The work of Denny [1] demonstrated the existence of hydrodynamic forces in mechanical face seals. He and Nau [3] both observed the "inward pumping" phenomenon. Nau [2], [3] also observed gas cavities in transparent seal experiments. Because he observed these two phenomena simultaneously he was led to the conclusion that the cavitation produced the pumping leakage. Lyman and Saibel [5], in their approximate cavitation seal analysis, tried to show theoretically that gas cavities did cause inward pumping in addition to hydrodynamic lift forces. Orcutt and Cheng [12] and Pape [13] also used approximate cavity solutions to demonstrate the relationship between this phenomenon on the hydrodynamic lifting force observed by Denny [1].

All these solutions [5], [12], [13], neglected to use conservation of flow boundary conditions (Swift-Floberg) at the edges of the cavities. Thus continuity of flow was not maintained. Pape [13] recognized this fact and Orcutt and Cheng [12] did not use their solution to calculate flow rates, for if they had, the same leakage rate would not have been obtained at both the inner and outer radii. This was the mistake that Lyman and Saibel [5] made. They integrated the local, radial flow rates at the inside radius of the seal and obtained an inward leakage when cavities were assumed. If, however, they had done the same at the outer radius they would have obtained an outward leakage for the same case. Thus a basic inconsistency existed in their solution and they were mislead to believe that cavitation produces inward pumping in face seals.

III. CAVITY EXPERIMENTS

A. WAVY SEAL

Although the cavity experiments were carried out on a misaligned seal, the analysis for a wavy seal interface that was carried out in Phase I [8] can

be used as an approximation. Thus, the film thickness variation for a misaligned seal is

$$H = 1 + \epsilon\ R \cos\theta \tag{35}$$

but can be approximated by

$$H = 1 + \epsilon \cos\theta \tag{36}$$

for R 1, i.e., small land width seal. For this case the upstream cavity boundary shape is given by the following expression

$$Y = \frac{1}{H^3}\ \frac{dH}{d\theta} = \frac{(P_o - P_i)}{\frac{\Lambda}{4}\left[2\ Rc^2\ \ln\frac{R_i}{R_c} + R_c^2 - R_i^2\right]} \tag{37}$$

where

$$\frac{1}{H^3}\ \frac{dH}{d\theta} = \frac{\epsilon\ \sin\theta}{(1 + \epsilon\ \cos\theta)^3} \tag{38}$$

Equation (38) is plotted in Figure 6 for various values of ϵ. In addition, the curve which represents the limit of application of equation (37) is shown. This occurs at

$$\frac{d}{d\theta}\left[\frac{1}{H^3}\ \frac{dH}{d\theta}\right] = 0 \tag{39}$$

which yields the following expression

$$\epsilon = \frac{-\cos\theta}{(3\ \sin^2\theta + \cos^2\theta)} \tag{40}$$

Values of Y corresponding to equations (39) and (40) are designated Y_{crit}.

In order to find the seal conditions for which a cavity will first appear, R_c should be set equal to R_o in equation (37). Therefore, from equation (37) we have

$$\Lambda = \frac{6\ \mu\ \omega}{p_i}\left(\frac{r_o}{\bar{h}_i}\right)^2 = \frac{13.57}{Y_{crit}} \tag{41}$$

where

$$R_i = \frac{r_i}{r_o} = \frac{d_i}{d_o} = \frac{2.250"}{3.50"} = 0.643$$

for the test seal. Using a 350 centistoke (4.95×10^{-5} psi-sec) (silicone oil) the speed-pressure ratio as a function of film thickness and misalignment can be computed from equation (41) as follows,

$$N/p_i = 1.426 \times 10^5 \frac{\bar{h}_i^2}{Y_{crit}} \text{ , rpm/psig} \tag{42}$$

Taking the values of Y_{crit} from Figure 6, the curves in Figure 7 were plotted.

The parameters $\bar{h}_i$ and ϵ are related to the minimum and maximum film thickness by the following expressions

$$h_{min} = \bar{h}_i (1-\epsilon) \tag{43}$$

$$h_{max} = \bar{h}_i (1+\epsilon) \tag{44}$$

$$\epsilon = \frac{h_{max} - h_{min}}{h_{max} + h_{min}} \tag{45}$$

$$\bar{h}_i = \frac{h_{max} + h_{min}}{2} \tag{46}$$

In the seal experiment it is the minimum and maximum film thicknesses that are set.

Once the cavity has formed and is of a finite size, the position of the cavity nose can be found by calculating Y from the following expression

$$Y = 1.426 \times 10^5 \bar{h}_i^2 \frac{p_i}{N} \tag{47}$$

and then finding θ from Figure 6 using the correct ϵ curve.

B. MISALIGNED SEAL

In the misaligned or tilted face seal the film thickness is a function of radius as well as θ. For this case the integration of the "short bearing" approximation to Reynold's equation is somewhat more complicated.

For the general case of seal misalignment and surface waviness the film thickness distribution is

$$H = (1 + \epsilon \cos n\theta) + R\left[\epsilon_t \cos(\theta + \psi)\right] \tag{48}$$

$$= a + b\,R \tag{49}$$

and

$$\frac{\partial H}{\partial \theta} = -\epsilon N \sin n\theta - R\,\epsilon_t \sin(\theta + \psi) \tag{50}$$

$$\frac{\partial H}{\partial R} = \epsilon_t \cos(\theta + \psi) = b\,. \tag{51}$$

The "short bearing" approximation to Reynold's equation for an eccentric face seal is

$$\frac{1}{R}\frac{\partial}{\partial R}\left(RH^3 \frac{\partial P}{\partial R}\right) = \Lambda\left\{-\epsilon_r \cos\beta \frac{\partial H}{\partial R} + \left(1 + \frac{\epsilon_r}{R}\sin\beta\right)\frac{\partial H}{\partial \theta}\right\} \tag{52}$$

or

$$\frac{\partial}{\partial R}\left(RH^3 \frac{\partial P}{\partial R}\right) = -\Lambda\left\{\left[\epsilon_r \sin\beta\ \epsilon\ n \sin n\theta\right] + \left[\epsilon_r \cos\beta \cdot b + \epsilon\ n \sin n\theta + \epsilon_r \sin\beta \cdot \epsilon_t \sin(\theta + \psi)\right] R + \left[\epsilon_t \sin(\theta + \psi)\right] R^2\right\}$$

$$= -\Lambda\left\{A(\theta) + B(\theta) \cdot R + C(\theta) \cdot R^2\right\}\,. \tag{53}$$

Integrating this expression we have

$$\frac{\partial P}{\partial R} = -\Lambda\left\{\frac{A}{H^3} + \frac{BR}{2H^3} + \frac{CR^2}{3H^3}\right\} + \frac{\Phi(\theta)}{RH^3} \tag{54}$$

and

$$P = -\Lambda\left\{A\int\frac{dR}{H^3} + B\int\frac{R\,dR}{2H^3} + C\int\frac{R^2 dR}{3H^3}\right\} + \Phi(\theta)\int\frac{dR}{RH^3} + \psi(\theta) \tag{55}$$

$$= -\Lambda\left\{F(R, \theta)\right\} + \Phi(\theta) \cdot G(R, \theta) + \psi(\theta)\,. \tag{56}$$

Applying the boundary conditions

$$P = P_i \text{ @ } R = R_i$$

$$P = P_c \text{ @ } R = R_i \text{ (at the cavity)} \tag{57}$$

the unknown functions $\Phi(\theta)$ and $\psi(\theta)$ can be determined, i.e.,

$$\Phi(\theta) = \frac{(P_i - P_c) - \Lambda \left[F(R_c,\theta) - R(R_i,\theta)\right]}{G(R_i,\theta) - G(R_c,\theta)} \tag{58}$$

$$\psi(\theta) = P_c + \Lambda\, F(R_c,\theta) - \Phi(\theta) \cdot G(R_c,\theta) \quad . \tag{59}$$

Substituting equations (58) and (59) into (54) and (56)

$$(P - P_c) = \Lambda \left[F(R_c,\theta) - F(R,\theta)\right] + \left\{(P_i - P_c) - \Lambda \left[F(R_c,\theta) - F(R_i,\theta)\right]\right\} \left\{\frac{G(R,\theta) - G(R_c,\theta)}{G(R_i,\theta) - G(R_c,\theta)}\right\} \tag{60}$$

$$\frac{dP}{dR} = \frac{\Lambda}{H^3} \left\{A + \frac{BR}{2} + \frac{CR^2}{3}\right\} + \frac{(P_i - P_c) - \Lambda \left[F(R_c,\theta) - F(R_i,\theta)\right]}{RH^3 \left[G(R_i,\theta) - G(R_c,\theta)\right]} \tag{61}$$

The integration indicated results in a singularity at the value of b = 0. Therefore, it was necessary to express the integral of equation (55) in the form of infinite series expansions. The functions of integration become:

$$F(R,\theta) = \frac{A}{a^3} \sum_{n=1}^{\infty} (-1)^{n+1} \frac{(n+1)}{2} \left|\frac{b}{a}\right|^{n-1} R^n + \frac{B}{2a^3} \sum_{n=1}^{\infty} (-1)^{n+1} \frac{n}{2} \left|\frac{b}{a}\right|^{n-1} R^{n+1}$$

$$+ \frac{C}{3a^3} \sum_{n=1}^{\infty} (-1)^{n+1} \frac{n(n+1)}{2(n+2)} \left(\frac{b}{a}\right)^{n-1} R^{n+2}$$

$$G(R,\theta) = \left[\frac{1}{a^3} \ell_n \frac{R}{H} + \frac{1}{a^2 H} + \frac{1}{2aH^2}\right] . \tag{62}$$

where

$$H = a + bR$$

$$a = (1+\epsilon \cos n\theta)$$

$$b = \left[\epsilon_t \cos (\theta + \psi)\right]$$

$$A = \left[\epsilon_r \sin \beta\ \epsilon\ n \sin n\theta\right]$$

$$B = \left[b\,\epsilon_r \cos \beta + \epsilon n \sin n\theta + \epsilon_r \epsilon_t \sin \beta \sin (\theta + \psi)\right]$$

$$C = \left[\epsilon_t \sin (\theta + \psi)\right]$$

Since the upstream cavity boundary condition is

$$\left(\frac{dP}{dR_c}\right) = 0 \tag{63}$$

equation (61) is set equal to zero and R_c is set equal to $R_o = 1$ since this is where the cavity will first appear for $P_c = P_o$. Thus, we have the following expression

$$\frac{P_i - P_c}{\Lambda} = \left\{AR + \frac{BR^2}{2} + \frac{CR^3}{3}\right\} (G_i - G_o) + (F_o - F_i) \tag{64}$$

If the reference pressure in Λ is taken as $(p_i - p_c)$, then $P_i - P_c = 1$. For the concentric seal ($\epsilon_r = 0$) then, equation (64) becomes

$$\frac{1}{\Lambda} = \frac{CR_o^3}{3} (G_i - G_o) + (F_o - F_i)$$

$$= \frac{C}{3}\left\{\ell n \left[\frac{R_i(1+b)}{1+bR_i}\right] + \frac{1}{1+bR_i} - \frac{1}{1+b} + \frac{1}{2}\left[\frac{1}{(1+bR_i)^2} - \frac{1}{(1+b)^2}\right]\right.$$

$$\left. + \sum_{n=1}(-1)^{n+1} \frac{n(n+1)}{2(n+1)} b^{n-1} 1-R_i^{n+2}\right\} \tag{65}$$

The series in equation (65) does not converge as fast as desirable. Therefore, the following technique was used. First it was noted that

$$\lim_{n \to \infty} (-1)^{n+1} \frac{n(n+1)}{2(n+2)} b^{n-1} \left(1-R^{n+2}\right) = \frac{n}{2} |b|^{n-1} \tag{66}$$

and

$$(-1)^{n+1} \frac{n(n+1)}{2(n+2)} b^{n-1} \left|1 - R_i^{n+2}\right| < \frac{n}{2}|b|^{n-1} \tag{67}$$

for $0 < R_i < 1$ and $b < .0$.

Therefore,

$$\sum_{n=1}^{\infty}(-1)^{n+1} \frac{n(n+1)}{2(n+2)} b^{n-1} \left|1-R_i^{n+2}\right| < \sum_{n=1} \frac{n}{2} |b|^{n-1} = \frac{1}{2(|b|)^2} \tag{68}$$

The series

$$\sum_{n=1} \frac{n}{2} |b|^{n-1} \tag{69}$$

converges faster than the series representing $(F_o - F_i)$. Also the expression

$$\frac{1}{2(1-|b|)^2} \tag{70}$$

gives an upper bound to the series. This information yields a series representation of $(F_o - F_i)$ which converges more quickly than the original one in equation (65). This new representation is

$$\frac{3}{C}(F_o - F_i) = \frac{1}{2(1-|b|)^2} - \lim_{n \to \infty} \left\{ \sum_{n=1}^{N} \frac{n}{2} |b|^{n-1} - \sum_{n=1}^{N}(-1)^{n+1} \frac{n(n+1)}{2(n+2)} b^{n-1} \left|1-R_i^{n+2}\right| \right\} \tag{71}$$

The listing of the Time Shared Computer program which calculates equations (65) and (71) is given in Table I. The numerical results are shown in Figs. 8 and 9. The line labeled $1/\Lambda_{crit}$ represents the conditions for which the cavity will first appear. The other curves labeled ϵ (= 0.1 for example) give the location of the nose of the cavity. The two figures represent conditions for two different test seals. The first one is for

$$R_i = \frac{ri}{ro} = \frac{di}{do} = \frac{2.25}{3.50} = 0.643 \quad .$$

The second is for

$$R_i = \frac{2.28}{2.75} = 0.83 \ .$$

These are the conditions for the two transparent test seals used in the seal experiments.

IV. SEAL PROGRAM (GE 635) IMPROVEMENTS

Although it is nice to have closed form analytical solutions to the various face seal problems, it sometimes becomes necessary to resort to numerical computer solutions. Once the basic problem has been set up on the computer it will usually handle various seal film geometries equally well, whereas the analytical solutions hold for more limited conditions. Therefore, the GE 635 SEAL PROGRAM has proven very useful. However, the computer solutions to the gas cavity problems require a large number of iterations and it is desirable to improve the numerical approach so as to reduce the computer time.

A method has been developed that not only conserves computer time but also gives a numerical solution to the "short bearing" approximation as the first iteration in the process. This method is a variation of a method described in Reference 16. In Reference 16 the film pressures in a bearing are obtained by direct solution of a finite set of simultaneous equations. This approach still requires a large number of computations and in some cases may not reduce the computer time over that required by an iterative solution.

It has been recognized that in the seal problem the influence of the circumferential pressure gradient is much less than that of the radial pressure gradient. Thus the "short bearing" approximation, wherein $\partial P/\partial \theta$ is neglected altogether, has resulted in very good solutions to the face seal problem.

The new method of solution used in the GE 635 SEAL PROGRAM makes use of the fact that a very good approximation can be obtained by neglecting $\partial P/\partial \theta$, and solves the "short bearing" approximation to Reynolds' equation numerically. However, this numerical solution is obtained by direct calculation of the simultaneous equations rather than by iteration. This is a very quick computation since the number of simultaneous equations is equal only to the number of radial grid points taken in the numerical approximation. Once the "short bearing" solution is calculated and printed out, the $\partial P/\partial \theta$ terms in Reynolds' equation are included as correction terms. Several corrective calculations are then made in order to obtain the two dimensional solution to Reynolds' equation.

The development of this new method of numerical solution starts from the numerical formulation of equation (1)

$$D_j P_{ij} = \frac{1}{2\Delta\theta^2}\left[P_{i+1,j} + P_{i-1,j}\right] + \frac{3}{4\Delta\theta H_{ij}}\left(\frac{\partial H}{\partial\theta}\right)_{ij}\left[P_{i+1,j} - P_{i-1,j}\right]$$

$$+ \frac{R_j^2}{2\Delta R^2}\left[P_{i,j+1} + P_{i,j-1}\right] + \frac{1}{4\Delta R}\left(\frac{3R_j^2}{H_{ij}}\frac{\partial H}{\partial R_{ij}} + R_j\right)\left[P_{i,j+1} - P_{i,j-1}\right]$$

$$- \frac{\Lambda R_j^2}{2H_{ij}^3}\left\{\frac{\partial}{\partial R}\left(U_r' H\right) + \left(\frac{U_r' H}{R}\right) + \frac{1}{R_j}\frac{\partial}{\partial\theta}\left(U_\theta' H\right)\right\}_{ij}$$

$$D_j = \left[\frac{1}{\Delta\theta^2} + R_j^2\frac{1}{\Delta R^2}\right]$$

$$H = (1 + a\xi + b\xi^2)^m + \epsilon\cos n\theta + \epsilon_t R\cos(\theta + \psi) + \epsilon_s .$$

These can be combined as follows

$$P_{ij} = A_{ij} P_{i+1,j} + A_{2j} P_{i-1,j} + A_{3j} P_{i,j+1} + A_{4j} P_{i,j-1} - A_{5j} \qquad (72)$$

where

$$A_{1j} = \left[(1/2\Delta\theta^2) + (3/4\Delta\theta H_{ij})(\partial H/\partial\theta)_{ij}\right] \Big/ D_j \qquad (73)$$

$$A_{2j} = \left[(1/2\Delta\theta^2) - (3/4\Delta\theta H_{ij})(\partial H/\partial\theta)_{ij}\right] \Big/ D_j \qquad (74)$$

$$A_{3j} = \left\{(R_j^2/2\Delta R^2) + (1/4\Delta R)\left[(3R_j^2/H_{ij})(\partial H/\partial R)_{ij} + R_j\right]\right\} \Big/ D_j \qquad (75)$$

$$A_{4j} = \left\{(R_j^2/2\Delta R^2) - (1/4\Delta R)\left[(3R_j^2/H_{ij})(\partial H/\partial R)_{ij} + R_j\right]\right\} \Big/ D_j \qquad (76)$$

$$A_{5j} = (\Lambda R_j^2/2H_{ij}^3)\left\{\frac{\partial}{\partial R}\left(U_r' H\right) + (U_r' H/R) + \frac{1}{R_j}\frac{\partial}{\partial\theta}\left(U_\theta' H\right)\right\} \Big/ D_j \qquad (77)$$

$$D_j = 1/\Delta\theta^2 + R_j^2/\Delta R^2 \qquad (78)$$

If it is assumed that the pressures in the circumferential direction

$$P_{i+1,j} \; P_{i-1,j}$$

are known or assumed, then one may start at one of the boundaries of the seal and work across the seal obtaining expressions for P_{ij} in terms of the starting point boundary pressure and $P_{i,j+1}$. Thus proceeding across the seal to the other boundary pressure the last $P_{i,j+1}$ is known, i.e., it is the second boundary pressure, and working back across the seal all P_{ij}'s are determined on that radial line. Going on to the next radial line the procedure is repeated.

The equations used for this procedure are

$$P_{ij} = X_j \; P_{i,j+1,} + Y_j \tag{79}$$

where

$$X_j = A_{3j}/(1 - A_{4j} \; X_{j-1}) \quad (j = 2, \ldots\ldots, j_{max}-1) \tag{80}$$

$$X_1 = 0 \tag{81}$$

$$Y_j = (A_{1j}P_{i+1,j} + A_{2j} \; P_{i-1,j} \; -A_{5j} + A_{4j} \; Y_{j-1})/(1-A_{4j} \; X_{j-1}); \; (j = 2,\ldots,j_{max}-1) \tag{82}$$

$$Y_i = P_m \text{ (first boundary pressure)} \tag{83}$$

$$P_{i,jmax} = P_n \text{ (second boundary pressure)} \tag{84}$$

The calculational procedure is as follows,

Step 1: Short Bearing Approximation, i.e., $\frac{\partial P}{\partial \theta} = 0$

(a) $A_{1j} = A_{2j} = 0$

(b) $D_j = R_j^2/\Delta R^2$

(c) Calculate X_j, Y_j, $(j = 2,3,\ldots, j_{max}-1)$; i fixed

(d) Calculate $P_{ij,_n,}$ $(j = j_{max-1}\cdot \ldots, 3,2)$; i fixed

(e) Repeat for all i's

Step 2: First Correction

(a) Calculate A_{1j}, A_{2j} from equations (73) and (74)

(b) Use $P_{i+1,j}$ and $P_{i-1,j}$ from Step 1

(c) Calculate X_j, Y_j, $(j = 2,3, \ldots, j_{max-1})$; i fixed

(d) Calculate P_{ij}, (Eq. 79), (J = j_{max-1}, ... , 3, 2); i fixed

(e) Repeat for all i's

Steps 3 to N: Additional Corrections

Repeat procedure under Step 2 always using the $P_{i+1,j}$ and $P_{i-1,j}$ values from the previous step (or iteration).

This method is now in use on the GE 635 SEAL PROGRAM and has proven to be very successful. The results obtained thus far indicate that for the full film seal the "short bearing" solution to Reynolds' equation is very close to the two dimensional solution.

V. TWO FLUID STUDY

The analysis of this problem has not been completed. Some of the basic relationships have been derived and the problem set up but not solved. Therefore, only a summary of the basic equations and approach to the solution will be given here.

The first step to this solution should be to take the single fluid, no cavity, misaligned seal solution and determine the regions in the seal interface occupied by the fluid coming from inside the seal and outside the seal. From this a general picture of the fluid regions will be obtained. This is needed for a better insight into setting up this problem.

From considering this problem qualitatively it appears that there may be multilayers of fluid in the seal. It looks quite likely that one fluid may be next to the two seal surfaces and the second fluid between these two strato. In the general case considered here only two layers of fluid have been considered in the boundary conditions.

The film cross-section geometry is shown in Fig. 12. For this case the problem is summarized as follows:

Two Fluid Problem in Polar Coordinates

Velocities

$$u_{r1} = \frac{1}{2\mu_1} \frac{\partial p}{\partial r} z\,(z-h_1) + U_{or}\left(1 - \frac{z}{h_1}\right) + \frac{z}{h_1} u_{ri}$$

$$u_{r2} = \frac{1}{2\mu_2} \frac{\partial p}{\partial r} \left[z\,(z-h_1) - h\,(z-h_1)\right] + U_{hr} \frac{(z-h_1)}{(h-h_1)} + u_{ri} \frac{(h-z)}{(h-h_1)}$$

$$u_{\theta 1} = \frac{1}{2\mu_1} \frac{1}{r} \frac{\partial p}{\partial \theta} z\,(z-h_1) + U_{o\theta}\left(1-\frac{z}{h_1}\right) + \frac{z}{h_1} u_{\theta i}$$

$$u_{\theta 2} = \frac{1}{2\mu_2} \frac{1}{r} \frac{\partial p}{\partial \theta} \left[(z-h)\,(z-h_1)\right] + U_{h\theta} \frac{(z-h_1)}{(h-h_1)} + u_{\theta i} \frac{(h-z)}{(h-h_1)}$$

Flows

$$q_{r1} = -\frac{h_1^3}{12\mu_1} \frac{\partial p}{\partial r} + U_{or} \frac{h_1}{2} + u_{ri} \frac{h_1}{2}$$

$$q_{r2} = -\frac{(h-h_1)^3}{12\mu_2} \frac{\partial p}{\partial r} + U_{hr} \frac{(h-h_1)}{2} + u_{ri} \frac{(h-h_1)}{2}$$

$$q_{\theta 1} = -\frac{h_1^3}{12\mu_1} \frac{1}{r} \frac{\partial p}{\partial \theta} + U_{o\theta} \frac{h_1}{2} + u_{\theta i} \frac{h_1}{2}$$

$$q_{\theta 2} = -\frac{(h-h_1)^3}{12\mu_2} \frac{1}{r} \frac{\partial p}{\partial \theta} + U_{h\theta} \frac{(h-h_1)}{2} + u_{\theta i} \frac{(h-h_1)}{2}$$

Continuity

$$\frac{\partial}{\partial r}(rq_r) + \frac{\partial q_\theta}{\partial \theta} = 0$$

$$\frac{\partial}{\partial r}\left[rh_1^3 \frac{\partial p}{\partial r}\right] + \frac{1}{r}\frac{\partial}{\partial \theta}\left[h_1^3 \frac{\partial p}{\partial \theta}\right] = 6\mu_1 \left\{ \frac{\partial}{\partial r}\left[rh_1(U_{or} + u_{ri})\right] + \frac{\partial}{\partial \theta}\left[h_1(U_{o\theta} + u_{\theta i})\right] \right\}$$

$$\frac{\partial}{\partial r}\left[r(h-h_1)^3 \frac{\partial p}{\partial r}\right] + \frac{1}{r}\frac{\partial}{\partial \theta}\left[(h-h_1)^3 \frac{\partial p}{\partial \theta}\right] = 6\mu_2 \left\{ \frac{\partial}{\partial r}\left[r(h-h_1)(U_{hr}+u_{ri})\right] + \frac{\partial}{\partial \theta}\left[(h-h_1)(U_{h\theta}+u_{\theta i})\right] \right\}$$

Shear Stress

$$\tau_{ri} = \mu_1 \left(\frac{\partial u_{r1}}{\partial z}\right)_i = \mu_2 \left(\frac{\partial u_{r2}}{\partial z}\right)_i$$

$$\tau_{\theta i} = \mu_1 \left(\frac{\partial u_{\theta 1}}{\partial z}\right)_i = \mu_2 \left(\frac{\partial u_{\theta 2}}{\partial z}\right)_i$$

$$\frac{\partial u_{r1}}{\partial z} = \frac{1}{2\mu_1} \frac{\partial p}{\partial r} (2z-h_1) - \frac{U_{or}}{h_1} + \frac{u_{ri}}{h_1}$$

$$\therefore \left(\frac{\partial u_{r1}}{\partial z}\right)_i = \frac{h_1}{2\mu_1} \frac{\partial p}{\partial r} + \frac{(u_{ri}-U_{or})}{h_1}$$

$$\frac{\partial u_{r2}}{\partial z} = \frac{1}{2\mu_2} \frac{\partial p}{\partial r} \left[2z-(h+h_1)\right] + \frac{U_{hr}}{(h-h_1)} - \frac{u_{ri}}{(h-h_1)}$$

$$\therefore \left(\frac{\partial u_{r2}}{\partial z}\right)_i = \frac{(h_1-h)}{2\mu_2} \frac{\partial p}{\partial r} + \frac{(U_{hr}-u_{ri})}{(h-h_1)}$$

$$\frac{\partial u_{\theta 1}}{\partial z} = \frac{1}{2\mu_1} \frac{1}{r} \frac{\partial p}{\partial \theta} (2z-h_1) - \frac{U_{o\theta}}{h_1} + \frac{u_{\theta i}}{h_1}$$

$$\therefore \left(\frac{\partial u_{\theta 1}}{\partial z}\right)_i = \frac{h_1}{2\mu_1} \frac{1}{r} \frac{\partial p}{\partial \theta} + \frac{(u_{\theta i}-U_{o\theta})}{h_1}$$

$$\left(\frac{\partial u_{\theta 2}}{\partial z}\right) = \frac{1}{2\mu_2} \frac{1}{r} \frac{\partial p}{\partial \theta} \left[2z-(h+h_1)\right] + \frac{(U_{h\theta}-u_{\theta i})}{(h-h_1)}$$

$$\therefore \left(\frac{\partial u_{\theta 2}}{oz}\right)_i = \frac{(h_1-h)}{2\mu_2} \frac{1}{r} \frac{\partial p}{\partial \theta} + \frac{(U_{h\theta}-u_{\theta i})}{(h-h_1)}$$

Shear Stress Boundary Conditions

$$\frac{h_1}{2} \frac{\partial p}{\partial r} + \mu_1 \frac{(u_{ri}-U_{or})}{h_1} = \frac{(h_1-h)}{2} \frac{\partial p}{\partial r} + \mu_2 \frac{(U_{hr}-u_{ri})}{(h-h_1)}$$

or

$$\frac{h}{2}\frac{\partial p}{\partial r} + u_{ri}\left[\frac{\mu_1}{h_1} + \frac{\mu_2}{(h-h_1)}\right] - \frac{\mu_1}{h_1}U_{or} - \frac{\mu_2 U_{hr}}{(h-h_1)} = 0$$

or

$$u_{ri} = \frac{-\frac{h}{2}\frac{\partial p}{\partial r} + \frac{\mu_1}{h_1}U_{or} + \frac{\mu_2 U_{hr}}{(h-h_1)}}{\left[\frac{\mu_1}{h_1} + \frac{\mu_2}{(h-h_1)}\right]}$$

$$\frac{h_1}{2}\frac{1}{r}\frac{\partial p}{\partial \theta} + \mu_1\frac{(u_{\theta i}-U_{o\theta})}{h_1} = \frac{(h_1-h)}{2}\frac{1}{r}\frac{\partial p}{\partial \theta} + \mu_2\frac{(U_{h\theta}-u_{\theta 1})}{(h-h_1)}$$

or

$$\frac{h}{2r}\frac{\partial p}{\partial \theta} + u_{\theta i}\left[\frac{\mu_1}{h_1} + \frac{\mu_2}{h-h_1}\right] - \frac{\mu_1 U_{o\theta}}{h_1} - \frac{\mu_2 U_{h\theta}}{h-h_1} = 0$$

or

$$u_{\theta i} = \frac{-\frac{h}{2r}\frac{\partial p}{\partial \theta} + \frac{\mu_1 U_{o\theta}}{h_1} + \frac{\mu_2 U_{h\theta}}{(h-h_1)}}{\left[\frac{\mu_1}{h_1} + \frac{\mu_2}{(h-h_1)}\right]}$$

Non-dimensional Form of Equations

$$R = \frac{r}{r_o}\ ,\ P = \frac{p}{p_o}\ ,\ H = \frac{h}{h_i}\ ,\ U' = \frac{U}{r_o\omega}$$

$$\frac{\partial}{\partial R}\left[RH_1^3\frac{\partial P}{\partial R}\right] + \frac{1}{R}\frac{\partial}{\partial \theta}\left[H_1^3\frac{\partial P}{\partial \theta}\right] = \Lambda_1\left\{\frac{\partial}{\partial R}\left[RH_1\,(U_{or}' + u_{ri}')\right] + \frac{\partial}{\partial \theta}\left[H_1\,(U_{o\theta}' + u_{\theta i}')\right]\right\}$$

$$\frac{\partial}{\partial R}\left[R(H-H_1)^3\frac{\partial P}{\partial R}\right] + \frac{1}{R}\frac{\partial}{\partial \theta}\left[(H-H_1)^3\frac{\partial P}{\partial \theta}\right] = \left(\frac{\mu_2}{\mu_1}\right)\Lambda_1\left\{\frac{\partial}{\partial R}\left[R(H-H_1)\,(U_{hr}'+u_{ri}')\right] + \frac{\partial}{\partial \theta}\left[(H-H_1)\,(U_{h\theta}'+u_{\theta i}')\right]\right\}$$

$$u'_{\theta i} = \frac{-\frac{3H}{\Lambda_1} \cdot \frac{1}{R}\frac{\partial P}{\partial \theta} + \frac{U'_{o\theta}}{H_1} + \frac{\mu_2}{\mu_1}\frac{U'_{hr}}{(H-H_1)}}{\left[\frac{1}{H_1} + \frac{(\mu_2/\mu_1)}{(H-H_1)}\right]}$$

For the case where

$U_o = 0$ and

$U'_{hr} = -\epsilon_r \cos\beta$

$U'_{h\theta} = R + \epsilon_r \sin\beta$,

the seal equations become,

$$\frac{\partial}{\partial R}\left[RH_1^3 \frac{\partial P}{\partial R}\right] + \frac{1}{R}\frac{\partial}{\partial \theta}\left[H_1^3 \frac{\partial P}{\partial \theta}\right]$$

$$= \Lambda_1 \frac{\partial}{\partial R}\left\{RH_1 \frac{\left[-\frac{3H}{\Lambda_1}\frac{\partial P}{\partial R} - \frac{\mu_2}{\mu_1}\frac{\epsilon_r \cos\beta}{(H-H_1)}\right]}{\left[\frac{1}{H} + \frac{(\mu_2/\mu_1)}{(H-H_1)}\right]}\right\}$$

$$+ \Lambda_1 \frac{\partial}{\partial \theta}\left\{\frac{H_1\left[\frac{-3H}{\Lambda_1}\cdot\frac{1}{R}\frac{\partial P}{\partial \theta} + \frac{\mu_2}{\mu_1}\frac{(R+\epsilon_r \sin\beta)}{(H-H_1)}\right]}{\left[\frac{1}{H_1} + \frac{(\mu_2/\mu_1)}{(H-H_1)}\right]}\right\}$$

$$\frac{\partial}{\partial R}\left[R(H-H_1)^3 \frac{\partial P}{\partial R}\right] + \frac{1}{R}\frac{\partial}{\partial \theta}\left[(H-H_1)^3 \frac{\partial P}{\partial \theta}\right]$$

$$= \left(\frac{\mu_2}{\mu_1}\right)\Lambda_1 \frac{\partial}{\partial R}\left\{R(H-H_1)\left[-\epsilon_r \cos\beta + \frac{-\frac{3H}{\Lambda_1}\frac{\partial P}{\partial R} - \frac{\mu_2}{\mu_1}\frac{\epsilon_r \cos\beta}{(H-H_1)}}{\frac{1}{H_1} + \frac{(\mu_2/\mu_1)}{(H-H_1)}}\right]\right\}$$

$$+ \left(\frac{\mu_2}{\mu_1}\right)\Lambda_1 \frac{\partial}{\partial \theta}\left\{(H-H_1)\left[(R+\epsilon_r \sin\beta) + \frac{-\frac{3H}{\Lambda_1}\cdot\frac{1}{R}\frac{\partial P}{\partial \theta} + \frac{\mu_2}{\mu_1}\frac{(R+\epsilon_r \sin\beta)}{(H-H_1)}}{\frac{1}{H_1} + \frac{(\mu_2/\mu_1)}{(H-H_1)}}\right]\right\}$$

$$u_{ri}' = \frac{\dfrac{-\bar{h}_i^2 p_o}{\mu_1 r_o^2 \omega}\ \dfrac{H}{2}\dfrac{\partial P}{\partial R} + \dfrac{U_{or}'}{H_1} + \dfrac{\mu_2}{\mu_1}\dfrac{U_{hr}'}{(H-H_1)}}{\left[\dfrac{1}{H_1} + \dfrac{\mu_2}{\mu_1}\cdot\dfrac{1}{(H-H_1)}\right]} = \frac{-\dfrac{3H}{\Lambda_1}\dfrac{\partial P}{\partial R} + \dfrac{U_{or}'}{H_1} + \dfrac{\mu_2}{\mu_1}\dfrac{U_{hr}'}{(H-H_1)}}{\left[\dfrac{1}{H_1} + \dfrac{(\mu_2/\mu_1)}{(H-H_1)}\right]}$$

First, it can be seen that a new parameter has been introduced into the set of simultaneous equations that must be solved. As might have been expected, this new parameter is the viscosity ratio, $\mu 2/\mu 1$. This parameter has been used in correlating the two fluid data in Appendix C.

Second, it should be obvious that the solution to P is the same for both differential equations. That is, the last two equations given are to be solved simultaneously for P and H_1, the two unknowns.

VI. CONCLUSIONS

1. The short bearing cavity solution presented in [6] has been confirmed experimentally.
2. The pumping theory developed in this Appendix has been confirmed experimentally.
3. In concentric face seals of fixed geometry, cavitation produces a net hydrodynamic lifting force and moment, but does not alter the leakage rate, i.e., it does not produce an "inward pumping" leakage.
4. Pumping leakage is produced by a combination of radial eccentricity and seal misalignment (tilt) or one wave waviness.
5. The above pumping effect can be either inward or outward depending upon the relationship between the radial eccentricity and misalignment, and the direction of rotation.
6. As long as a complete fluid film exists in the seal interface, the hydrostatic pressure differential does not affect the pumping leakage and produces a leakage which is independent of speed and, of course, always in the direction of decreasing pressure.
7. The existence of gas cavities in the film reduces the pumping effect, in eccentric seals, rather than causing it as heretofore postuated.

VII. FUTURE WORK

An experimental program has been completed to verify the predicted effects of fluid inertia [10], [11], and to study the influence of having fluids of different viscosities on either side of the seal. The solution to the two fluid problem and the single fluid pumping problem with cavities should be completed and included in the digital SEAL PROGRAM.

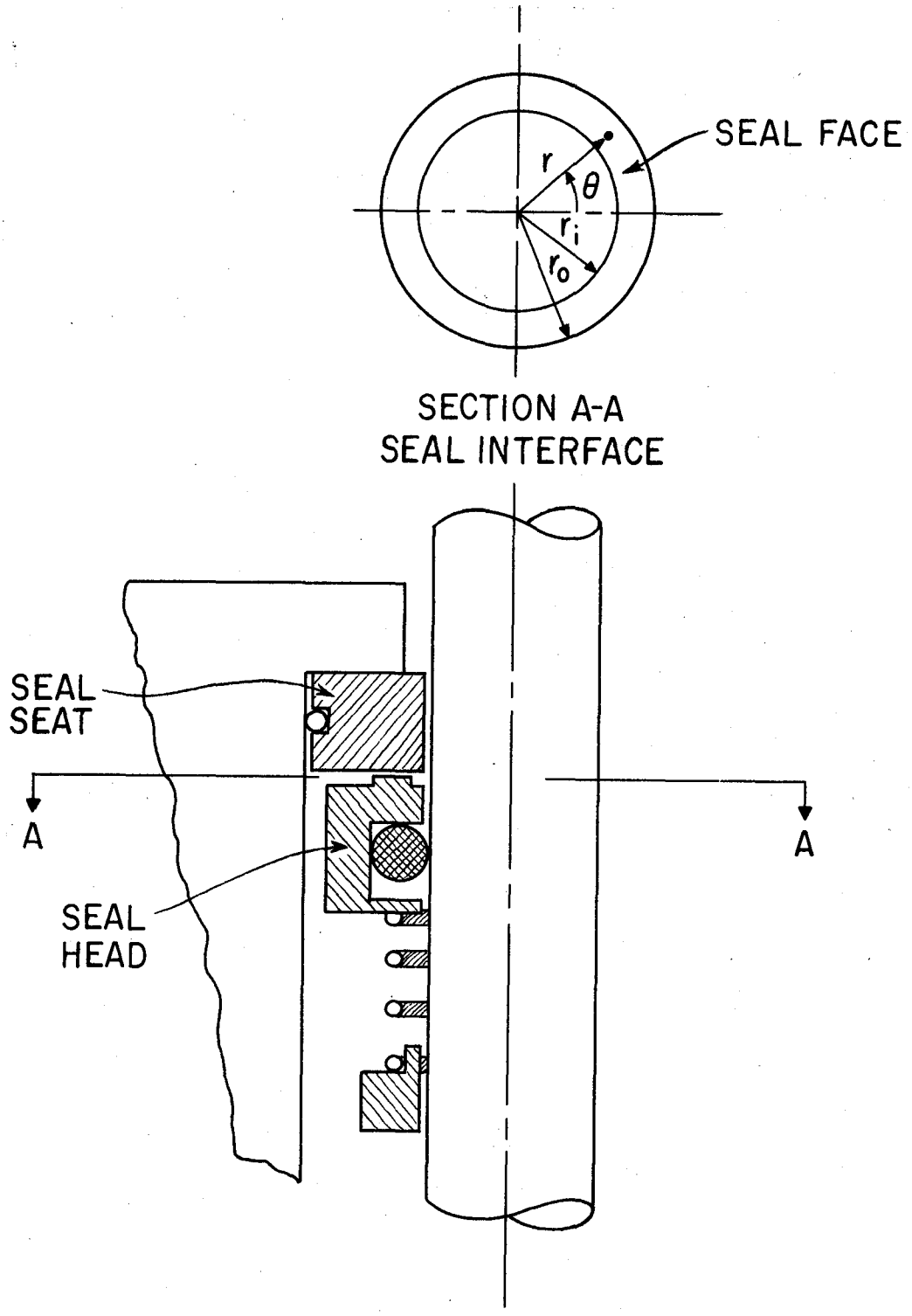

Figure 1

Mechanical Face Seal Geometry

FIXED SEAL, ROTATING SHAFT

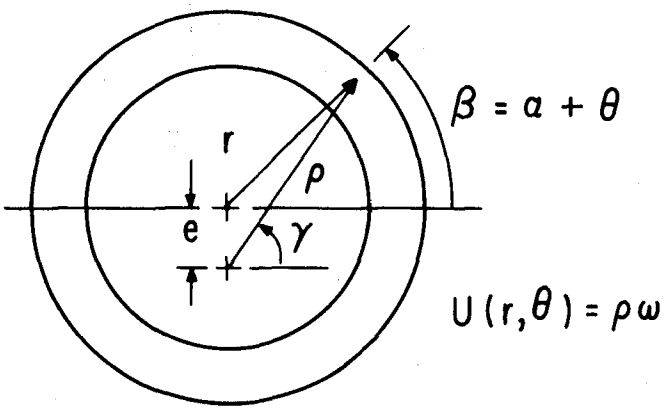

SEAL COORDINATES ARE r, θ

$$U'_r = \frac{U_r}{r_0 \omega} = -\epsilon_r \cos\beta$$

$$U'_\theta = \frac{U_\theta}{r_0 \omega} = R + \epsilon_r \sin\beta$$

FILM THICKNESS

$$H = 1 + \epsilon \cos\theta$$

$$0 \leq \epsilon \leq 1$$

r is measured from the center of the seal

ρ is measured from the center of rotation

Figure 2

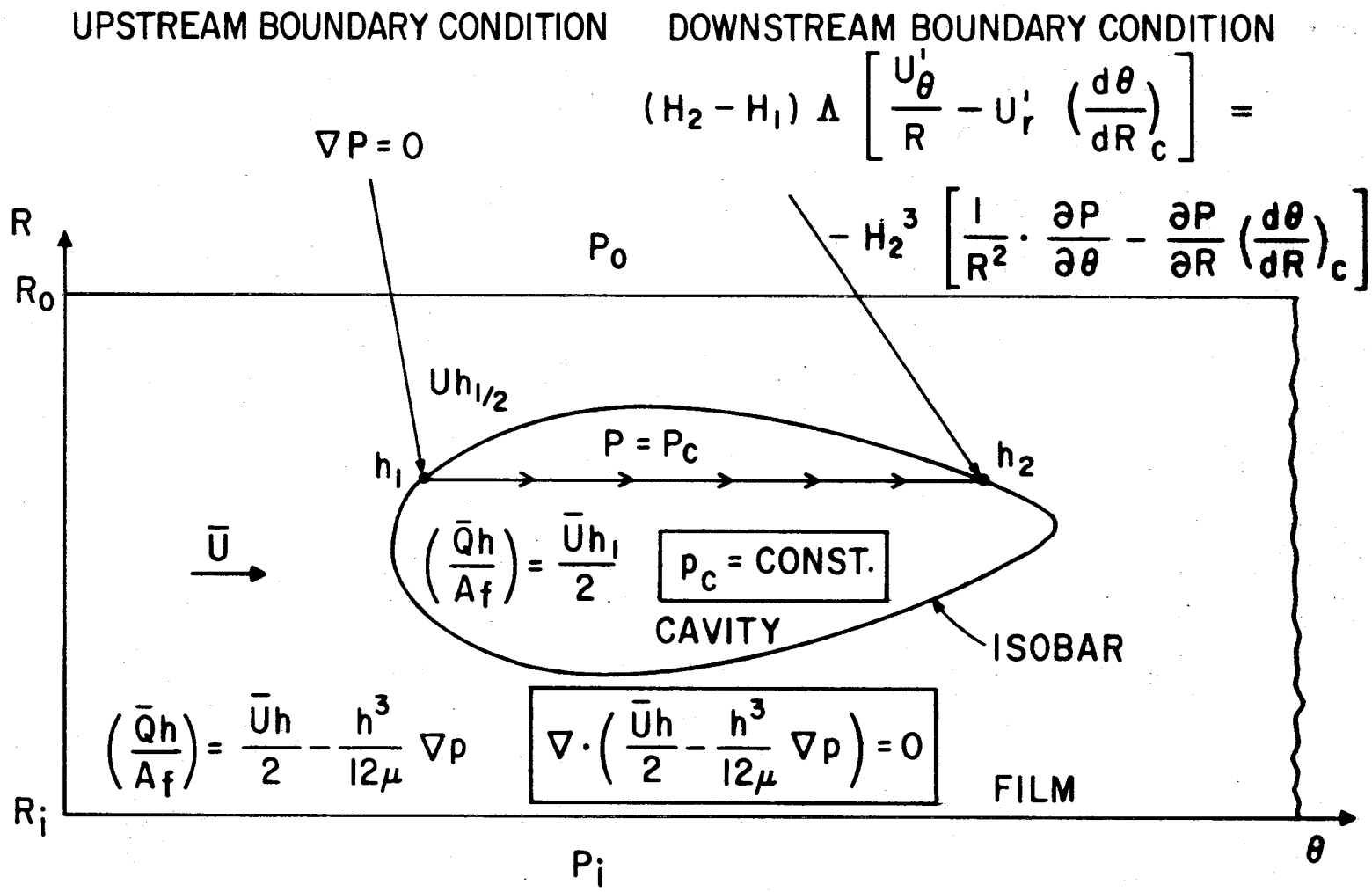

Figure 3

Cavity Boundary Conditions

FIGURE 4

HYDROSTATIC FLOW COEFFICIENT
FOR
MISALIGNED SEAL

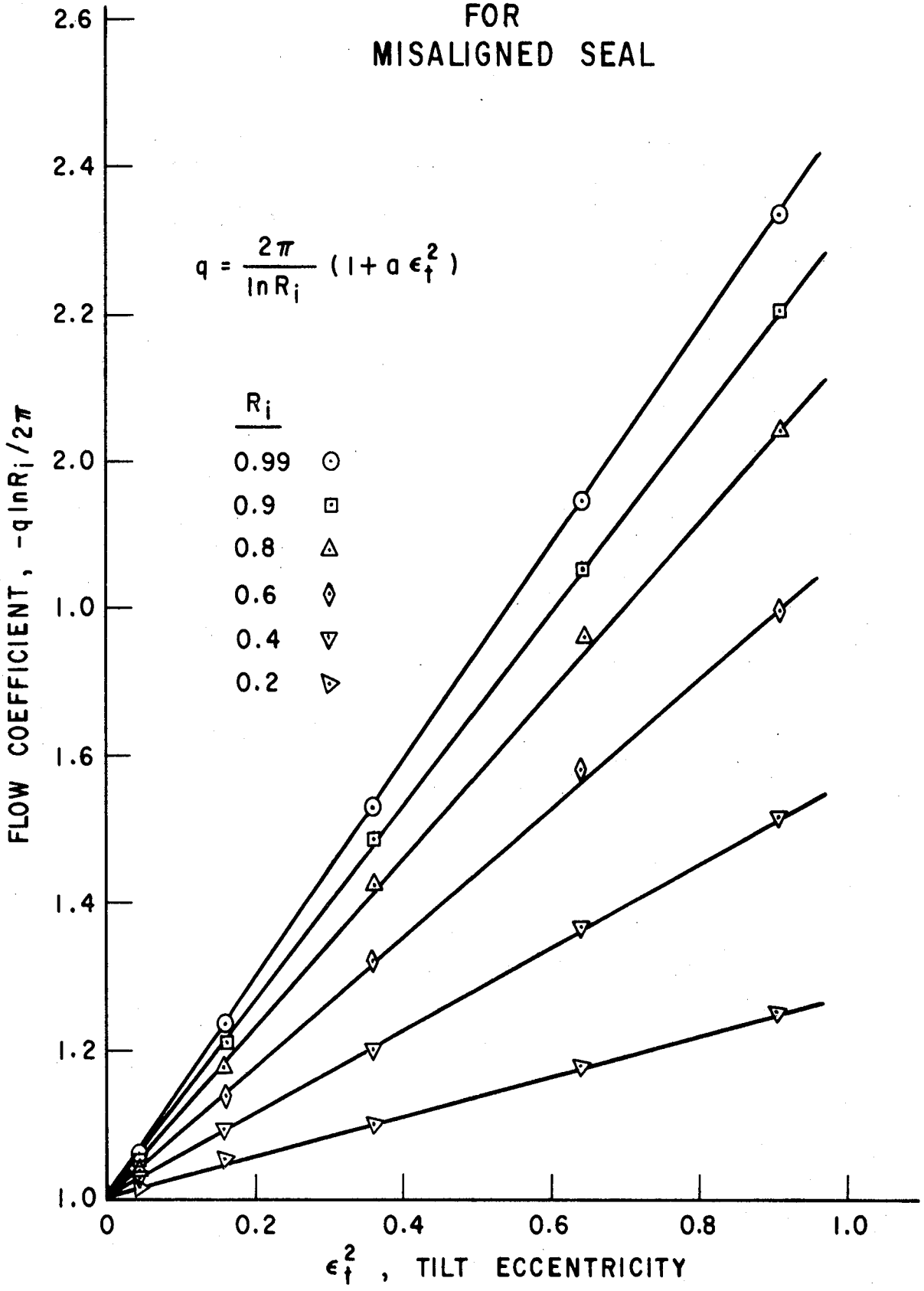

FIGURE 5

HYDROSTATIC FLOW CONSTANT
FOR
MISALIGNED SEAL

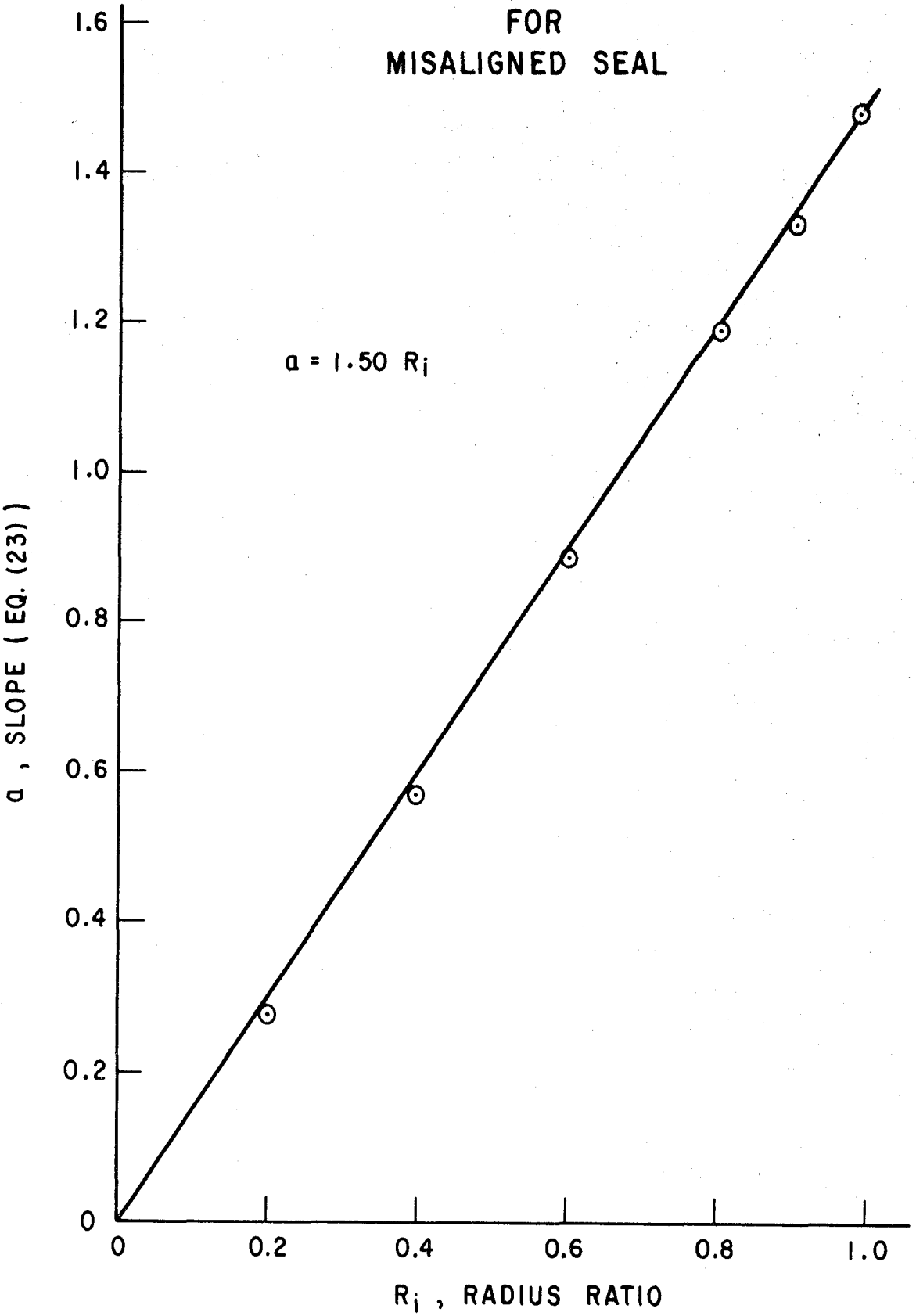

FIGURE 6

BOUNDARY FUNCTION Y

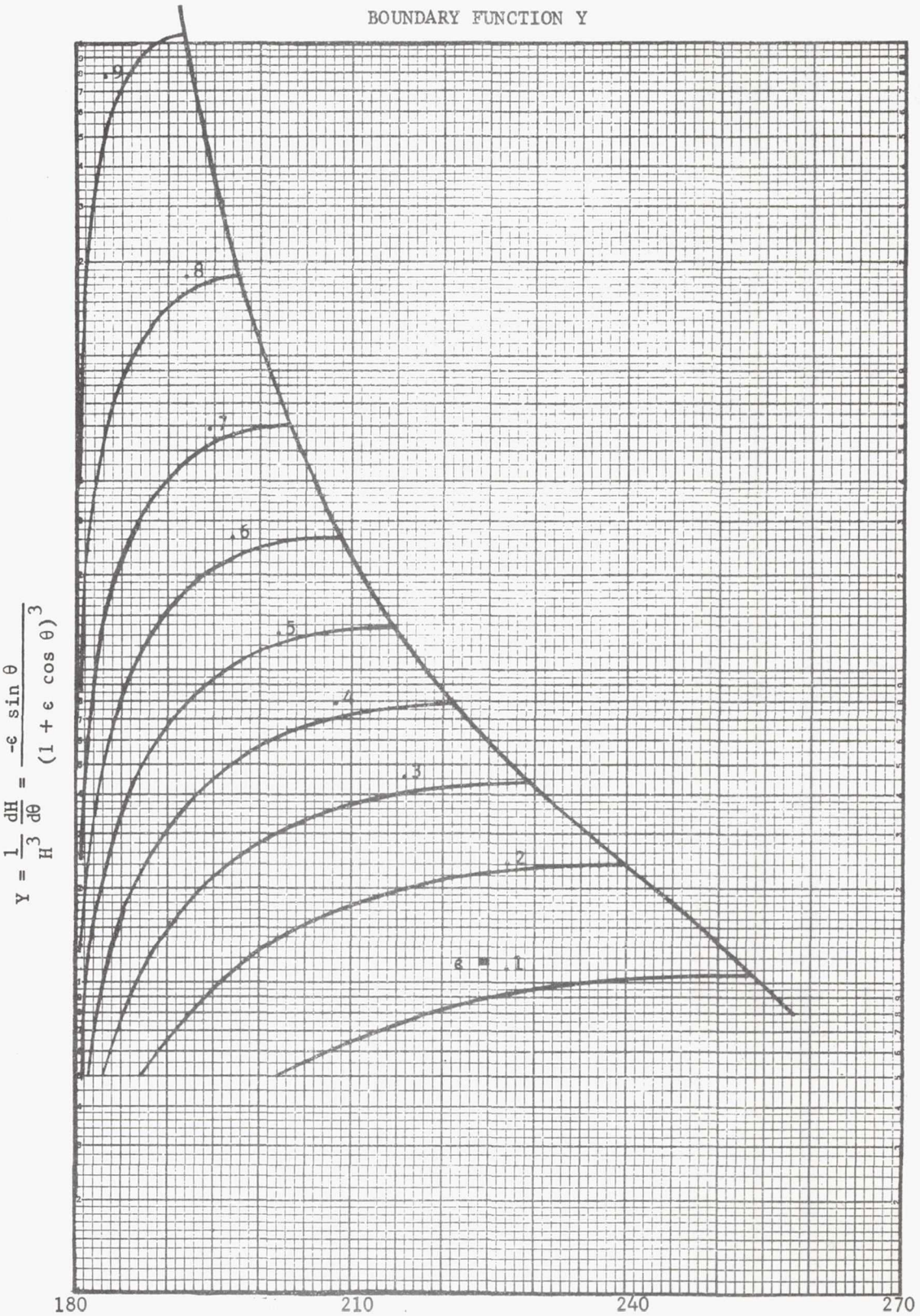

FIGURE 7

SEAL CONDITIONS FOR INITIATION OF CAVITY

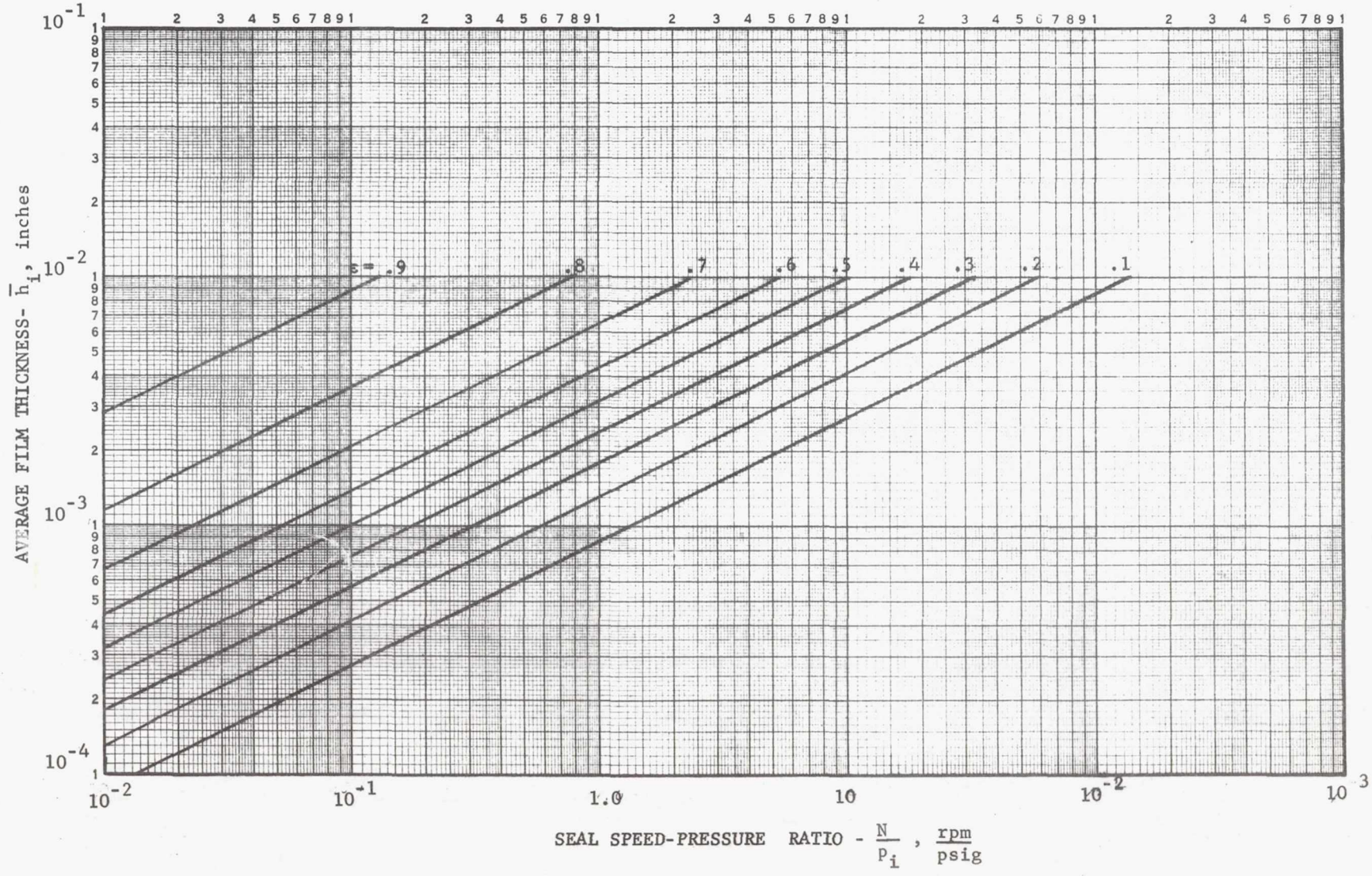

FIGURE 8

LOCATION OF INITIAL CAVITY (Λ_{crit})

AND CAVITY NOSE

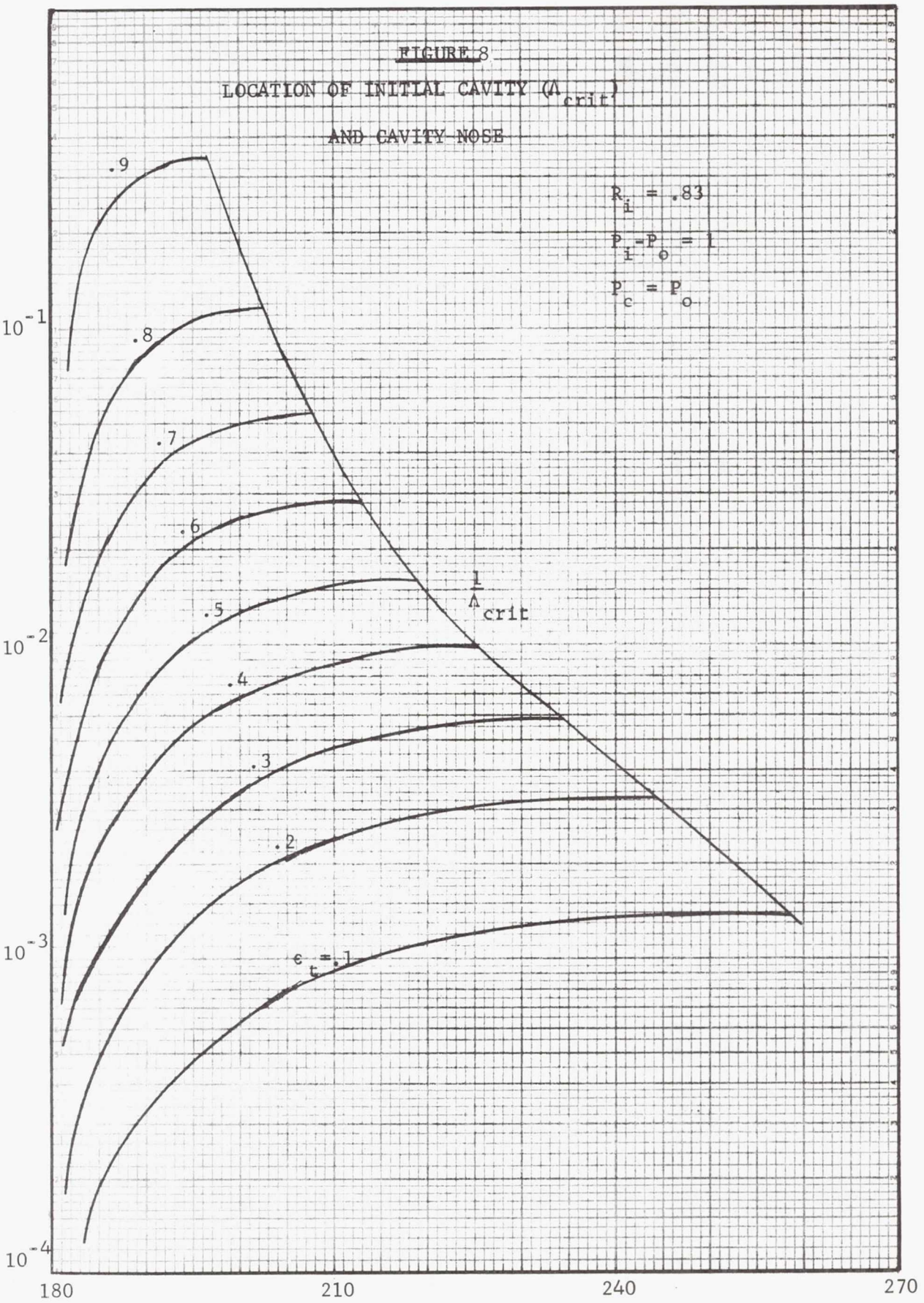

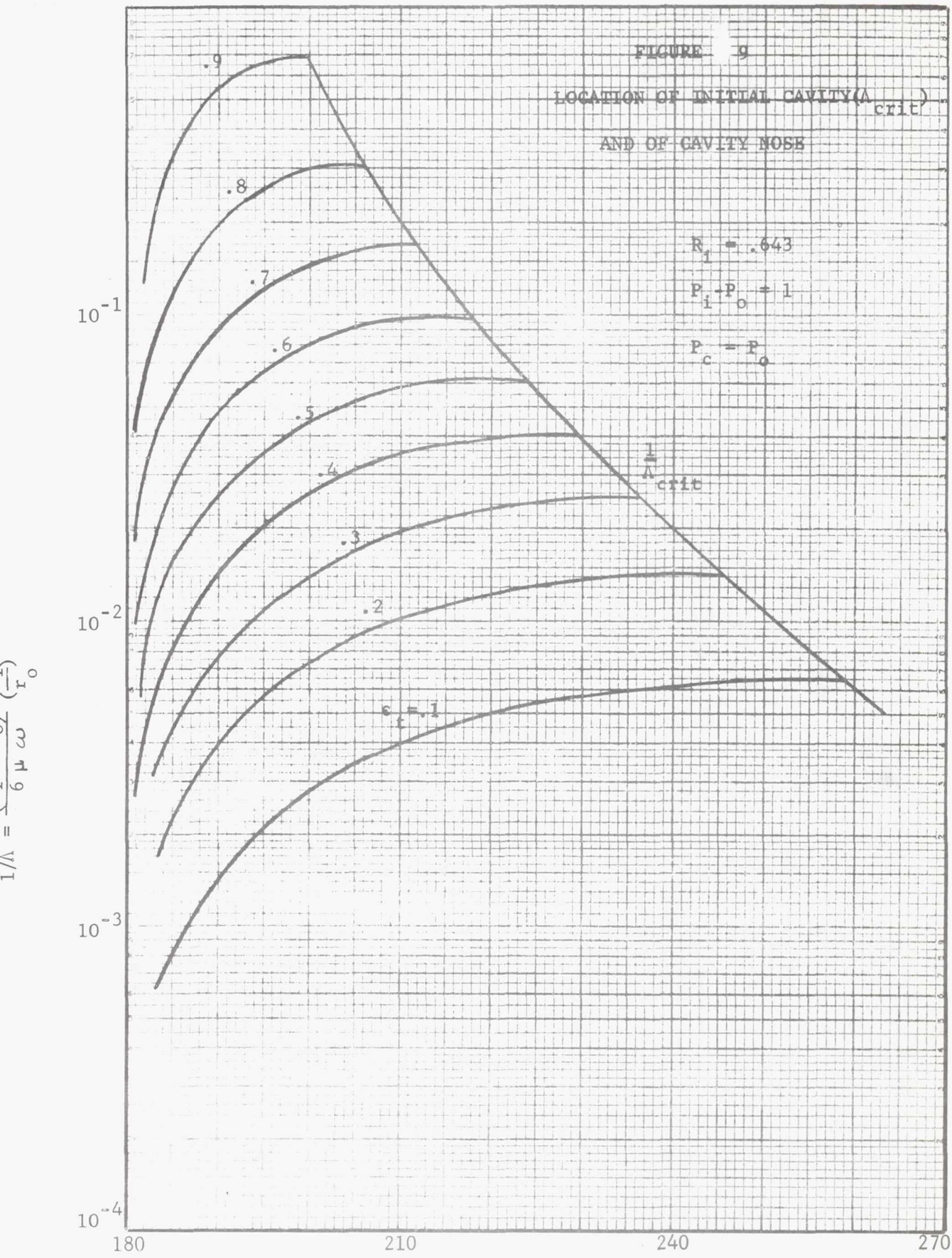
FIGURE 9
LOCATION OF INITIAL CAVITY(Λ_{crit})
AND OF CAVITY NOSE
$R_1 = .643$
$P_i - P_o = 1$
$P_c = P_o$
$\frac{1}{\Lambda_{crit}}$
$\epsilon_t = .1$
.9
.8
.7
.6
.5
.4
.3
.2
10^{-1}
10^{-2}
10^{-3}
10^{-4}
180
210
240
270
θ, Degrees
$1/\Lambda = \frac{(P_i - P_o)}{6\mu\omega} \frac{\bar{h}_i^2}{(\frac{r_i}{r_o})}$

Figure 10

SEAL PUMPING LEAKAGE
DUE TO RADIAL ECCENTRICITY

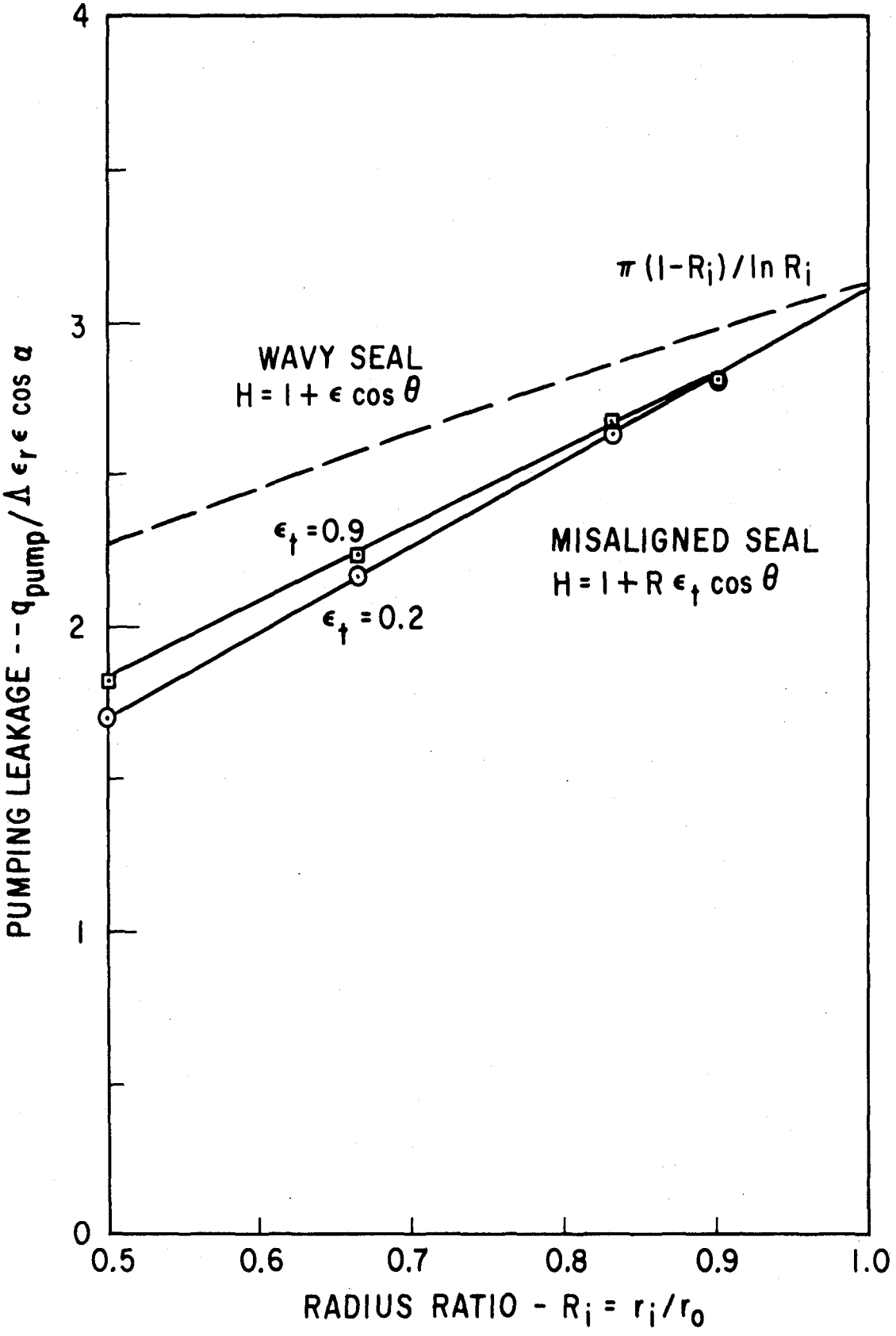

FIGURE 11

SEAL LEAKAGE

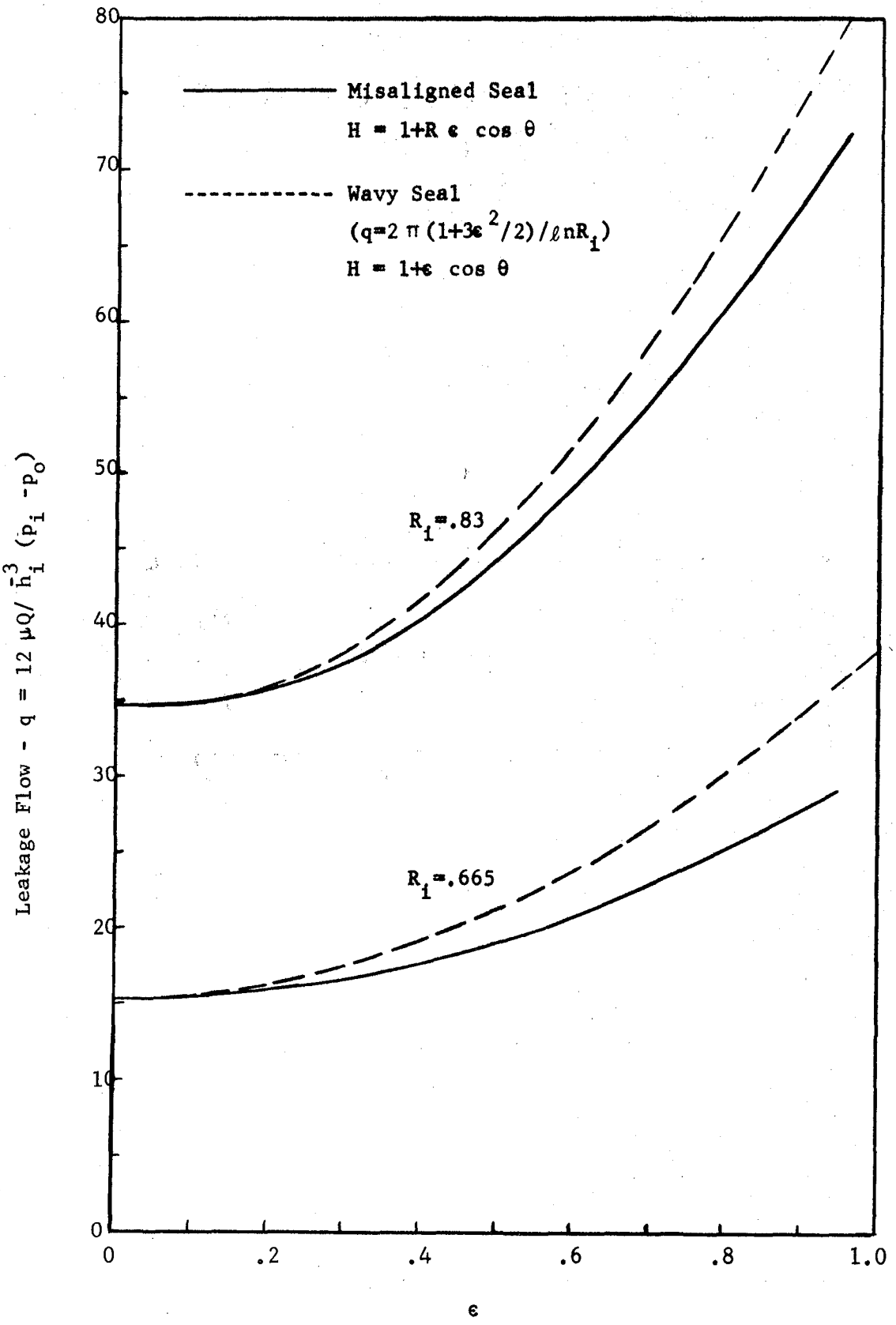

Figure 12

FLUID FILM GEOMETRY
FOR THE
TWO FLUID PROBLEM

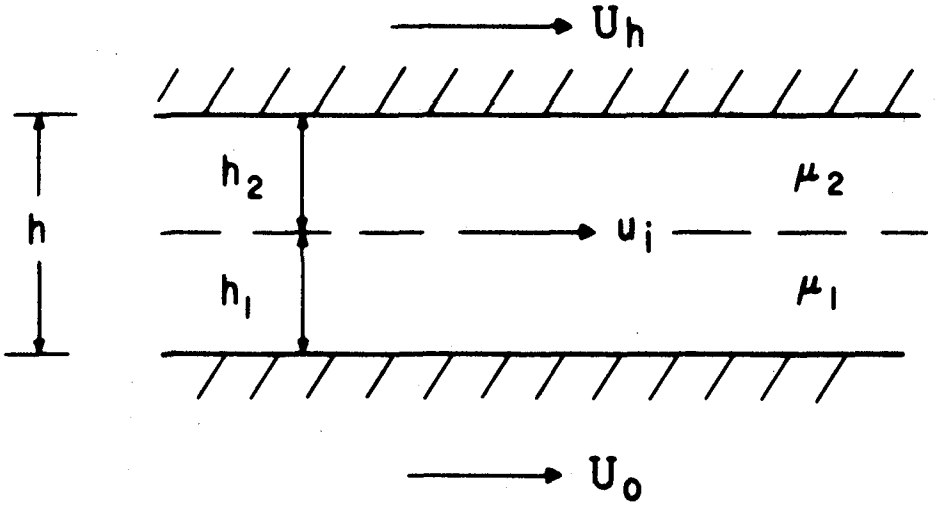

FIGURE 13

EFFECT OF RADIAL MISALIGNMENT

ON SEAL LEAKAGE

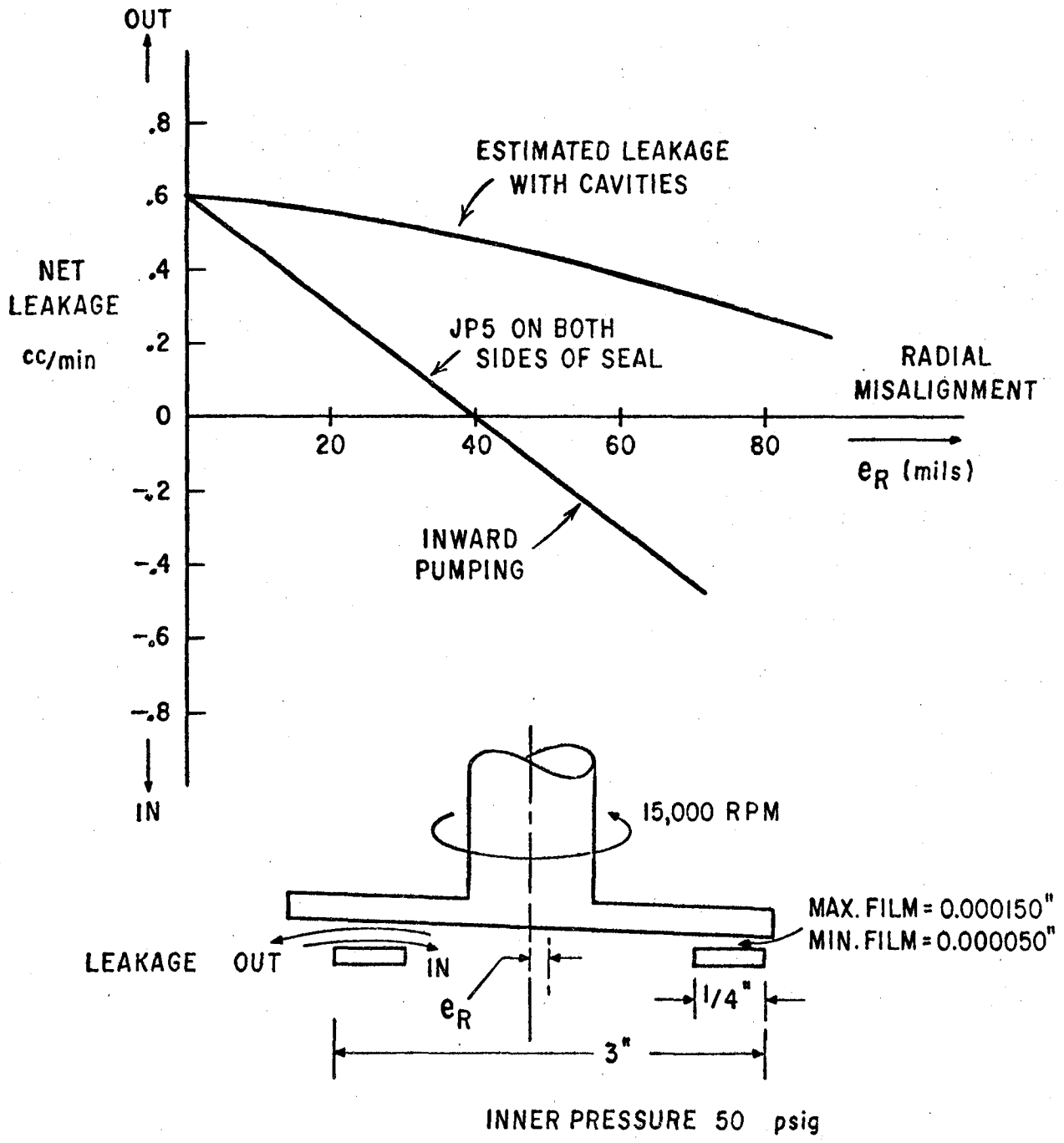

NOMENCLATURE

A - seal area, in^2

A_f - flow area, in^2

h - film thickness, in

$\bar{h}_i$ - average film thickness at inside radius, in

e - displacement between seal center and shaft center, in

y - coordinate across the film, in

ρ - coordinate measured from center of shaft, in

ρ - density, lb/in^3

r - coordinate measured from center of seal, in

θ - angular coordinate, radian

β - $\alpha + \theta$, radian

α - phase angle between waviness and eccentricity, radian

γ - angle measured to ρ, radian

ψ - tilt phase angle, radian

t - time, seconds

U - fluid velocity, in/sec

ω - rotational speed, radian/sec

Q - flow rate, in^3/sec

p - pressure, psi

τ - shear stress, psi

W - seal load capacity, lb_f

SM - shaft friction moment, $in\text{-}lb_f$

C_p - specific heat, Btu/lb^oF

k - thermal conductivity, $Btu/sec\ in^oF$

T - temperature, ^oF

Φ - dissipation function, sec^{-1}

μ - dynamic viscosity, psi-sec

Dimensionless Terms

R - radius ratio = r/r_o

H - film thickness ratio = $h/\bar{h}_i$

P - pressure ratio = p/p_o

Λ - seal number = $\frac{6\mu\omega}{p_o}\left(\frac{r_o}{h_i}\right)^2$

ϵ - waviness parameter

ϵ_r - radial eccentricity

ϵ_t - tilt eccentricity

C_L - load coefficient = $\frac{W}{p_o r_o^2}$

C_f - friction coefficient = $\frac{SM}{\bar{h}_i^3 p_o r_o^2/6}$

q - flow coefficient = $\frac{12\mu Q}{\bar{h}_i^3 p_o}$

U' - pumping velocity variable = $\frac{U}{r_o\omega}$

ξ - radius variable = $\frac{r - r_i}{r_o - r_i}$

λ - film thickness variable = $\frac{h_o - \bar{h}_i}{h_i}$

n - number of circumferential waves

E_{ij} - numerical grouping

D_i - numerical grouping

Subscripts

o - at the outside radius of the seal

i - at the inside radius of the seal

C - within the cavitated film

TABLE I

TIME SHARING COMPUTER PROGRAM
FOR CALCULATING 1/Λ (EQUATIONS 65 AND 71)

```
10 DIM T(50),I(50)
15 READ NO
20 FØR I=1 TØ NO
30 READ I(I)
35 LET T(I) = I(I) * 3.14159/180
40 NEXT I
45 LET P=0
50 READ R1,E
55 PRINT "TILT ECCENTRICITY =",E
59 PRINT
60 PRINT "THETA","1/L(FN)","1/L(FT)","N","CØNSTANT TERM"
70 FØR J= 1 TØ NO
72 LET TO=0
73 LET A=0
74 LET LO=0
76 LET B= E* CØS(T(J))
79 LET C= E*SIN(T(J))
81 LET A1=0
85 LET B1 =0
90 LET Y= R1
92 LET L= 1/2*1/(1-ABS(B))↑2
110 PRINT
200 LET X1= (LØG(Y*(1+B)/(1+B*Y)))+(1/(1+B*Y)-1/(1+B))
210 LET X2 = .5*((1/(1+B*Y)↑2)-(1/(1+B)↑2))
220 LET X3= X1+ X2
225 FØR N= 1 TØ 100
230 LET T=(-1)↑(N+1)*((N+1)/(N+2))*N/2*B↑(N-1)*(1-Y↑(N+2))
235 LET TO= TO+T
236 LET L1= 1/2*(N*(ABS(B)↑(N-1)))
237 LET LO= LO+L1
240 LET D= L-(LO-TO)
242 IF ABS((D-TO)/D) < .01 THEN 300
260 NEXT N
261 PRINT " CØNDITIØNS NØT MET IN 100 TERMS"
263 GØ TØ 320
300 LET X4 = (X3+TO)*C/3
302 LET F= (X3+D)*C/3
304 PRINT I(J),F,X4,N,X3
320 NEXT J
900 DATA 27
910 DATA 180,182,184,186,188,190,192,194,196,198,200,202,204,206,208
911 DATA 210,212,214,216,218,220,222,224,226,228,230,232
920 DATA .643,.9
99999 END
```

REFERENCES

1. Denny, D. F., "Some Measurements of Fluid Pressures Between Plane Parallel Thrust Surfaces with Special Reference to Radial-Face Seals," Wear, Vol. 4, No. 1, Jan./Feb. 1961, pp. 64-83.

2. Nau, B. S., "A Reconsideration of Pressure Generation in Radial-Face Seals," BHRA, RR 699, Sept., 1961.

3. Nau, B. S., "Centripetal Flow in Face Seals," ASLE Paper No. 68 AM 4B-3, ASLE Annual Meeting, Cleveland, Ohio, May 6, 1968.

4. Nau, B. S., "Hydrodynamics of Face Seal Films," Paper F5, Second International Conference on Fluid Sealing, BHRA, Canfield, England, April, 1964.

5. Lyman, F. A. and Saibel, E., "Leakage Through Rotary Shaft Seals," Proceedings of the Fourth U. S. National Congress of Applied Mechanics, Vol. 2, 1962.

6. Findlay, J. A., "Cavitation in Mechanical Face Seals," ASME Paper No. 67-WA/Lub-20.

7. Findlay, J. A., "Cavitation in Mechanical Face Seals," MS thesis, Union College, Schenectady, New York, March, 1967.

8. Final Report, "Study of Dynamic and Static Seals for Liquid Rocket Engines, Vol. I NASA Contract No. NAS 7-434, Feb. 1967.

9. Quarterly Report No. 3, Phase II, "Study of Dynamic and Static Seals for Liquid Rocket Engines," NASA Contract No. NAS 7-434, January 17, 1968.

10. Sneck, H. J., "The Effects of Geometry and Inertia on Face Seal Performance-Laminar Flow," ASME Paper No. 67-WA/Lub-15.

11. Sneck, H. J., Vol. II, Final Report, "Study of Dynamic and Static Seals for Liquid Rocket Engines," NASA Contract No. NAS 7-434, February, 1967.

12. Orcutt, F. K. and Cheng, H. S., "Preliminary Analytical Investigation of Radial Face Seals," Mechanical Technology Inc., Report No. MTI 64TR22, April 24, 1964.

13. Pape, J. G., "Fundamental Research on a Radial Face Seal," ASLE Paper No. 68 AM 5B-3, ASLE Annual Meeting, Cleveland, Ohio, May 6, 1968.

14. Nau, B. S., "Cavitation in Thin Films," British Hydromechanics Research Association TN 832, Nov., 1964.

15. Jackobsson, B. and Floberg, L., "The Finite Journal Bearing, Considering Vaporization," Transactions of Chalmers University of Technology, No. 190, 1957, Gothenburg, Sweden, (Report No. 3 from the Institute of Machine Elements).

16. Castelli, V., and Privics, J., "Equilibrium Characteristics of Axial-Groove Gas-Lubricated Bearings," ASME Paper No. 65-LUB-16.

APPENDIX E

SEAL DESIGN II

BY

H.J. SNECK

I. INTRODUCTION

Included in this section are several analyses which are directed at furthering our understanding of mechanical face seals operating under hydrodynamic conditions with a Newtonian lubricant.

The first study examines the effects of heat generation in the face seal due to viscous shearing of the fluid. One of the purposes of this study is to evaluate the constant viscosity assumption made in our previous analyses. That is, how much does the fluid temperature (and thus the fluid viscosity) vary across the seal face. As one might expect from the fact that leakage rates through the seals are low, the conclusion of this study was that the fluid in the seal interface film is almost isothermal. Thus the assumption of constant viscosity is a valid one for most seal problems. However, each seal application should be evaluated individually.

The second study examines the interaction of the fluids on either side of a face seal due to inertia effects. That is, the fluids being separated by the seal may come in contact in the seal film and inertia forces may cause a reverse flow through the seal against the hydrostatic pressure drop. The analysis solves for the streamline separating the two fluids and determines the conditions for which this streamline will span the width of the seal and result in an interchange of fluid across the seal.

II. THERMAL EFFECTS WITHIN AN ALIGNED FACE SEAL - LAMINAR FLOW

A. INTRODUCTION

In the previous analyses of face seal performance (Ref. 1) it was always assumed that the flow through the seal was isothermal. Since the density and especially the viscosity of the sealant fluid are reasonably sensitive to temperature changes, it is important to establish the accuracy of this assumption.

B. ANALYSIS OF LAMINAR FLOW

Because of its simplicity, the aligned, laminar, flat seal will be

analyzed and the results of the analysis extended to seals in general.

It was shown in Ref 1 that the radial and tangential velocity profiles in laminar flow are given by the equations

$$u = \left(\frac{Z^2 - cZ}{2\mu}\right)\frac{\partial p}{\partial r} - \frac{\rho r \omega^2}{12\mu c^2}\left(Z^4 - Zc^3\right) \tag{1}$$

$$v = r\omega\left(\frac{Z}{c}\right) \tag{2}$$

where it is assumed that ρ and μ are independent of Z.

The pressure distribution is given by the formula

$$p = P_1 + \frac{3\rho\omega^2}{2o}\left(r^2 - R_1^2\right) - \frac{6\mu Q}{\pi c^3}\ell n\left(\frac{r}{R_1}\right) \tag{3}$$

Equations (1), (2) and (3) will be particularly useful in evaluating the various terms of the energy equation which is

$$\frac{\partial}{\partial Z}\left(-k\frac{\partial T}{\partial Z}\right) + \rho C_p u\frac{\partial T}{\partial r} = u\frac{\partial p}{\partial r} + \mu\left[\left(\frac{\partial u}{\partial Z}\right)^2 + \left(\frac{\partial v}{\partial Z}\right)^2\right] \tag{4}$$

Since the liquid film is quite thin it seems reasonable to assume that the temperature variation across the film in the axial (Z) direction is relatively small. This is consistant with the previous assumption that μ and ρ are not functions of Z. With this assumption the energy equation may be integrated across the fluid film in the axial direction.

The first term in the energy equation (4) represents the axial conduction of thermal energy, which when integrated between the seal surfaces yields the total local heat transfer flux exchanged between the fluid and the surroundings. That is,

$$\int_o^c \frac{\partial}{\partial Z}\left(-k\frac{\partial T}{\partial Z}\right) dZ = -\left(k\frac{\partial T}{\partial Z}\right)_c - \left(-k\frac{\partial T}{\partial Z}\right)_o \tag{5}$$

$$= \dot{q}_w'' = \text{total local heat flux out of fluid}$$

The second and third terms (associated with the radial transport of energy) take the form when integrated in the axial direction

$$\left(\rho C_p\frac{\partial T}{\partial r} - \frac{\partial p}{\partial r}\right)\int_o^c u\,dz \tag{6}$$

where

$$\int_0^c u\,dz = \frac{Q}{2\pi r} \tag{7}$$

Differentiating the pressure equation (3) and rearranging yields

$$\int_0^c u\,dz = \frac{Q}{2\pi r} = \frac{c^3}{12\mu}\left[\frac{3\rho r\,\omega^2}{10} - \frac{\partial p}{\partial r}\right] \tag{8}$$

for the integral coefficient in equation (6).

The last term in equation (4) represents the energy converted by viscous dissipation within the fluid film. From the radial velocity distribution given by equation (1) the dissipation associated with the radial flow is

$$\int_0^c \mu\left(\frac{\partial u}{\partial z}\right)^2 dz = \frac{c^3}{12\mu}\left(\frac{\partial p}{\partial r}\right)^2 - \frac{c^3}{20\mu}(\rho r\,\omega^2)\frac{\partial p}{\partial r} + \frac{1}{7}\frac{c^3}{\mu}\left(\frac{\rho r\,\omega^2}{4}\right)^2 \tag{9}$$

The tangential flow contribution to the dissipation is

$$\int_0^c \mu\left(\frac{\partial v}{\partial z}\right)^2 dz = \frac{\mu(r\,\omega)^2}{c} \tag{10}$$

With the aid of the foregoing evaluations, the energy equation integrated across the fluid film now takes the form

$$\dot{q}_w'' + \rho C_p\left(\frac{Q}{2\pi r}\right)\frac{\partial T}{\partial r} = \frac{c^3}{12\mu}\frac{\partial p}{\partial r}\left[\frac{3\rho r\,\omega^2}{10} - \frac{\partial p}{\partial v}\right] + \frac{c^3}{12\mu}\left(\frac{\partial p}{\partial r}\right)^2 - \frac{c^3}{20\mu}(\rho r\,\omega^2)\frac{\partial p}{\partial r} + \frac{1}{7}\frac{c^3}{\mu}\left(\frac{\rho r\,\omega^2}{4}\right)^2 + \mu\frac{(r\,\omega)^2}{c} \tag{11}$$

or, after some cancellation and rearranging

$$\dot{q}_w'' + \rho C_p\left(\frac{Q}{2\pi r}\right)\frac{\partial T}{\partial r} = -\frac{c^3}{20\mu}(\rho r\,\omega^2)\frac{\partial p}{\partial r} + \frac{1}{7}\frac{c^3}{\mu}\left(\frac{\rho r\,\omega^2}{4}\right)^2 + \frac{\mu(r\,\omega)^2}{c} \tag{12}$$

In order to integrate equation (12) in the radial direction , it will be assumed for the time being that ρ and μ are independent of the radial coordinate. This is, of course, not known apriori. As a matter of face, it is the possibility of just such a radial variation which is under investigation here. The results to follow will fortunately justify this seemingly bold assumption.

When equation (12) is integrated radially it becomes

$$\frac{\int_{R_1}^{R_2} 2\pi r\, \dot{q}_w''\, dr}{Q} + \rho C_p (T_2 - T_1) = \frac{3}{20}\rho\omega^2(R_2^2 - R_1^2) + \left[\frac{2\pi\mu\omega^2}{Qc} + \frac{9}{100}\frac{(\rho\omega^2)^2\pi C^3}{Q\mu}\right]\left(\frac{R_2^4 - R_1^4}{4}\right) \tag{13}$$

The numerator of the first term is obviously the total heat transfer exchanged with the surroundings $\dot{q}_w'' = \int_{R_1}^{R_2} 2\pi r\, \dot{q}_w''\, dr$

With this definition the energy equation may be rewritten as

$$\frac{\dot{q}_w}{Q} + \rho C_p (T_2 - T_1) = \frac{3}{5}\rho\left(\frac{R_2\omega}{2}\right)^2\left[1 - \left(\frac{R_1^2}{R_2}\right)^2\right] \cdot \left\{1 + \frac{3}{20}\left[\frac{\rho R_2\omega^2}{\frac{\mu Q}{\pi C^3 R_2}}\right]\left[1 + \frac{200}{9}\left(\frac{\mu}{\rho\omega C^2}\right)^2\right]\left[1 + \left(\frac{R_1}{R_2}\right)^2\right]\right\} \tag{14}$$

where the heat transfer, enthalpic, and kinetic energy terms are easily identified.

C. ANALYSIS OF TURBULENT FLOW

The basic difference between the laminar and turbulent flow analyses is the way in which the dissipation (viscous) term in the energy equation is formulated. The general form of this term in dyadic notation is

$$\tau : \nabla V \tag{15}$$

where τ is the stress dyadic and V is the velocity vector. For face seal flow this quantity may be approximated by

$$\tau : \nabla V = \tau_{\theta z}\left(\frac{\partial u}{\partial z}\right) + \tau_{rz}\frac{\partial v}{\partial z} \tag{17}$$

When the flow is laminar then

$$\tau : \nabla V = \mu\left[\left(\frac{\partial u}{\partial z}\right)^2 + \left(\frac{\partial v}{\partial z}\right)^2\right] \tag{18}$$

which appears in equation (4). For isotropic turbulent flow it has been shown that (Ref. 1)

$$\tau_{rz} = \tau_{\theta z}\left(\frac{\partial u}{\partial z}\Big/\frac{\partial v}{\partial z}\right) \tag{19}$$

which means that

$$\tau : \nabla V \cong \tau_{\theta z}\left[\frac{\partial v}{\partial z} + \left(\frac{\partial u}{\partial z}\right)^2\Big/\frac{\partial v}{\partial z}\right] \tag{20}$$

where

$$\tau_{\theta z} = \tau_{\theta z_w} = 0.0225\ \rho\ (\nu)^{1/4} \left[\frac{(\frac{r\omega}{2})^7}{c/2}\right]^{1/4} \tag{21}$$

Following the same procedure used in the laminar analysis, the integrated form of the energy equation for turbulent flow is

$$\dot{q}_w'' + \rho C_p \frac{\partial T}{\partial r}\int_o^c u dZ = r\omega\ \tau_{\theta z_w} + \frac{\rho}{r}\int_o^c v_r\ (v_\theta)^2\ dZ \tag{22}$$

Noting that $Q = \int_o^c 2\pi r u dZ$, the working form of the energy equation can be written as

$$\dot{q}_w'' + \frac{\rho C_p Q}{2\pi r}\frac{\partial T}{\partial r} = r\omega\ \tau_{\theta z_w} + \rho_r \int_o^c u(v)^2\ dz \tag{23}$$

The velocity distributions to be used when evaluating the last term of this equation will be the same as used in Reference 1

$$u\ \tau_{z\theta_w} = -(\frac{r\omega}{2})(\frac{c}{2})\frac{dp}{dr}F(\frac{Z}{c/2}) + \frac{\rho}{r}(\frac{r\omega}{2})^3(\frac{c}{2})\ G(\frac{Z}{c/2} \tag{24}$$

$$v = \begin{cases} v_1 = (\frac{r\omega}{2})(\frac{Z}{c/2})^{1/7}, & 0 < Z < c/2 \\ v_2 = r\omega\left[1 - 1/2\ (\frac{c-z}{c/2})^{1/7}\right], & c/2 < z < c \end{cases} \tag{25}$$

The pressure gradient from the same reference is

$$\frac{dp}{dr} = \frac{835}{816}\rho r\ (\frac{\omega}{z})^2 - \frac{0.0195}{\pi}\ (\frac{\rho^3 \mu\ \omega^3}{rc^9})^{1/4}\ Q \tag{26}$$

The evaluation of the last term in equation (23) leads to

$$\tau_{ze_w}\frac{\rho}{r_o}\int_o^c u(v)^2 dz = -1.2090\ \frac{\rho}{r}(\frac{r\omega}{2})^3(\frac{c}{2})^2\frac{835}{816}\left[\rho r(\frac{\omega}{2})^2 - \frac{0.0195}{\pi}(\frac{\rho^3\mu\ \omega^3}{rc^9})^{1/4} Q\right] +$$

$$1.7228\ (\frac{\rho}{r})^2(\frac{r\omega}{2})^5(\frac{c}{2})^2 \tag{27}$$

or

$$\frac{\rho}{r}\int_0^c u(v)^2 dz = \left\{\frac{1}{0.0225\rho(\nu)^{1/4}\left[\frac{(\frac{\omega}{2})^7}{c/2}\right]^{1/4}}\right\} \cdot$$

$$\left\{0.48568\ (\frac{c\rho}{2})^2\ (\frac{\omega}{2})^5\ r^{5/4} + 1.2090\ (\frac{0.0195}{\pi})\ (\frac{\rho^3 \mu\ \omega^3}{c^9})^{1/4}\ \rho Q\ (\frac{\omega}{2})^3\ (\frac{c}{2})^2\right\} \qquad (28)$$

It should be observed that this rather complicated expression is really a simple function of the radius of the form

$$\frac{\rho}{r}\int_0^c u(v)^2 dz = Ar^{5/4} + B \qquad (29)$$

Returning to equation (23) and integrating with respect to r yields

$$\int_{R_1}^{R_2} 2\pi r \dot{q}_w'' \, dr + \rho Q C_p \int_{R_1}^{R_2} \frac{\partial T}{\partial r}\, dr = 0.0225\ \rho(\nu)^{1/4}\ \omega \left[\frac{(\frac{\omega}{2})^7}{c/2}\right]^{1/4} \int_{R_1}^{R_2} 2\pi r^{15/4}\, dr +$$

$$2\pi \int_{R_1}^{R_2} Ar^{9/4}\, dr + 2\pi \int_{R_1}^{R_2} Br\, dr \qquad (30)$$

Carrying out the integration assuming that A and B are independent of the radius yields

$$\dot{q}_w + \rho Q C_p\ (T_2 - T_1) = 0.0225\ \rho(\nu)^{1/4}(2\pi\ \omega) \cdot$$

$$\left[\frac{(\frac{\omega}{2})^7}{c/2}\right]^{1/4} (\frac{4}{19})\ (R_2^{19/4} - R_1^{19/4}) + 2\pi A\ (\frac{4}{3})\ (R_2^{13/4} - R_1^{13/4})$$

$$+ 2\pi\ B\ (\frac{1}{2})\ (R_2^2 - R_1^2) \qquad (31)$$

Rearranging and replacing A and B with their earlier representations gives the final form

$$\frac{\dot{q}_w}{Q} + \rho C_p\ (T_2 - T_1) = \frac{4}{19}\ (\frac{2\pi}{Q})\ R_2^2 (R_2\omega)\left[1 - (\frac{R_1}{R_2})^{19/4}\right] \cdot$$

$$\left\{0.0225\ \rho(\nu)^{1/4}\left[\frac{(\frac{R_2\omega}{2})^7}{c/2}\right]^{1/4}\right\} + \frac{2\pi}{Q}\ (\frac{4}{13})\left[1 - (\frac{R_1}{R_2})^{13/4}\right] \cdot$$

$$\left\{\frac{0.48568\left(\frac{\rho c}{2}\right)^{2}\left(\frac{R_2\omega}{2}\right)^{5}}{0.0225\,\rho(\nu)^{1/4}\left[\frac{\left(\frac{R_2\omega}{2}\right)^{7}}{\frac{2}{c/2}}\right]^{1/4}}\right\} + \left[1-\left(\frac{R_1}{R_2}\right)^{2}\right]\left\{\frac{0.0195(1.2090)\left(\frac{\rho^{3}\mu\omega^{3}}{R_2 c^{9}}\right)^{1/4}\rho R_2\left(\frac{R_2\omega}{2}\right)^{3}\left(\frac{c}{2}\right)^{2}}{0.0225\,\rho(\nu)^{1/4}\left[\frac{\left(\frac{R_2\omega}{2}\right)^{7}}{\frac{2}{c/2}}\right]^{1/4}}\right\} \tag{32}$$

This equation plays the same role for turbulent flow which equation (14) plays in laminar flow.

D. CONCLUSIONS

The implications of equation (15) may be most conveniently assessed by first considering the case when Q=0. The equilibrium temperature of the fluid trapped in the clearance space is determined by the equation

$$(\dot{q}_w)_{Q=0} = \frac{9}{100}\,\rho\left(\frac{R_2\omega}{2}\right)^{2}\left[\frac{\rho R_2\omega^{2}}{\frac{\mu}{\pi c^{3}R_2}}\right] \cdot$$

$$\left[1+\frac{200}{9}\left(\frac{\mu}{\rho\omega c^{2}}\right)^{2}\right]\left[1+\left(\frac{R_1}{R_2}\right)^{2}\right] \tag{33}$$

The term $\dot{q}_w$, which contains the ambient temperature and the fluid film temperature, is determined by heat transfer characteristics of the seal support and surroundings.

Since the leakage rate through the seal is by design small, the temperature level within the seal even with non-zero leakage is expected to be very nearly equal to the equilibrium temperature determined by equation (33). This means that the temperature change across the seal is approximated by

$$\rho C_p\,(T_2-T_1) = \frac{3}{5}\,\rho\left(\frac{R_2\omega}{2}\right)^{2}\left[1-\left(\frac{R_1}{R_2}\right)^{2}\right] \tag{34}$$

So it would seem that the level of the temperature within the seal fluid is mainly established by equation (33), with the external heat transfer characteristics of the seal support system as the major controlling influence. This temperature level is then perturbed by through-flow leakage which does not substantially change the level, only the distribution of the temperature within the seal around that level.

Calculations of the temperature rise predicted by equation (34) for typical operating conditions indicates that this rise is ordinarily small, the order of 10°F or less. The most important temperature for the evaluation of the fluid properties is, therefore, the temperature level, calculated from equation (33).

It is now clear that the sealant leaks through the seal nearly isothermally relative to the no-leakage equilibrium temperature (the temperature level). This supports the isothermal assumption which was made during the analysis. The analysis itself has provided the means of estimating the isotherm to be used when selecting μ and ρ.

Furthermore, it appears unnecessary to investigate the temperature distributions in misaligned, eccentric, wavy, or other seal configurations, since the temperature variations caused by these aberrations are undoubtedly small and inconsequential relative to the operating temperature level.

The arguments presented above apply with equal validity to laminar or turbulent flow. The heat transferred in turblent flow with Q = 0 is

$$(\dot{q}_w)_{Q=0} = \frac{4}{19}\, 2\pi R_2^2\, (R_2\omega) \left[1 - \left(\frac{R_1}{R_2}\right)^{19/4}\right] \left\{0.0225\, \rho\, \nu^{1/4} \left[\frac{\frac{R_2\omega}{2}^7}{c/2}\right]^{1/4}\right\} + 2\pi \left(\frac{4}{13}\right) \left[1 - \left(\frac{R_1}{R_2}\right)^{13/4}\right] \left\{\frac{1.59865 \left(\frac{\rho c}{2}\right)^2 \left(\frac{R_2\omega}{2}\right)^5}{0.0225\, \rho(\nu)^{1/4} \left[\frac{\left(\frac{R_2\omega}{2}\right)^7}{c/2}\right]^{1/4}}\right\}$$

which establishs the temperature level.

For $\dot{q}_w \approx (\dot{q}_w)_{Q=0}$, the temperature rise across the seal is given approximately by

$$\rho C_p (T_2 - T_1) = \left[1 - \left(\frac{R_1}{R_2}\right)^2\right] \left\{\frac{0.0195(1.2090)\left(\frac{\rho^3 \mu\omega^3}{R_2 c^9}\right)^{1/4} \rho R_2 \left(\frac{R_2\omega}{2}\right)^3 \left(\frac{c}{2}\right)^2}{0.0225\, \rho(\nu)^{1/4} \left[\frac{\left(\frac{R_2\omega}{2}\right)^7}{c/2}\right]^{1/4}}\right\} \tag{36}$$

Estimates of the temperature rise associated with this term using typical seal data indicates values of the order of $1.0^{\circ}F$ or less, again validating the isothermal assumption.

REFERENCES

1. "Study of Dynamic and Static Seals for Liquid Rocket Engines," Final Report, Volume 2, February 14, 1967, NASA Contract No. NAS 7-434.

NOMENCLATURE

c	=	seal clearance
C_p	=	fluid specific heat
k	=	fluid thermal conductivity
p	=	fluid pressure
P_1	=	supply pressure
Q	=	volumetric leakage rate
$\dot{q}''_w$	=	total local heat transfer flux from seal
$\dot{q}_w$	=	total heat transfer from seal
r	=	radial coordinate
R_1	=	inner seal radius
R_2	=	outer seal radius
T	=	temperature
T_1	=	temperature at inner radius
T_2	=	temperature at outer radius
u	=	radial velocity component
v	=	tangential velocity component
z	=	axial coordinate
μ	=	viscosity
ν	=	μ/ρ
ρ	=	density
ω	=	angular velocity of seal surface
τ_{zr}	=	radial shear stress
$\tau_{z\theta_w}$	=	tangential shear stress at the wall

III. A STUDY OF REVERSED FLOW REGIMES IN FARALLEL FACE SEALS - LAMINAR AND TURBULENT FLOW

A. INTRODUCTION

In an earlier investigation (Ref. 1) it was noted that when the net leakage rate was zero or nearly zero the radial velocity was directed outward along the rotating disk and inward along the stationary disk. The hydrodynamic features of this multi-directional flow were not explored in the earlier study, other than to suggest that a zero net leakage rate did not necessarily mean that there was no exchange of sealant fluid between the inner and outer boundaries of the seal.

The analysis which follows is a more detailed investigation of the nature of these reversed flow regimes.

B. STREAM FUNCTION - LAMINAR FLOW

The analysis of the reversed flow regimes is most conveniently carried out with the aid of the stream-function for the stream surface in this axisymmetric flow. In Reference 1 it was shown that the continuity and momentum equations were satisfied by a stream-function of the form

$$\psi(r,\xi) = r\omega\ \mathrm{Re}\ c\ W(\xi) + \frac{Q}{2\pi r} U(\xi) \tag{1}$$

where, to a first order approximation,

$$U \cong U_1 = 2\xi^3 - 3\xi^2 \tag{2}$$

$$W \cong W_1 = -\frac{1}{20}\xi^2 + \frac{7}{60}\xi^3 - \frac{1}{12}\xi^4 + \frac{1}{60}\xi^5 \tag{3}$$

$$\mathrm{Re} = \frac{c^2\omega}{\nu}$$

In the above equations $\xi = \frac{z}{c}$ where z is measured from the rotating surface toward the stationary one. The values of the stream-surface at the bounding surfaces are

$$\psi\ (r,o) = 0$$
$$\psi\ (r,1) = -\frac{Q}{2\pi r} \tag{4}$$

C. CASE OF LAMINAR NET RADIAL OUTFLOW ($Q \geq 0$)

In this case we seek a stream-surface separating internal and external fluids which branches from the stream-surface for the stationary surface, $\psi(r,1)$. For this purpose equation (1) will be written in the form

$$W(1) - W(\xi) + \beta\left[U(1) - U(\xi)\right] = 0 \tag{5}$$

where

$$\beta = \frac{\mu Q}{2\rho(r\omega)^2 c^3 \pi} \tag{6}$$

From the initial investigation it is known that reversed laminar flows occur when

$$-\frac{6}{5} < \frac{36\mu Q}{\rho(r\omega)^2 c^3 \pi} < \frac{4}{5} \tag{7}$$

or

$$-0.01666 < \beta < 0.01111 \tag{8}$$

The shape of the stream-surface separating the fluid coming from the inside and the fluid coming from the outside is determined by obtaining the roots of equation (5) for β in the range given relation (8). Figure 1 shows the result of such an evaluation for $0 < \beta < 0.01111$ $(Q > 0)$.

In a practical sense, after having designed a seal and determined its leakage rate using the analysis given in Reference 1, one would next calculate β with $r = R_1$. If $\beta < 0.01111$, then for $R_1 < r < R_2$, β will be in the range given by expression (7) and reversed flow will be present. Figure 1 allows one to calculate the shape of the separating stream-surface, and in particularly at what radius it branches from the stationary surface.

A typical plot will look like that shown in Figure 2. If the separating stream-surface branches within the seal itself as shown in Figure 2, no external fluid will reach the inside. If, on the other hand, this stream-surface branches at a radius less than R_1 there will be an exchange of external and internal fluids even though the net flow is radially outward.

D. CASE OF LAMINAR NET RADIAL INFLOW ($Q < 0$)

In this case the separating stream-surface branches from the rotating

surface, so we seek zeros of the equation

$$W(\xi) + \beta\ U(\xi) = 0 \tag{9}$$

with

$$-\ 0.01666 < \beta < 0.$$

Whether there is an exchange of inner and outer fluids is determined, as above, using in this case Figure 3. If it is determined that the separating stream-surface branches at a radius greater than R_2, as shown in Figure 4, there will be an exchange of inner and outer fluid.

E. CASE OF ZERO NET RADIAL FLOW (Q = 0)

The case of no-net flow is special situation which cannot be treated the same way as the two previous cases. In this case the streamfunction reduces to

$$\psi\ (r,\xi) = r\,\omega\ Re_c\ W(\xi) \tag{10}$$

From equations (4) it is clear that the z axis, as well as the stationary and rotating disks, lie on the same stream-surface, ψ=0. From Reference 1 it is obvious that $W(\xi)$ is roughly parabolic in the range $0 \leq \xi \leq 1.0$ so that ψ is multivalued at any given radius. It is not difficult then to show that the radial velocity vanishes on a surface $\xi_t = 0.475$ for all radii. With this information the general streamline picture can be sketched (see Figure 5).

The solution given by equation (10) is actually valid for disks with R_1=0 as shown in Figure 5. When $R_1 > 0$ the stream-surfaces shown in Figure 5 for the region $r < R_1$ are, of course, meaningless. The flows shown in Figure 2 and 5 being the limiting case of Figure 2, where the separating stream-surface has merged into the rotating surface.

Once again there is an exchange of inner and outer fluids, the separating stream-surface being the one which just reaches the inner radius before turning around and returning to the outside. The number value of this particular stream line is obtained by inserting the coordinates of the turning point into equation (10), i. e.,

$$\psi_{separating} = \psi(R_1,\ 0.475) = R_1\omega\ Re\ C\ W(0.475) = -0.00262\ R_1\omega\ Re\ c \tag{11}$$

The inflow and outflow leakage rates are equal in magnitude and given by the equation

$$q_t = 0.00262\ (2\pi R_1)\ R_1\ \omega\ Re\ c \tag{12}$$

It should be noted at this point that when the separating stream-surface branches from the seal surfaces, as in the earlier cases studied(see Figure 4), the fluid exchanges are determined in exactly the same way as just described. These exchanges will not be equal in magnitude, of course, but their algebraic difference will be equal to the net flow rate Q.

To find the turning point coordinates of the stream-surface just reaching a radial boundary in the cases where $Q \neq 0$, one would calculate ξ_t from the formula

$$\xi_t = 1 - \frac{1}{2}\left[\sqrt{1 + 4\left(\frac{4}{5} - A\right)} - 1\right] \tag{13}$$

setting r equal to R_1 or R_2 in

$$A = \frac{36\,\mu\,Q}{\rho\pi c^3 (r\omega)^2} \tag{14}$$

Inserting the proper r and ξ_t into equations 1, 2 and 3 yields the number value of the streamline bounding the exchange flows. Using the relations given in equation (4) the exchange rates of the inner and outer flows can be calculated.

F. TURBULENT FLOW

Since the equations of motion for the turbulent case are more conveniently solved in integral rather than differential form, the streamline technique of laminar flow will not be used with turbulent flow. An alternative approach is to calculate the flow rate through a cylindrical area whose height is measured from the seal surface and determine at what distance from the surface the net flow-rate equals zero. In this way it is possible to construct a functional relationship between the separating stream-surface and the radial coordinate.

From reference 1 we have the following relationships for the radial velocity component and the pressure gradient

$$u\,\tau_{z\theta_w} = -\left(\frac{r\omega}{2}\right)\left(\frac{c}{2}\right)F\left(\frac{z}{c/2}\right)\frac{dp}{dr} + \frac{\rho}{r}\left(\frac{r\omega}{2}\right)^3\left(\frac{c}{2}\right)G\left(\frac{z}{c/2}\right) \tag{15}$$

and

$$\frac{dp}{dr} = \frac{835}{816}\rho r\left(\frac{\omega}{2}\right)^2 - \frac{0.0195}{\pi}\left(\frac{\rho^3 \mu\, \omega^3}{rc^9}\right)^{1/4} Q \tag{16}$$

These equations may be combined to give

$$\frac{u\tau_{z\theta}}{(\frac{c}{2})(\frac{r\omega}{2})\frac{\rho}{r}(\frac{r\omega}{2})^2} = G\left(\frac{z}{c/2}\right) + \left[\left(\frac{0.0195}{9}\right)\left(\frac{36\mu Q}{\pi\rho c^3(r\omega)^2}\right)\cdot \left(\frac{\rho r\omega c}{\mu}\right)^{3/4} - \frac{835}{816}\right] F\frac{z}{c/2} \tag{17}$$

where

$$F\left(\frac{z}{c/2}\right) = \left(\frac{z}{c/2}\right)^{1/7}\left[1 - \frac{1}{8}\left(\frac{z}{c/2}\right),\right] \quad 0 \le z \le c/2$$

$$= \left(\frac{h-z}{c/2}\right)^{1/7}\left[\frac{3}{4} + \frac{1}{8}\left(\frac{z}{c/2}\right)\right], \quad c/2 \le z \le c \tag{18}$$

$$G\left(\frac{z}{c/2}\right) = \left(\frac{z}{c/2}\right)^{1/7}\left[\frac{35}{36} - \frac{7}{90}\left(\frac{z}{c/2}\right)^{9/7}\right], \quad 0 \le z \le c/2$$

$$= \left(\frac{c-z}{c/2}\right)^{1/7}\left[\frac{1}{12} + \frac{1}{2}\left(\frac{z}{c/2}\right) + \frac{7}{18}\left(\frac{c-z}{c/2}\right)^{8/7} - \frac{7}{90}\left(\frac{c-z}{c/2}\right)^{9/7}\right], c/2 \le z \le c \tag{19}$$

It should be noted that z in this case is measured from the stationary surface.

Defining the net flow-rate through the cylindrical surface of height z as

$$q = \int_0^z u\,dz \tag{20}$$

the position of the stream-surface is determined by the zeros of the expression

$$0 = \int_0^z G\left(\frac{z}{c/2}\right) dz + \left[\left(\frac{0.0195}{9}\right)\left(\frac{36\,\mu\,Q}{\pi\rho c^3(r\omega)^2}\right)\cdot \left(\frac{\rho r\omega c}{\mu}\right)^{3/4} - \frac{835}{816}\right]\int_0^z F\left(\frac{z}{c/2}\right) dz \tag{21}$$

For this purpose the following integrals are required:

$$0 \le z \le c/2$$

$$\int_0^z F\left(\frac{z}{c/2}\right) dz = \frac{7}{8}\left(\frac{c}{2}\right)\left(\frac{z}{c/2}\right)^{8/7}\left[1 - \frac{1}{15}\left(\frac{z}{c/2}\right)\right]\int_0^z G\left(\frac{z}{c/2}\right) dz$$

$$= \frac{c}{2}\left[\frac{35}{36}\left(\frac{7}{8}\right)\left(\frac{z}{c/2}\right)^{8/7} - \frac{7}{90}\left(\frac{7}{17}\right)\left(\frac{z}{c/2}\right)^{17/7}\right] \tag{22}$$

$$c/2 \leq z \leq c$$

$$\int_0^z F\left(\frac{z}{c/2}\right) dz = \frac{c}{2}\left(\frac{7}{8}\right)\left\{\frac{28}{15} - \left[\left(\frac{c-z}{c/2}\right)^{8/7} - \frac{1}{15}\left(\frac{c-z}{c/2}\right)^{15/7}\right]\right\}$$

$$\int_0^z G\left(\frac{z}{c/2}\right) dz = \frac{c}{2}\left\{\left[\frac{13}{12}\left(\frac{7}{8}\right) - \frac{1}{2}\left(\frac{7}{15}\right) + \frac{7}{18}\left(\frac{7}{16}\right) - \left(\frac{7}{90}\right)\left(\frac{7}{17}\right) + \frac{35}{36}\left(\frac{7}{8}\right) - \frac{7}{90}\left(\frac{7}{17}\right)\right] - \left[\frac{13}{12}\left(\frac{7}{8}\right)\left(\frac{c-z}{c/2}\right)^{8/7} - \frac{1}{2}\left(\frac{7}{15}\right)\left(\frac{c-z}{c/2}\right)^{15/7} + \frac{7}{18}\left(\frac{7}{16}\right)\left(\frac{c-z}{c/2}\right)^{16/7} - \frac{7}{90}\left(\frac{7}{17}\right)\left(\frac{c-z}{c/2}\right)^{17/7}\right]\right\} \tag{23}$$

G. CASE OF TURBULENT NET RADIAL OUTFLOW ($Q < 0$)

It was determined analytically in reference 1 that reversed flow would occur when

$$-27.7 \leq \left(\frac{36\,\mu Q}{\rho \pi c^3 (r\omega)^2}\right)\left(\frac{\rho r \omega c}{\mu}\right)^{3/4} \leq 23.6 \tag{24}$$

The zeros of equation (21) for values in this range are the only ones which need be considered. They are most conveniently determined with the aid of a computer. Figure 6 shows the computed results for the positive portion of the range given in (24). In order to be consistant with the laminar results, relation 24 is re-written as

$$-0.385 \leq \beta\left(\frac{\rho r \omega c}{\mu}\right)^{3/4} \leq 0.328 \tag{25}$$

and the product $\beta\left(\frac{\rho r \omega c}{\mu}\right)^{3/4}$ is plotted as a function of $\xi = 1 - z/c$. The stream-surface for these conditions looks like that sketched in Figure 2.

H. CASE OF TURBULENT NET RADIAL INFLOW($Q < 0$)

Since the separating stream-surface for this situation will look like the one sketch in Figure 4, the zeros of the following equation must be found

$$0 = \int_0^z u\,dz - \int_0^z u\,dz \tag{26}$$

The results of this computation are plotted in Figure 7.

I. CASE OF ZERO NET RADIAL FLOW

The case of zero net flow once again requires special treatment. Referring to Figure 5, the exchange flow is determined by first locating the separating stream-surface. On this surface u = o so that ξ_t is found from equation (17) by setting u = Q = 0, i. e.,

$$0 = G\left(\frac{z}{c/2}\right) - \frac{835}{816} F\left(\frac{z}{c/2}\right) \tag{27}$$

Using the function F and G from reference 1 yields

$$z_{t/c} = 0.55 \tag{28}$$

Since the inflow and outflow exchange rates are equal, the exchange rate can be calculated from

$$q_t = \frac{1}{2}\left[2\pi R_1 \int_{z_t = 0.55c} u(R_1, z)\, dz\right] \tag{29}$$

where

$$u(R_1,z) = \left[\frac{\frac{c}{2}\left(\frac{R_1\omega}{2}\right)\frac{\rho}{R_1}\left(\frac{R_1\omega}{2}\right)^2}{\tau_{\theta z_\omega}(R_1)}\right]\left[G\left(\frac{z}{c/2}\right) - \frac{835}{816} F\left(\frac{z}{c/2}\right)\right] \tag{30}$$

$$\tau_{\theta z_\omega}(R_1) = 0.0225\, \rho(\nu)^{1/4}\left[\frac{\left(\frac{R_1\omega}{2}\right)^7}{c/2}\right]^{1/4} \tag{31}$$

Carrying out the indicated integration yields

$$q_t = -0.01696\,(2\pi R_1)\,\omega c^2\left[\frac{\frac{c}{2}\left(\frac{R_1\omega}{2}\right)}{\nu}\right]^{1/4} \tag{32}$$

which is the equation for turbulent analogous to equation (12) for turbulent flow.

J. CONCLUSION

The means for determining whether reversed flow conditions result in an exchange of inner and outer fluids have been developed. When there is an exchange, a technique for dividing the net flow-rate into individual exchange rates is outlined. The results are restricted to the case where both inner and outer boundaries are continually immersed in the same fluid.

Because the special case of no net leakage (Q=0) results in a simple stream-surface geometry, the equations for the exchange flows can be deduced without reference to other the specifics of the seal operation. These equations (12) and (32) and Figures (1,3,5,6) provide a complete description of the reversed flow phenomena.

FIGURE 1

STREAM-SURFACE BRANCHING FROM STATIONARY DISK (Q70)

LAMINAR

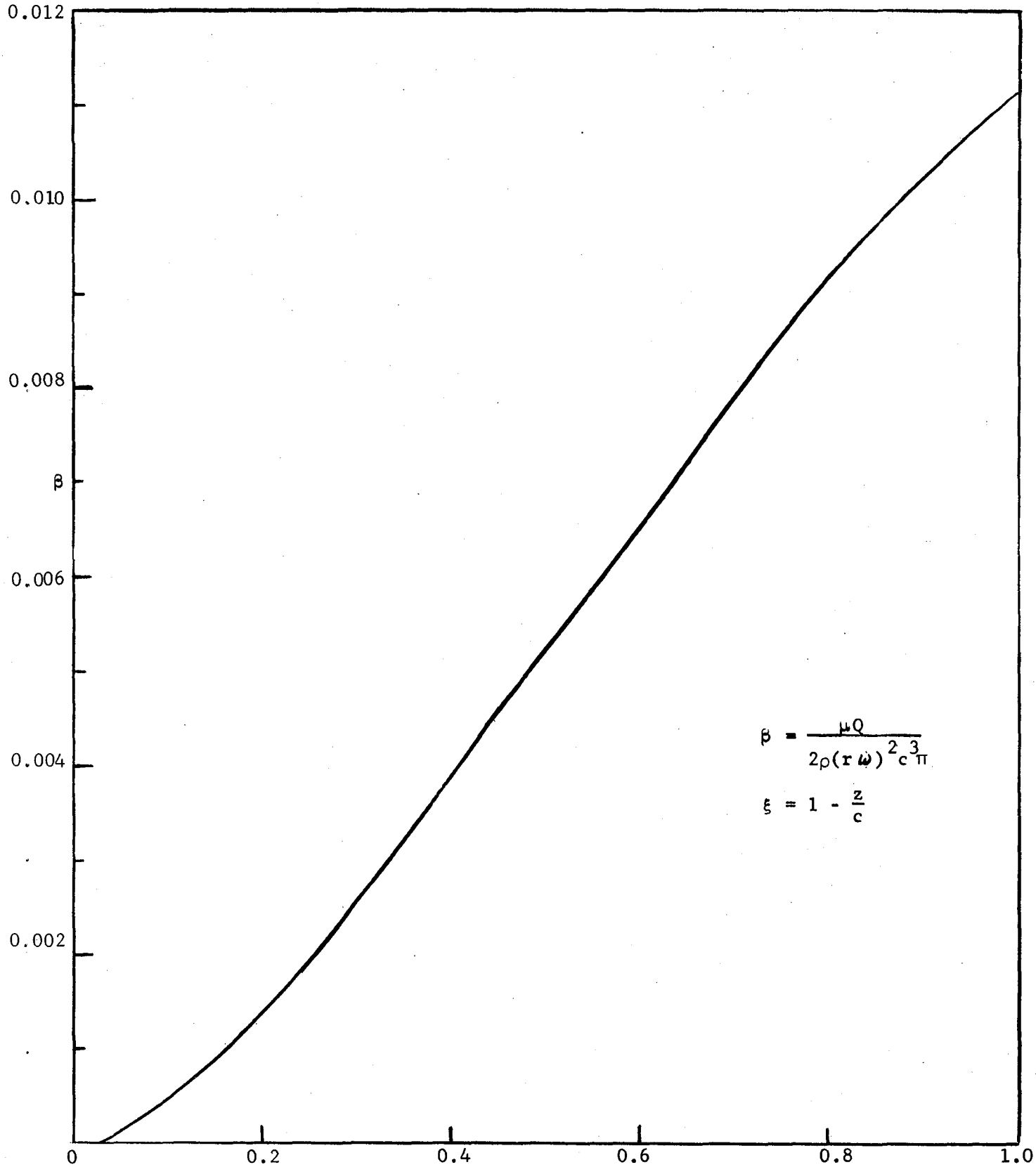

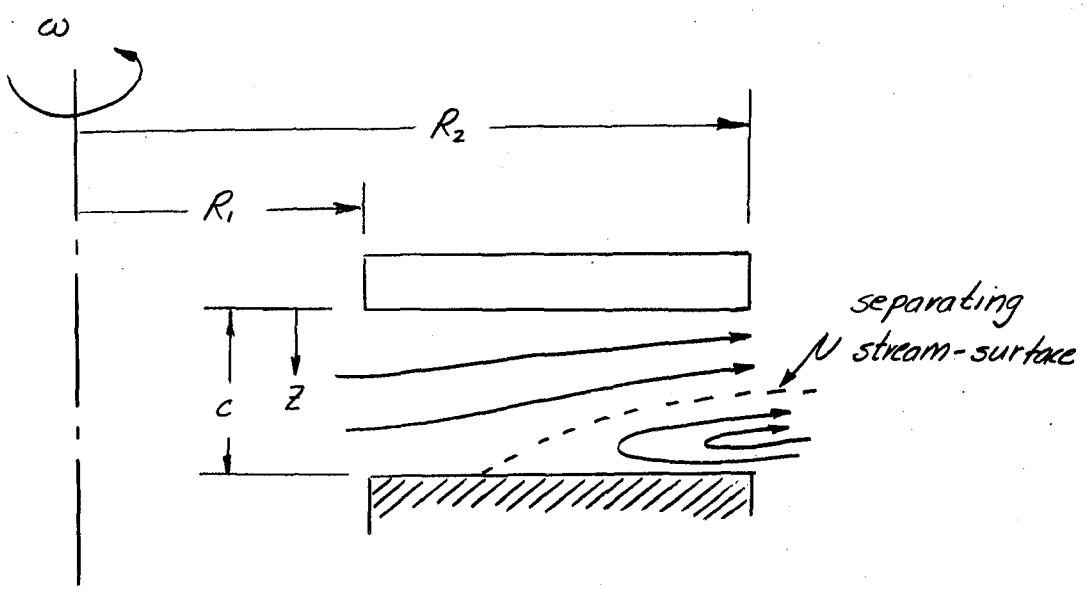

FIGURE 2

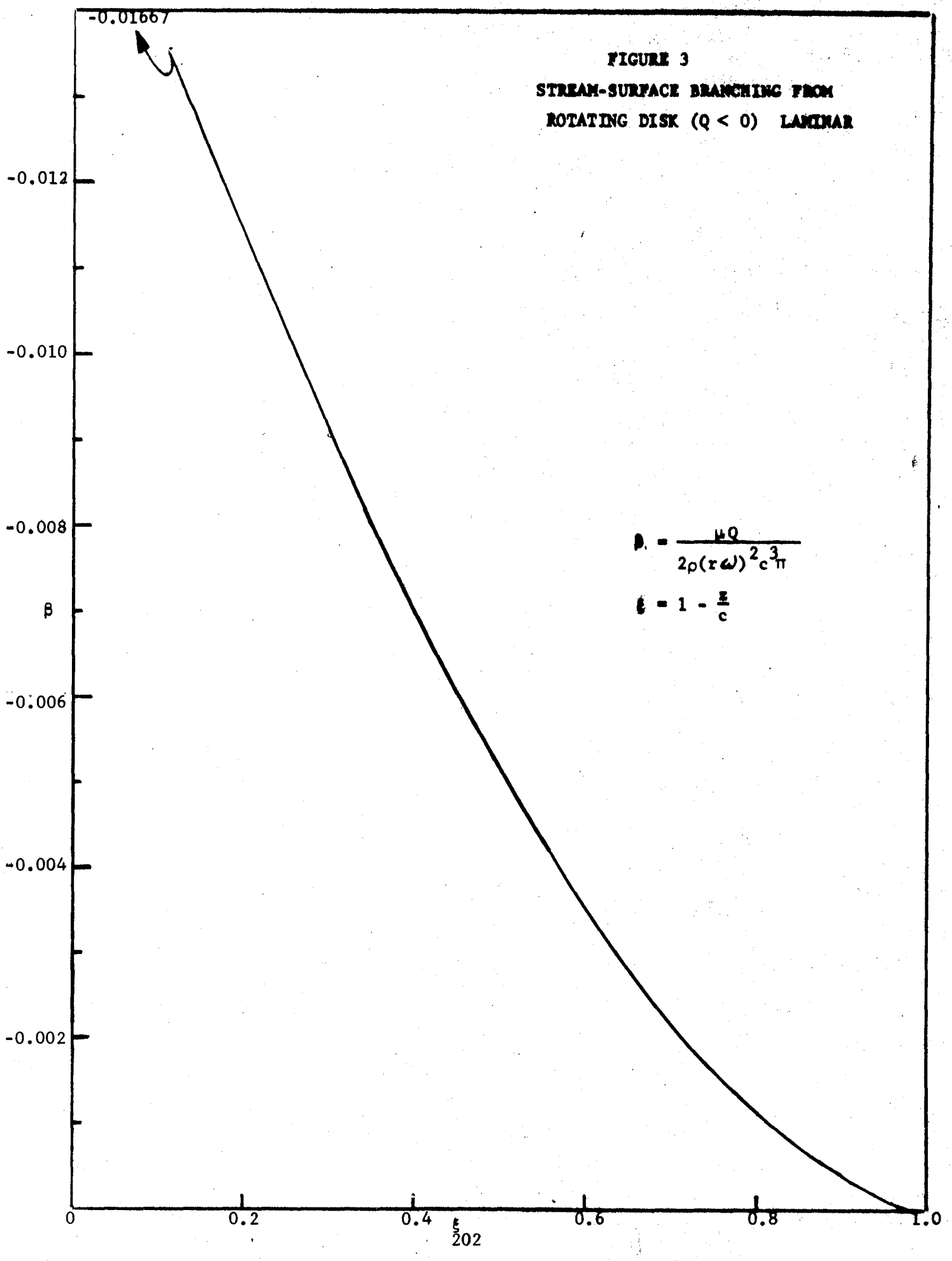

FIGURE 3

STREAM-SURFACE BRANCHING FROM ROTATING DISK ($Q < 0$) LAMINAR

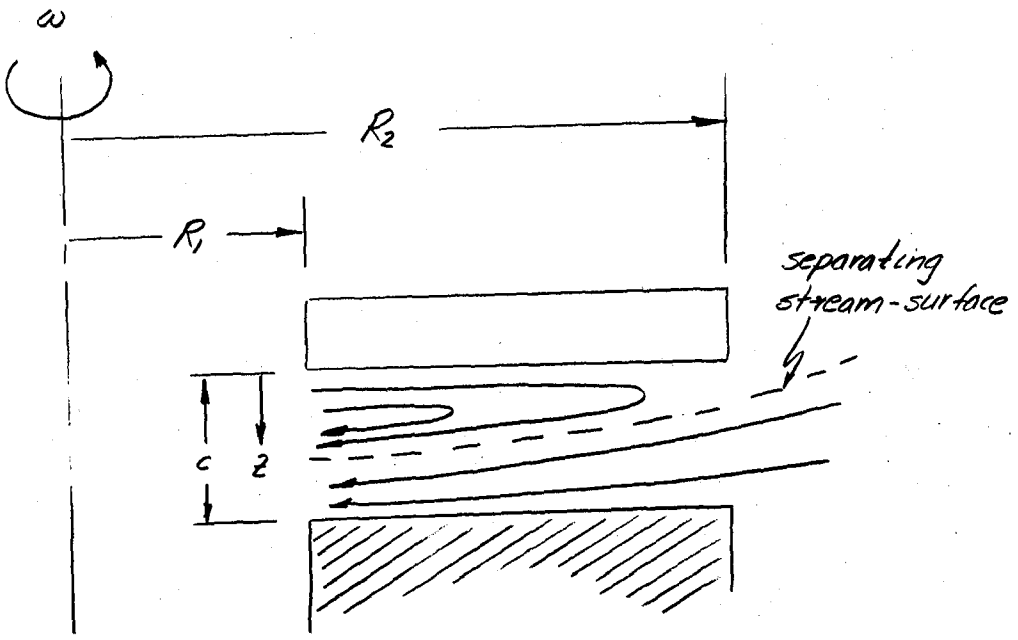

FIGURE 4

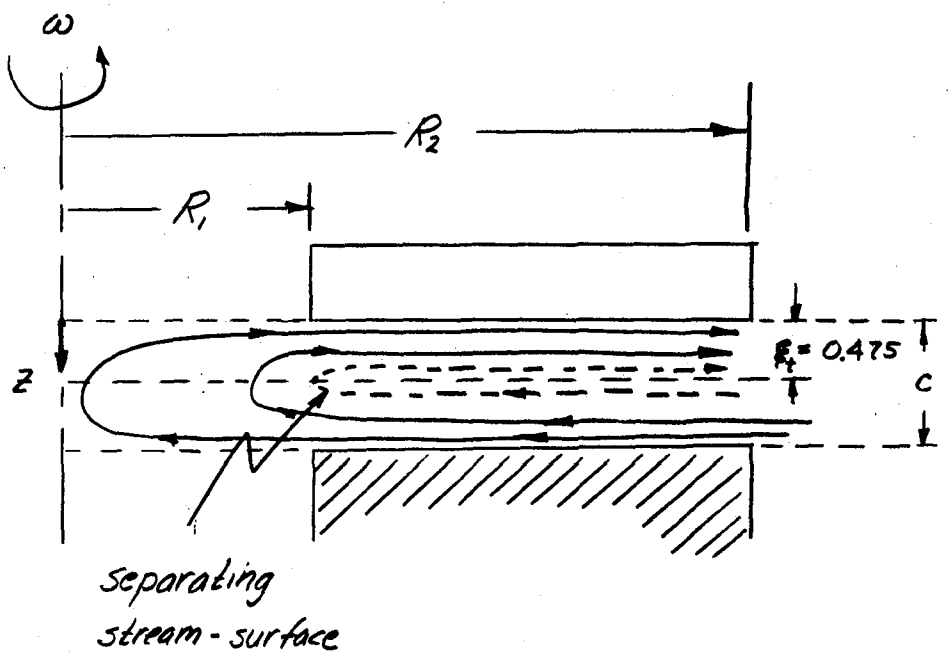

FIGURE 5

FIGURE 6

STREAM-SURFACE BRANCHING FROM STATIONARY DISK (Q70)

TURBULENT

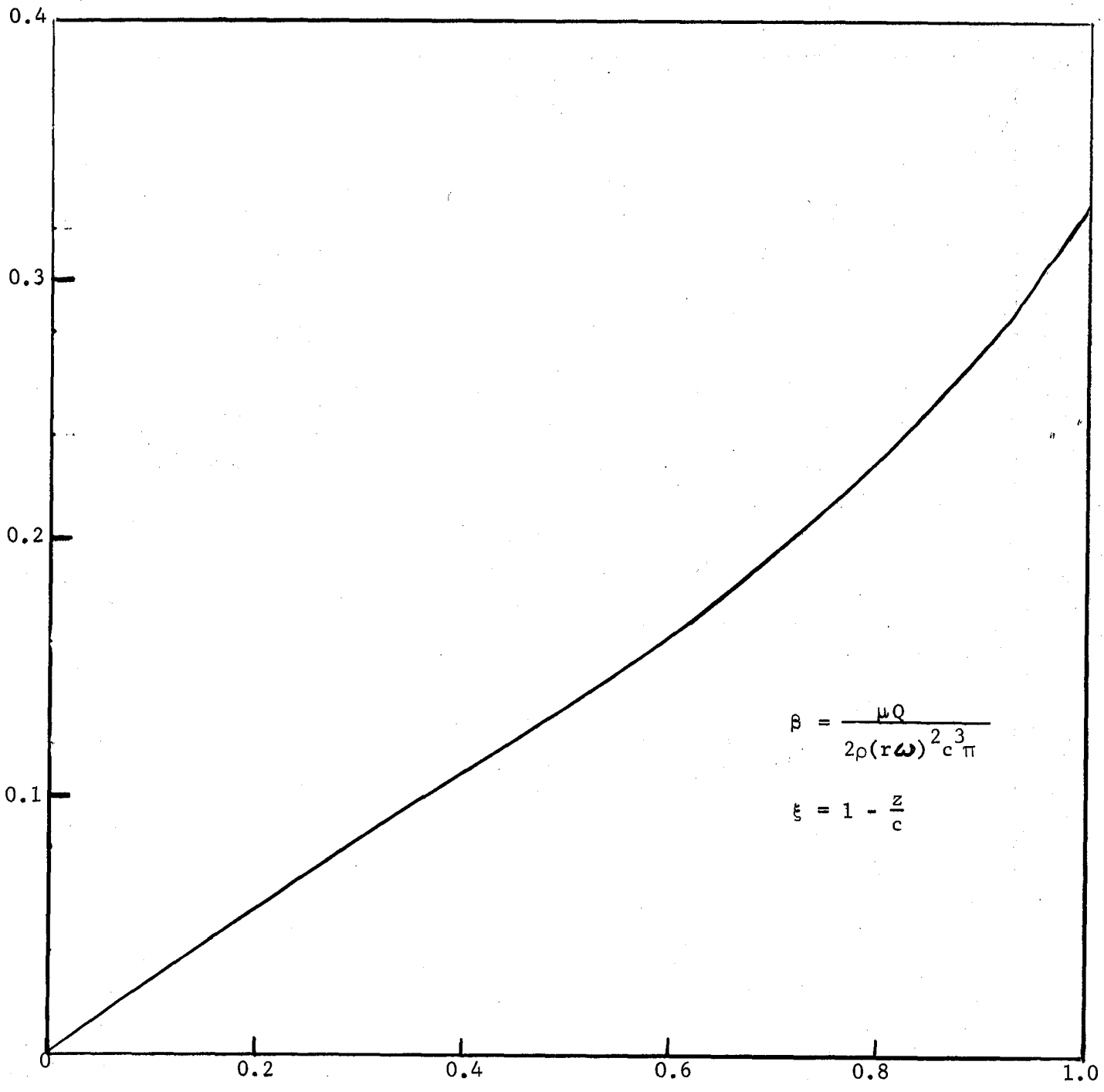

FIGURE 7

STREAM-SURFACE BRANCHING FROM ROTATING DISK ($Q < 0$)

TURBULENT

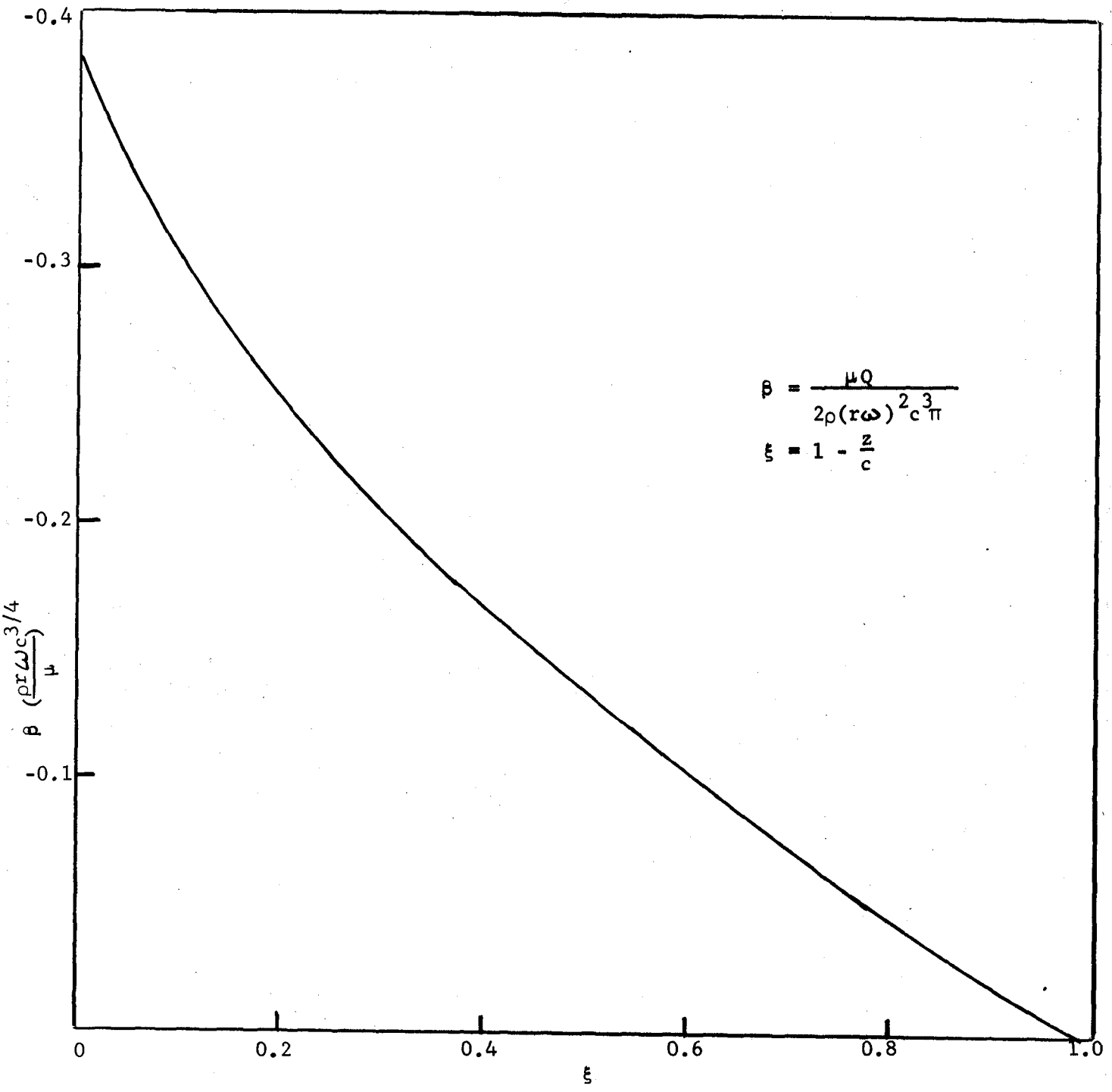

REFERENCES

1. "Study of Dynamic and Static Seals for Liquid Rocket Engines", Final Report, Vol. 2, February 14, 1967, NASA Contract No., NAS 7-434.

NOMENCLATURE

$A = \dfrac{36\,\mu Q}{\rho\,\pi c^3 (r\,\omega)^2}$

c = Axial clearance

q_t = Exchange leakage rate for Q=0

Q = Net leakage rate

r = Radial Coordinate

R_1 = Inner Radius

R_2 = Outer radius

$Re = \dfrac{c^2\omega}{\nu}$

u = Radial velocity

U_1 = First approximation to U

W_1 = First approximation to W

z = Axial coordinate measured from non-rotating disk

$\beta = \dfrac{\mu Q}{2\rho(r\,\omega)^2 c^3 \pi}$

μ = viscosity

$\nu = \mu/\rho$

$\xi = 1 - z/c$

ξ_t = Coordinate of streamline turning point at seal radial boundary

ρ = Density

$\tau_{z\theta_w}$ = Tangential wall shear stress

ψ = Stream function

ω = Angular velocity of rotating disk

APPENDIX F

SEAL DESIGN III

BY

H.J. Sneck

ECCENTRIC FACE SEAL WITH A TANGENTIALLY VARYING FILM THICKNESS

I. INTRODUCTION

Previous investigations of the effects of geometry on the performance of face seals have considered such aberrations as misalignment waviness in the tangential direction, and film thickness variations in the radial direction (Ref.1). In each case, however, it was assumed that the seal faces themselves were centered on a common centerline. It has been suggested by Findlay (Ref.2) that the anomolous pumping effects observed in face seals might be attributed to the eccentricity of the seal faces which occurs when their centers are not on a common centerline. Preliminary analytical and experimental studies of the effects of such eccentricities indicate that the proposed pumping effect is indeed initiated with the introduction of an eccentricity (Ref.3). In the analysis to follow the effects of tangential fluid film thickness variations and eccentricity will be investigated in order to determine how, and to what degree, they influence face seal performance.

II. ALIGNED FLAT SEAL WITH ECCENTRICITY

Before launching into the analysis of the seal with a tangentially varying fluid film thickness it should be demonstrated that the geometric effect of eccentricity alone cannot cause a face seal to perform in any unusual way.

Figure 1 shows the geometry of the problem. The velocity of a point in the lower surface relative to the origin is given approximately by the formula

$$\bar{V}_{\Omega} \cong \Omega \left\langle \left[\epsilon \, \mathrm{Sin}(\Phi - \theta) \right] \bar{e}_r + r\bar{e}_\theta \right\rangle \tag{1}$$

The tangential velocity of the fluid in the clearance space (Ref.1) is given by

$$v = r\,\Omega \left(\frac{z}{c}\right) \tag{2}$$

The equation of motion governing the fluid flow within the clearance space has been shown to be (Ref.1)

$$\frac{\partial p}{\partial r} = \rho \frac{v^2}{r} + \mu \frac{\partial u^2}{\partial z^2} \tag{3}$$

Integrating equation (3) with the aid of equation (2) yields for the radial velocity distribution

$$u = \frac{\partial p}{\partial r}\left(\frac{z^2}{2\mu}\right) - \rho\left(\frac{r\Omega^2}{c^2}\right)\frac{z^4}{12} + f(r,\theta)z + g(r,\theta) \tag{4}$$

Because of the seal eccentricity, the radial velocity must satisfy the boundary conditions

$$\begin{aligned} u &= \epsilon\Omega \,\mathrm{Sin}(\Phi - \theta) \quad , \; z = c \\ u &= 0 \qquad\qquad\qquad\quad , \; z = 0 \end{aligned} \tag{5}$$

This results in a radial velocity distribution of the form

$$u = \left(\frac{z^2 - cz}{2\mu}\right)\frac{\partial p}{\partial r} - \rho\left(\frac{r\Omega^2}{c^2}\right)\left(\frac{z^4 - c^3 z}{12\,\mu}\right) + \epsilon\Omega\left(\frac{z}{c}\right)\mathrm{Sin}(\Phi - \theta) \tag{6}$$

The integral form of the continuity for this case is

$$\int_0^c \frac{1}{r}\frac{\partial}{\partial r}(ur)\,dz = 0 \tag{7}$$

This results in a differential equation for the pressure distribution

$$\frac{\partial}{\partial r}\left(\frac{rc^3}{12\mu}\frac{\partial p}{\partial r}\right) = \frac{3}{5}\left(\frac{\rho\Omega^2 c^3 r}{12\,\mu}\right) + \frac{\epsilon\Omega c\,\mathrm{Sin}\,(\Phi - \theta)}{2} \tag{8}$$

The net leakage rate is computed from equation (6) using the formula

$$Q = r\int_0^{2\pi}\left[\int_0^c u\,dz\right]\,d\theta \tag{9}$$

The separating force is obtained from the integration of equation (8) for p which is then inserted in

$$F = \int_0^{2\pi}\int_{R_1}^{R_2} p\; r\,dr\,d\theta \tag{10}$$

Since the determination of Q and F both require θ integrations from 0 to 2π, it is obvious that the calculated flow-rate and separating force will be the same as the concentric seal due to the periodicity of Sin $(\Phi - \theta)$. The mathematical reason for this is the assumption of a uniform clearance c as will be demonstrated in the analysis to follow.

III. ALIGNED WAVY SEAL WITH ECCENTRICTY - LAMINAR FLOW

A. Velocity Distribution

If the upper surface is allowed to be wavy, as shown in Figure 2, while the lower surface is eccentric and rotates, the tangential velocity distribution can be represented by

$$v = r\Omega \left(1 - \frac{z}{h}\right) \tag{11}$$

where h is a function of θ only. When this equation is combined with equation (3) and the result when integrated is

$$u = \frac{z^2}{2\mu} \frac{\partial p}{\partial r} - \frac{\rho r \Omega^2}{\mu} \left[\frac{z^2}{2} - \frac{z^3}{3h} + \frac{1}{12} \frac{z^4}{h^2}\right] + F(r,\theta)\, z + G(r,\theta) \tag{12}$$

The boundary conditions to be applied to this equation are

$$\begin{aligned} u &= \Omega \epsilon \operatorname{Sin} (\Phi - \theta) \quad , z = 0 \\ u &= 0 \qquad\qquad\qquad\quad , z = h \end{aligned} \tag{13}$$

so that the radial velocity distribution finally takes the form

$$u = \frac{1}{2\mu} (z^2 - hz) \frac{\partial p}{\partial r} - \frac{\rho r \Omega^2}{\mu} \left[-\frac{zh}{4} + \frac{z^2}{2} - \frac{z^3}{3h} + \frac{1}{12} \frac{z^4}{h^2}\right] + \Omega \epsilon \operatorname{Sin} (\Phi - \theta) \left[1 - \frac{z}{h}\right] \tag{14}$$

B. Pressure Distribution

The integrated form of the continuity equation for this case is

$$\int_0^h \frac{1}{r} \frac{\partial}{\partial r} (ur)\, dz + \int_0^h \frac{1}{r} \frac{\partial v}{\partial \theta}\, dz + \int_0^h \frac{\partial w}{\partial z}\, dz = 0 \tag{15}$$

Using the boundary conditions that w (0) = w(h) = 0, this equation reduces to

$$\frac{\partial}{\partial r} \left[r \int_0^h u dz\right] + \int_0^h \frac{\partial V}{\partial \theta}\, dz = 0 \tag{16}$$

The second term in equation (16) can be simplified as follows

$$\frac{\partial}{\partial \theta} \int_0^h v dz = \int_0^h \frac{\partial v}{\partial \theta}\, dz + v(h) \frac{\partial h}{\partial \theta} \tag{17}$$

with the aid of Leibnitz Rule. Since v(h) = 0

$$\int_0^h \frac{\partial v}{\partial \theta}\, dz = \frac{\partial}{\partial \theta} \int_0^h v dz \tag{18}$$

This simplification, along with the velocity distributions given by equations (11) and (12), result in a partial differential equation for the pressure distribution

$$\frac{\partial}{\partial r}\left(\frac{rh^3}{12\mu}\frac{\partial p}{\partial r}\right) = \frac{3}{5}\left(\frac{\rho\Omega^2 h^3 r}{12\mu}\right) + \frac{\varepsilon\Omega h \sin(\Phi - \theta)}{2} + \frac{r\Omega}{2}\frac{\partial h}{\partial \theta} \tag{19}$$

This equation, of course, reduces to equation (8) when h = c and also consistent with the earlier analysis of Reference 1 when $\varepsilon = 0$. Recalling that h is a function of θ only, equation (19) may be easily integrated to yield

$$p = \frac{3}{20}\rho r^2\Omega^2 + \left(\frac{6\mu\Omega\varepsilon r}{h^2}\right)\sin(\Phi - \theta) + \left(\frac{3\mu r^2\Omega}{2h^3}\right)\frac{\partial h}{\partial \theta} - \frac{12\mu f(\theta)}{h^3}\ell nr + g(\theta) \tag{20}$$

The arbitrary functions of integration are determined using the pressure boundary conditions

$$\begin{aligned} p &= P_1 \ , \ r = R_1 \\ p &= P_2 \ , \ r = R_2 \end{aligned} \tag{21}$$

The pressure distribution satisfying these conditions is given by

$$\begin{aligned} p - P_2 = {} & \frac{3}{20}\rho\Omega^2(r^2 - R_2^2) + \left(\frac{6\mu\Omega\varepsilon}{h^2}\right)\sin(\Phi - \theta)(r - R_2) \\ & + \left\{\frac{3\mu\Omega}{2h^3}(r^2 - R_2^2)\frac{\partial h}{\partial \theta} + \frac{\ell n\frac{r}{R_2}}{\ell n\frac{R_1}{R_2}}\right\}(P_1 - P_2) \\ & - \left\{\frac{3}{20}\rho\Omega^2(R_1^2 - R_2^2) - \frac{3\mu\Omega}{2h^3}(R_1^2 - R_2^2)\frac{\partial h}{\partial \theta}\right. \\ & \left. - \left(\frac{6\mu\Omega\varepsilon}{h^2}\right)\sin(\Phi - \theta)(R_1 - R_2)\right\} \end{aligned} \tag{22}$$

C. Leakage Flow

The net leakage-rate is computed from the equation

$$Q = \int_0^{2\pi}\int_0^h u\,dz\,r\,d\theta \tag{23}$$

Performing the first integration with the aid of equation (14) gives

$$Q = \int_0^{2\pi}\left[-\frac{r\Omega}{4}\frac{\partial h}{\partial \theta} + \frac{f(\theta)}{r}\right] r\,d\theta$$

$$= \int_0^{2\pi} f(\theta)\, d\theta$$

$$= \frac{1}{12\mu \ell n \frac{R_2}{R_1}} \int_0^{2\pi} \left\{ \left[P_1 - P_2 + \frac{3}{20} \rho\Omega^2 (R_2^2 - R_1^2) \right] h^3 \right.$$

$$\left. + 6\mu\, \Omega\, \epsilon h \sin(\Phi - \theta)(R_2 - R_1) \right\} d\theta \qquad (24)$$

If it is now assumed that the surface waviness is approximated by the film thickness equation

$$h = c\,(1 + a \cos k\theta) \qquad (25)$$

the formula for the leakage rate is

$$Q = \frac{\pi}{6\mu \ell n \frac{R_2}{R_1}} \left\{ c^3 \left[P_1 - P_2 + \frac{3}{20} \rho\Omega^2 (R_2^2 - R_1^2) \right] \left(1 + \frac{3}{2} a^2\right) \right.$$

$$\left. \pm \frac{6\mu\, \Omega\, \epsilon c a (R_2 - R_1) \sin \Phi}{2\pi} \int_0^{2\pi} \cos k\theta \cos\theta\, d\theta \right\} \qquad (26)$$

The total leakage rate consists of two parts, one due to the waviness alone and one due to eccentricity and waviness together. The waviness contribution is same as found earlier (Ref. 1). The eccentricity contribution is seen to exist only if there is a "once-per-rev" (k=1) distortion of the type observed by Nau(Ref. 4). Then equation (26) becomes

$\underline{k = 1}$

$$Q = \frac{\pi}{6\mu \ell n \frac{R_2}{R_1}} \left\{ c^3 \left[P_1 - P_2 + \frac{3}{20} \rho\Omega^2 (R_2^2 - R_1^2) \right] \left(1 + \frac{3}{2} a^2\right) \right.$$

$$\left. + 3\mu\, \Omega\, \epsilon (R_2 - R_1)\, ca \sin \Phi \right\} \qquad (27)$$

Whether the eccentricity cases inward or outward pumping depends on

i) the direction seal rotation

ii) the phase angle of the waviness relative to the line of centers, Φ.

Since it is quite difficult to determine the phase angle Φ, it is not surprising to find reports of both inward pumping effects and outward pumping effects exhibited by the same seal. A very logical explanation is a shift in Φ between disassembly

and reassembly, or a change in rotational direction.

D. Torque

Since the tangential velocity distribution is the same as the one used earlier (Ref. 1) the torque is uneffected by eccentricity, being given by the formula

$$T = \frac{\pi\mu\Omega}{2c}(R_2^4 - R_1^4)\left(1 + \frac{a^2}{2}\right) \tag{28}$$

neglecting terms of order a^4.

E. Separating Force

The separating force is computed from equation (10) using the pressure distirbution given by equation (22). It will be noted that integration with respect to θ will eliminate terms containing $\frac{1}{h^3}\frac{\partial h}{\partial \theta}$ if the film thickness is described by equation (25). The remaining terms fall into two catagories, those which contain ϵ and those which do not. The terms which do not contain ϵ do not contain h either, so their contribution to the separating force is the same as a concentric, aligned, flat-surface seal.

The eccentricity effects the separting force through the terms containing $\frac{\mathrm{Sin}(\Phi - \theta)}{h^2}$. This expression can be expanded using equation (25) as follows

$$\frac{\mathrm{Sin}(\Phi - \theta)}{h^2} = \left(\frac{\mathrm{Sin}\,\Phi\,\mathrm{Cos}\,\theta - \mathrm{Sin}\,\theta\,\mathrm{Cos}\varphi}{c^2}\right) \cdot$$

$$(1 - 2a\,\mathrm{Cos}\,k\theta + 3a^2\,\mathrm{Cos}^2\,k\theta + \cdots\cdot) \tag{29}$$

If $k = 1$

$$\int_0^{2\pi} \frac{\mathrm{Sin}(\Phi - \theta)}{h^2}\,d\theta \cong \frac{-2a\,\mathrm{Sin}\,\Phi}{c^2}\int_0^{2\pi} \mathrm{Cos}^2\,\theta\,d\theta = \frac{-2a\pi\,\mathrm{Sin}\,\theta}{c^2} \tag{30}$$

The total separating force using this approximation for $k = 1$ is

$$F \cong \pi P_1(R_2^2 - R_1^2) + \frac{\pi}{2}\left(\frac{3\rho\Omega^2}{20}\right)(R_2^2 - R_1^2)^2 +$$

$$2\pi\left[\frac{P_2 - P_1 - \left(\frac{3\rho\Omega^2}{20}\right)(R_2^2 - R_1^2)}{\ell n\, R_2/R_1}\right]\left[\frac{R_2^2\,\ell n\, R_2/R_1}{2} - \left(\frac{R_2^2 - R_1^2}{4}\right)\right]$$

$$+\left(\frac{12\mu a\Omega\pi\epsilon R_2^3\,\mathrm{Sin}\,\theta}{c^2}\right)\left\{\frac{1}{2}\left[1 - \left(\frac{R_1}{R_2}\right)^2\right]\right.$$

$$- \frac{1}{3}\left[1 - \left(\frac{R_1}{R_2}\right)^3\right] + \left[\frac{1 - R_1/R_2}{\ell n\ R_2/R_1}\right]\left[\frac{1}{2}\left(\frac{R_1}{R_2}\right)^2 \ell n\ \left(\frac{R_2}{R_1}\right) - \frac{1 - (R_1/R_2)^2}{4}\right]\Bigg\}, \quad \underline{k = 1} \tag{31}$$

The geometric factor contained in the last term is shown in Figure 3.

F. Numerical Example

Equation (27) for the net leakage is comparable to that reported earlier (Ref 2) with the exception that the inertia contribution is included here. Using the same data as assumed in Ref. 2 for a sample calculation, we have

$R_1 = 1.125"$

$R_2 = 1.75"$

$\mu = 4.95(10^{-5})$ psi/sec

$c = 10^{-3}$ inches

$a = 1.0'$

$\epsilon = 0.003"$

$\Omega = (10^3)\ \frac{2\pi}{60}$

$\Phi = 90^\circ$

The contribution to the total leakage rate due to the eccentricity alone is given by

$$Q_\epsilon = \frac{\pi}{2}\left[\frac{\Omega\ \epsilon\ ca\ (R_2 - R_1)\ \text{Sin}\ \Phi}{\ell n(R_2/R_1)}\right]$$

$$= \frac{\pi(10^3)\ \frac{2\pi}{60}\ (0.003)(10^{-3})(1.75 - 1.125)}{2\ \ell n\ \left(\frac{1.75}{1.125}\right)}$$

$$= 5.86\ (10^{-4})\ \text{in}^3/\text{sec.}$$

$$= 5.86\ (10^{-4})\ (3600)(24)$$

$$= 50.6\ \text{in}^3/\text{day}$$

The load carrying capacity contribution due to eccentricity done is given by

$$\frac{12\ \mu a\ \Omega\ \epsilon\ R_2^3 \text{Sin}\ \Phi}{c^2}\left\{\frac{1}{2}\left[1 - \left(\frac{R_1}{R_2}\right)^2\right] - \frac{1}{3}\left[1 - \left(\frac{R_1}{R_2}\right)^3\right]\right.$$

$$+\left[\frac{1 - R_1/R_2}{\ell n\ R_2/R_1}\right]\left[\frac{1}{2}\left(\frac{R_1}{R_2}\right)^2 \ell n\left(\frac{R_2}{R_1}\right) - \frac{1 - (R_1/R_2)^2}{4}\right]\Bigg\}$$

$$= \frac{12(4.95)(10^{-5})\ 10^3\ (\frac{2\pi}{60})\ (0.003)(1.75)^3}{10^{-6}} \left\{ 0.00382 \right\}$$

$$= 3.82\ lb_f$$

IV. ALIGNED WAVY SEAL WITH ECCENTRICITY - TURBULENT FLOW

A. Velocity Distribution

For turbulent flow the tangential velocity profile will be taken to be the 1/7 power law measured from the surfaces. Using the velocity matching condition that the mid-channel velocity is one-half the rotating surface velocity, the tangential velocity profile is then given by

$$v_1 = r\ \Omega \left[1 - \frac{1}{2}\left(\frac{z}{h/2}\right)^{1/7}\right],\ 0 \le z \le h/2 \qquad (32)$$

$$v_2 = \frac{r\Omega}{2}\left(\frac{h-z}{h/2}\right)^{1/7},\quad h/2 \le z \le h \qquad (33)$$

It will be recalled that these profiles are consistent with the concept that the tangential shear stress is constant across the clearance space assuming that the shear flow follows the "law of the wall", Ref. 1. It is easily verified that equations (32) and (33) also have the same slope at mid-channel with the result that the velocity profile is "smooth" all across the clearance space.

The radial velocity profile can now be computed from the equation of motion

$$u\,\tau_{z\theta_w} = v\left[f(r,\theta) + \frac{\partial p}{\partial r}\,z - \frac{\rho}{r}\int v^2 dz\right]$$

$$+ \int \frac{\rho}{r} v^3 dz - \int v\,\frac{\partial p}{\partial r}\,dz + g(r,\theta) \qquad (34)$$

which was derived in Ref. 1 with the aid of the concept of isotropic viscosity.

This radial velocity profile must satisfy the boundary conditions given in equation (13). Evaluating the arbitrary functions $f(r,\theta)$ and $g(r,\theta)$ yields

$$u\tau_{z\theta_w} = \left[\frac{v\ \epsilon\ \tau_{\theta z_w}}{r}\right] \mathrm{Sin}\ (\Phi - \theta) +$$

$$\frac{\rho}{r}\left[\frac{v}{r\Omega}\int_o^h v^3dz - v\int_o^z v^2dz + \int_o^z v^3dz - \int_o^h v^3dz\right] + \left[vz - \frac{v}{r\Omega}\int_o^h vdz - \int_o^z vdz + \int_o^h vdz\right]\frac{\partial p}{\partial r} \tag{35}$$

When the velocities given by equations (32) and (33) are inserted into equation (35) the radial velocity distribution takes the form

$$u\,\tau_{z\theta_w} = \left(\frac{r\Omega}{2}\right)\left(\frac{h}{2}\right)\frac{\partial p}{\partial r}\,F\left(\frac{z}{h/2}\right) - \frac{\rho}{r}\left(\frac{r\Omega}{2}\right)^3\left(\frac{h}{2}\right)G\left(\frac{z}{h/2}\right) \tag{36}$$

where

$$F\left(\frac{z}{h/2}\right) = \left(\frac{z}{h/2}\right)^{1/7}\left[1 - \frac{1}{8}\left(\frac{z}{h/2}\right)\right], \quad 0 \le z \le h/2$$

$$= \left(\frac{h-z}{h/2}\right)^{1/7}\left[\frac{3}{4} + \frac{1}{8}\left(\frac{z}{h/2}\right)\right], \quad h/2 \le z \le h \tag{37}$$

and

$$G\left(\frac{z}{h/2}\right) = \left(\frac{z}{h/2}\right)^{1/7}\left[+\frac{13}{12} + \frac{1}{2}\left(\frac{z}{h/2}\right)^{8/7} + \frac{7}{18}\left(\frac{z}{h/2}\right)^{9/7} - \frac{7}{90}\left(\frac{z}{h/2}\right)^{10/7}\right], \quad 0 \le z \le h/2$$

$$= \left(\frac{z}{h/2}\right)^{1/7}\left[\frac{35}{36} - \frac{7}{90}\left(\frac{h-z}{h/2}\right)^{9/7}\right], \quad h/2 \le z \le h \tag{38}$$

With the exception of a sign change due to a change in direction of rotation, equation (36) is identical to one reported earlier for turbulent flow (Ref. 1). It should also be noted that z is measured from the rotating surface in this analysis, whereas it was previously measured from the stationary surface.

B. Pressure Distribution

The radial pressure gradient is determined from the continuity equation (16) with the aid of equations (32), (33), (36), (37) and (38). The result is

$$\frac{\partial p}{\partial r} = \frac{835}{816}\ \rho\ (\frac{\Omega}{z})^2\ r + \frac{f(\theta)}{r^{1/4}} - 0.0225\ \frac{\rho}{2}\ (\nu)^{1/4}\ (\frac{30}{49})\ \left[\frac{|\frac{r\Omega}{2}|^{3/4}\ (\frac{r\Omega}{2})}{(h/2)^{9/4}}\right]\ \frac{\partial h}{\partial \theta}$$

$$- 0.0225\rho\ (\nu)^{1/4}\ \epsilon\Omega\ (\frac{30}{49})\ \left[\frac{|\frac{r\Omega}{2}|^{3/4}}{h/2^{5/4}}\right]\ \text{Sin}\ (\Phi - \theta) \qquad (39)$$

Integrating this equation with respect to r yields the general solution

$$p = \frac{835}{816}\ \frac{\rho}{z}\ (\frac{\Omega r}{2})^2 - 0.0225\ (\frac{30}{49})(\frac{4}{11})\ \frac{\rho}{2}\ (\nu)^{1/4}\ \cdot$$

$$r^{11/4}\ \left[\frac{|\frac{\Omega}{2}|^{3/4}\ (\frac{\Omega}{2})}{(h/2)^{9/4}}\right]\ \frac{\partial h}{\partial \theta} - 0.0225\rho\ (\nu)^{1/4}\ \epsilon\Omega\ \text{Sin}\ (\Phi - \theta)\ \cdot$$

$$\frac{4}{7}\ (\frac{30}{49})\ \left[\frac{|\frac{\Omega}{2}|^{3/4}}{(h/2)^{5/4}}\right]\ r^{7/4} + \frac{4}{3}\ f\ (\theta)\ r^{3/4} + g\ (\theta) \qquad (40)$$

The arbitrary functions f(θ) and may now be evaluated using the pressure boundary conditions

$$p = P_1\ @\ r = R_1 \qquad (41)$$

$$p = P_2\ @\ r = R_2$$

The pressure distribution which results is given by the formula

$$p - P_2 = \frac{835}{816}(\frac{\rho}{2})(\frac{\Omega}{2})^2(r^2 - R_2^2)$$

$$+ 0.0225\ (\frac{30}{49})\ (\frac{4}{11})\ \frac{\rho\nu}{2}^{1/4}\ \left[\frac{|\frac{\Omega}{2}|^{3/4}\ (\frac{\Omega}{2})}{(h/2)^{9/4}}\right]\ (r^{11/4} - R_2^{11/4})\ \frac{\partial h}{\partial \theta}$$

$$+ \left[\frac{r^{3/4}R_2^{3/4}}{R_1^{3/4}R_2^{3/4}}\right]\ \left\{ P_1 - P_2 + \frac{835}{816}\ \frac{\rho}{2}\ (\frac{\Omega}{2})^2 (R_2^2 - R_1^2)\right.$$

$$\left. - 0.0225\ (\frac{30}{49})\ (\frac{4}{11})\ \frac{\rho}{2}\ (\nu)^{1/4}\ \left[\frac{|\frac{\Omega}{2}|^{3/4}\ (\frac{\Omega}{2})}{(h/2)^{9/4}}\right]\ (R_1^{11/4} - R_2^{11/4})\ \frac{\partial h}{\partial \theta}\right\}$$

$$+ 0.0225\ \rho\ (\nu)^{1/4}(\frac{4}{7})(\frac{30}{49})\ \epsilon\Omega\ \text{Sin}\ (\Phi - \theta)\ \left[\frac{|\frac{\Omega}{2}|^{3/4}}{(h/2)^{5/4}}\right]\ (r^{7/4} - R_2^{7/4})$$

$$-\left[\frac{r^{3/4} - R_2^{3/4}}{R_1^{3/4} - R_2^{3/4}}\right] \left[0.0225\ \rho\ (\nu)^{1/4}\ (\tfrac{4}{7})(\tfrac{30}{49})\ \epsilon\Omega\ \mathrm{Sin}\ (\Phi - \theta)\right.$$

$$\left.\left(\frac{\left|\frac{\Omega}{2}\right|^{3/4}}{(h/2)^{5/4}}\right)\ (R_1^{7/4} - R_2^{7/4})\right] \qquad (42)$$

When $\epsilon = 0$ this equation reduces to the earlier result given in Ref. 1 with the sign of the angular velocity reversed.

C. Leakage Flow

The net leakage-rate is calculated from equation (23) using for the velocity profile the formulations given by equation (36) and (39). The resulting leakage rate is given approximately by

$$Q \cong \frac{P_1 - P_2 + \frac{835}{816}\ (\frac{\rho}{2})\left(\frac{R_2\Omega}{2}\right)^2 \left[1 - (\frac{R_1}{R_2})^2\right]\left[1 + \frac{45}{64}\ a^2\right]}{\frac{0.0195}{\pi}\ \left|\frac{\rho^3\mu\Omega^3}{c^9}\right|^{1/4}\ (\frac{4}{3})\ (R_2^{3/4} - R_1^{3/4})}$$

$$+\ \frac{3}{7}\ (\frac{\epsilon\Omega}{2})\left[\frac{R_1^{7/4} - R_2^{7/4}}{R_1^{3/4} - R_2^{3/4}}\right] \int_0^{2\pi} h\ \mathrm{Sin}\ (\Phi - \theta)\ d\theta \qquad (43)$$

neglecting terms of the order a^4.

The last term in this equation is the contribution due to eccentricity. As in the laminar case the integral in this term is non-zero only when $\underline{k = 1}$. In this case

$$\int_0^{2\pi} h\ \mathrm{Sin}\ (\Phi - \theta)\ d\theta = \pi\ ca\ \mathrm{Sin}\ \Phi\ ;\quad \underline{k = 1} \qquad (44)$$

so that the total leakage rate for $\underline{k = 1}$ is

$$Q \cong \frac{P_1 - P_2 + \frac{835}{816}\ (\frac{\rho}{2})(\frac{R_2\Omega}{2})^2 \left[1 - (\frac{R_1}{R_2})^2\right]\left[1 + \frac{45}{64}\ a^2\right]}{\frac{0.0195}{\pi}\ \left|\frac{\rho^3\mu\Omega^3}{c^9}\right|^{1/4}\ (\frac{4}{3})\ (R_2^{3/4} - R_1^{3/4})}$$

$$+ \frac{3}{7}\left(\frac{\Omega}{2}\right) \epsilon R_2 \, ca\,\pi \, \text{Sin}\,\Phi \left[\frac{1-\left(\frac{R_1}{R_2}\right)^{7/4}}{1-\left(\frac{R_1}{R_2}\right)^{3/4}}\right] \tag{45}$$

Once again it should be noted that eccentricity alone is not sufficient to cause additional leakage, it must be coupled with a specific kind of surface waviness ($k = 1$). Even then the additional leakage can be outward or inward depending on the phase angle Φ or the direction of rotation.

D. Torque

The total torque exerted by the fluid on the rotating foace of the seal is given by

$$T = \int_0^{2\pi} \int_{R_1}^{R_2} \tau_{z\theta_w} r^2 \, r dr d\theta \tag{46}$$

The wall shear stress used to obtain equation (39) is the same as used in Ref. 1, namely

$$\tau_{z\theta_w} = 0.0225 \, \rho \, (\nu)^{1/4} \left(\frac{r\Omega}{2}\right) \left[\frac{\left|\frac{r\Omega}{2}\right|^{3/4}}{h/2}\right]^{1/4} \tag{47}$$

If the film thickness relation given by equation (25) is expanded binomially before integration with respect to θ, it is clear that the torque is the same as for the concentric case, i.e.,

$$T = 0.00335\pi \left[\frac{\rho^3 \mu \Omega^7 R_2^{19}}{c}\right]^{1/4} \left[1 - \left(\frac{R_1}{R_2}\right)^{19/4}\right]\left[1 + \frac{5}{64} a^2\right] \tag{48}$$

neglecting terms of the order a^4.

E. Separating Force

The last two terms in the expression for the pressure distribution present the contribution of the eccentricity. The separating force is determined by the integral

$$F = \int_0^{2\pi} \int_{R_1}^{R_2} p \, r dr d\theta$$

When this integration is carried out the separating force for the concentric case will be retrieved with the addition of a term proportional to ϵ. Since both eccentricity terms of equation (42) contain $\frac{\text{Sin}(\Phi - \theta)}{(h/2)^{5/4}}$ the integral of this factor

will be determined first. Using the film thickness relation given by equation (25)

$$\int_0^{2\pi} \frac{\sin(\Phi - \theta)\, d\theta}{(h/2)^{5/4}} = \frac{1}{(c/2)^{5/4}} \int_0^{2\pi} \left[\frac{\sin\Phi \cos\theta - \cos\Phi \sin\theta}{(1 + a \cos k\theta)^{5/4}} \right] d\theta =$$

$$\frac{1}{(c/2)^{5/4}} \int_0^{2\pi} (\sin\Phi \cos\epsilon - \sin\theta \cos\Phi)\left(1 - \frac{5}{4} a \cos k\theta + \cdots\right) d\theta$$

$$= -\frac{5}{4}\left[\frac{a\pi}{(c/2)^{5/4}}\right] \sin\Phi , \qquad \underline{k = 1} \tag{49}$$

It should again be noted that only if $k = 1.0$ is there any contribution of eccentricity to the order of a^2.

The total separating force for $\underline{k = 1}$ and small a computed from equations (10) and (42) is approximately

$$F \cong \pi P_1 (R_2^2 - R_1^2) + \frac{\pi}{2}\left(\frac{835}{816}\right)\frac{\rho}{2}\left(\frac{\Omega}{2}\right)^2 (R_2^2 - R_1^2)^2$$

$$+ 2\pi \left[\frac{P_2 - P_1 - \frac{835}{816}\left(\frac{\rho}{2}\right)\left(\frac{\Omega}{2}\right)^2 (R_2^2 - R_1^2)}{R_2^{3/4} - R_1^{3/4}}\right]\left[\frac{4}{11}\left(R_2^{11/4} - R_1^{11/4}\right)\right.$$

$$\left. - \frac{R_1^{3/4}}{2}(R_2^2 - R_1^2)\right] + 0.0225 \left(\frac{10}{7}\right)\left(\frac{30}{49}\right) \rho (\nu)^{1/4} \cdot$$

$$a\epsilon R_2^2 \pi \left|\frac{R_2\Omega}{2}\right|^{3/4} \left(\frac{R_2\Omega}{2}\right)\left[\frac{\sin\Phi}{(c/2)^{5/4}}\right] \left\{ \frac{4}{11}\left[\frac{1 - \left(\frac{R_1}{R_2}\right)^{7/4}}{1 - \left(\frac{R_1}{R_2}\right)^{3/4}}\right] \cdot \right.$$

$$\left[1 - \left(\frac{R_1}{R_2}\right)^{11/4}\right] - \frac{4}{15}\left[1 - \left(\frac{R_1}{R_2}\right)^{15/4}\right]$$

$$\left. + \left[1 - \left(\frac{1 - \left(\frac{R_1}{R_2}\right)^{7/4}}{1 - \left(\frac{R_1}{R_2}\right)^{3/4}}\right)\right]\left[\frac{1 - \left(\frac{R_1}{R_2}\right)^2}{2}\right]\right\} ; \quad \underline{k = 1} \tag{50}$$

The geometric factor contained in the last term is shown in Figure 4.

V. CONCLUSIONS

From the analysis of both laminar and turbulent flow it is clear that eccentricity contributes to both the flow-rate and separating force if the surface is wavy.

For small amplitudes of waviness relative to the nominal clearance (c) this contribution is proportional to the product of the eccentricity and waviness, which means that the eccentricity will have no effect unless the surface is also wavy. The analysis also indicates that a "once per rev" waviness ($k = -1$) is the primary contributor to the pumping effect.

An unusual feature of the pumping due to eccentricity is the effect of rotation and phase angle (Φ). Depending on the direction of rotation and the magnitude of Φ, the pumping contribution due to eccentricity can be positive or negative augmenting diminishing the leakage due to pressure difference, centrifugal forces and waviness. Since in a practical sense the phase angle and eccentricity are uncontrollable factors, one would expect to see some random variations in leakage and separating force between apparently identical seals which were actually assembled differently.

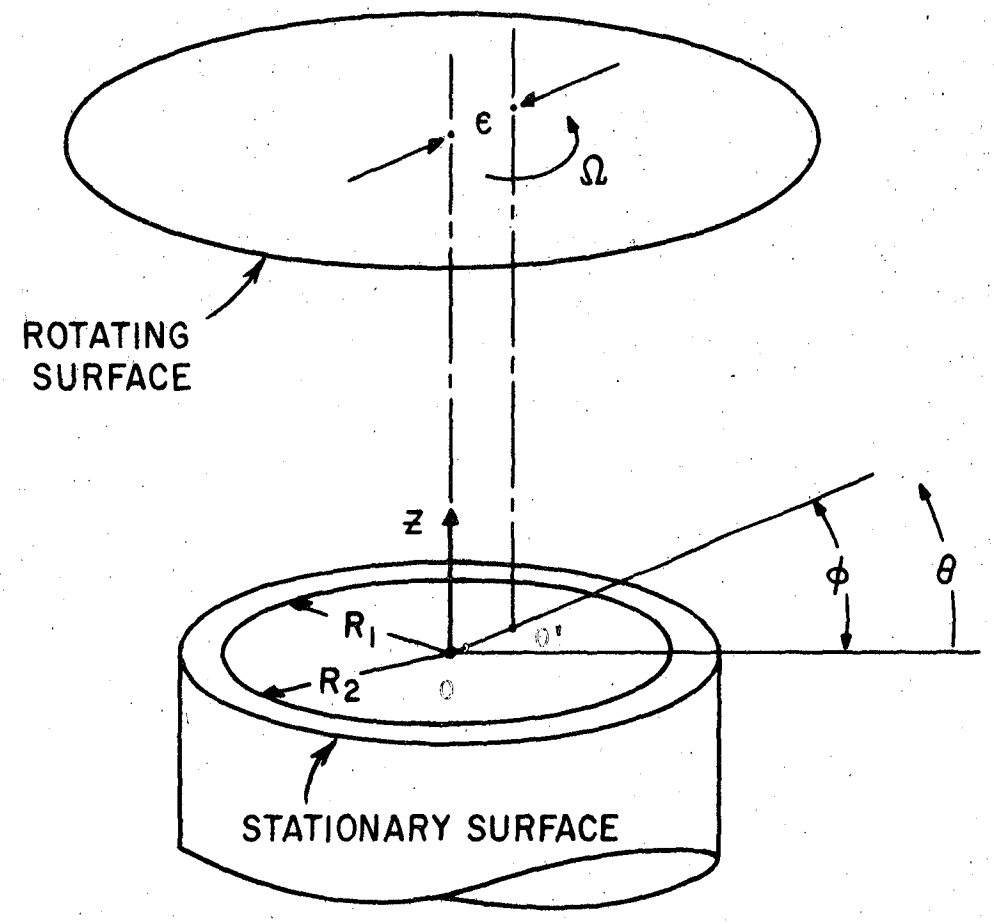

FIGURE 1

SEAL GEOMETRY FOR PARALLEL SURFACES AND
RADIAL ECCENTRICITY

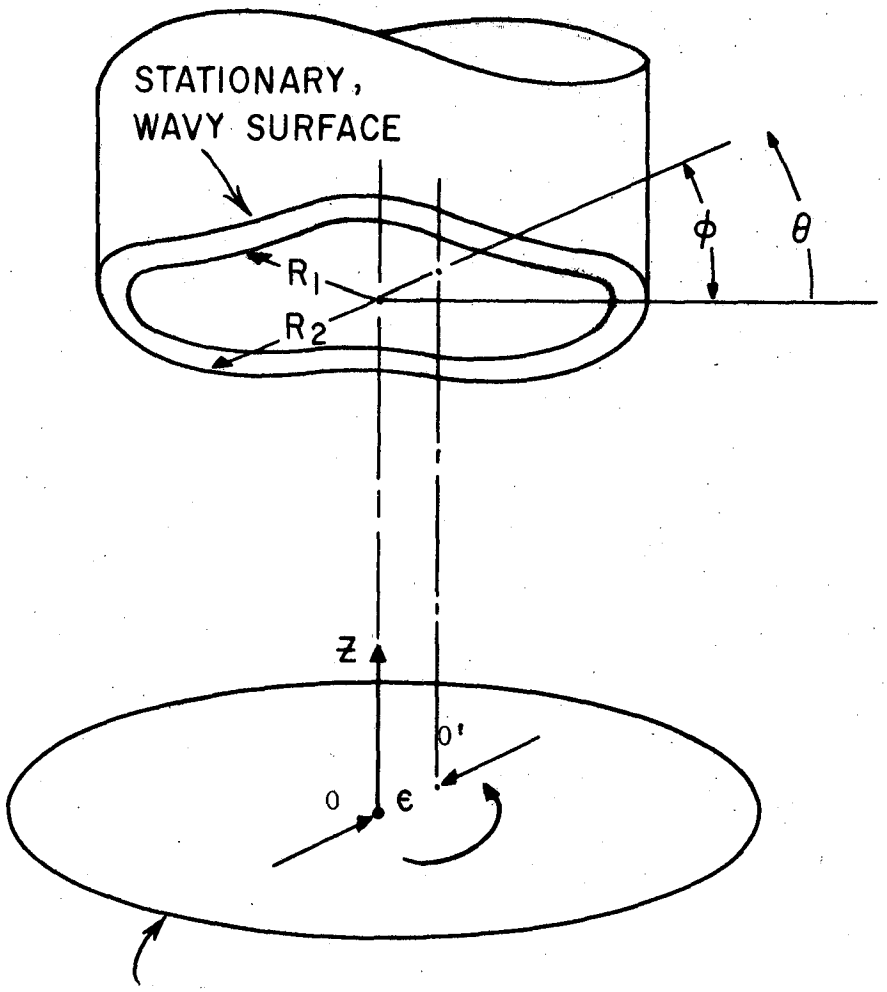

FIGURE 2

SEAL GEOMETRY FOR A WAVY SURFACE AND RADIAL ECCENTRICITY

FIGURE 3
GEOMETRY FACTOR FOR LAMINAR FLOW
EQUATION (31)

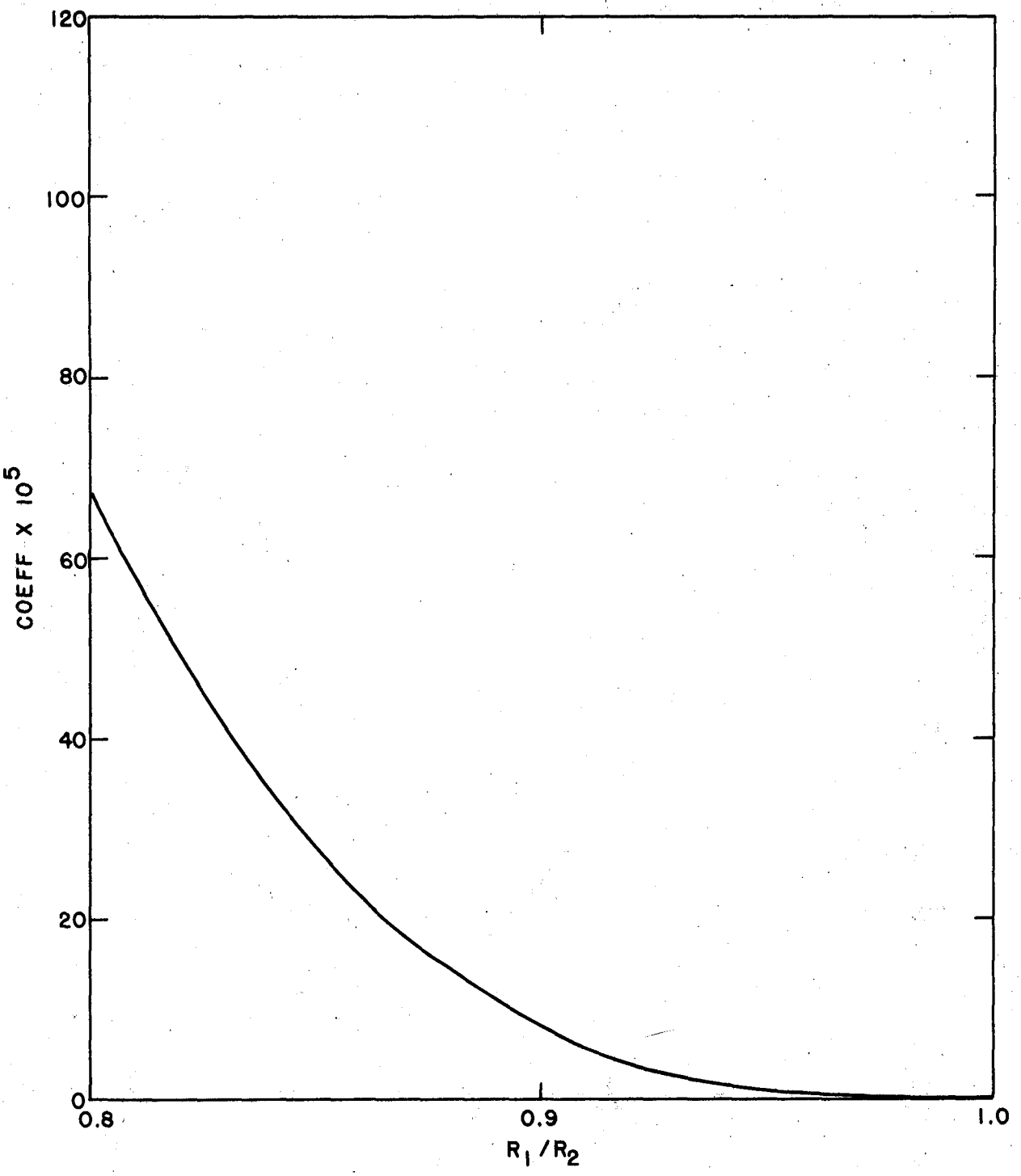

FIGURE 4
GEOMETRY FACTOR FOR TURBULENT FLOW
EQUATION (50)

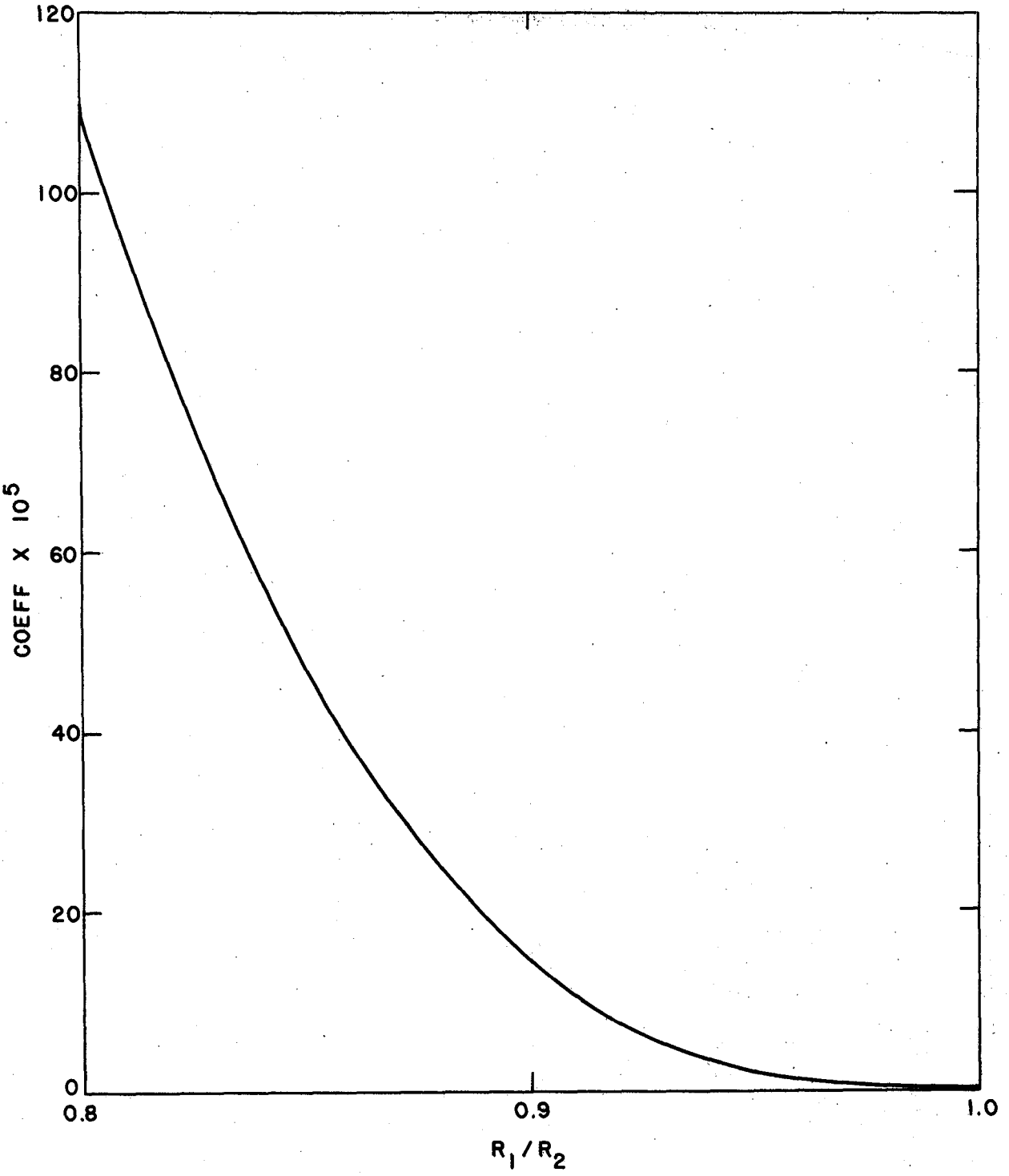

NOMENCLATURE

a	=	ratio of the waviness amplitude to the nominal clearance
c	=	nominal clearance
$\bar{e}_r, \bar{e}_\theta$	=	unit vectors
F	=	total force in clearance space tending to separate the seal surfaces
h	=	local film thickness
k	=	an integer
p	=	pressure in clearance space
P_1	=	pressure at the inner radius of the seal
P_2	=	pressure at the outer radius of the seal
Q	=	volumetric leakage - rate
r	=	radial coordinate
R_1	=	inside radius of seal
R_2	=	outside radius of seal
T	=	total torque on seal face
u	=	temporal mean radial velocity component
v	=	temporal mean tangential velocity component
$\bar{V}_\Omega$	=	seal surface velocity vector
w	=	temporal mean axial velocity component
z	=	axial coordinate
ϵ	=	seal eccentricity
θ	=	tangential coordinate
μ	=	fluid viscosity
ν	=	μ/ρ
ρ	=	fluid density
τ	=	shear stress
Φ	=	phase angle between eccentricity line of centers and waviness reference line
Ω	=	seal surface angular velocity

REFERENCES

1. H. J. Sneck, "Study of Dynamics and Static Seals for Liquid Rocket Engines" Final Report, Volume 2, Period 1 January 1966 to 14 February 1967, NASA Contract Number NAS 7-434.

2. J. A. Findlay, "Study of Dynamic and Static Seals for Liquid Rocket Engines", Quarterly Report Number 1, Period 1 April 1967 to 1 July 1967, NASA Contract Number 7-434, Phase II.

3. "Study of Dynamic and Static Seals for Liquid Rocket Engines", Quarterly Report No. 2, Period 1 July 1967 to 30 September, 1967, NASA Contract No. 7-434, Phase II.

4. B. S. Nau, "An Investigation into the Nature of the Interfacial Film, the Pressure Generation and Centripetal Pumping in Mechanical Seals", Brit. Hydromechanics Res. Assoc., Report RR 754, January 1963.

APPENDIX G

LITERATURE REVIEW

A. J. ORSINO

J. A. REILLY & H. T. ROBISON

I. INTRODUCTION

An important part of the technical work under this contract is the review of available literature on seals and sealing mechanisms. Such a review permits a continuously expanding background upon which to evaluate and appraise the new fundamental knowledge as well as the general broad technology of seals and sealing mechanisms.

The original work in this area, completed in February, 1963, produced a rather extensive bibliography of all the available data and information on seals and sealing mechanisms. Over 2200 documents were considered for abstract and entry into the bibliographies which were published as part of the final report for contract NAS 7-102. Subsequent phases of NAS 7-102 continued the review of the available literature and the results have been issued as a part of the subsequent final reports. It is expected that a separate addendum or supplement will eventually be required to formally update the original bibliographies.

A considerable portion of the material which was reviewed was of a purely theoretical nature and was essentially an engineering data gathering to obtain information for use in conjunction with the various main task efforts. This material appears referenced in the appropriate sections where it is treated more extensively rather than being listed here in abstract form as part of this literature review. The remaining references obtained are included in this appendix and are arranged alphabetically according to author; or, as in the case of NASA documents, were arranged numerically by accession number. Some minor departure from this pattern may be present but this is not considered sufficiently critical to detract from the usefulness of the material listed. Where possible the listed reference contains an abstract prepared from a reading of the text. For some references the author's prepared abstract was used. In several instances no text was available, however, the document was included since it was considered to contain information of interest in some area of seals and sealing mechanisms.

II. DESCRIPTION OF REVIEW

In the original work more than twenty-two separate sources from the English and American literature were completely reviewed. These sources are fully

identified in NASA report N63-19597, which is the bibliography on the open literature developed under the original study. The bibliography of over 700 abstracts from the Defense Documentation Center (formerly ASTIA) is contained in NASA report N63-19596.

The review conducted for contract NAS 7-434 was concerned with a further updating of the bibliographies by searching the more recent issues of the various primary sources. The references chosen, along with suitable summaries or abstracts, are contained in this Appendix as supplements to material presented in previous reports.

The following sources were reviewed, to the dates indicated, as a continuation of previous reviews conducted on this study contract and contained in NASA reports N63-19596, N63-19597, X64-16399 and X65-10582.

Source	Date
Applied Science and Technology Index	January 1968
ASM Review of Metal Literature	January 1968
Chemical Abstracts	January 1968
Engineering Index	January 1968
International Aerospace Reports	January 1968
Nuclear Science Abstracts	January 1968
Science Abstracts (A) (Physics)	January 1968
Science Abstracts (B) (Elec. Eng'g.)	January 1968
Scientific and Technical Aerospace Reports	January 1968
Technical Translations	January 1967
U.S. Government Research Reports	January 1967

III. BIBLIOGRAPHY SUPPLEMENTAL MATERIAL

The supplemental material developed in the course of updating of the bibliographies is present here. The "Supp" numbers used follow sequentially from previous reports. Additional references, primarily of a theoretical nature, are contained in the text presented as a report of the work effort for each major task.

SUPPLEMENTAL BIBLIOGRAPHY OF

OPEN LITERATURE ON SEALS*

*(See introductory text of this appendix for a full description of this supplement and other bibliographic material issued under NASA Contract NAS 7-102 and NAS 7-434, Phase I)

Supp. 200

Anonymous NSA21-67 3225

Loads to Deform Elastomer O Seals in Grooves and Between Plain Flanges
Atomic Weapons Research Establishment, Aldermaston, (England), October 1966, 27 pp. (AWRE-O-82/66)

The loads necessary to deform O seals in various types of grooves and between plain flanges have not been extensively investigated. As there is a recurrent demand for this information, a series of practical tests was carried out. The results of 210 tests are presented on a nomogram.

Supp. 201

Anspach, W. F. Eng. Ind., July 1967

Hydrofluorocarbon High Temperature Integral Fuel Tank Sealants
Rubber Chem. & Technology, Vol. 39, No. 4, Pt. 2, September 1966, pp. 1200-1214

Interim solution to critical fuel tank sealant problem in March 3 aircraft; high temperature sealant based on mixture of high and low molecular weight hydrofluorocarbon polymers has solids contents of 85% and cures at moderate temperatures; it is one-component system stable for several weeks at ambient temperatures; sealant exhibits good room temperature and high temperature. Mechanical properties both before and after aging in hydrocarbon fuel and fuel vapor at temperatures up to 500F adhesion to metal substrates is good.

Supp. 202

Appleton, B. Eng. Ind., January 1967

Design Considerations for Polyurethane Sealing Devices
Nat'l Conference on Fluid Power, Proc., Vol. 19, 1965, pp. 79-83

Designer must examine carefully what is ultimately required of seal and what fringe benefits seal material can yield to product to which it is to be fitted; chemical and chemical properties required in seal, cost of material and cost of processing must be considered. Types of seals made from polyunethane resins include: O-rings, U-cups, V-rings, flange packings, cup packings, rod wipers, scrapers, bellows, diaphragms, and special balljoint and bearing seals.

Supp. 203

Bazzarre, D. F., Spain, R. G., Withers, J. C. Eng. Ind., July 1967

Metal Clad Elastomeric Cone Seals for Liquid Rocket Propellants
Products Finishing, Vol. 31, No. 1, October 1966, pp. 66-77

Development of seals resistant to storable liquid rocket propellants was motivated by two facts, i.e., (a) that current storable propellants differ widely in composition and necessitate elastomeric vulcanizater to secure reasonable compatibility, and (b) that propellants are new fluids and existing elastomers are eliminated rather quickly as elergetics of these fluids advance; fabrication and preliminary evaluation of limited quantities of metal clad O-rings, using variety of metals in thickness of 1 to 10 mils; determination of techniques for preparing conductive surface on O-ring and application of metals by electroplating; evaluation of metal clad O-rings in N_2O_4 and in acetone at 75F.

Supp. 204

Bellanca, C. F., Salyer, J. O. Eng. Ind., July 1967

Effect of Liquid Rocket Fuels and Oxidizers on Elastomeric O-Ring Seals

Rubber Chem. and Technology V. 39, No. 4, Part 2, September 1966 pp. 1215-1221

Tests of selected elastomeric and compliant materials were made at 73F with N_2O_4, ClF_3, and 90% H_2O_2 (oxidizers) and with mixed hydrazines, pentaborane and hybaline A-5 (fuels); at 73F only polytetrafluroethylene was resistant to all fluids; butyl and ethylene propylene rubber appear satisfactory for long-term storage in presence of mixed hydrazines and hybaline A-5; fluorocarbons appear best suited for use with pentaborane and hydrogen peroxide.

Supp. 205

Billington, J. J., Toronchuk, J. P. Eng. Ind., December 1967

Characteristics of Self Energized Hydrostatic Seals for Rotating Shafts

Eng. Inst. Canada Trans. Paper EIC-66-MECH 7, May 1966, 10 pp.

Theoretical and experimental study of controlled leakage shaft seals with fixed gap maintained between rotating and stationary members is described; fixed gap is by self-energized hydrostatic actuators; effect of various geometrical parameters on seal performance was investigated theoretically; good correlation was obtained between experiment and theory when operating in low viscosity fluid (water); effects of pressure-induced seal face deformation and effects of thermal transients were studied.

Supp. 206

Billington, J. J., Fitzsimmons, T. E. NSA67-21 17432

Final Report on Shaft Seal Development

A coolant pump shaft seal development program is summarized; particular reference is made to the final endurance test series on hydrostatic self-energized, finite clearance seals. The endurance program resolved the seal geometry and materials.

Supp. 207

Bupara, S. C., Walowit, J. A., Allen, C. M. IAA67-22705 10-15 1658

Gas Lubrication and Distortion of High Pressure Mainshaft Seals for Compressors

B.H.R.A., Int. Conf. on Fluid Sealing, 3rd; Cambridge, England, April 1967, Paper B3, 24 pp., 7 ref.

Theoretical analyses and static experiments have been performed for high-pressure, gas lubricated face seals of the type used for mainshaft seals for jet-engine compressors. The analyses consider the combined effects of seal-element distortion and gas flow through the seal interface.

Supp. 208
Davies, A. R., O'Donoghue, J. P. Eng. Ind., June 1967
Lubrication of High-Pressure Face Seals
ASME-Paper 66-WA-LUB-7 for Meeting November-December 1, 1966, 8 pp., 12 Refs.

Theoretical analysis of lubrication conditions of hp face seal is presented which uses very simple treatment for estimating effects of elastic and thermal distortion. Agreement between theory and experimental results obtained for carbon seal is good; from results obtained, it is concluded that there is inherent stiffness in seal and this enables leakage to be controlled by load clamping seal faces together. Effect of speed on temperature and problems of hydrodynamic pressure generation under seal face are discussed; it seems that from order of pressure used (1000 lb. ft./sq. in.) hydrodynamic effects are not of major importance.

Supp. 209
Decker, O. Eng. Ind., September 1967
Advances in Dynamic Seal Technology
ASME-Paper 67-DE-50 for Meeting May 15-18, 1967, 16 pp.

Need for advanced seal concepts has been brought about by increasingly severe requirements imposed by applications such as supersonic transport, dynamic space power machinery, nuclear applications cryogenic machinery, and liquid-metal technology; conventional sealing techniques prove inadequate to meet challenges improved by such applications; recent trends and technological developments are solving advancement sealing problems; some dynamic seals are described in applications employing liquid metals, gas, and move standard organic fluids for both ground, aerospace and space turbomachinery.

Supp. 210
Decker, O. IAA67-28881 14 2328
Advances in Dynamic Seal Technology
ASME, Design Engineering Conf. & Show N.Y., May 1967, Paper, 67-DE-50, 17 pp., 21 Refs.

Description of recent trends and technological developments in solving advanced sealing problems. A variety of dynamic seals is described in applications employing liquid metals, gas and more standard organic fluids for ground, aerospace and space turbomachinery.

Supp. 211
Dickenson, R. W. NSA21-67-14356
Bearing and Seal Requirement for Large Liquid Metal Cooled Reactor Systems
Atomics International, Canoga Park, Calif., MTI-66TR66, pp. 8, 1, 1-6

The requirements of bearings and seals in pumps for high power output liquid-metal cooled reactors are outlined. Present and potential uses of sodium lubricated bearings are described. The need for a reliable, economical seal for mechanisms in sodium reactors is emphasized.

Supp. 212

Eibert, P. NSA21-67 8002

Nuclear Reactor Coolant Circulator with a Liquid Shaft Sealing

To Siemeas-Schuckerverke Aktiengesellschaft German Patent 1, 218, 076, June 2, 1966, Filed September 29, 1962

The sealing comprises an annular gap portion between the shaft and the housing filled with a sealing liquid, and a second gap portion filled with a sealing gas, the latter portion being located adjacent to the interior of the reactor vessel. In the middle of the annular portion which is filled with gas there is a chamber connected to a storage tank containing clean reactor coolant gas. The liquid sealed portion and the gas sealed portion are separated by another chamber connected to the interior of the housing, into which the sealing liquid and the sealing gas escape and which is provided with an exit through which the gas-liquid mixture is drawn off.

Supp. 213

Gerlach, T. Eng. Ind., January 1967

Self-Adjusting Seal with Fluid Friction

Polska Akadenia, Prace Instytutu Maszyn Prezeplywouych, No. 22, 1965, pp. 15-33

Self-adjusting seal, with constant clearance between seal elements independent of pressure and fluid viscosity, enabling frictionless transfer of dynamic loads in beariig test rigs; equation of equilibrium of sealing element is analyzed; dynamic properties of seal are examined for constant load and for periodically changing load occuring in test rig operation; sufficient conditions for attenuation of vibrations are determined. Results of experimental tests verify theoretical assumptions. In Polish.

Supp. 214

Green, J., Levine, N. B., Sheehan, W. Eng. Ind., July 1967

Elastomers Resistant to Rocket Propellants

Rubber Chem. & Technology, Vol. 39, No. 4, Pt. 2, September 1966, pp. 1222-1232

Resistance of polymers to hydrazine - type fuels, hybaline A-5, nitrogen tetroxide, and fluorine - containing oxidizers; butyl and ethylene propylene rubber are found compatible with hydrazine; carboxy-nitrose rubber is recommended for long-term exposure to N_2O_4 at 165F; fluoro-carbon plastics and silicone rubber are most suitable for use with oxygen difluoride, chloryl fluoride-tetrafluoro-hydrazine mixture; teflon, Kel-F81, and uncured nitrose rubber gum are suitable for limited applications in chlorine trifluoride.

Supp. 215
Halliger, L. Eng. Ind., June 1967
Sealing of Anti-Friction Bearings
T2 Fuer Praktische Metallbearbeitung, Vol. 60, No. 4, April 1966, pp. 207-218

Important features and properties of common shapes of protective seals are described and factors to consider in their selection indicated; development of grease-charged bearings with built-in seals for maintenance-free bearings; examples of seal combinations which proved satisfactory under plant conditions. In German.

Supp. 216
Hamaker, J. Eng. Ind., January 1967
New Materials in Mechanical Face Seals
Nat'l Conference on Fluid Power, Proc., Vol. 19, 1965, pp. 58-65

Fundamentals of seal operation, basic seal types, available and advantages and limitations inherent in seal's design and materials of construction are discussed; special emphasis is given to materials introduced in recent years; materials for secondary seals and seal rings.

Supp. 217
Hawkins, R. J. NSA21-67 8007
Improvements in or Relating to Sealing Means
To Babcock and Wilcox, Ltd., British Patent 1,045,910, October 19, 1966, Filed September 11, 1964

A method is described for making nuclear reactor seals by means of which a flow path for coolants, from the reactor core to heat exchangers, is formed. Ducts which provide for circulation of coolants are given a sealing contact by sliding blocks of graphite. The blocks are held in place, against movement caused by thermal expansion, by springs, pins, or toggle arms, but may be moved vertically or horizontally.

Supp. 218
Hazard, R. E. Eng. Ind., September 1967
Testing Seals for Aerospace
Fluid Power Int., Vol. 32, No. 373, April 1967, pp. 38-40

New sealing technique developed in view of increasingly higher temperatures and pressures required to work aerospace hydraulic equipment; design of testing machine at British Aircraft Company at Stevenage, England, for evaluating dynamic performance of seals and to control temperature and pressure of hydraulic fluid, fluid leakage part seals and piston movement; types of seals investigated were metal, plastic and combined metal and plastic.

Supp. 219

Hooke, C. T., Lenis, D. J., O'Donaghue, J. P.

Elasto Hydrodynamic Lubrication of O-Ring Seals

IME Proc., Vol. 181, Pt. 1, No. 9, 1966-1967, pp. 205-210

The paper presents a theoretical solution to the ideal problem of an O-ring seal constructed of an isotropic elastic material moving at a constant axial velocity along a cylinder. The net leakage past the seal, which is the difference between the fluid flow across the seal when it is "pumping" against the pressure and that when the seal is "monitoring" or moving with the pressure, is shown to increase with sealed pressure.

Supp. 220

Hummel, B. L. - Editor IAA67-22610 09-15 1509

Seals: Reference Issue (3rd Edition)

Machine Design, Vol. 39, March 9, 1967, 219 pp.

The Design Data section contains completely revised and updated information which clearly and concisely describes how to select and apply seals and sealants. The all-new Product Directory is set up so that the reader in search of information about manufacturers of seals and sealants can easily find exactly which company can fill his needs.

Supp. 221

Johnson, D. F. Eng. Ind., January 1967

Controlled Gap and Segmental Seals

Nat'l Conference on Fluid Power, Proc. Vol. 19, 1965, pp. 39-43

Performance materials and construction of controlled gap and segmental carbon shaft riding type seals are discussed; seals can operate to 1400F for short periods of time and to 1200F for long periods of time; they are easy to install over shaft and have capability to handle axial tolerance or shaft movements.

Supp. 222

Kinsbury, J. E. IAA67-15788 04-18 0642

New and Proposed Cryogenic Temperature Resistant Plastics

Society of Automotive Engineers, Aeronautics and Space Engineering and Manufacturing Meeting, Los Angeles, Calif., Oct. 3-7, 1966, Paper 660638, 5 pp.

Discussion of the need for cryogenic-temperature-resistant plastic material in the space program; the selection of a plastic material for cryogenic application in dependent on the cryogenic fluid with which it will come in contact. Problem areas discussed are insulation of cryogenic materials, adhesives used on plastics, use of seals and gaskets and the expulsion of cryogenic propellant in a zero gravity environment. It is believed that although the research being done in this field at present appears to have limited applications in the aerospace industry, it may be of great significance for the future.

Supp. 223
Koehler, H. Eng. Ind., January 1967
Apparatus for Sealing in Plastic Forming Machines
U. S. Patent 3,238,566, March 8, 1966

Seal for sealing space between two members having sheet of plastic material interposed there between when one of the members is moved into engagement with sheet; continuous, seal receiving groove around outer edge of one of members and yieldable sealing member mounted in groove, sealing member being formed upwardly angled flat surface with projects above upper edge of said groove, and centrally disposed, continuous passage provided in one side wall of seal member.

Supp. 224
Lawrie, J. M., Summersgill, J. Eng. Ind., March 1967
Design Specifications for Hydraulic Seals
Fluid Power Int., Vol. 31, No. 368, November 1966, pp. 330-334

Information required for seal design specifications; categories considered include applications, fluid to be sealed, temperature, pressure, relevant dimensions, additional technical information, special, life, function limitations, permissible leakage and form of lubrication.

Supp. 225
Lindsey, M. H.
Mechanical Seals: Carbons Key Role
Chemical Engineering, Vol. 74, No. 5, February 27, 1967, p..160

Carbon's unique qualities have made carbon sealing ring an indispensable part of the mechanical seal. Now, a denser, more impervious carbon is widening mechanical seal applications, and a new type of components is reducing costs. Carbon - because it is self-lubricating, resists chemical attack excellently, withstands large and rapid temperature change, and can be machined readily by conventional methods - finds wide application in the petroleum and petrochemical industries which handle many gases and liquids that cannot provide the lubrication that is necessary between moving surfaces.

Supp. 226
McManus, S. P., Piken, S. Eng. Ind., July 1967
Elastomeric Seals for Army's Lance Missile
Rubber Chem. & Technology, Vol. 39, No. 4, Pt. 2, September 1966, pp. 1233-1246

Missile propulsion system requires dynamic and static seals which must operate under extremely severe conditions for short periods; resin-cured chlorobutyl rubber meets requirements for low and high temperature operation and retains properties on exposure to propellants; comparisons with vinylidene fluoride-hexafluoropropylene copolymer (Viton). 19 Refs.

Supp. 227

Moore, B. C., Bergquist, L. E., Clements, P. R. Eng. Ind., July 1967

Cryogenic Low-Pressure Seal

J. Vacuum Science & Technology, Vol. 4, No. 1, January-February 1967, pp. 45-46

Communication to Editor describes development of simple, reliable metallic seal aluminum or stainless steel flanges at low pressures and cryogenic temperatures; self metal wire gasket is retained in rectangular groove in aluminum spaces.

Supp. 228

Mowers, R. E. IAA67-31990 17 2864

Static and Dynamic Seals Used on Rocketdyne Engines

Soc. Auto. Eng. Aerospace Systems Conf., Calif., June 1967

The paper reviews typical sealing concepts and materials used throughout the propellent feed systems and pneumatic and hydraulic control systems of liquid propellent rocket engines. Emphasis is placed on the sealing concepts utilized to compensate for extreme conditions.

Supp. 229

Murray, F. S. NSA21-67 14345

Bearing and Seal Materials for Liquid Metal Fabrications

Mechanical Technology Inc., Latham, N.Y., MTI-66TR66, pp. 6.3.1-26

Flame and plasma-sprayed hard coatings for bearing and seal components of process-fluid lubricated bearing systems are evaluated. The effectiveness of some of these coatings in protecting the surfaces against sliding damage in inert environments has been demonstrated in a number of practical applications. All of the test results show that these coatings can be used effectively for liquid metal-lubricated systems. The coatings simplify the design and fabrication of the bearing and seal components, but have the disadvantage of lack of adequate quality control. Necessary quality control procedures for the use of coatings must be developed to ensure a reliable product.

Supp. 230

Nau, B. S. IAA67-27889 14-15 2324

Hydrodynamic Lubrication in Face Seals

B.H.R.A. Int. Conf. on Fluid Sealing, 3rd, Cambridge, England, April 1967, Paper H3, 48 pp., 54 Refs.

The literature of fundamental studies of face seals is reviewed in detail with the emphasis on the conditions in the interface region. Attention is concentrated on hydrodynamic face seals. Among the subjects covered are the effects of surface roughness; wear-rates; leakage and inward pumping; and film thickness measurements.

Supp. 231
Paxton, R. R. Eng. Ind., December 1967
Carbon and Graphite Materials for Seals, Bearings, and Brushes
Electrochem Technology, Vol. 5, No. 5-6, May-June 1967, pp. 174-82

Developments of past ten years in carbon and graphite materials for seals, bearings, and electric motor brushes are briefly reviewed; properties of wide range of currently available materials are compared, and variety of applications are described indicating type of carbon or graphite which has been found suitable for each; bibliography of recent literature is included. 242 Refs.

Supp. 232
Ruhl, F. F., Wendt, A. B., Dalenberg, P. N.
A New Approach to Face Type Sealing
Lubrication Eng. 23(6), pp. 241-244, 1967, England

The following 17 major factors affect face type seal wear: design, materials, speeds, temperatures, pressure, alignment, lubrication or lack of it, cooling, mechanical forces, chemical potential, abrasive foreign material, care in assembly, the medium being sealed, secondary mechanical factors, secondary chemical factors, possible electrical effects, and the interactions of all factors. These factors are appraised in relation to each other and in relation to the overall problem.

Supp. 233
Schnetzer, E. NSA21-67 14353
Alkali Metal Bearing and Seal Development at Space Power and Propulsion Section
General Electric Co., Cincinnati, Ohio, Space Power and Propulsion Section, MTI-66TR66, pp. 6.2.1-46, Includes Appendices A through E

Three major programs associated with the development of Rankine cycle power conversion technology for space applications were undertaken; low viscosity bearing stability investigation, development of dynamic seals, and preparations for a liquid metal bearing test, simulating the conditions of a space generator. All programs were supported by a corresponding analytical effort, presently geared towards predicting bearing-rotor response. Experimental results are expected in 1966 and 1967. Screw seals, rotating channel and slinger squeeze seals were investigated in the dynamic seal program. Interface instability was identified as one of the major problems. It was resolved for the case of the slinger squeeze seal, which was successfully tested in potassium.

Supp. 234
Shevckenka, R. P. IAA67-22537 09-28 1560
Shaft, Bearing and Seal Systems for a Small Engine
Society of Automotive Engineers, Automotive Engineering Congress, Detroit, Mich., January 9-13, 1967, Paper 670064, 10 pp.

Discussion of the key mechanical difficulties inherent in designing shaft bearing and seal systems for three high-speed turbine engines. A review is made of the bearing, shaft and seal system of a family of large turbine engines which has demonstrated its high reliability, high efficiency, and low cost per unit of power as the thermodynamic, material and structural component technology has been improved and as the design power requirement has been reduced. Three different solutions to the problems discussed are presented; two for sophisticated, efficient engines for weapon system consideration, and the third for a potential industrial, low cost, high-efficiency, moderately heavy engine.

Supp. 235
Smaley, E. M. Eng. Ind., March 1967
Sealing with Gaskets
Machine Design, Vol. 38, No. 25, October 27, 1966, pp. 171-187

Design guide presented shown best practices for creating seal in gasketed joints and insuring seals longevity; two sets of parameters are surveyed, those that create seal and those that affect life in service, e.g., flange movement; gaskets considered are cork composition, cork and rubber asbestos fiber and rubber cellulose fiber and rubber, or rubber above; flat and grooved - face types of flanges are discussed.

Supp. 236
Stair, W. K., Hale, R. H. IAA67-22706 10-15 1659
The Turbulent Visco Seal - Theory and Experiment
B.H.R.A. Int. Conf. on Fluid Sealing, 3rd, Cambridge, England, April 1967, Paper #2, 32 pp., 12 Refs.

Experimental evaluation of the laminar viscosial for a number of seal geometrics has shown that the Boon and Tal's analysis is in better agreement with experiment than any other analytical approach available. It has been observed further that the seal performance improved and became dependent upon Reynold's number as turbulent conditions were encountered.

Supp. 237
Stair, W. R. IAA67-15356 04-15 0630
Effect of Groove Geometry on Viscoseal Performance
ASME Winter Annual Meeting and Energy Systems Exposition, New York, N.Y., November 27-December 1, 1966, Paper 66-WA/FE 28, 8 pp., 19 Refs.

An experimental investigation of the effect of groove geometry on the performance of the grooved-shaft viscoseal is being conducted. Using distilled water as the sealed fluid, the concentric and eccentric performance of ten seals has been determined under laminar and turbulent conditions. An approximate method is devised to predict the empirical factors in the turbulent sealing equation. The findings reveal that the optimum seal geometry for laminar operation is not optimum for turbulent operations. The seal eccentricity has slight effect on performance, and the phenomenon of air injection may present a major problem in the application of the viscoseal.

Supp.. 238
Ward, J. R. Eng. Ind., June 1967
Piston Seal Development for Oil-Free Compressors
Naval Engrs. J., Vol. 78, No. 6, December 1966, pp. 995-1002

Report of experimental work at U. S. Navy Marine Engineering Laboratory leading to design of nonlubricated seal for air compressors intended for shipboard use, which successfully operated 1500 hrs. at discharge pressure of 4500 psi; seal consisted of sleeve made of 25% glass-filled TFE and follower made of polyimide material; long term operation occured in chromium-plated cylinder bore; in later evaluations, follower material was charged to metal impregnated carbon-graphite.

Supp. 239
Wasil, T. J., McCleary, G. P.
Sealing Corrosive Materials
Lubrication Engineering, Vol. 23, No. 6, June 1967, pp. 234-240

This paper discussed tungsten carbide, tungsten titanium carbide, and titanium carbide as applied to axial mechanical sealing materials for sealing corrosive fluids. It states that the corrosive resistance of the carbides is dependent mainly upon the compatibility of the corrosive media with the carbide binder material. The tungsten carbide grains are inert to most corrosive fluids. The general mechanism of the carbide corrosion is explained. Galvanic corrosion, concentration cell corrosion, erosion corrosion, direct chemical attack and oxidation are discussed in detail.

Supp. 240
Zuck, J., Strom, T. N., Ludwig, L. P., Johnson, R. L., IAA67-28797 14-15 2327
Convective Inertia and Gas Ingestion Effects on Flow Regimes of the Viscoseal - Theory and Experiment
ASLE, Annual Meeting, 22nd, Toronto, May 1967, Paper, 61 pp., 39 Refs.

An experimental and visual investigation of the viscoseal operating regions was conducted. Importance of convective inertia forces and changes in the functional relations between variables in the super laminar flow regime are discussed. Correlation between modified Reynolds number and sealing capacity improvement is found.

*SUPPLEMENTAL REFERENCES FROM

SCIENTIFIC AND TECHNICAL AEROSPACE REPORTS (STAR)

AND

TECHNICAL ABSTRACT BULLETINS (TAB)

*The major portion of the references included in this listing are the result of government sponsored research and development.

N67-11171 AD 638972

Air Force Systems Command, Wright-Patterson AFB, Ohio, Foreigh Tech. Div.

Operation of Cascade Contact Seals

A. M. Yevtushenko, 31 August 1966, 25 pp., Refs., (FTD-HT-66-281; 77-66-62243)

Translation of Russian research: operation of cascade contact seals.

N67-13998

Atomic Energy of Canada, Ltd., Ottawa (Ontario)

Performance Testing of Conical-Face High Pressure Rotary Shaft Seals

R. D. Watson, November 1965, 36 pp., Refs. (AECL-2551)

The performance characteristics of a special type rotary shaft seal have been determined at pressures up to 1000 lb ft/in^2 gage and speeds at 1900 rev/min. The seal is made up of two rings, with one flat face ring in contact with the very slightly cone-shaped face of the other ring. Leakage rates for the seal were studied.

N67-17506

NASA Lewis Research Center, Cleveland, Ohio

Screw-Seal Performance in Vacuum Environment

J. C. Hudelson and L. P. Ludwig, Washington, NASA, February 1967, 16 pp., Refs. (NASA-TN-D-3842)

Non-contact seals are being proposed for use in space power systems. The non-contact seals offer reliable operational lifetimes of over 10,000 hours. The leakage rate of an ether lubricant through a non-contact slinger pump and screw-seal assembly to a simulated space environment was measured.

N67-19126

Pratt and Whitney Aircraft, East Hartford, Conn.

Development of Main Shaft Seals for Advanced Air Breathing Propulsion Systems

Semiannual Report No. 2, 1 January-30 June, 1966

R. L. Thomas, A. J. Parks, and R. M. Slayton, 9 September 1966, 130 pp. (Contract NAS3-7609) (NASA-CR-82453; PWA-2879)

Detailed analytical studies of all seal configurations to be tested are continued. Approval was received for the following seal concepts: orifice compensating hydrostatic face seal and face contact seal with bellows secondary.

N67-22711

Royal Aircraft Establishment, Farnborough (England)
Temperature Limitations of Polymeric Materials. Part 6: Elastomers
G. Wood, April 1964, 40 pp., Refs. (RAE-TN-CPM-52)

Elastomers find many applications in aircraft, e.g., seals (static and dynamic), sealants, gaskets, O-rings, and different properties are significant for particular cases. This report reviews the properties of the more important commercial elastomers and sealants.

N67-23037

British Hydro Mechanics Research Association, Cranfield (England), Information Dept.
References on or Related to Screw-Type Rotary Shaft Seals
March 1966, 14 pp., Refs. (BIB-22)

A compilation of abstracts related to screw-type rotary shaft seals of interest to hydromechanics is presented. Areas covered include screw viscosity pumps, the sealing action of a viscous fluid, helical groove seals, high speed lubricating oil pumps, and screw seals in laminar and turbulent operation.

N67-25487

Pratt and Whitney Aircraft, East Hartford, Conn.
Development of Compressor End Seals, Stator Interstage Seals, and Stator Pivot Seals in Advanced Air Breathing Propulsion Systems
Semi-annual Report, 1 January-30 January 1966
R. M. Hawkins, 20 July 1966, 249 pp., Refs. (Contract NAS3-7605)
(NASA-CR-83786; PWA-2875; SAR-2)

The design of compressor end seals, stator interstage seals and stator pivot seals is discussed in detail. One-side floated shoe seals, two-side floated shoe seals, and thin strip seal designs are considered.

N67-25842

NASA Lewis Research Center, Cleveland, Ohio
Improving Performance of Face Contact Seal in Liquid Sodium (400° to 1000°F) by Incorporation of Spiral-Groove Geometry
L. P. Ludwig, T. N. Strom, G. P. Allen and R. L. Johnson, Washington, NASA, May 1967, 39 pp., Refs. (NASA-TN-D-3942)

Conventional face contact seal performance was improved by incorporation of spiral-groove geometry. In comparison with conventional face contact seals, seals with spiral grooves had negligible leakage. The wear and contact patterns indicated that the spiral-groove seal operated with separation of the sealing surfaces, which is necessary for long life.

N67-26213

Atomic Weapons Research Establishment, Aldermaston (England)
Loads to Deform Elastomer O-Seals (Toroidal Sealing Rings) in Grooves and Between Plain Flanges

The loads necessary to deform O-seals in various types of grooves and between plain flanges have not been extensively investigated. This report describes and presents the results of 210 tests in the form of a nomogram.

N67-31128

Pratt and Whitney Aircraft, East Hartford, Conn.
Development of Main-Shaft Seals for Advanced Air-Breathing Propulsion Systems
Semiannual Report, 1 July-31 December 1967, 85 pp. (Contract NAS3-7609) (NASA-CR-85908; PWA-2996; SAR-3)

Four main-shaft seals for advanced gas turbine applications have been designed. The seals studied are an orifice-compensated hydrostatic face seal, an extremely pressurized hydrostatic face seal, a carbon-face-contact seal with a bellows secondary seal, and a carbon-face-contact seal with a piston-ring secondary seal.

N67-31151

Pratt and Whitney Aircraft, East Hartford, Conn.
Development of Compressor End Seals, Stator Interstage Seals, and Stator Pivot Seals in Advanced Air Breathing Propulsion Systems
Semiannual Report, 1 July-31 December 1966
R. M. Hawkins and A. H. McKibbin, 20 January 1967, 94 pp., Refs.
(Contract NAS3-7605) (NASA-CR-85891; PWA-2995; SAR-3)

The basic design concept for the "OC" diaphragm thin strip seal is discussed. The final design of the one-side floated shoe seal is discussed in some detail. The final designs of the vane pivot seals and test rig are also discussed.

N67-31390

Tennessee Univ., Knoxville, Dept. of Mechanics and Aerospace Engineering
Theoretical and Experimental Studies of Visco Type and Buffered Shaft Seals
Semiannual Progress Report, 15 October 1966-15 April 1967
William K. Stair and C. F. Fisher, Jr., May 1967, 25 pp., Refs.
(Grant NsG-587) (NASA-CR-85893; ME-67-587-9)

This report outlines progress made on the investigation of the viscoseal and the buffered seal. The experimental performances of fine grooved shaft viscoseal are presented.

N67-35568

NASA Marshall Space Flight Center, Huntsville, Alabama

Conference on Design of Leak-Tight Separable Fluid Connectors, Vol. 1

25 March 1964, 340 pp., Refs. Proc. held 24-25, March 1964 (NASA-TM-X-60234)

Contains twelve papers given at the conference.

AD-379 053L Fld. 21/5

Pratt and Whitney Aircraft, East Hartford, Conn.

Component Propulsion Program for Future High-Performance Strategic Aircraft. Vol. XVI Seals

Semiannual Report No. 3, 1 August 66-31 January 67

R. C. Barningham, Contract AF33(657)-14903, Proj. AF-61139A

Confidential Report